INVESTIGATIONS OF THE NUCLEAR PROPERTIES OF ^{124}Te AND ^{154}Gd USING A DUAL-PARAMETER ENERGY-TIME SPECTROMETER

George Mardirosian

B.Sc. (Aleppo), M.Sc. (London)

A Thesis Submitted for the Degree of

Doctor of Philosophy

in the

University of London.

Physics Department

Bedford College

London

1983.

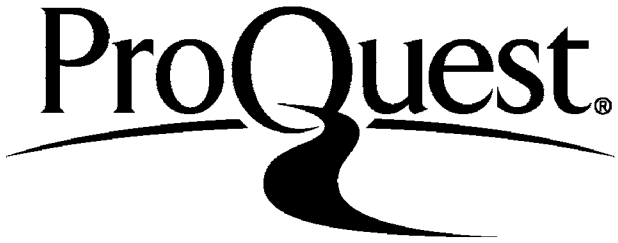

Abstract

Two large volume Ge(Li) detectors and a plastic scintillation counter incorporated in a dual-parameter energy-time spectrometer are used to measure gamma-gamma coincidences following the beta decay of ^{124}Sb and ^{154}Eu. Such an assembly of the detectors also allowed the lifetime of the first excited state of ^{154}Gd to be determined.

A 12 % efficient Ge(Li) detector, an intrinsic Ge detector and a Compton suppression system have been employed in the measurement of gamma-ray energies and relative intensities, allowing the log ft values, multipolarities, spins/parities and transition probabilities to be deduced for the two medium mass isotopes ^{124}Te and ^{154}Gd. Consequently following the coincidence measurements, the energy level schemes for both nuclei are built up incorporating several new energy levels and transitions; evidence is also found regarding levels which had been tentatively reported earlier, and are now considered as confirmed from the coincidence data.

The apparent vibrational shape of ^{124}Te and the deformation mode of ^{154}Gd are investigated in light of the experimental results concerning their positive parity states. Negative parity states are also considered in terms of Coriolis coupling acting between three octupole bands in the ^{154}Gd nucleus. The calculated electric dipole transition probabilities show good agreement with the experimental values.

Comparisons are made with the predictions of current nuclear models. In particular the application of the group theoretical symmetries of the interacting boson approximation are discussed. The calculations are carried out using the program package PHINT for determining the energy levels, in conjuction with FBEM for evaluating the transition rates. In case of ^{154}Gd the consequences of using the hybrid parameters, resulting from proton subshell closure at Z=64, are considered. Earlier nuclear models applied to both nuclei are discussed and compared with the present nuclear predictions.

CONTENTS

List of Figures.

List of Tables.

CHAPTER I
INTRODUCTION

1.1 General.

In low energy physics, gamma-ray spectroscopy is by far the most comprehensive way of dealing with the properties of decay schemes and therefore nuclear structure. However, nuclear spectroscopy is mainly concerned with the study of the manner in which nuclei absorb and emit energy. These discrete amount of energy result from relatively long-lived nuclear states. The description of nuclear states is always associated with some parameters which are of particular importance. One of the main objects of the experimental work in nuclear spectroscopy is to obtain as much information as possible on these parameters, i.e. the energy of excited states, relative intensities, angular momentum, parities, isotopic spins,width or lifetime of excited states, electric and magnetic moments, etc.. Theoretical work however, attempts to relate the experimental data by models to the behaviour of nucleons in nuclei.

A large variety of techniques in experiments and theories have developed out of the field of α-, β- and γ-ray spectroscopy. Continuous progress in spectroscopic resolution now allow a detailed insight into the level schemes.

During the course of this work, the two level schemes of ^{124}Te and ^{154}Gd have been studied on the basis of gamma-gamma coincidence technique. The system of the Dual-Parameter Energy-Time Spectrometer is basically suitable for γ-γ coincidence studies, providing a great advantage over the conventional fast-slow coincidence technique and enabling complicated decay schemes to be handled efficiently by incorporating 4096 X 4096 matrix spectra stored on large capacity magnetic tape. With two large volume Ge(Li) detectors and a plastic scintillator, the assembly of the system also enables the lifetime measurement of nuclear excited states in the nanosecond region. A full description of the system, functions and operations are discussed in Chapter III together with a general description of the experimental procedures made to set up the experimental work.

Despite many attempts to overcome the difficulties which followed previous studies on ^{124}Sb and ^{154}Eu decay, it

has been found that there are many gaps still unfilled by experiments, which certainly require further investigations. Furthermore, the choice of the present isotopes, which predominantly exhibit harmonic (^{124}Te) and deformed (^{154}Gd) types of nuclei, is particularly important since they provide an interesting and challenging problem concerned with general nuclear collective motions. They also provide a strict test of nuclear models as they may not be adequately described by assuming some simple symmetric geometrical shapes. Full studies on ^{124}Sb decay are given in Chapter IV, and Chapter V is dedicated to the studies of ^{154}Eu decay.

In Chapter I, an introductory prescription to specific and basic modes in nuclear physics are briefly outlined and sometimes explicitly written down consistent with the essential requirement of this work. The theory of some important and distinctive nuclear models given in Chapter II mainly focusses the attention onto those models having direct applicability to the nuclides under considerations.

1.2 Radioactivity.

Radioactivity is the process following the change of one kind of nuclide to another by the emission of radiations. The discovery of natural radioactivity and the associated phenomena of β-decay, as well as α- and γ-decay, signalled the start of nuclear physics. All radioactive materials decay according to an equation of the form

$$N = N_0 \, e^{-\lambda t} \qquad (1.2.1)$$

where N_0 is the number of radioactive atoms at time t=0 and λ is the radioactive decay constant which related to the mean life τ of the radioactive substance $\lambda=1/\tau$. Therefore the time for half of the radioactive atoms to decay is termed the half value period or half-life T.

$$T = \ln 2 \, / \, \lambda \qquad (1.2.2)$$

If the radioactive substance decays by more than one mechanism, the total probability of decay of the atom in time dt is $\sum_i \lambda_i dt$ and the mean life of the substance is $1/\sum_i \lambda_i$.

In addition to the naturally occurring radioactive substances, radioisotopes are also obtained either by bombardment of suitable target materials with neutrons, or charged particles, or from fission products. Those radioisotopes produced by neutron bombardment are by far the largest class, and have been responsible for the very extensive development in the use of radioisotopes in the last twenty years or more. The latter method is used to prepare the radioactive elements used in the present work. This was achieved by exposing the material element to thermal neutrons using the facilities provided by the University of London Reactor Centre (ULRC). The 100 kW water tank reactor which produces a neutron flux of about 10^{12} n cm^{-2} sec^{-1} is most suitable for short irradiation purposes. In addition the irradiations in low flux reactors prevents the burn up of the target nuclei. Therefore, for negligible neutron absorption cross-section of the product isotope, the specific activity of product nuclei in curies per gramme of target element's

$$S = \frac{0.6\ \phi\sigma(1-e^{-0.693t/T})}{3.7\times10^{10}\ W} \qquad (1.2.3)$$

where ϕ is the effective neutron flux in neutrons per cm^2 per second. σ is the activation cross-section of the target material in barns. W is the atomic weight of target material, and t is the irradiation time.

1.3 Beta decay.

Beta decay is classified according to the radioactive decay process in which the mass number of the nucleus remains unchanged, but the atomic number changes, and is therefore referred to as the conversion of nucleons.

$$N \longrightarrow P + e^- + \bar{\nu} \qquad \beta^- \text{ decay} \qquad (1.3.1)$$

$$P \longrightarrow N + e^+ + \nu \qquad \beta^+ \text{ decay} \qquad (1.3.2)$$

$$P + e^- \longrightarrow N + \nu \qquad \text{Electron Capture} \qquad (1.3.3)$$

Here, the main discussion will concentrate on the

first two types of transitions that show a broad electron spectra from zero to a finite maximum energy (end-point energy) which is characteristic of the nuclide. The spectra also involved with the intermediate excited states which proceed to the ground state in an appreciable fraction by the internal conversion process, i.e. a line spectrum of conversion electrons will be superimposed on the broad beta-ray spectrum (see later).

Because the beta particles emitted from radioactive nuclei have velocities approaching that of the velocity of light, their motion must be described by the special theory of relativity instead of the classical mechanics. Based on Pauli's neutrino hypothesis, Fermi (1933, 1934) gave a complete descriptive theory of beta-decay which explains satisfactorily beta process. This theory states that the interaction which exists between the nucleon, electron and neutrino causing the transition, depends on the spin states of the particles but not on their linear or angular momentum. Thus the derivation of the transition probability makes use of the time dependent perturbation theory. The theoretical treatment of Segrè (1977) is rather lengthy from which the results are quoted. It is worth noting that Fermi assumed the conservation of parity. Although it turned out not to be so, his calculation still stands in large measure because the calculation involved scalar quantities.

The probability per second for emission of an electron having a momentum in the interval between P_e and (P_e + dP_e) is

$$N(n)dn = \frac{g^2 m^5 c^4}{2\pi^3 \hbar^7} |M_{if}|^2 F(Z,\varepsilon)(\varepsilon_0-\varepsilon)^2 n^2 dn \quad (1.3.4)$$

where $\varepsilon=E_e/mc^2$ and $n=P_e/mc$ the energy and momentum of the electron and their maximum values ε_0 and n_0 respectively. $F(Z,\varepsilon)$ is Fermi function which is necessary to apply a correction due to the Coulomb field Ze affecting the emission of ±e particles [tables of $F(Z,\varepsilon)$ are listed in Grove et al. (1971)]. g is a constant representing the magnitude of the weak interaction i.e. $g^2/\hbar c \simeq 10^{-13}$, for gravitational force is $\sim 10^{-39}$, the strong interaction is $f^2/\hbar c \simeq 1$ and the coupling constant for the electromagnetic interaction $e^2/\hbar c \simeq 10^{-2}$.

The matrix element M_{if}

$$M_{if} = \int \Psi_f^* \, e^{i(k_e+k_\nu)\cdot r} \, \Psi_i \, dv \qquad (1.3.5)$$

where $k=P/\hbar$ is the propagation of both electron and neutrino. $\Psi_i = u_i$ describes the nucleus before decay whereas Ψ_f is the product of u_f which describes the nucleus in the final state times $\Psi_e(\propto e^{ik_e\cdot r})$ times $\Psi_{\bar{\nu}}(\propto e^{ik\cdot r})$ the wave functions of the electron and antinutrino appearing in the final state. dv is a small volume. By expanding the exponential term in a power series

$$e^{i(k_e+k_\nu)\cdot r} = 1+i(k_e+k_\nu)\cdot r - \frac{[(k_e+k_\nu)\cdot r]^2}{2!}+\ldots \qquad (1.3.6)$$

when the emission of the electron and neutrino does not depend upon their energies i.e. 1 is larger than the other terms, such transitions are called allowed transitions. Hence, the plot of $[N(n)/n^2F(Z,\varepsilon)]^{\frac{1}{2}}$ versus ε should give a straight line known as a Fermi-Kurie plot able to find ε_0 the end-point energy. However, departures from the straight line are attributed to a dependence of M_{if} on P_e such as occurs in "forbidden transitions" according to Eq.(1.3.6). Also the slight difference near the upper energy limit referred to a limit of the neutrino rest mass being considered to be zero in the calculation.

The disinte gration constant λ is obtained by the integration of Eq.(1.3.4) from 0 to n_0. This gives for $F(Z,\varepsilon)=1$

$$\lambda = \frac{1}{\tau} = \frac{\log_e 2}{T} = \frac{g^2 m^5 c^4}{2\pi^3 \hbar^7} \, |M_{if}|^2 f(n_0) \qquad (1.3.7)$$

where $$f(n_0) = \int_0^{n_0} [(1+n_0^2)^{\frac{1}{2}} - (1+n^2)^{\frac{1}{2}}]^2 \, n^2 \, dn \qquad (1.3.8)$$

Then Eq.(1.3.7) leads to

$$ft = \frac{\text{constant}}{|M_{if}|^2} \qquad (1.3.9)$$

where, f is the function given by Eq.(1.3.8) which includes the Coulomb correction, t is the half-life of beta decay and the product ft is called the comparative life-time. It is seen that the expression $1/|M_{if}|^2$ depends on the nuclear structure. Eq.(1.3.9) allows to extract from experimental data, which is affected by the energy of the decay and Z, the information about $|M_{if}|^2$ that is relevant to the nuclear problem. The evaluation of $\log_{10} ft$ is rather complicated and have been much simplified by Moszkowski (1951) and Verrall et al. (1966). This is provided by graphs and the log ft value based on the sum of two terms.

$$\log ft = \log (f_0 t) + \log c \qquad (1.3.10)$$

To define the degree of forbidden transitions based on log ft values, it was found that transitions with log ft value between 3 to 6 are allowed and those which lie between ~6 and ~9 as first forbidden. For the second forbidden transitions, the log ft value is greater than 9 and so on for the higher forbiddness. On the other hand, the transitions with log ft less than 4 are the super-allowed transitions. It is clear that a small value of log ft indicates a large matrix element. This occurs when the spin difference of the initial and final states $\Delta I = \pm 1, 0$ without change of parity (transition from S state). Since the electron and antineutrino are emitted without orbital angular momentum, they carry away no orbital angular momentum if they are emitted with spins antiparallel (singlet state), or a total angular momentum of 1 if they are emitted with parallel spins (triplet states). In the first case, the spin of the nucleus does not change at all in beta decay $\Delta I = 0$ and such transitions are due to Fermi selection rules (denoted F). In the second case, $\Delta I = \pm 1$ or 0, but not the transitions $0 \rightarrow 0$, are referred to Gamow Teller (denoted GT). In both cases, the nuclear eigen-function must not change parity.

Forbidden transitions occur not only because Ψ of the electron and neutrino occupy the entire volume of the nucleus (case of higher waves i.e. p or d), but also the higher terms of Eq.(1.3.6) are considered which introduce the powers of P_e and P_ν into the matrix element. As a consequence, the form of beta spectrum changes and the introduction to a "shape factor" is important to explain the departure from the straight line. Therefore, the selection rules for forbidden transitions depend on the term of the interaction producing the transition. For instance, when the second term of Eq. (1.3.6) describes the interaction, the leptons are emitted in a wave with $\ell=1$ and the parity changes. Hence F selection rules give as second approximation $\Delta I=\pm 1$, 0 (except $0 \nrightarrow 0$); with change of parity. GT rules give $\Delta I=\pm 2$, ± 1, 0 (except $0 \nrightarrow 0$; $\frac{1}{2} \nrightarrow \frac{1}{2}$; $0 \nrightarrow 1$) with change of parity. For more details about forbidden transitions see for example Enge (1966).

1.4 Gamma emission.

The emission of gamma-rays has always played an important role in nuclear physics. Gamma-rays emitted from nuclei yield information on the energy and quantum numbers of nuclear states, and for this reason they are a powerful tool in analyzing nuclear phenomena. Fundamentally, one distinguish two aspects of this study, first is essentially electromagnetic theory, the other is the application to nuclear problems.

The semiclassical description of the gamma radiation process is well documented. Here, a review of the general principles of gamma-ray spectroscopy is given with some useful consequences of the theory as well as the basic aspects of multipole radiations are discussed. The quantum theory of radiation is given by Blatt and Weisskopf (1952). The classical picture describes a nucleus consisting of a charge-current distribution confined to a region about the nuclear origin and undergoing periodic motion whose frequency ω is related to the energy involved in a nuclear transition between two levels by $\omega=(E_i-E_f)/\hbar$. Then the calculation of the power radiated from an oscillating charge assembly involves the solution of Maxwell's equations outside and inside the charge region (the nucleus), and an integration of Poynting's vector over an area

surrounding the nucleus. The simplest treatment was found in considering the wave length λ of the electromagnetic radiation is large compared with the nuclear dimension R, ($R<<\lambda$ relates to the fact that the probability of emission of radiation decreases rapidly with the increase of multipole order).

Since each nuclear state has a definite angular momentum I, its component m and parity π, a gamma-ray transition (photon) must take out an angular momentum L (its eigenvalue λ and component μ), and parity π in accordance with conservation laws

$$L = I_i - I_f \qquad (1.4.1)$$

$$\pi_i \times \pi = \pi_f \qquad (1.4.2)$$

where the scripts i,f indicate the initial or final state.

The angular momentum of the photon λ defines the multipolarity of the radiation. Therefore for a given multipolarity λ there are two kinds of radiations namely, electric with 2^λ pole ($E\lambda$) and magnetic 2^λ pole ($M\lambda$). In addition, the electric and magnetic multipole have different symmetry properties, hence the selection rules could be derived immediately from the parity properties of the wave function of the nuclear states involved. Consequently, the electric multipole radiation of order L has parity as $\pi_i.\pi_f=(-1)^L$ and for magnetic multipole $\pi_i.\pi_f=(-1)^{L+1}$. On the other hand, two momentum selection rules restrict the permitted range of multipolarities and is expressed in the triangular relation

$$|I_i - I_f| \leq L \leq |I_i + I_f| \qquad (1.4.3)$$

These conditions are necessary but not sufficient for radiation transitions. For example, transitions from 0_i to 0_f states are always forbidden and can only occur by mechanisms different from electromagnetic radiation, namely, by the emission of conversion electrons or by formation of electron-positron pairs. The types of radiations that have been observed in practice are E1 to E6 inclusive, and M1 to M5 inclusive. In almost all cases, except the pairs E2-M1 and E1-M2, only a single type of radiation occurs in a given

transition.

If for certain order of multipole, the matrix elements that determine the transition probability, vanish exactly, the transition is forbidden and that multipole component of the electromagnetic field is absent.

The transition probability is the basis feature of an electromagnetic transition, and a very useful property for the analysis of empirical data. Derivations of the formulae are given in many text such as Blatt and Weisskopf (1952).

$$T(\sigma\lambda,\mu) = \frac{8\pi(\lambda+1)}{\lambda[(2\lambda+1)!!]^2}\frac{1}{\hbar}\left(\frac{\omega}{c}\right)^{2\lambda+1}|\langle f|M(\sigma\lambda,\mu)|i\rangle|^2 \quad (1.4.4)$$

$$T(\lambda;\ I_i \to I_f) = \sum_{\mu,m_f} T(\lambda,\mu;I_i m_i \to I_f m_f)$$

$$= \frac{8\pi(\lambda+1)}{\lambda[(2\lambda+1)!!]^2}\frac{1}{\hbar}\left(\frac{\omega}{c}\right)^{2\lambda+1} B(\lambda;\ I_i \to I_f) \quad (1.4.5)$$

where σ is either for electric (E) or magnetic (M) type of radiation, and the quantity

$$B(\lambda;\ I_i \to I_f) \equiv \sum_{\mu,m_f}|\langle I_f m_f|M(\lambda,\mu)|I_i m_i\rangle|^2 \quad (1.4.6)$$

is the reduced transition probability. It is noticed that while the transition probability depends on the transition energy, being related to $E^{2\lambda+1}$, the reduced transition probability does not depend on energy, but is the squared of transition matrix element. It is therefore convenient to convert $T(\lambda)$ into $B(\lambda)$. Usually $B(E\lambda)$ is expressed in units of $e^2R^{2\lambda}$ and $B(M\lambda)$ in units of $\mu_N^2 R^{2\lambda-2}$.

The evaluation of formulas such as $B(\sigma\lambda)$ requires a detailed knowledge of the nucleus. Detailed calculations are possible only for low-lying states. A notable case is that of only one nucleon radiating, this single particle aspect assumes the excitation of only one nucleon and provides

valuable reference to nuclear models. The Weisskopf estimate provides a rough and simple estimate for a single-particle transition probability for each multipolarity. It is a very useful unit with which gamma-ray transition probabilities can be compared. In calculating the Weiskopf estimate, the statistical factor S is taken to be unity, and the nuclear radius is taken as $1.2A^{1/3}$ fm.

$$B_w(E\lambda) = \frac{1}{4\pi}\left(\frac{3}{\lambda+3}\right)^2(1.2)^{2\lambda}\, A^{2\lambda/3} \quad \text{in units } e^2fm^{2\lambda} \qquad (1.4.7)$$

$$B_w(M\lambda) = \frac{10}{\pi}\left(\frac{3}{\lambda+2}\right)^2(1.2)^{2\lambda-2}A^{(2\lambda-2)/3} \text{ in units } \mu_N^2 fm^{2\lambda-2} \qquad (1.4.8)$$

In practice, when small admixtures of magnetic multipole with the electric multipole radiations are present i.e. E2 and M1, the relative magnitudes and phases of the E2 and M1 matrix element can yield information on the nature and size of the nonvibrational component of the excited states, and is given by the mixing ratio δ as:

$$\delta = \frac{\langle I_f| \ |E2| \ |I_i\rangle}{\langle I_f| \ |M1| \ |I_i\rangle} \qquad (1.4.9)$$

The evaluation of the total transition probability of a nuclear level, P(level), is the sum of the transition probabilities of all depopulating (electromagnetics and particles) transitions P_d and can be measured by knowing the half life T or the level width Γ of that particular level.

$$P(\text{level}) \equiv \sum_d P_d = [\tau(\text{level})]^{-1} \quad \text{in sec}^{-1} \qquad (1.4.10)$$

$$\tau(\text{level})\,\Gamma(\text{level}) = \hbar \simeq 6.58\text{X}10^{-16} \text{ eV sec.} \qquad (1.4.11)$$

The experimental gamma-ray transition probability is relevant to the theoretical partial gamma-ray transition probability $T(\sigma\lambda) \equiv P_\gamma(\sigma\lambda)$, which can be calculated as following

$$P_\gamma(\sigma\lambda) = P(\text{level})\ I_\gamma(\sigma\lambda)/\sum_d I_d \qquad (1.4.12)$$

where $\sum_d I_d$ is the sum of the intensities of all transitions depopulating the level of interest in the same relative units as the intensity $I_\gamma(\sigma\lambda)$ of the gamma-ray transition with multipolarity $\sigma\lambda$ for which $P_\gamma(\sigma\lambda)$ is to be calculated. This is being calculated like this

$$\sum_d I_d = \sum_d I_\gamma\ (1+\alpha_T) \qquad (1.4.12)$$

considering no interference occurs between mixed electric and magnetic multipole radiations. The definition of the total conversion electron coefficient α_T is given in section (1.5). Then using Eq.(1.4.5) one ends with the relations :

$$B(E1;\ I_i \rightarrow I_f) = 6.288\ 10^{-16}\ E_\gamma^{-3}\ P_\gamma(E1;\ I_i \rightarrow I_f) \qquad (1.4.13)$$

$$B(E2;\ I_i \rightarrow I_f) = 8.161\ 10^{-10}\ E_\gamma^{-5}\ P_\gamma(E2;\ I_i \rightarrow I_f) \qquad (1.4.14)$$

$$B(M1;\ I_i \rightarrow I_f) = 5.687\ 10^{-14}\ E_\gamma^{-3}\ P_\gamma(M1;\ I_i \rightarrow I_f) \qquad (1.4.15)$$

where the transition energy E_γ is given in MeV.

For single depopulating gamma-ray transition with E2/M1 mixing, the relation between the partial gamma-ray transition probability and the total transition probability of the level can be given as a function of the total internal conversion coefficient α_T and the multipole ratio δ:

$$P_\gamma(M1) = P(\text{level})/[1 + \delta^2 + \alpha_T(M1) + \delta^2\alpha_T(E2)] \qquad (1.4.16)$$

$$P_\gamma(E2) = P(\text{level})/[1 - \delta^{-2} + \alpha_T(E2) + \delta^{-2}\alpha_T(M1)] \qquad (1.4.17)$$

For transitions having different multipole mixing order see Löbner et al. (1972). The above relations are used in the calculation given in Chapters IV and V.

1.5 Internal Conversion.

An inevitable parallel process to the normal electromagnetic transitions for which a single photon is emitted, is internal conversion in which an orbital electron emerges carrying away the energy of deexcitation. This process is complementary to photon emission, and to first order does not diminish the rate of photon emission but rather provides an additional mechanism to the process.

Two types of information that may be derived are the conversion coefficients α and the conversion ratios. The K conversion coefficient is the ratio

$$\alpha_K = N_K / N_\gamma \qquad (1.5.1)$$

where N_K and N_γ are the relative probabilities for emission of K-conversion electrons and gamma-rays respectively. Therefore conversion coefficients for other shells or subshells are similarly defined and the total conversion coefficient is

$$\alpha_T = \alpha_K + \alpha_{LI} + \alpha_{LII} + \ldots \qquad (1.5.2)$$

The internal conversion coefficients are important because of their sensitivity to the energy, to the multipole order and parity change involved in the transition, and of course to the radius and atomic number of the nucleus. But not to a specific nuclear model. Hence the study of either the magnitude of the internal conversion coefficient or the conversion ratio α_K/α_L can determine the polarity of the radiation and

so the parity. This process is also important because the longitudinal electromagnetic field can contribute to transitions that cannot proceed via the transverse electromagnetic field such as the $0^+ \rightarrow 0^+$, the so called E0 or electric monopole, can occur. It is possible for an orbital electron to participate in the transition of an excited nucleus due to the electromagnetic interaction between the electron and the nucleus. The magnitude of the effect depends partly on the amplitude of the electron wave function and hence the most strongly bound electrons will generally have the largest conversion probabilities.

As the conversion coefficients depend on the atomic properties of the electron, calculation of these properties could be measured accurately. Therefore the conversion coefficients for different shells as a function of the energy, the type of radiation and of Z, have been extensively tabulated, such as by Rose et al.(1937, 1955, 1958). These tables cover different atomic subshells nuclear charges and transition energies. The calculation of the total transition probabilities must, of course, include the internal conversion process. The experimental value of the conversion coefficients can be compared with the theoretical calculation to assist in assigning the characteristic of a transition. However, the procedure for calculating the internal conversion coefficients involves several model considerations. Nevertheless the assumptions, which underlie the calculation, require the application of a second order perturbation theory of quantum electrodynamics with the inclusion of the electron dynamics, penetration and screening effects and finite nuclear size effect.... The model that is described by Rosel et al.(1978) has been used in the present work. It covers a wide energy range and provides the calculation for higher shells with very good accuracy.

1.6 Introduction to nuclear structure physics.

In the last two decades, the knowledge that concerns the structure of nuclei has been tremendously improved through the development of nuclear models. The ultimate goal of nuclear structure physics is to account for the properties of

complex nuclei in terms of a collection of A bodies (Z protons and N=A-Z neutrons) interacting with each other through instantaneous two body potentials. Such a microscopic description of the nucleus, in terms of the properties of its constituents, defines the direction in which nuclear structure physics moves in the quest for a fundamental theory of nuclei.

However, the microscopic investigations in nuclear structure theory makes a direct contact to the shell model. Its later development helped in understanding the nuclear properties, which thereafter, led to the dynamical model with strong spin-orbit force which was developed by Feenberg (1949), Haxel et al.(1949), Mayer (1949, 1950), Mayer et al.(1955) and Jensen (1964). This was very successful in correlating spins and parities of ground states, magic numbers, alpha and beta decay systematics, etc.. Despite the great successes of the shell model in many aspects, its predictions of some nuclear properties, especially in the regions between closed shells, was not adequate enough to explain the empirically observed behaviours.

From a theoretical point of view, the description of observed phenomena in terms of a shape phase transition, is a very interesting and challenging problem. For such studies, the natural sequence moves towards examining first the systematics of the ground state properties and then goes on to look for the patterns in spectra of low-lying excited states. This description is rather related to the most "macroscopic" aspects of the nuclear droplet. Such rules indicate that nuclei with a wildly differing ground-state structure respond in similar ways when they acquire a small amount of energy i.e. they rotate. However the effect of the rotational motion seems to be different for different ground state structure (highly deformed or stable nuclei with simple rotation), so that the moment of inertia is almost independent of angular velocity. Unstable and less deformed nuclei show a tendency to become more deformed as they rotate faster.

The essential contribution of Bohr (1952) and later Bohr & Mottelson (1953) was in recognizing the static shape,

the orientation of a deformed nucleus and the collective deformation variables of a spherical nucleus, were related to each other. The properties of rotational bands strengthened Bohr & Mottelson's conviction that a deformed nucleus has cylindrical symmetry so that the component K of the total angular momentum along the axis of symmetry is a good quantum number. The deformed nucleus was assumed to be an essentially incompressible spheroid of constant density in which neutrons and protons are uniformly distributed. In addition to the rotational motion, two types of quadrupole vibrations of considerably higher frequency than that of the rotations ($\hbar\omega \simeq 1$ MeV) were thought to be most prominent; beta vibrations around the equilibrium deformation, for which K=0, and for which the spin sequence of the superimposed rotational band is 0, 2, 4,...., even parity, and the as ymmetry producing gamma vibrations with K=2 and spin sequence 2, 3, 4, 5 ...., even parity. The deformation parameter β provides a measure of the departure from spherical symmetry, while the as ymmetry parameter γ is an angular coordinate so that for $\gamma=0$ or π the deformation is symmetric about the axis of symmetry, and of prolate and oblate shape respectively. For $\gamma=30^0$, the assymmetry is at maximum.

The fully microscopic nuclear model approach gives reliable results only in the limiting situations for either spherical or strongly deformed regions. In general, the phenomenological collective models have been used to describe the low-lying states of even-even nuclei; those nuclei fall conveniently into three distinguished groups. The first consists of closed shell nuclei with magic neutron or proton numbers. Their low excited states can often be described adequately on the basis of the shell model. A second group contains those even nuclei with atomic weight A in the ranges 20-28; 150-190 and 220 upwards. These nuclei have a spectrum of electric quadrupole γ-vibration rates up to 300 times the value calculated for a single particle transition so that many particles must contribute to the transition. Outside the rotational regions and excluding the closed-shell nuclei there is a third group whose members show large quadrupole motion but do not have a rotational energy spectrum. Low levels of

many of these nuclei can be described by the surface vibration model introduced by Bohr et al.(1957, 1958-a and -b) and Scharff-Goldhaber et al.(1955, 1958). Morinaga (1966) was the first to suggest that the decrease of the energy spacings at higher I than required by the I(I+1) rules of Bohr & Mottelson was due to an increase in the moment of inertia $\mathcal{J}$. He proposed the term softness for the percentage increase of $\mathcal{J}$ per unit change of I, $\Delta\mathcal{J}/\mathcal{J}\Delta I$ and discussed the form of the dependence of this quantity on I as a function N and Z. An attempt to give a physical explanation of the increase of $\mathcal{J}$ was made by Diamond et al.(1964), who suggested a semiclassical model based on the idea of a spinning nucleus being stretched out under the influence of a centrifugal force, the so-called beta-stretching model. A similar attempt was made by Harris (1965) who proposed a consistent expansion of the energy and moment of inertia in powers of ω^2 as an alternative to the I(I+1) expansion. The latter is a generalisation of the Inglis cranking model. The equivalence of the variable moment of inertia (VMI) model with Larri's fourth-order cranking model was also proven [Mariscotti et al.(1969)]

Other collective models have been developed to describe also intermediate situations. Among the latter approaches, the most familiar ones are the pairing-plus-quadrupole model of Kumar and Baranger (1968 a, b and c) and the boson expansion model of Tamura et al.(1979) and Kishimoto et al.(1976). Attempts have been also made to describe these collective properties in terms of boson degrees of freedom instead of fermion degrees of freedom. Some methods involved infinite expansions, i.e. boson operators of ever-increasing order [see Brink et al.(1965) and Kishimoto et al.(1976)], and others contain boson operators of finite order such as the work of Janssen et al.(1974). Since these methods utilize only quadrupole operators (obey the commutation relations of U(6) Lie algebra), their expansion consists only of quadrupole bosons (J=2). The second approach is that of Arima & Iachello (1976, 1978, 1979), Iachello (1979), Scholten et al.(1978), known as the Interacting Boson Model (IBM) which contains monopole (J=0), s bosons, as well as quadrupole, d bosons. The distinctive differences of the IBM from earlier boson

models is that the total number of bosons is conserved, $n_s+n_d=N=$constant. This important feature directly links the IBM to the number of valence fermions (outside a closed shell) and thereby to the underlying single particle or shell-model structure of the nucleus. Consequently, the IBM provides a possible method of simultaneously interpreting nuclear collective properties in terms of a simple model. Also it contains only few parameters in a model space much smaller than the usual shell-model space. On the other hand, the analytic solutions of the Hamiltonian in terms of complete chains of a six-dimensional space group SU(6) gave rise to three possible dynamical symmetrics (chains) and three possible analytic solutions appeared in SU(5), SU(3) and O(6) limits referred to the vibrational, rotational and γ-unstable structure respectively. The usefulness of the interacting boson approximation is the possibility to depart from these three limited cases to take into account the intermediate limits i.e. the transitional limits of SU(5)-SU(3), SU(5)-O(6) and SU(3)-O(6) covering a wide range of nuclei in the periodic table.

Since in nuclei, one has both proton and neutron pairs, it was possible to introduce proton (s_π, d_π) and neutron (s_ν, d_ν) bosons. The model that explicitly distinguishes between the proton and neutron bosons is commonly referred to as IBA-2, whereas the conditions when no distinction is made is often referred to as IBA-1.

Although the various nuclear models are not completely independent of each other, the nuclear application is approximately peculiar and depends on the mass number, as well as, on the nuclear properties exhibited by the nucleus under consideration. Ultimately the nuclear models are all facets or approximations of a theory that is not complete . Chapter II will deal briefly with the latest nuclear models, and explicitly with those relevant to the nuclei under investigation.

1.7 Detection methods for nuclear radiation.

The measurement of gamma-ray energies with precision

is related to the ability to determine precisely the channel position of the centre of the peaks in the corresponding pulse-height spectrum. This in turn associated with the shape of the peaks and with the spectrometer energy resolution.

The development of semiconductor detectors with an energy resolution which is vastly superior to that of the high efficiency scintillation detector has an important application in the detection of nuclear events in the last twenty years. On the other hand organic scintillators (plastic) have an extremely fast response, of the order of 10^{-9} sec, especially when matched by good photomultipliers. But because of their low density and low Z, their efficiency for gamma-ray conversion is not high. However, inorganic crystals are used instead, such as NaI or CsI, activated with some impurity of Tl. They have an excellent efficiency for gamma-ray conversion due to their high Z (the photoelectric effect is proportional to Z^5 and pairproduction to Z^2). But the light output from inorganic crystals is spread over a much longer time interval of the order 10^{-6} sec.

The semiconductor crystals of silicon and germanium have been found to be very useful as high resolution detectors. In addition they are produced of purity and crystal perfection, many orders of magnitude, better than any other available materials. As a gamma-ray of energy E enters the intrinsic region of a semiconductor detector, part of this energy is going into formation of ion pairs and part of it going into heating the lattice crystal structure (phonon or thermal energy). The latter case is undesired and causes statistical fluctuation which involves what is called Fano factor [Fano (1947)]

$$F = \frac{\sigma^2}{E/\varepsilon} \qquad (1.7.1)$$

where $$\Delta E = 2.35\varepsilon\sigma = 2.35\ (\varepsilon EF)^{\frac{1}{2}} \qquad (1.7.2)$$

σ^2 is the mean square variation of the number of electron-hole pairs produced by E. ε is the average number of electron-volts

that result in the production of an ion pair.

A strong electric field is required in order to accelerate the electrons and holes to maximum velocity within the intrinsic germanium region, and to avoid carrier trapping or the recombination effect which is the main inconvenience in these counters. At the same time, Fano factor would be unity if the energy lost by ionization were dissipated solely through thermal vibration of the lattice, hence the number of electron-hole pairs are subject to normal statistical fluctuation. On the other hand, if the energy was completely converted into ionization energy, the number of electron-hole pairs would not fluctuate. The actual situation found for Ge and Si materials is with F about 0.12 (Goulding 1966) and the rise time would vary between 50-250 n.sec depending on the detector's type. One inconvenience of semiconductor detectors is that they must be operated at low temperature in order to reduce the leakage current existing at room temperature. Usually, field effect transistors (FET) are used in the first stage of amplification for best electronic devices,as far as noise is concerned. The specification of detectors, in particular semiconductor detectors, and the problems concerned are fully discussed by Siegbahn (1965), Bertolini & Coche (1968) and Helmer et al.(1975). A sphere for a solid-state Ge(Li) detector provides the greatest full-energy peak efficiency, the least probability of Compton scattering and loss of the gamma-ray energy. Although this shape is obviously impractical because a centre contact could not be made, the true right circular cylinder (TRCC) coaxial detector approximates a sphere more closely than other designs. Small volume pure Ge detectors have low efficiency for high energy gamma-rays which means that the background due to Compton scattering is low.

To obtain the best resolution, capacitance at the preamplifier should be minimized by keeping the connecting cable between the detector and amplifier as short as possible. In addition, when resolution is the prime criterion in the experiment, every effort must be made to reduce the count rate at about less than 100 count per second. This could be achieved by a proper selection of a source strength, geometrical

position, etc.. But some experimental situations demand high count rate and yet need the benefit of the highest possible resolution. In these circumstances, selection of the pulse shaping method with a variable shaping amplifier is necessary as well as the use of pole-zero-cancelled preamplifiers and amplifiers. The use of a base line restorer should also improve the resolution at high count rates. However the pulse shaping method yields optimum signal-to-noise ratio enhancement and is always in conflict with the optimum method for overlap prevention. This conflict requires some compromise in the design of an experiment (the overlap happens when an event was not eliminated within a time that is short compared to the average spacing of the pulses. It always creates errors in amplitude measurements if not prevented). The lifetime of nuclear levels for γ-ray decay are usually much shorter than the charge collection time in a Ge(Li) detector. When two or more γ-rays are emitted in cascade, any two of them may deposit energy in the detector to form a composite pulse indistinguishable from that due to a single event. Thus correction for peak areas (gamma-ray intensity) must be made for true and random coincidence summing effects. In the case of a cascade and cross-over transition relationship, real coincidence summing will increase the apparent intensity of the cross-over transition. Therefore the consequences of true coincidence summing that are independent of counting rate (depend solely upon the experimental geometry and the specific features of the decay scheme), become progressively more important as the distance of the source-detector is reduced especially in those cases where the cross-over transition intensity is much less than that of the cascade gamma-rays. High count rates can also give rise to pile up effects which causes nonlinearity of the preamplifier output.

A rapidly increasing interest in basic research and direct applications that involve the timing of events primarily include measurements of very short lifetimes of excited nuclear states; coincidence experiments, positron annihilation studies, are some of many application in atomic, nuclear and elementary particle physics. In general, extremely short-time events are associated with the emission of photons or particles, and

therefore, a radiation detector and fast electronic techniques are necessary to convert the received information.

In the following, it is important to point out the cause of some of the problems associated with timing measurements. This directly involves the use of nonlinear circuits which convert the detector output pulses to the input of the time analyser. Shaping stages for this purpose have to come close to fulfilling the conditions for obtaining high time resolution. Still the major inaccuracies of time derivation are caused by two basic factors, jitter and walk. Large Ge(Li) detectors, have walk that is caused by variations in rise times as well as amplitudes. Thus individual pulses will cross the discriminator level at different times with respect to their actual times of occurrence. This problem is difficult to avoid when using a leading-edge discriminator in an experiment. Therein the effect could be minimized by lowering the leading-edge discriminator level as much as possible without triggering on random noises in the system, or by restricting the information to the dynamic range in setting the discriminator level at that fraction of pulse height where experiments show the best results. However, walk recently became less effective in timing systems following the technique of zero-crossing point which found an accurate timing device in the Constant Fraction timing discriminator (CFD). This problem was superceded by the Amplitude and Rise-time Compensator (ARC) technique which provides well improved timing results and differs from CF timing in the amount of delay of the full amplitude with respect to the rise time of the pulse.

Jitter on the other hand, is defined by the time error that is introduced by noise fluctuation on the signal. It causes a discriminator response either sooner or later than would be the case if no noises were present. In the system in which noise is relatively constant, the higher energy signals have a larger time uncertainty due to the increased effect of jitter on the smaller slope.

Principally the achievement of taking direct time measurements in the nanosecond region depends on two main tasks;

the coincidences of events or the measurement of time intervals between them when they are correlated in time and the processing and counting of like events which occur at nanosecond intervals. However, the choice of the appropriate time derivation method and the specific instruments used to perform the time derivation depends upon the detector being used, the constraints of the experiment and the time resolution derived.

Following advances in nuclear electronics (such as the time to pulse height converter, time pick off and timing filter amplifiers) the use of integrated circuits and microprocessors are replacing the conventional multichannel analyzer for their flexibility in operating complicated devices. For intance, the use of multiparameter data collection systems has increased the capabilities of the conventional fast-slow coincidence, giving enormous advantages in building up decay schemes, and flexibility in data handling purposes. Some very useful sources of information dealing with electronic devices and the associated operational problems can be found in the Instrument For Research (ORTEC-Catalogue 1002) and references such as Meiling et al.(1968) and Nicholson (1974). The details concerning the Dual-Parameter Data Collection system used in the present work are discussed in Chapter III together with the timing resolution of the system involved.

CHAPTER II
NUCLEAR MODELS

2.1 Nuclear shell model.

For many years, the main objective of the shell model was to interpret the magic numbers at 2,8,20,28,50,82 and 126. As more developments were introduced, it was found that this model was able to explain many other nuclear properties besides the magic numbers. However, there are various versions of the shell model, notably the extreme single particle model, the single particle model and the independent particle model, all of which posses a common property, that is, the particles in the nucleus are assumed to move in a mean potential independent of each other. This potential is strongly dependent on a spin-orbit type of coupling force.

In the extreme single particle model, the properties of the nucleus are assumed to be attributed to the single unpaired nucleon. With the single particle model the nucleus is visualised as consisting of filled shells that contain the maximum number of neutrons and protons permitted by the Pauli exclusion principle, and unfilled shells containing the remaining number of nucleons. The independent particle model considers the nucleons moving freely in a single particle potential which depends on the nucleons' spatial, spin and charge coordinates, i.e. a system of independent non-interacting fermions with appropriate density [De-Shalit & Feshbach (1974)].

The single particle estimate of gamma transition probability, normally referred to as Weisskopf estimates [see section (1.4)], provides a crude but useful estimate of the order of magnitude of this quantity. This estimate constitutes convenient units in which the experimentally observed properties can be expressed.

By introducing a deformed potential as in the Nilsson (1955) model, the motion between the single particle and collective degrees of freedom can be correlated.

2.2 Collective model and its extension.

As going farther away from closed shells, some new and systematic features start to show up for some nuclei. In the mass number, A in the range 20-28; 150-190 and 220 upwards, nuclei in these regions are characterised by exceptionally large positive quadrupole moments, Q; even-even nuclei in the same region all have a rather low-lying first excited state with $I=2^+$ and electric quadrupole radiation is strongly enhanced (up to 300 times the value calculated for a single particle transition). These nuclei have a regular spectrum of excited states with spin sequence I=0,2,4 and energies, $E \alpha I(I+1)$, which led Bohr & Mottelson (1953) to the suggestion that these nuclei have a non-spherical shape and the energy sequence is produced by a rotation of this shape. As the ground state of an even nucleus has spin I=0, hence no magnetic moment is allowed. Excited states have a magnetic moment due to the collective rotation of the nuclear charge. The magnetic moment operator is proportional to the angular momentum = $g_R I$, where g_R is the collective g-factor. If the neutrons and protons move quite together in the collective rotation, g_R should have the value Z/A. As more experimental information is obtained, the regularities observed in even-even nuclei are becoming more obvious, and especially those with simple characteristics of rotational spectra are explained with accuracy by the Bohr & Mottelson (1953) strong coupling collective model.

Outside the rotational regions and excluding the few closed-shell nuclei, there may be nuclei which have a tendency to deform, but the deformation may have fluctuations large compared with the magnitude of the deformation. If these fluctuations in shape have dynamical properties, these should be nuclear excitations analogous to waves on the nuclear surface. The customary expressions specifying the shape of the surface in terms of a radius R referred to an equilibrium radius R_0 employ a spherical-harmonic expansion. It takes the form

$$R = R_0[1 + \Sigma \alpha_{LM} Y_{LM}(\theta,\phi)] \qquad (2.2.1)$$

the coefficients α_{LM} vary with time even though the shape remains fixed. If L=0 the deformation represented is a uniform dilatation. The case L=1 corresponds to a centre of mass translation, hence plays no part in describing excited states, while L=2,3 describe quadrupole and octupole surface deformations. The system can be quantized as a set of independent oscillators and the ground state has angular momentum I=0. The lowest excited state associated with the coordinate α_{LM} has angular momentum (L,M), parity $(-1)^L$, and an excitation energy $\hbar\omega$ above the ground state. The states of a set of independent oscillators can always be described by "quasi-particle" picture and n^{th} excited state associated with the coordinate α_{LM} is said to have n phonons (or surfons) in the state (L,M). Many even-even nuclei are known which have a first excited state with spin I=2 and a second excited state with I=2 or 4 at approximately twice the excitation of the first excited state. In some cases, I=0,2 and 4 states are seen close together in this position as predicted by the model. All these nuclei have enhanced electric quadrupole γ-transition probabilities.

The vibrational model predicts the energies and spins of second excited states and in addition there are certain selection rules and intensity rules. For small deformations the quadrupole operator is proportional to $\alpha_{2\mu}$, hence it has matrix elements only between adjacent vibrational states. A selection rule follows that the cross-over transition between the second 2^+ excited state and the ground state is forbidden. The same argument shows that excited states corresponding to quadrupole vibrations should have zero quadrupole moment. However, higher terms in the expansion of the quadrupole operator violate this selection rule and allow the cross-over transition. The ratio of the reduced transition rates of the cross-over to the stop-over transition is $(2'-0)/(2'-2) = 2\beta^2/7\pi$ where $(\beta$ -) is the deformation parameter whereas $(2'-2)/(2-0) = 2.0$. A magnetic dipole photon carries off an angular momentum $\hbar$, while a phonon has angular momentum $2\hbar$. Hence follows a selection rule for M1 radiation that a transition involving a change in the phonon number is forbidden. In particular the M1

transition from the second 2^+ state to the first 2^+, which is allowed by total angular momentum and parity selection rules, is forbidden (empirically it is reduced by factors ~100 below the single particle value). It is known however, that M1 radiation occurs because g-factors deviate from the value Z/A and depend on the details of the intrinsic structure [Scharenberg & Goldring (1958)]. A simple hypothesis in the spirit of the collective model is to assume that the collective g-factor depends on the nuclear deformation

$$\frac{B(M1;\ 2' \rightarrow 2)}{B(E2;\ 2' \rightarrow 2)} = \frac{80}{7}\,\frac{\mu_0\ g_R'}{2Z\ R_0^2} \qquad (2.2.2)$$

where g_R' is a factor which determines the dependence of g-factor on the deformation and μ_0 is the nuclear magneton.

The above discussion is based on a small vibrational approximation where only the lowest terms are retained in an expression of the kinetic and potential energies in the deformation parameters $\alpha_{2\mu}$. Another set of coordinates used by Wilets & Jean (1956) to describe the anharmonicity of the nuclear surface oscillations, are the two quadrupole deformation parameters γ, β and the three Euler angles specifying the orientation of the quadrupole θ, ϕ, ς. β and γ serve to relate the intrinsic radii of the ellipsoid to its average radius R_0. Therefore, the Hamiltonian of Bohr (1952) can be rewritten in a most general form consistent with the requirements of invariance under rotations and time-reversal

$$H = V(\beta,\gamma) + T_{rot} + T_{vib} \qquad (2.2.3)$$

where $V(\beta,\gamma)$, is the potential energy of deformation, T_{rot} and T_{vib} are the rotational and vibrational kinetic energy. Wilets & Jean (1956) generalized the model by taking two simple anharmonic forms for $V(\beta)$, depending only on β (γ-unstable), but allowing any as ymmetry to occur. Thus the harmonic degeneracies are split producing a second excited 0^+ state and third 2^+ state disappeared up into the high

excitation region. The 4^+ and 2^+ second excited states remain degenerate at an excitation which is slightly greater than twice the energy of the first excited state, the B(E2) cross-over transition is still forbidden. Possibly the most striking change is the displacement upwards of the first excited 0^+ state and the B(E2) ratio $(2' \rightarrow 2)/(2 \rightarrow 0)$ is reduced to 1.43.

Studies on the departure from the simple rotational model, due to oscillations in the nuclear shape, raised [Alder et al. (1956)] the deformation parameter β and the as ymmetry parameter γ; the β-vibration, has zero angular momentum about the nuclear symmetry axis in any vibrational model, while the γ-vibration, has angular momentum K about the symmetry axis, K being either zero or an even integer. Corresponding to any intrinsic vibrational state, there is a sequence of rotational states with I>K, i.e. if K is zero I=0,2,4, whereas if K is not zero I=K, K+1, K+2,... with I=K the lowest state in the band.

Kumar & Baranger (1967-a and -b) have developed the Hamiltonian of Bohr (1952) by proceeding from the two limiting cases (vibrational, rotational) to consider a wide range between the vibrational and the rotational limits, using perturbation methods. This numerical approximation method includes the conditions of boundry as well as symmetry to the adiabatic approximation, which is the intrinsic motion following the collective motion of nucleons. Again the potential energy of deformation $V(\beta,\gamma)$ has taken the main consideration [Eq.(2.2.3)], leaving the shape, and hence, the intrinsic state of the nucleus free to change from one nuclear state to another. The resultant potential contains in its formation several terms, such as for surface energy, Coulomb energy of deformation of a liquid drop model and a term attributed to shell effects. The latter term should disappear at large deformation and doesnot affect the nuclear fission aspect of the nucleus [condition of Myers & Swiatecki (1966)].

2.3 Variable Moment of Inertia (VMI) model.

In this model, the energy levels of the g.s bands

in even-even nuclei could be interpreted on the basis of a semi-classical term in which the plan was to include, in addition to strongly deformed nuclei, the transitional, vibrational and perhaps even magic nuclei. In searching for such an expression the following considerations were taken:

a. The expansion of g.s. band energies in terms of $I(I+1)$ diverges [Mallman (1955)] from the observed behaviour close to the adiabatic limit [Bohr & Mottelson (1953)].

b. The moment of inertia $\mathcal{J}$ deduced from energy spacings in g.s. bands, increases steadily with increasing I [Morinaga (1966)].

c. The static quadrupole moment found in spherical nuclei for 2^+ states indicates a non-vanishing moment of inertia in the 2^+ state.

d. The scaling law depends on only two quantities E_2 and E_4, it should be possible to find a two-parameter expression for the curves $R_I = E_I/E_2$ as a function $R_4=E_4/E_2$ (Mallman's universal curves).

The level energy is thus given by

$$E_I(\mathcal{J}) = \tfrac{1}{2}\, C(\mathcal{J}-\mathcal{J}_0)^2 + \tfrac{1}{2}[I(I+1)]/\mathcal{J} \qquad (2.3.1)$$

The equilibrium condition

$$\delta\, E(\mathcal{J}) \;/\; \delta\mathcal{J} = 0 \qquad (2.3.2)$$

determines the moment of inertia $\mathcal{J}_I$ (given in units of $\hbar^2$). The parameters C and $\mathcal{J}_0$ are the stiffness parameter and g.s. moment of inertia (for $\mathcal{J}_0>0$) respectively and both introduce the softness parameter σ such that

$$\sigma = \tfrac{1}{2}\, C\, \mathcal{J}_0^3 \qquad (2.3.3)$$

The confidence in the VMI model was considerably

strengthened when it was found that fitting the two lowest-level energies (E_2,E_4) alone also permits a good fit to higher levels. The range of validity of this model defined by the variation of R_I for the two cases when $\sigma=0$ and $\sigma \to \infty$ [Mariscotti et al. (1969)]

$$[\frac{1}{6} I(I+1)]^{2/3} \leqslant R_I \leqslant \frac{1}{6} I(I+1) \qquad (2.3.4)$$

2.4 Pairing-plus-quadrupole model (PPQM).

The pairing-plus-quadrupole model has gained popularities in the late sixties-early seventies in attempts at understanding nuclear structure of various types of nuclei. Its success is mainly due to a particular combination of forces which led to the two most important residual effects in nuclear structure, namely paring effects and quadrupole deformations. The later force attempts to deform the shape of the nucleus while the former force trying to keep it spherical. Therefore the Hamiltonian of the model consists of three parts

$$H = H_s + H_p + H_Q \qquad (2.4.1)$$

The first part is the spherical, single particle energy, the second is a pairing force and the third is the quadrupole force. Baranger & Kumar (1965) have greatly simplified in the formation with the following approximations:

a. The contribution of the pairing force to the self-consistent field was neglected.

b. The contribution of the quadrupole force to the pairing potential was neglected.

c. The exchange term coming from the quadrupole force is also neglected.

As such, predictions of many nuclear properties for many nuclei of the periodic table were calculated by Baranger & Kumar (1965, 1968-a and b) and by Kumar & Baranger (1968-a and b) where the single-j shell nuclei (nuclear shell consisting of only one single particle level with angular momentum j), rare earth region as well as deformed nuclei were predicted.

2.5 Boson Expansion technique.

The boson expansion method was first proposed by Belyaev & Zelevinsky (1962) by attempting to obtain a microscopic Hamiltonian for describing the anharmonic correction of the quadrupole oscillations of spherical nuclei in terms of a fermion creation and annihilation operators. Two basis bilinear products of the fermion operators were explained in power of boson creation and annihilation operators. Sorenson (1967, 1968, 1970) later extended the idea and expanded the Hamiltonian to fourth order terms, consequently getting the main features of actual vibrational nuclei.

Kishimoto & Tamura (1972, 1976) and Tamura et al. (1979) refined Sorenson's Hamiltonian to give various expressions in a more compact and transparent way. They noticed from the accumulated experiments that nuclei of spherical shapes, which had been thought to have a quite different form from that of deformed nuclei, might not be so different, and nuclei of high spin states resembled spherical as well as deformed excited levels. The Hamiltonian is therefore a sum

$$H = H_{sp} + H_{ph} + H_{pair} \qquad (2.5.1)$$

of a single-particle Hamiltonian H_{sp}, a particle-hole type quadrupole-quadrupole interaction H_{ph} and a pairing interaction of both monopole and quadrupole types H_{pair}. This Hamiltonian was made to describe spherical and deformed nuclei, and consequently the transitional nuclei as well. So far the boson expansion theory worked well for deformed nuclei, seemingly better than it did for non-deformed nuclei.

2.6 The interacting boson model.

In its simplest form, the interacting boson model assumes that the structure of low-lying levels of nuclei is dominated by excitations of the valence particles, i.e. the particles outside the major closed shell at 2,8,20,28,50,82 and 126. Furthermore, it assumes that the important particle configurations in the low-lying levels of even-even nuclei, are those in which identical particles are paired together in states with total angular momentum L=0 and L=2. These pairs are treated as bosons. Proton (neutron) bosons with angular momentum L=0 are denoted $s_\pi(s_\nu)$, while proton (neutron) boson with angular momentum L=2 are denoted by $d_\pi(d_\nu)$. In order to take into account the particle-hole configuration in the particle space, the number of proton, N_π, and neutron, N_ν, bosons is counted from the nearest closed shell, i.e. if more than half of the shell is full, $N_\pi(N_\nu)$, is taken as the number of hole pairs. A detailed description of the properties of nuclei must treat separately proton and neutron pairs. This description, often referred as IBA-2, will not be discussed. Only the case in which no distinction is made between proton and neutron bosons is considered. In this approximation, often referred to as IBA-1 an even-even nucleus is treated as a system of $N = N_\pi + N_\nu$ bosons.

In the IBM it is assumed that the Hamiltonian contains only one-body&two-body terms, thus introducing creation $(s^\dagger, d^\dagger_\mu)$ and annihilation (s, d_μ) operators, where the index $\mu = 0, \pm1, \pm2$. The most general Hamiltonian can be written as

$$H = \varepsilon'' n_d + a_0(P^\dagger.P) + a_1(L.L) + a_2(Q.Q) + a_3(T_3.T_3) + a_4(T_4.T_4) \qquad (2.6.1)$$

where

$$\left.\begin{aligned} n_d &= (d^\dagger.\tilde{d}) \\ P &= \tfrac{1}{2}(\tilde{d}.\tilde{d}) - \tfrac{1}{2}(\tilde{s}.\tilde{s}) \\ L &= \sqrt{10}[d^\dagger \times \tilde{d}]^{(1)} \end{aligned}\right\} \qquad (2.6.2)$$

$$\left.\begin{aligned} Q &= [d^{\dagger}\times\tilde{s}+s^{\dagger}\times\tilde{d}]^{(2)}-\tfrac{1}{2}\sqrt{7}[d^{\dagger}\times\tilde{d}\,]^{(2)} \\ T_3 &= [d^{\dagger}\times\tilde{d}]^{(3)} \\ T_4 &= [d^{\dagger}\times\tilde{d}]^{(4)} \end{aligned}\right\} \qquad (2.6.2)$$

and $$\tilde{d}_{\mu} = (-1)^{\mu}d_{-\mu} \quad , \qquad \tilde{s} = s \qquad (2.6.3)$$

Eq.(2.6.1) contains 6 independent parameters ε'', $a_i(i=0\text{-}4)$, usually referred to terms as d-boson energy, pairing, angular momentum, quadrupole, octupole and hexadecupole respectively. Several other equivalent ways of writing the Hamiltonian are explicitly given by Arima & Iachello (1981) and Iachello (1979).

In general the residual interaction between bosons and the energy difference $\varepsilon=\varepsilon_d-\varepsilon_s$ split the degeneracy and give rise to a definite spectrum. The eigen-values and eigen-states can be found by diagonalizing the Hamiltonian in an appropriate basis. In order to find these solutions, the advantage of the group structure of the problem had been taken since five ($\mu=0,\pm1,\pm2$) components of the d-boson and the single component of the s-boson span a six-dimensional space and the group structure of the problem is that of U(6) (or SU(6) for a fixed boson number N). Analytical solutions can be found whenever the Hamiltonian is written in terms of invariants only of a complete chains of subgroups of SU(6). Once a group chain has been identified, its first important application is in constructing a basis in which the Hamiltonian H can be diagonalized.

Another operator of interest is the one-body transition operator which in the second quantized form can be written as

$$T^{(\ell)}_{m} = \alpha_2\delta_{\ell 2}[d^{\dagger}\times\tilde{s}+s^{\dagger}\times\tilde{d}]^{(2)}_{m}+\beta_{\ell}[d^{\dagger}\times\tilde{d}]^{(\ell)}_{m}+\gamma_0\delta_{m0}\delta_{\ell 0}[s^{\dagger}\times\tilde{s}]^{(0)}_{0} \qquad (2.6.4)$$

Eq.(3.6.4) gives rise to the following operators

$$T^{(E0)}_{0} = \beta_0 [d^\dagger \times \tilde{d}]^{(0)}_{0} + \gamma_0 [s^\dagger \times \tilde{s}]^{(0)}_{0} \qquad (2.6.5)$$

$$T^{(M1)}_{m} = \beta_1 [d^\dagger \times \tilde{d}]^{(1)}_{m} \qquad (2.6.6)$$

$$T^{(E2)}_{m} = \alpha_2 [d^\dagger \times \tilde{s} + s^\dagger \times \tilde{d}]^{(2)}_{m} + \beta_2 [d^\dagger \times \tilde{d}]^{(2)}_{m} \qquad (2.6.7)$$

Once the parameters α, β and γ have been fixed, all multipole transition rates can be calculated. An example of a detailed study of E2 transition rate can be found by Warner et al. (1980). A good review of all the tests performed up to 1980 can be found in two articles by Casten (1980, 1981).

In addition to L=0,2 (s,d), the active fermion pairs can also be coupled to other values of the angular momentum L. Of particular importance is the case L=3, the octupole mode, hereafter denoted by f. In order to construct states of octupole character, Arima & Iachello (1976) considered a system of two different kinds of bosons, N quadrupole d-bosons able to occupy a L=2 and a L=0 level, and N′ octupole f-bosons able to occupy a L=3 and L=0 level. The most general Hamiltonian describing this system is

$$H = H_d + H_f + V_{fd} \qquad (2.6.8)$$

where H_d is the Hamiltonian describing the quadrupole mode [Eq.(3.6.1)], H_f is the Hamiltonian describing the octupole mode and V_{fd} represents the octupole-quadrupole interaction. Further discussion for the octupole influence in IBA can be found in Arima & Iachello (1976, 1978) and Scholten et al. (1978).

2.6.1 SU(5) group — The vibrational limit.

When the energy $\varepsilon(\varepsilon=\varepsilon_d-\varepsilon_s)$ is much larger than all interacting terms, the states are characterized by the number

of bosons occupying the L=2 level, n_d, therefore n_s plays no role in this case, and the general Hamiltonian is given

$$H = \varepsilon \sum_m d_m^\dagger d_m + \sum_L \tfrac{1}{2}(2L+1)^{\frac{1}{2}} c_L[(d^\dagger d^\dagger)^{(L)}(dd)^{(L)}]^{(0)}$$

$$+ v_2\{[(d^\dagger d^\dagger)^{(2)}d]^{(0)}(1-(n_d/N))^{\frac{1}{2}}+(1-((n_d-1)/N))^{\frac{1}{2}}[d^\dagger(dd)^{(2)}]^{(0)}$$

$$+ v_0\{(d^\dagger d^\dagger)^{(0)}((1-(n_d/N))(1-((n_d+1)/N)))^{\frac{1}{2}}$$

$$+ ((1-((n_d-1)/N))(1-((n_d-2)/N)))^{\frac{1}{2}}(dd)^{(0)}\} \qquad (2.6.9)$$

In the parametrization (2.6.1), this case of above correspond to $a_0=a_2=0$. The group chain here is

$$U(6) \supset U(5) \supset O(5) \supset O(3) \supset O(2)$$

An analytical solution to the eigenvalue peoblem is achieved by diagonalising in the basis $|[N],n_d,v,n_\Delta,L,M>$ which lables the totally symmetric irreducible representations of SU(5), where N is the usual total boson number, and M the projection of angular momentum L along the z axis. Additional quantum numbers specifying the wave function are n_Δ, counts boson triplets coupled to zero angular momentum and n_β which counts boson pairs coupled to zero angular momentum. The quantum number v is linearly dependent on n_β such that

$$v = n_d - 2n_\beta \qquad (2.6.10)$$

and n_d is then given by

$$n_d=2n_\beta + 3n_\Delta + \lambda \qquad (2.6.11)$$

where $L = \lambda, \lambda+1, \lambda+2, \ldots\ldots 2\lambda-2, 2\lambda.$, but not $(2\lambda-1)$. Thus the eigenvalues of the interacting d-boson is given

with parameters ε, α, β and γ Arima & Iachello (1976)

$$E = \varepsilon n_d + \frac{\alpha}{2} n_d(n_d-1) + \beta(n_d-v)(n_d+v+3) + \gamma[L(L+1)-6n_d] \qquad (2.6.12)$$

which do not depend on n_Δ and M. One has

$$C_4 = \alpha + 8\gamma$$

$$C_2 = \alpha - 6\gamma$$

$$C_0 = \alpha + 10\beta - 12\gamma$$

Any spectrum of SU(5) [see Fig.(2.1)] is presented with bands Y, X, Z, X′, Z′, β, Δ with the following functions

Y-band	$\mid n_d, n_d, 0, L=2n_d, M >$
X-band	$\mid n_d, n_d, 0, L=2n_d-2, M >$
Z-band	$\mid n_d, n_d, 0, L=2n_d-3, M >$
X′-band	$\mid n_d, n_d, 0, L=2n_d-4, M >$
Z′-band	$\mid n_d, n_d, 0, L=2n_d-5, M >$
β-band	$\mid n_d, n_d-2, 0, L=2n_d, M >$
Δ-band	$\mid n_d, n_d, 1, L=2n_d-6, M >$

The operator for E2 transition rate [Eq.(2.3.7)] when taken between states of SU(5) limit has selection rules $\Delta n_d = 0, \pm 1$. The first part of this operator, which satisfies the selection rule $\Delta n_d = 1$, gives rise to transitions from one n_d multiplet to another, while the second part, which satisfies $\Delta n_d = 0$, gives rise to transitions within the same multiplet and to quadrupole moments. Analytic expressions for the reduced matrix elements of both terms are given in Arima & Iachello (1976). Of particular importance are those between members of g.s. band

$$B(E2;L+2\to L) = \alpha_2^2 \frac{1}{4}(L+2)(2N-L) = \frac{(L+2)(2N-L)}{4N} B(E2;2\to 0) \qquad (2.6.15)$$

Thus $$B(E2;\ 2_1^+ \rightarrow 0_1^+) = \alpha_2^2 N \qquad (2.6.16)$$

The quadrupole moments of the states in the g.s. band are given by

$$Q(L) = \beta_2 (16\pi/70)^{\frac{1}{2}}\ L \qquad (2.6.17)$$

A consequence of (2.6.16) is that in the limit of an exact SU(5) symmetry, one has

$$\frac{B(E2;\ 4 \rightarrow 2)}{B(E2;\ 2 \rightarrow 0)} = 2\left(\frac{N-1}{N}\right) < 2 \qquad (2.6.18)$$

This feature is observed in vibrational nuclei. An interesting discussion for the vibrational character of the SU(5) symmetry and comparison with the traditional harmonic vibrator of Bohr (1952) are made by Arima & Iachello (1976) and Scholten et al. (1978).

2.6.2 SU(3) group – The rotational limit.

In the case when ε is small, the group chain here is

$$U(6) \supset SU(3) \supset O(3) \supset O(2)$$

The lables which characterize the irreducible representations of the various groups appear in the basis $|[N], (\lambda,\mu), K, L, M>$, where [N] lables the totally symmetric irreducible representations of U(6), (λ,μ) lables the representations of SU(3), L angular momentum lables O(3) and its Z projection (M) lables O(2). The K quantum number is added, referring to states having same λ,μ and L. It is related to L along the body-fixed axis as in the geometrical description.

In the form of Eq.(2.6.1), it turns out [Arima & Iachello (1978)] that the Hamiltonian of this symmetry arises when $\varepsilon'=0$, $a_0=a_3=a_4=0$.

$$H = -k\ Q.Q - k'L.L \qquad (2.6.19)$$

For the two parameters k and k′, the eigenvalues are

$$E = \left(\frac{3}{4} k - k' \right) L(L+1) - k[\lambda^2 + \mu^2 + \lambda\mu + 3(\lambda+\mu)] \tag{2.6.20}$$

The decomposition for the totally symmetric representations [N] of U(6) into representations (λ,μ) of SU(3) is

$$\begin{aligned} [N] = (2N,0) \oplus (2N-4,2) \ldots. & \begin{bmatrix} (0,N) \\ (2,N-1) \end{bmatrix} \quad \begin{matrix} N = \text{even} \\ N = \text{odd} \end{matrix} \\ \oplus (2N-6,0) \oplus (2N-10,2) \ldots. & \begin{bmatrix} (0,N-3) \\ (2,N-4) \end{bmatrix} \quad \begin{matrix} N-3 = \text{even} \\ N-3 = \text{odd} \end{matrix} \\ \cdot \qquad \cdot & \\ \cdot \qquad \cdot & \end{aligned} \tag{2.6.21}$$

while the reduction of each representation (λ,μ) of SU(3) into a representation of O(3) gives

$$L = K, (K+1), (K+2) \ldots. (K+\max\{\lambda,\mu\}) \tag{2.6.22}$$

where

$$K = \text{integer} = \min\{\lambda,\mu\}, \min\{\lambda,\mu\}-2, \ldots. 1 \text{ or } 0 \tag{2.6.23}$$

with the exception of K=0 for which

$$L = \max\{\lambda,\mu\}, \quad \max\{\lambda,\mu\}-2, \qquad \ldots. 1 \text{ or } 0 \tag{2.6.24}$$

A typical structure of the energy spectrum which arises from this symmetry is schematically shown in Fig.(2.1).

For E2 transition rate, it turns out that the first term in Eq.(2.6.7) is much larger than the second in region where the SU(3) symmetry applies. This however corresponds with the selection rules $\Delta\lambda=0$, $\Delta\mu=0$.

The B(E2) values and the quadrupole moments of the states in the ground state band are given by

$$B(E2,\ L+2 \rightarrow L) = \alpha_2^2 \frac{3}{4} \frac{(L+2)\ (L+1)}{(2L+3)(2L+5)} (2N-L)(2N+L+3) \qquad (2.6.25)$$

$$Q_L = -\alpha_2 \sqrt{\frac{16\pi}{40}} \frac{L}{2L+3} (4N+3) \qquad (2.6.26)$$

The N^2 dependence is responsible for the observed large enhancement of $B(E2;\ 2 \rightarrow 0)$ in rotational nuclei.

The SU(3) group plays the dominant role in the collective states and describes the rotational spectra as reported by Arima & Iachello (1978) who showed its correspondence to the axially symmetric rotor. Recently, Warner & Casten (1982) investigated the E2 operator of deformed nuclei in the SU(3) structure of IBA model. They showed the validity of the parameters α_2, β_2 remarking the fact that the relative B(E2) values of transitions between different representations are independent of the parametrization chosen for the operator.

2.6.3 The O(6) limit.

The eigenvalue problem of the Hamiltonian can be solved when H is written in terms of a generator of subgroup $G \subset SU(6)$. For $G \equiv O(6)$ in the present case, the complete chain of subgroups is

$$U(6) \supset O(6) \supset O(5) \supset O(3) \supset O(2)$$

The quantum numbers N, σ, τ, L and M label the representations of the groups U(6), O(6), O(5), O(3) and O(2) respectively. The first and last two labels have been previously defined, while the quantum number σ, which characterize the totally symmetric irreducible representations of O(6), takes the values

$$\sigma = N,\ N-2,\ \ldots.\ 0 \text{ or } 1 \qquad (2.6.27)$$

and the quantum number τ of O(5) symmetry

$$\tau = \sigma,\ \sigma-1,\ \ldots.\ 0$$

In addition to the five labels, a quantum number v_Δ, which counts d-boson triplets coupled to zero angular momentum, partition τ as

$$\tau = 3v_\Delta + \lambda \quad , \qquad v_\Delta = 0,1, \ldots . \tag{2.6.29}$$

and taking

$$L = 2\lambda, 2\lambda-2, \ldots . \lambda+1, \lambda. \tag{2.6.30}$$

The expectation value of the Hamiltonian, which in the parametrization (2.6.1) corresponds to vanishing coefficients $\varepsilon=a_2=a_4=0$, in the basis $|[N],\sigma,\tau,v_\Delta,L,M,>$ has eigenvalues

$$E = \frac{A}{4}(N-\sigma)(N+\sigma+4) + \frac{B}{6}\tau(\tau+3) + CL(L+1) \tag{2.6.31}$$

A partial spectrum of (2.6.31) for positive parameters A, B and C is shown in Fig.(2.1). It consists of repeating patterns 0^+; 2^+; 4^+, 2^+; .... corresponding to various values of σ. Within each pattern there are several levels corresponding to the values of τ, v_Δ and L. The effect of a positive A is that of placing the representation $\sigma=N$ lowest in energy, while a positive B gives the ordering 0_1^+, 2_1^+, 4_1^+ ...., finally for C>0, the 2_2^+ state is placed below 4_1^+ etc. noting that when C=0 the energy spacings between states with the same value of σ are given by the second term in (2.6.31) and are identical to those of the γ-unstable model of Wilets & Jean (1956).

It turns out that in regions where the O(6) symmetry applies, the first term in the transition operator (2.6.7) is the dominant one i.e. $\beta_2=0$. This operator, when taken between states $|[N],\sigma,\tau,v_\Delta,L,M>$, has selection rules

$$\Delta\sigma = 0 \quad , \qquad \Delta\tau = \pm 1 \tag{2.6.32}$$

the first being a consequence of the fact that $[d^\dagger\times\tilde{s}+s^\dagger\times\tilde{d}]^{(2)}_m$, of (2.6.7), is a generator of O(6), and thus cannot connect different O(6) representations. The B(E2) values along the ground state band

$$B(E2) = \alpha_2^2 \frac{L+2}{2(L+5)} \frac{1}{4} (2N-L)(2N+L+8) \qquad (2.6.33)$$

Because of the second selection rule in (2.6.32), all quadrupole moments are zero in O(6), if the E2 operator is strictly given for $\beta_2=0$. It is possible to calculate analytically other B(E2) values and quadrupole moments as described by Arima & Iachello (1979).

2.6.4 Transitional regions.

Only few nuclei can be described by the three limiting cases described above. Most nuclei display spectra intermediate between the limiting cases. In order to describe these transitional nuclei, one must return to H[Eq.(2.6.1)] and diagonalize it numerically. These transitional nuclei are conveniently divided into four classes:

A) nuclei with spectra intermediate between SU(5) and SU(3)

B) nuclei with spectra intermediate between SU(3) and O(6)

C) nuclei with spectra intermediate between O(6) and SU(5)

D) nuclei with spectra intermediate among all three limiting cases.

Nuclei in the transitional class D are obviously the most difficult to treat from a phenomenological point of view, because they require the use of all the operators n_d, $P^+.P$, L.L, Q.Q, $T_3.T_3$ and $T_4.T_4$ appearing in (2.6.1). However, only few of these operator may suffice for the studies of nuclei belonging to the transitional classes A, B and C. A study of transitional class A has been done Scholten et al. (1978), the transitional class B was done by Casten & Cizewski (1978) and a typical type of transitional class C have recently been done by Stachel et al.(1982).

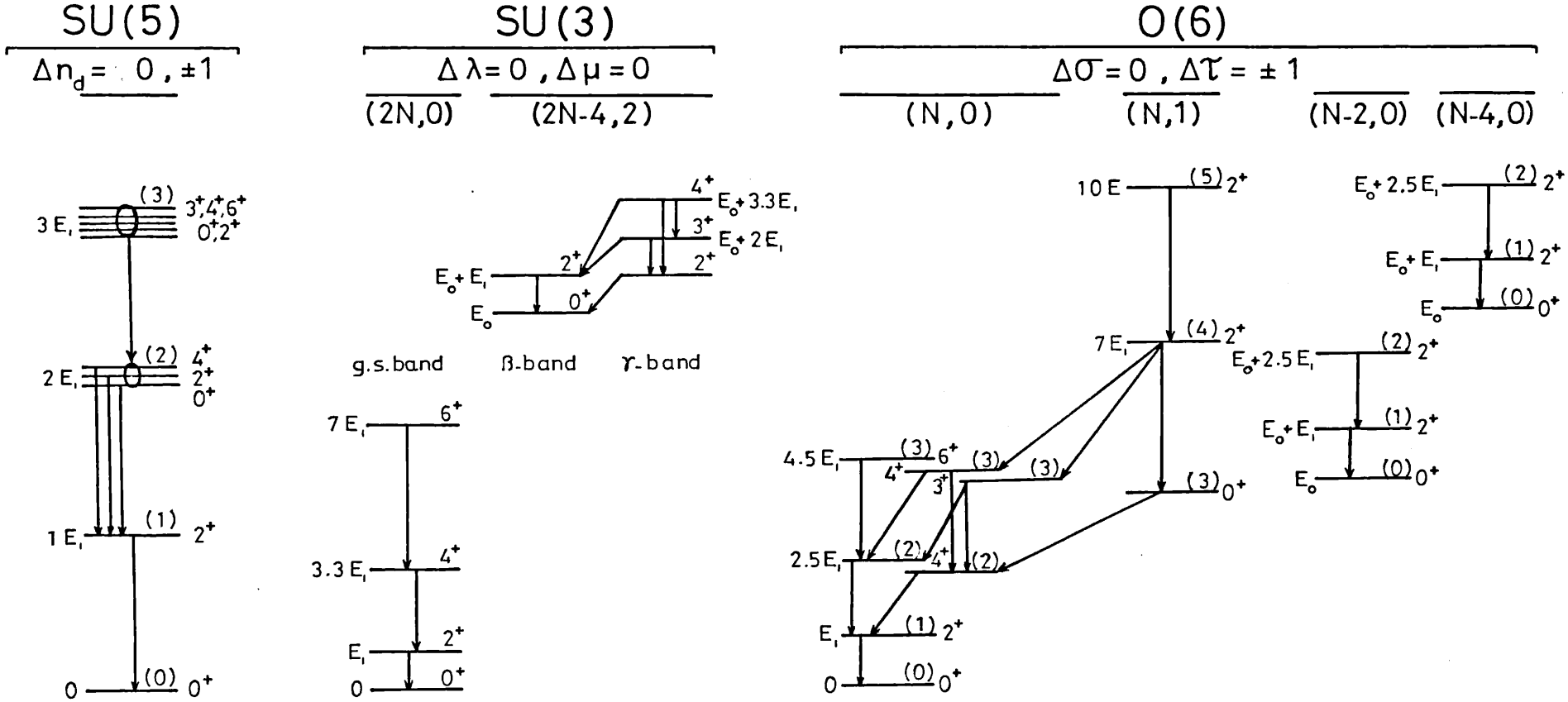

Fig.(2.1). The first few collective states for SU(5), SU(3) and O(6) limits of IBA-1. The states are grouped for different values of the quantum numbers (λ,μ) of SU(3), (σ, v_Δ) of O(6); and in addition, they are labelled by the quantum numbers L, n_d (for SU(5)) and τ (for O(6)). States corresponding to the β and γ-vibrational bands of deformed axial rotor are indicated in the SU(3) limit. The allowed E2 transitions are also shown in the three limits for the selection rules stated on the top.

2.6.5 The Computer codes PHINT & FBEM.

In order to find the spectrum, one diagonalizes H, in one of its forms, in an appropriate basis provided by the totally symmetric irreducible representations of the unitary group in six dimensions, U(6). A computer program for this diagonalization, called PHINT, has been written by Scholten (1975, 1980) for this prupose. The program-package "PHINT contains the programs to perform calculations for even-even nuclei in the framework of the IBA model including the program FBEM to calculate transition rates. The programs are coded in Fortran IV and written for a CDC-7600 computer. In its standard version, the program can handle up to 16 bosons.

Two forms of H are used in PHINT, the first is equivalent to that of Eq.(2.6.1) with parameters EPS, PAIR, ELL, QQ, OCT and HEX such that

$$\varepsilon' = \text{EPS} \quad , \quad a_0 = \text{PAIR} \quad , \quad a_1 = \text{ELL}/2$$
$$a_2 = \text{QQ}/4 \quad , \quad a_3 = 5\sqrt{7}\ \text{OCT} \ , \quad a_4 = 15\ \text{HEX} \qquad (2.6.34)$$

The completely equivalent H to that of (2.6.1) is also specified as

$$\begin{aligned} H = \text{HBAR} \times n_d + \sum_{L=0,2,4} \frac{1}{2}(2L+1)^{\frac{1}{2}}\, C\left(\frac{L+2}{2}\right)\left[(d^\dagger d^\dagger)^{(L)}(dd)^{(L)}\right]^{(0)} \\ + F \times \left[(d^\dagger d^\dagger)^{(2)}(ds)^{(2)} + (s^\dagger d^\dagger)^{(2)}(dd)^{(2)}\right]^{(0)} \\ + G \times \left[(d^\dagger d^\dagger)^{(0)}(ss)^{(0)} + (s^\dagger s^\dagger)^{(0)}(dd)^{(0)}\right]^{(0)} \qquad (2.6.35) \\ + \frac{\text{CHI}}{2} \times \left[(s^\dagger s^\dagger)^{(0)}(ss)^{(0)}\right]^{(0)} + \sqrt{5}\ \text{CH2} \times \left[(d^\dagger s^\dagger)^{(2)}(ds)^{(2)}\right]^{(0)} \end{aligned}$$

The parameters HBAR, C(I = (L+2)/2), F, G, CH1 and CH2 are referred to variable names used in the program and related to those (2.6.34) of above [Scholten (1980)].

In order to use PHINT, one essentially has to feed

into the program some useful data; the total boson number N of the nucleus under investigation must be included, and an initial estimation of the parameters that are relevant to the region where the nucleus lies in the periodic table (vibrational region, rotational, ...). These parameters can therefore be gradually altered suitably to the experimental data keeping their values within the physical sense. Least square fittings to a given positive parity levels can also be used to determine the appropriate parameters (with great caution as these parameters may not be physically correct).

With the program FBEM, it is possible to calculate the electromagnetic transition rates. The parametrization of Eq.(2.6.7) are then given

$$\text{E2SD} = \alpha_2$$

$$\text{E2DD} = \sqrt{5}\,\beta_2 \qquad (2.6.36)$$

To calculate the energies and eigenvectors for negative parity states, H_f and V_{df} of (2.6.8) must be included to the Hamiltonian (2.6.35). This is constructed through the inclusion of one $L^{\pi} = 3^{-}(f)$ boson giving rise to other parameters HBAR3, FELL and FQQ to be included in the program. A reasonable fit can be obtained by using the multipoles FELL and FQQ while the energy of f-boson, HBAR3, has only the effect of shifting all the negative parity states by an equal amount and does not change the wave function.

CHAPTER III

EXPERIMENTAL ARRANGEMENTS.

3.1 Single spectra measurements.

During the course of this work, γ-ray spectra have been taken using true-coaxial Ge(Li) detectors and a Ge detector. Their efficiencies, equivalent volumes and measured performance characteristics are listed in Table (3.1).

Table(3.1). Specifications of the detectors used during the course of this work.

No	Detector	Approximate volume	Relative efficiency	Energy* resolution	Peak/Compton ratio*
1	ORTEC Ge(Li)	70 cc	12 %	2.21(5)	36
2	ORTEC Ge(Li)	60 cc	10 %	1.94(4)	38
3	HARSHOW Ge(Li)	70 cc	11 %	2.40(5)	37
4	ORTEC Ge	$2cm^2 \times 2.5cm$		0.5′,1.62	
5	NE102A(Plastic)	1"×1"			

′ The FWHM of the 122 keV.

* For the peak at 1332 keV of ^{60}Co.

Each of these detectors is equipped with a cooled FET low noise pre-amplifier. The output signals were fed into an amplifier [ORTEC 472 or 572] with variable time constants for pulse shaping before proceeding to the Northern Scientific Analogue to Digital Converter [ADC model NS 628]. The signals are then fed into a Northern Scientific memory unit [model No.630] and pulse height spectra were recorded on 4096 channels.

Low isotope activities have been used (~10 μCi) with a source-to-detector distance of 25 cm. This standard requirement enables total counting rates to be kept below 2000

count/sec. to avoid pile-up effects and minimize coincidence summing correlations.

3.2 Energy and efficiency calibrations.

The energy and efficiency calibrations were obtained using the chemical standard source set consisting ^{241}Am, ^{133}Ba, ^{54}Mn, ^{57}Co, ^{22}Na, ^{60}Co and ^{137}Cs (these radioactive materials available from the Radiochemical Centre, Amersham, Buckinghamshire, U.K.) for energies below 1.3 MeV and ^{226}Ra for higher energy region. The latter was prepared and calibrated at the University of London Reactor Centre (ULRC) and the specifications of the transitions involved were taken from [Thein (1977)].

Essentially, the uncertainties in energy determination can be attributed to two main sources, the listed calibration uncertainty, and that due to the nonlinearity of the apparatus. The latter is always more difficult to estimate since it depends on many factors such as the condition of the apparatus, the energy region under investigation and pulse shaping. However, the energy calibration was determined by the least squares fit to an n'th degree polynomial to the γ-ray energies using the program code SAMPO [Routti (1969), Routti & Prussin (1969)]. Although the program takes the uncertainty in finding the centroid of the peak into the calculation of the errors, the accepted energy of a transition and its uncertainty was determined from more than one set of singles spectra.

The program SAMPO uses two methods for including the efficiency calibrations in intensity calculations. The first makes the use of calibrated points and interpolates logarithmically between these points. The second employs an approximate functional representation of the efficiency curve expressed as a function energy E

$$\varepsilon = P_1[E^{P_2} + P_3 \, Exp(P_4 E)] \qquad (3.2.1)$$

where the parameters $P_i (i=1,4)$ are determined by the least squares fitting method. The calibration uncertainties are expressed as a band round the efficiency curve, the width of

which is obtained by interpolating between given values. Indeed this method of determining the uncertainty of an interpolated point is a rough approximation and not reliable or exact. Instead, the function introduced by Ahmad et al.(1981) has been used in this work.

$$\varepsilon = [P_1+P_2 \ln E+P_3(\ln E)^2+P_4(\ln E)^3+P_5(\ln E)^5+P_6(\ln E)^7]/E \qquad (3.2.2)$$

This function is linearly dependent on the parameters $P_i(i=1,6)$, and the least squares fitting provides an exact solution with an uncertainty band along the fitted curve that is due to the errors of the calibrated points. The flexibility and advantages offered by Eq.(3.2.2) over Eq.(3.2.1) has been fully discussed by Ahmad (1982) and the absolute efficiency curves for three detectors No. 1, 3 and 4 are given Figs.(3.1-3.3) respectively.

Therefore, the relative intensities have been calculated using Eq.(3.2.2) to determine the efficiency at a particular transition, and using SAMPO to obtain the net areas of the fitted peaks.

3.3 Compton suppression spectrometer.

In the Compton suppression system a large volume of NaI scintillator acts as a single large detector surrounding the Ge(Li) detector in order to collect scattered photons. A coincidence system is used to establish the time coincidence between the Compton event in the Ge(Li) detector and the scattered photon detected in the scintillator. The event is then eliminated from the energy spectrum by the anticoincidence timing correlation; with the result that a spectrum with a greatly reduced Compton background is obtained.

The system provided by ULRC [Fig.(3.4)] consists of a Ge(Li) detector [No.3 in Table (3.1)] and a 20cm diameter X 20cm long NaI(Tℓ) crystal viewed by four photomultipliers. Signals driven from the dual-sum & inverter unit, which combines the output signals of the photomultipliers, are fed in the time

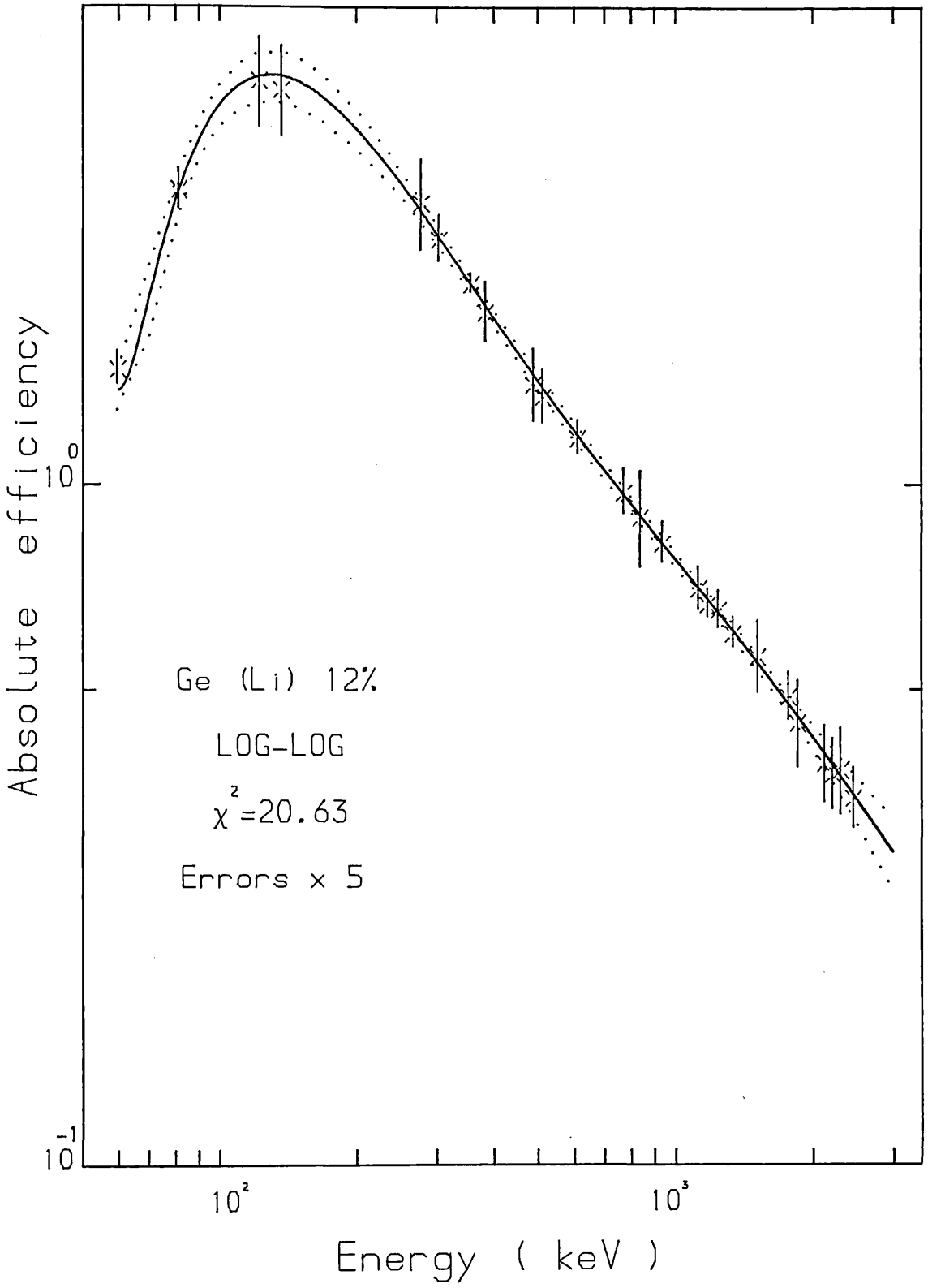

Fig.(3.1). The absolute efficiency-energy curve for the 12% efficient Ge(Li) detector.

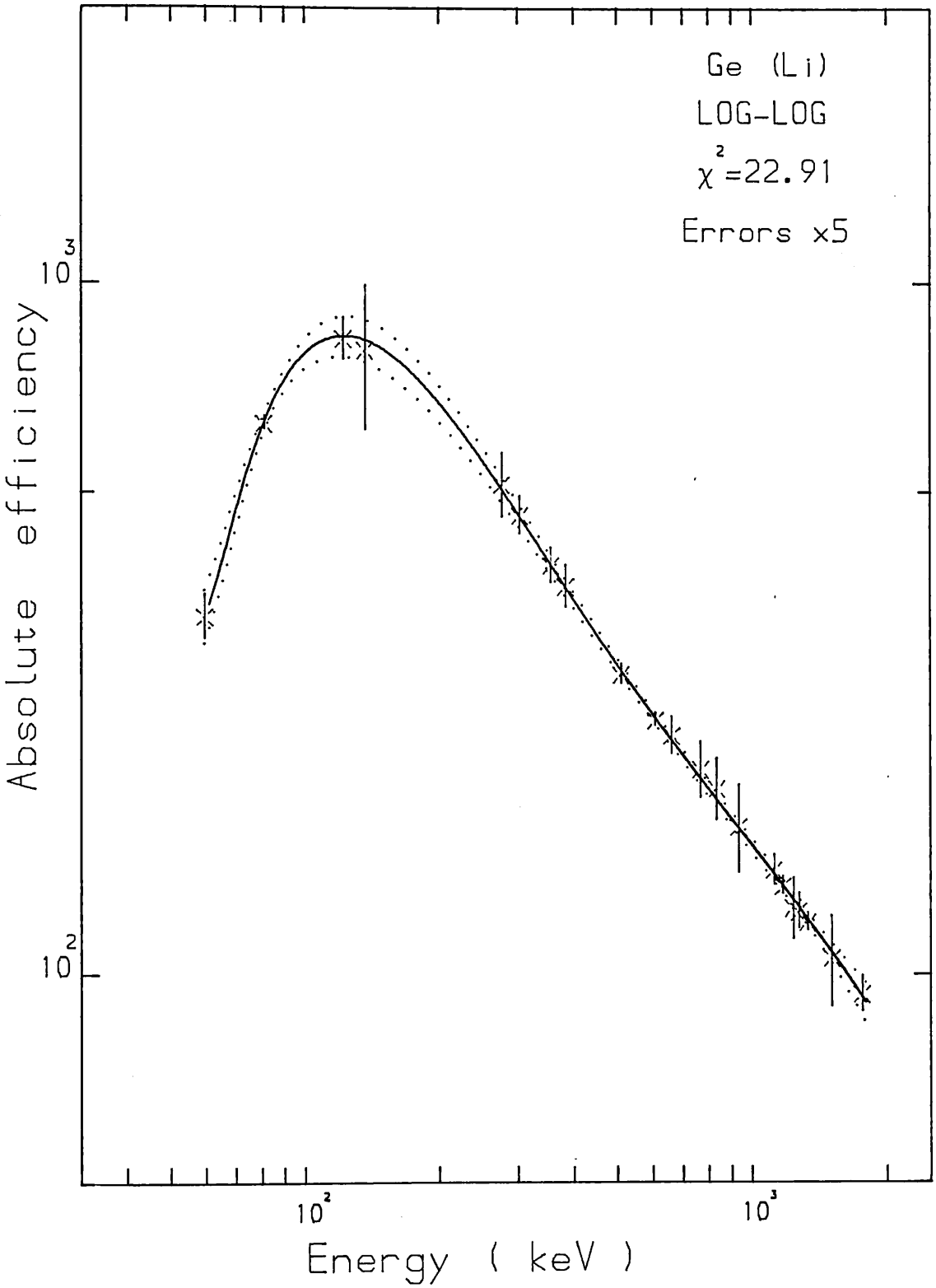

Fig.(3.2). The absolute efficiency-energy curve for the 11% efficient Ge(Li) detector.

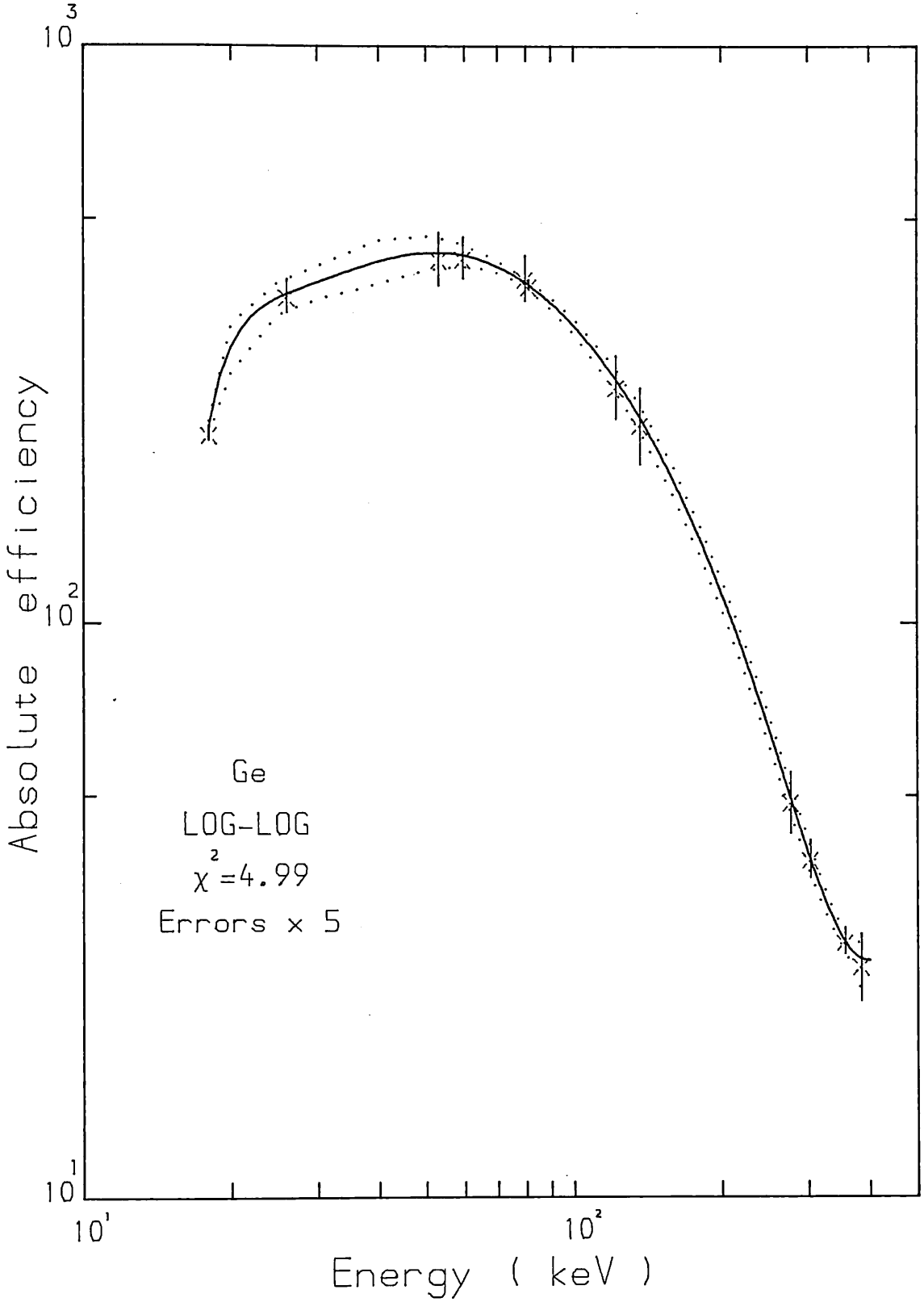

Fig.(3.3). The absolute efficiency-energy curve for the intrinsic Ge detector.

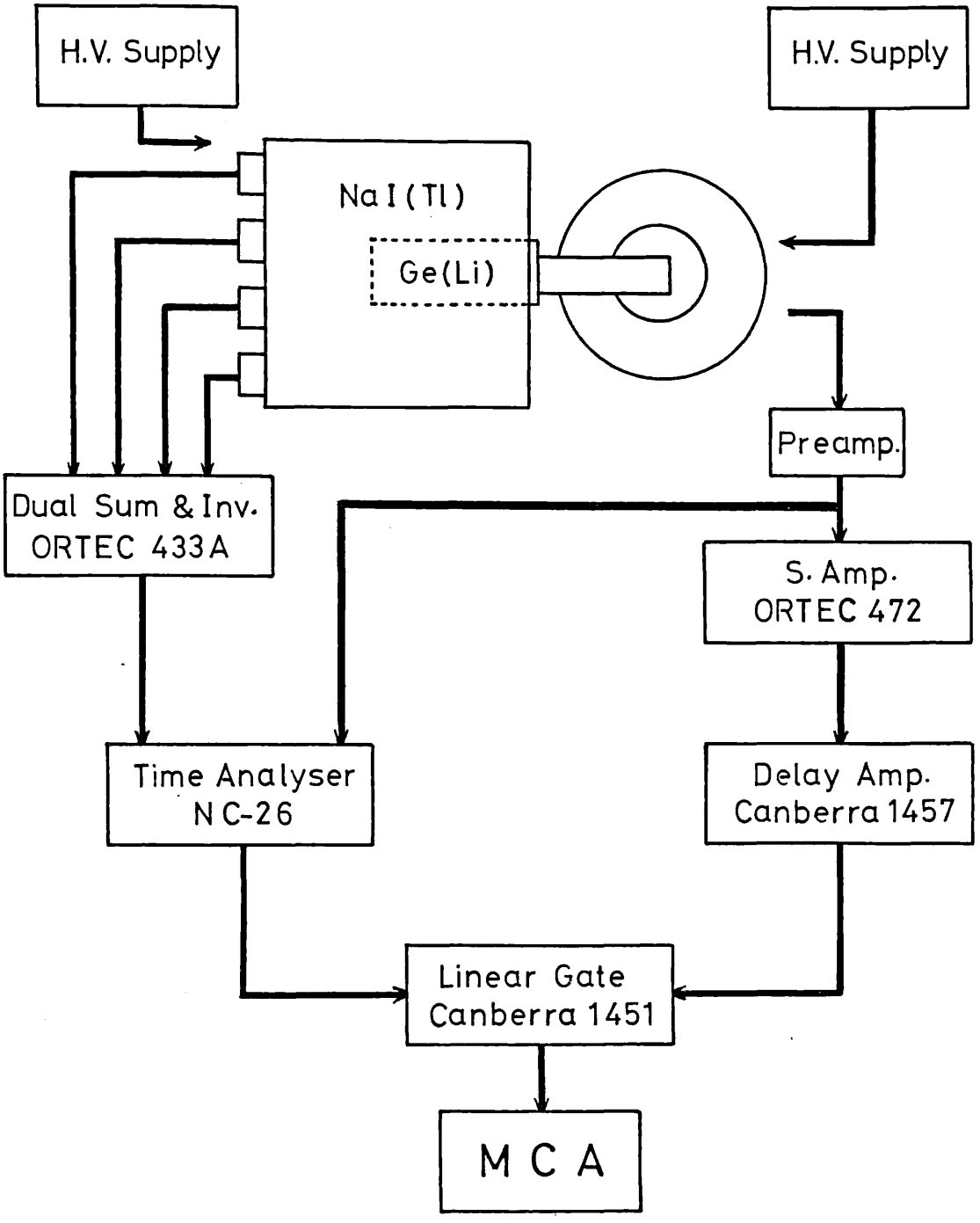

Fig.(3.4). A block diagram of the Compton suppression spectrometer.

analyser together with the signals generated in the Ge(Li) detector. The time analyser can measure time relationships between the Ge(Li) primary detector and the NaI(Tℓ) guard detector and generates logic level output signals. These signals provide the gating input of the linear gate unit. Meanwhile the linear input of the linear gate is driven from the amplifier of the Ge(Li) detector, which then suitably delayed to match the delay time taken to process the signals in the time analyser. By operating the linear gate in anti-coincidence position, the resulting outputs can display in the MCA a pulse height spectrum with greatly reduced Compton scattering regions.

3.4 Energy-time spectroscopy.

If a nucleus undergoes emission of two radiations in succession, their correlations can be divided into essentially two kinds, spatial correlations and time correlations. In many cases, the purpose of the time correlation studies is the determination of the coincidence intensities of two transitions, i.e. the number of transitions of the first following (or preceding) the other, in the construction of decay schemes. The devising of a nuclear decay scheme by gamma-gamma coincidence technique is normally arranged by fast-slow coincidence system. This system usually comprises two detectors coupled in simple two fold coincidence circuit with elements that give an output pulse whenever two input pulses occur "simultaneously" within a certain resolving time, but give no output when only one of the input pulses is present. Hence, signals from each of these two detectors, in addition to going to a fast coincidence circuit, also go to energy amplification circuits and one of these divisions (namely from the gating detector) goes to a single pulse channel height analyser which is set to accept those signals that fall in a narrow amplitude range. The output signals from the pulse height analyser is combined with the output of the fast coincidence circuit in a slow coincidence unit, which in turn, opens the gate to the linear signals coming from the other energy division in the multichannel analyser. Therefore, by setting the multichannel analyser in coincidence, it only allows the registration of pulses having coincidence relat-

ship with that of the gating window set in the single channel analyser

A dual-parameter energy-time spectrometer, which employs such coincidence arrangements, is used in this work, and has been found to be very efficient and capable of giving useful information for studying the levels schemes of nuclei [Sulaiman & Thomas (1979), Stewart & Shaban (1980), El-Daghmah & Stewart (1983)]. The spectrometer involves two Ge(Li) detectors (No. 1 and 2) and a plastic detector (No. 5). Two main sections are distinguished; timing section that couples one Ge(Li) detector with the plastic scintillator for the purpose of studying lifetimes of nuclear excited states, and a section on the dual-parameter data collection system which correlates γ-ray events in the two Ge(Li) detectors in gamma-gamma coincidences. A block diagram of the dual-parameter energy-time spectrometer is shown in Fig.(3.5).

3.4.1 Timing spectrometer.

For every decaying nucleus, the time analyser measures the interval t between the birth and death of an excited state (its lifetime), which is performed in a coincidence curve. With the delayed coincidence method, the time difference between the population and the depopulation of a nuclear excited state can be, perhaps most comprehensively, measured. Usually, the measuring assembly comprises two detector devices, one for the preceding event and the second for the delayed event (the populating event which feeds the excited state of interest is called the "preceding event", and the deexciting event to the lower state is the "delayed event"). With the use of TPHC, which converts time differences to pulse heights proportional to the time differences, one can detect the distribution of time intervals between the two signals in a multichannel analyser.

To obtain a good time and energy resolution, a plastic scintillator (No. 5) mounted on a fast RCA8575 photomultiplier, and a Ge(Li) detector (No. 2) are used in this work in a fast-slow coincidence circuit with two main distinct arms,

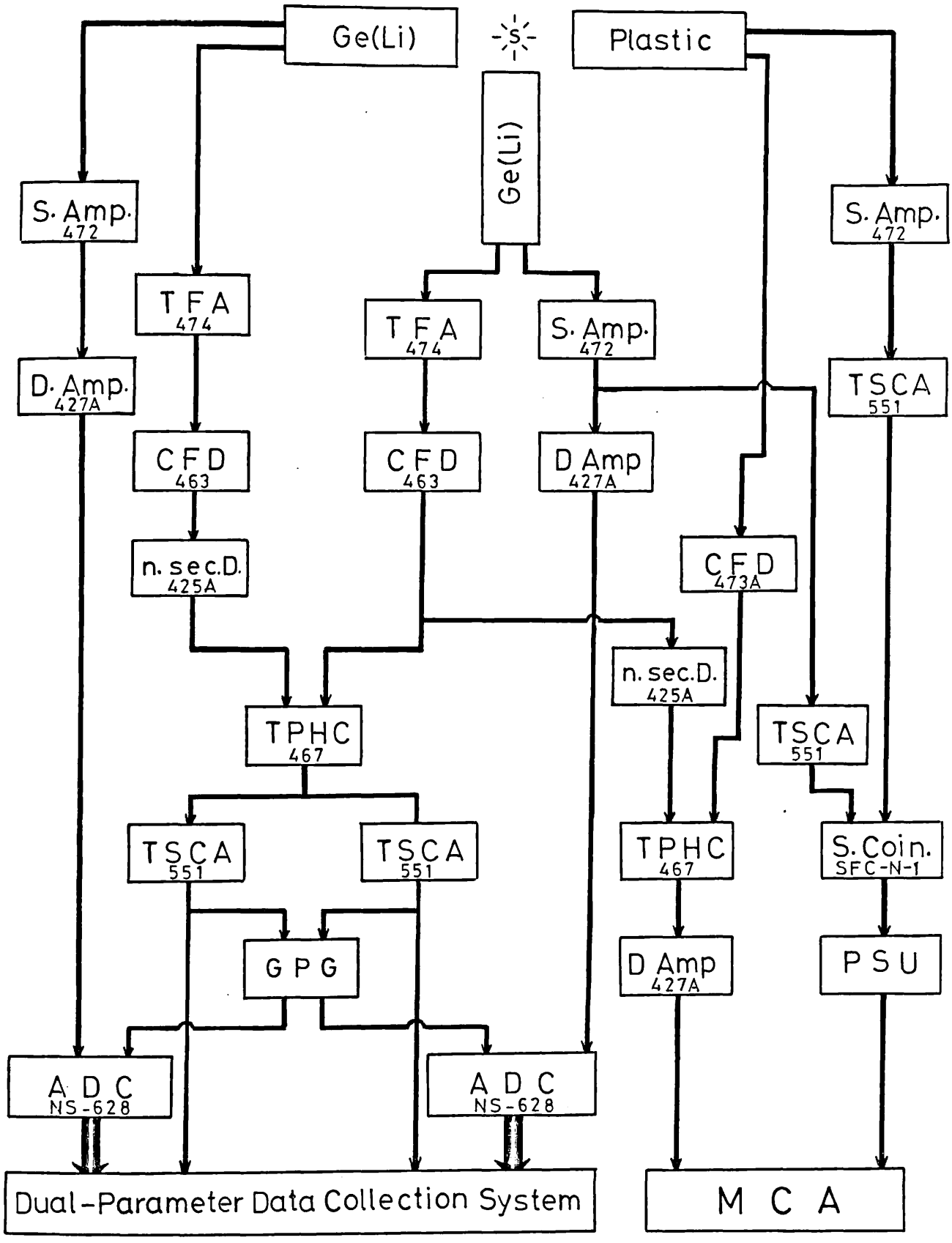

Fig.(3.5). Block diagram of the dual-parameter energy-time spectrometer.

namely fast arms and slow arms. The fast arms are the electronics that process the fast risetime (anode pulses of the plastic detector, which pinpoint the nuclear event in time, and the timing signals generated from the smaller volume Ge(Li) detector), while the slow arms process the slow rise time (dynode pulses of the plastic detector and the energy output of the preamplifier in the Ge(Li) detector), which perform energy discrimination so that events corresponding to the birth and death of the level can be monitored.

As the timing signal from the Ge(Li) detector (20mV) is too small to be analysed in the constant fraction discriminator CFD, it was first driven into a timing filter amplifier TFA, so that manipulation of pulse shaping and amplification could be made. The signal then passes the timing information to stop the TPHC while the start signal is processed directly from the anode plastic detector (3V) into CFD into the start input of the TPHC. The nanosecond delay unit inserted before the stop input of the TPHC affects only the absolute magnitude of the timing difference between the start and stop arrival of pulses. This is unimportant in assessment of the performance of the system.

All detectors and auxiliary electronics show statistical fluctuations in the time necessary to develop an appropriate pulse for the TPHC. Because of these fluctuations, a finite time resolution is obtained which is usually called prompt time distribution. The prompt time distribution is characterized by two quantities, the full width at half maximum FWHM, sometimes also called time resolution, and the experimental slopes which can be expressed as apparent half-lives. The prompt curve can be measured on decay of ^{60}Co, or on two 511 keV positron annihilation quanta, and the FWHM of a prompt curve usually defines the resolving time $2\tau_0$.

When uncorrelated events occur during resolving time, they are also accepted as coincidence. This is called chance coincidence N_c, and its ratio to the rate of genuine coincidences N_g must be minimized

$$N_c/N_g = 2\,\tau_0 N \qquad (3.4.1)$$

This is independent of counter efficiency but is determined by the source activity N and the resolving time.

The contribution of the energy coincidence in the fast arms, that often referred to slow coincidence, assess another conditions to the assembly. The two energy selection branches connected in parallel to allow the registration of only coincidences of pulses having the desired information. The energy pulses from the two detectors are amplified in two separate units to permit the energy selection process in the two timing single channel annalysers TSCA. One of these TSCAs may set its energy window ΔE to the corresponding preceded event and the other window to the delayed event of the excited state under consideration. Both logic outputs of the TSCAs (4.5 V) are connected into the slow coincidence unit, which generates a logic coincidence pulse whenever two input pulses are coincided within an accepted resolving time.

The coincidences between the fast signals, in the form of the TPHC output, and the slow signals, in the form of the slow coincidence unit output is achieved by stretching the slow coincidence unit output pulse and delaying the TPHC output pulse so that the two coincided in time, the former overlapping the latter. The output from the slow coincidence unit was passed through a pulse shaper which outputs a 4.5 volt logic output pulse of variable width for any positive input pulses. The width is variable from about few μs to about 10 μs by means of an internal variable resistor. The other output from the TPHC is passed through a linear delay which could be set exactly by lining up the two oscilloscope pulses so that the stretched pulse overlapped the TPHC pulse evenly (by means of external triggering). Having set the appropriate delay, the TPHC output is fed into the high level input of the multichannel analyser and the stretched slow coincidence pulse fed into the coincidence input as the gate pulse. A whole system arrangement is shown in block diagram on the right hand side of Fig.(3.5).

If the half-life to be measured is approximately two factors longer than the apparent half-life of the prompt time distribution, the slope method is usually used to determine the half-life of the level quite efficiently [Meilling & Stray (1968)]. The life-time can be measured from the slope of the coincidence curve which is a straight line on a semilogarithmic plot.

3.4.2 The Dual-Parameter Data Collection System (DPDCS).

In a conventional fast-slow coincidence experiment, a major proportion of the useful information is inevitably lost in a single measurement. The limitation of observing coincidence information is overcome when employing a dual-parameter system since all potentially useful information is recorded in a storage unit. The (DPDCS) has a 4096 by 4096 γ-γ coincidence spectra generated from two Ge(Li) detectors [No. 1 and 2 in Table(3.1)] stored in a large capacity magnetic tape. These detectors are placed at 90° to minimize detector-to-detector Compton scattering effect. Detector No.2, which is employed to provide the gating spectrum, generates the start pulse to the time-to-pulse-height converter (TPHC) unit, while the pulses from the second arm (timing channel of the spectrum detector No.1) is used to stop the (TPHC), as explicitly shown in the block diagram of the system on the left side of Fig.(3.5). The output amplitude of the (TPHC) contains a time distribution for the events in the two detectors, which in turn, furnished into two timing single channel analysers (TSCA). The accuracy of the coincidence results mainly depends on this time distribution, since it presents the so-called total timing coincidence (true + chance), of which is allowed by one of the (TSCA)s, while the second (TSCA) selects only the tail end of the timing distribution being considered totally chance. Either of these coincidences can generate a pulse in the gating pulse generator unit (GPG), which consequently open the gates at the respective gating and spectrum (ADC)s, enabling the linear signals from the two detectors to be digitized. At this stage, the processed signals, carrying the useful information, are ready to enter the (DPDCS) to be analysed, when the latter is not accessable (not busy).

A summary about the (DPDCS) will be described in the remainder of this section, while a detailed descriptions of the units involved, characteristic of the components and the process of data handling, are found in the original works by Sulaiman (1977), Shaban (1980) and Sulaiman & Thomas (1979).

An interface between the coincidence section and the magnetic tape storage is called the write interface. Another dual-parameter interface is used between the magnetic tape transport and the memory unit is the read interface. The block diagram that presents the whole system is shown in Fig.(3.6).

In the write interface, the timing pulse which is connected to the respective total and chance coincidence inputs is suitably delayed to match the time required for the conversion process in the two (ADC)s. When this conversion is completed, the recording process is initiated and therefore passed to the multiplexer units to facilitate changing the binary addresses into binary decimals in the binary to BCD converter units. The data are then made available to the multiplexer units which converts the parallel data into serial form connected to the input tracks that suits the buffer of the magnetic tape recorder. The total chance indicator signifies the words on the tape according to whether a total or chance coincidence event is being recorded. When a coincidence event initiated, it also enables a temporarily counter that inhibits the system from collecting further data. This is made as coincidence events happen randomly in time and to allow sufficient time the recording process. The system is live again when this is ended.

The tape transport is an SE 8000 series synchronous type with read-after-write configuration. Its variable recording capacity was chosen to correspond to 7-track mode in this system. For every coincidence event, there are altogether nine words written along the tape. The first is the indicator or tag word which is used to signify whether the event following it arises from total or chance coincidence. It has all zeros on the first four tracks (2^0, 2^1, 2^2, 2^3) and either (11) for total coincidence or (01) for the chance on the 5^{th} and

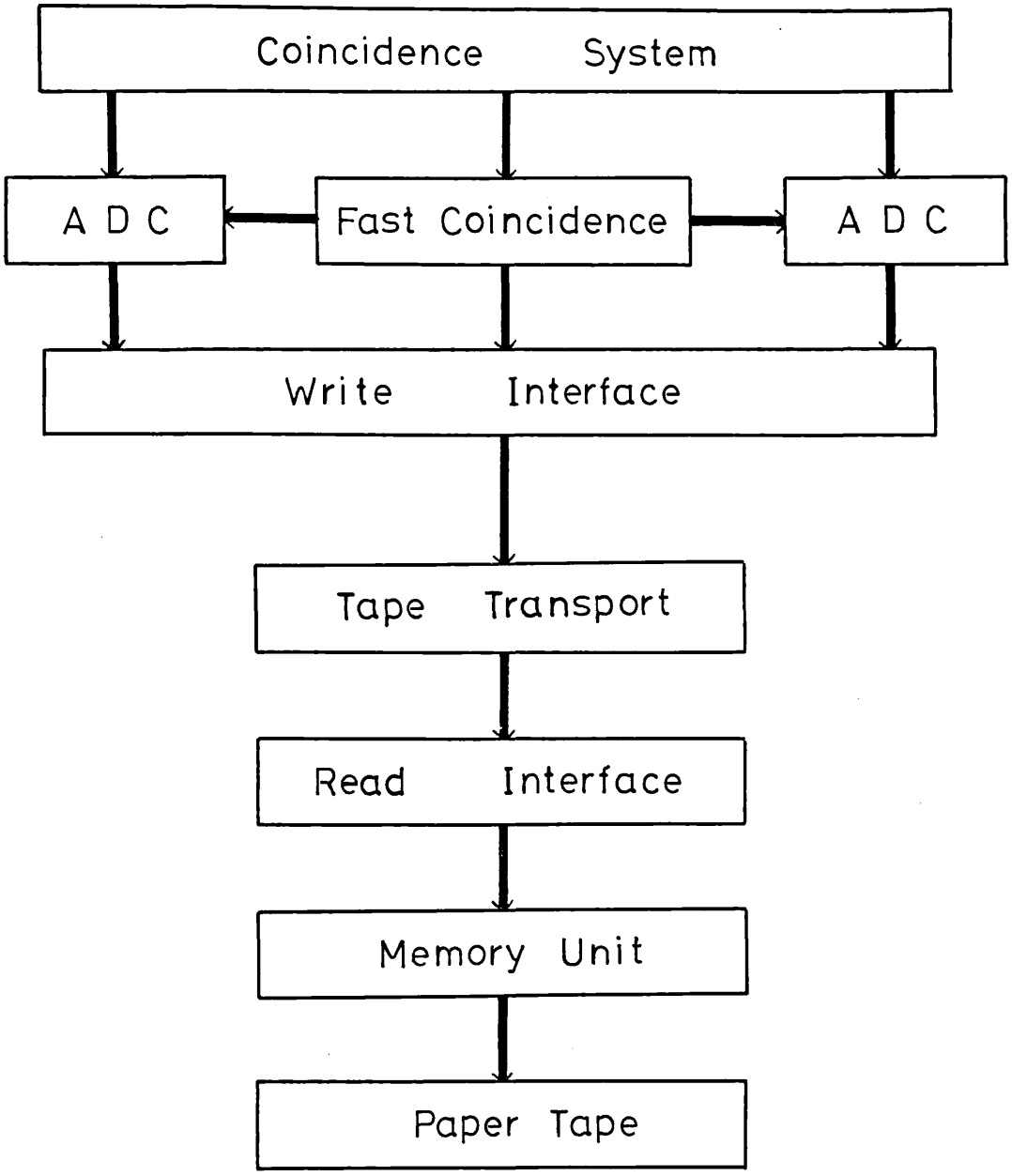

Fig.(3.6). A block diagram of the dual-parameter data collection system.

6^{th} tracks. The seventh track is not relevant in this system. The remaining eight words that follow the indicator word are addresses from the two (ADC)s. The first four are addresses from the gating ADC and the other four from the spectrum (ADC). In all eight words only zeros are recorded on the tracks 5 and 6. With a temporary storage buffer of 2048 bytes, its contents are dumped synchronously onto the magnetic tape forming a block of data of 225 coincidence events corresponding to 9 bytes X 225 events = 2025 bytes. The tape transport has a recording speed of 45 inches per second and a recording capacity of 556 bytes per inch. Therefore, the time taken to transfer the 2025 words in the buffer onto the magnetic tape is about 81msec.

A total-chance indicator (front panel toggle) selects the total or chance event by sensing the corresponding tag word on the magnetic tape in the read interface. The serial data are converted back to parallel in the shift register unit before proceeding to the BCD-to binary data to be read in the memory unit (N.S.630). At the same time a selecting gate unit compares the incoming data in the shift register with window boundaries that correspond to the lower and upper channel limits of the gate peaks. These are available with levels set on two thumbwheel switches acting as lower and upper level window. In this way, the spectrum in coincidence with this region are allowed through the BCD-to binary converter into the memory unit. The latter resets the read interface, that is dead for reading the whole addresses from the (ADC)s, to permit further read data to be compared. In the analyser memory, the window boundaries is particularly useful when the effect of spectrum backgrounds on the coincidence peaks is to be subtracted. The accumulated information in the analyser memory can be transferred through paper tape to be analysed later with the ULCC 7600 computer.

3.5 System performance.

3.5.1 Timing performance.

Before analysing any sample, it was neccessary to

determine the timing calibration of the timing system. The calibration procedure is as follows; the TPHC output is connected to the high level input of a multichannel analyser (N.S.630), and then the start and stop inputs are fed by a pulse generator whose output can be shaped to represent almost those timing outputs from the two detectors [No. 2 and 5 in Table(3.1)]. One output is taken and split by means of T-piece, the first cable is leading to the start input of the TPHC via CFD, and the second via CFD and variable nanosecond delay line unit to the stop input. The calibration was then made for different conversion gains of the MCA, and that resulting from the 1024 conversion gain is shown in Fig.(3.7) at different TPHC ranges. The slopes have been calculated using the least squares fit.

As mentioned in section (3.4.1), the time resolution of the timing system was tested using a 10 μCi ^{60}Co source positioned between the two detectors (the distance between the surface of the two detectors is 20cm). The analysis was made until about 10^4 counts obtained in the highest count channel of the Gaussian shaped peak. The prompt curve is shown in Fig.(3.8) with a FWHM of 3.91 ± 0.08 n.sec, FWTM=9.09 ± 0.16 n.sec and the apparent lifetime is 0.86 ± 0.04 n.sec.

With $2\tau_0$=3.91 n.sec, a sample of the time spectrum obtained from positron annihilation in a lucite sample was selected. A common isotope that in most general use is ^{22}Na which emits a prompt 1275 keV γ-ray signalling that a positron has been produced. When the energetic positron then enters condensed matter (Lucite) it rapidly loses almost all of its energy by collisions with electrons, and after a longer period (relative to the emission of 1275 keV γ-ray) its annihilation is signalled by the emission of two 511 keV γ-ray at 180°. By a measurement of the time difference between the emission of the 1275 keV γ-ray and one of the 511 keV γ-rays, a direct measurement of the positron lifetime is made. Thus, the anode of the plastic detector (the rise time is of the order of 4 or 5 nanoseconds) with its associated electronics are set to process all the start signals i.e. the 1275 keV γ-ray pulses and the timing output of the Ge(Li) detector and its associated electronics to process all of the stop signals i.e. the 511 keV

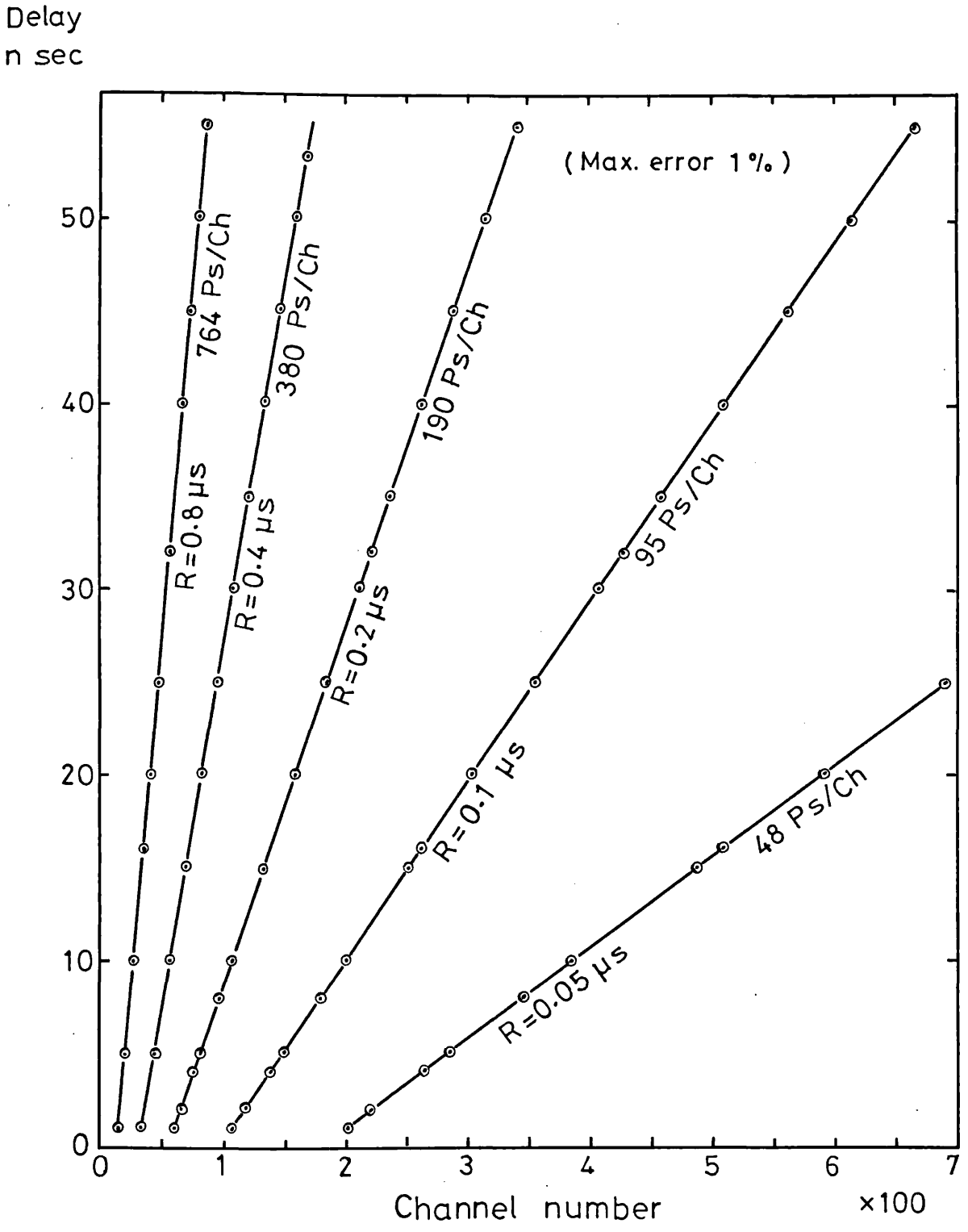

Fig.(3.7). The time calibration of the MCA (conversion gain 1024) for different TPHC ranges.

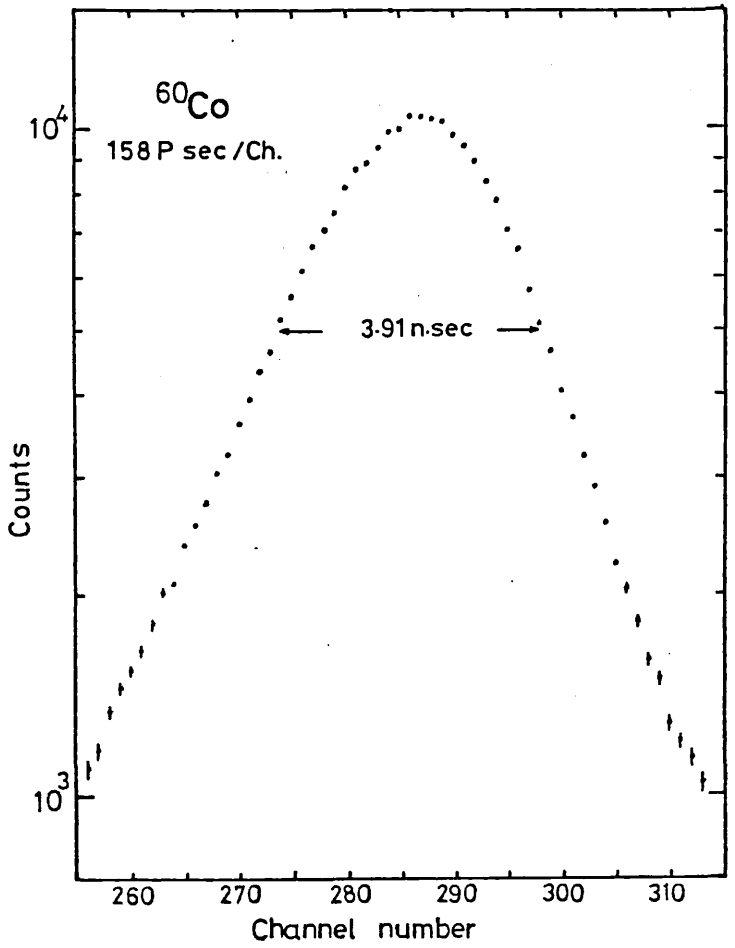

Fig.(3.8). Prompt life-time spectrum of ^{60}Co.

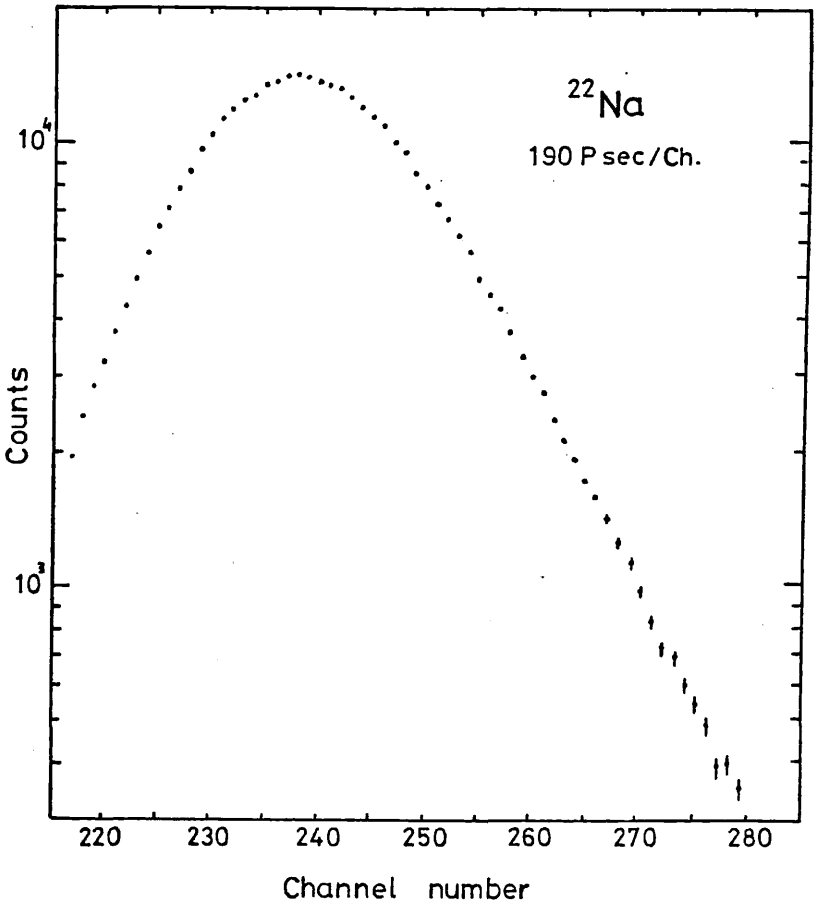

Fig.(3.9). Positron life-time in Lucite $[CH_3CH_2C(OCOCH_3)]_n$ sample at room temperature.

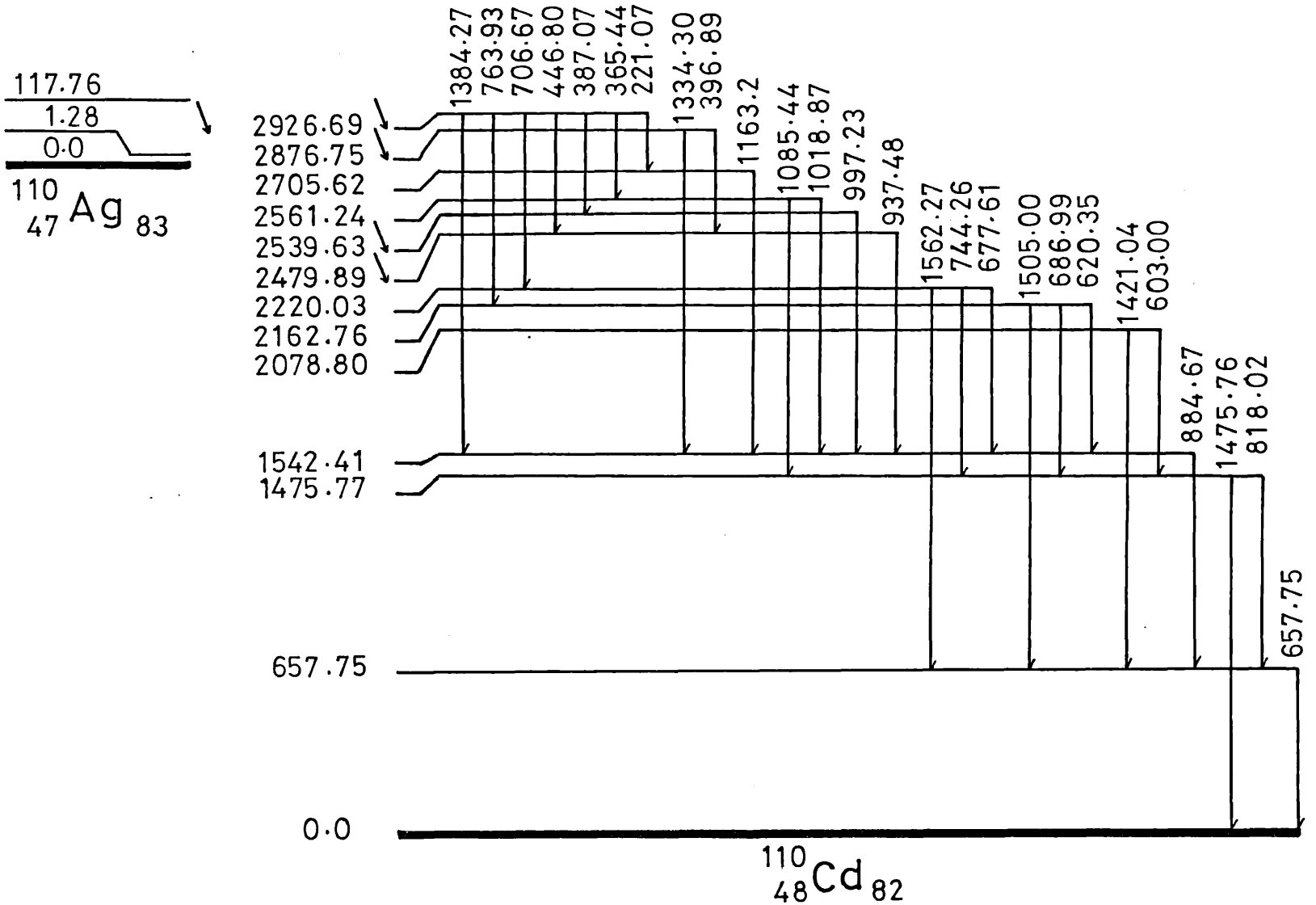

Fig.(3.10). The level scheme of ^{110}Cd nucleus .

γ-ray pulses. The 511 keV peak is well defined in the pulse height spectrum of Ge(Li) detector and is gated at the TSCA window of the energy division, while the TSCA of the plastic dynode pulses was set at discrimination level just above the noise and background pulses so that not to miss the Compton plateau of the 1275 keV transition. The system was kept over a month (at room temperature) period to accumulate enough counts, and the consequent positron lifetime spectrum [Fig.(3.9)] was analysed leading to a half life value of 1.24 ± 0.05 n.sec. This value appears in good agreement with the results given by Broseclose & Loper (1965) and by Wilson et al.(1963). The former recorded their measurement at temperature 26 ± 0.5 degrees centigrade obtaining $T_{1/2}$=1.32 ± 0.03 n.sec, while the latter reported the value 1.18 ± 0.14 n.sec at 30°C.

3.5.2 The DPDCS performance.

The performance of the DPDCS can be tested by measuring the coincidence spectra of a well established decay scheme; ^{110} Ag(252 d), which decays to ^{110}Cd by emitting β^- particles, was selected for this purpose. As shown in Nuclear Data sheets (1977), all β-decays populate the high energy levels of the ^{110}Cd spectrum [Fig.(3.10)], which in turn cascade through γ-rays to the ground state.

Corrected spectra were obtained with four energy gates are 658, 764, 818 and 885 keV as explicitly shown in Fig.(3.11 to 20). In each gate, chance and background coincidences were subtracted from the uncorrected spectrum which was obtained by setting the upper and lower energy window at the appropriate line on the gating spectrum. Whereas the background was selected by setting the window on either side of the corresponding line (with equal width to that of the gate) made to minimize the background continuum and to reduce the peak height of the gate to the minimum. A summary of the results of the γ-γ coincidence experiment is given in Table(3.2). The observation of a γ-ray in coincidence with a γ-ray energy gate is indicated in Table(3.2) by one of the following entries: VS (Very Strong), S(Strong), W(Weak) or VW(Very Weak). These entries represent the percentage intensity of a transition

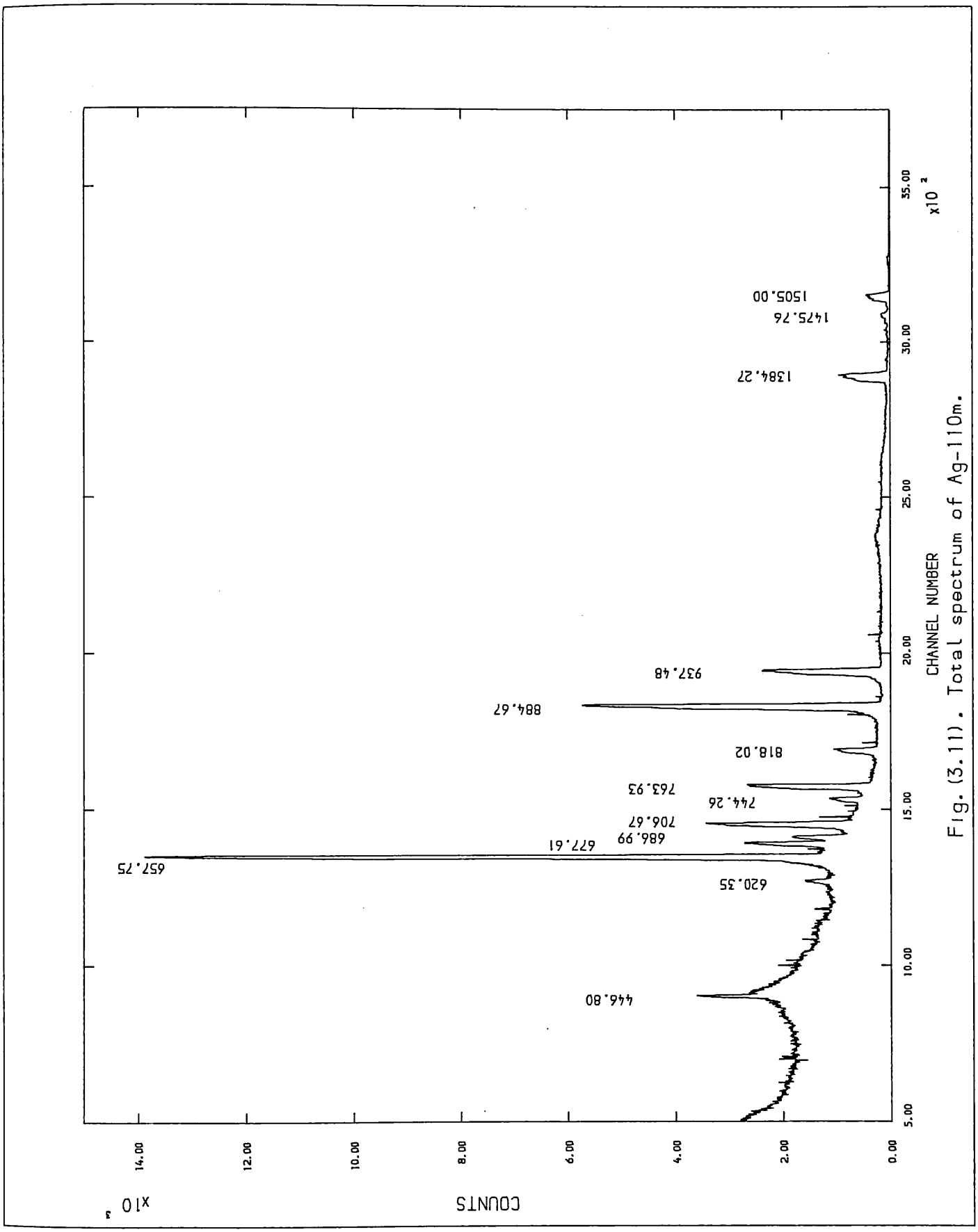

Fig. (3.11). Total spectrum of Ag-110m.

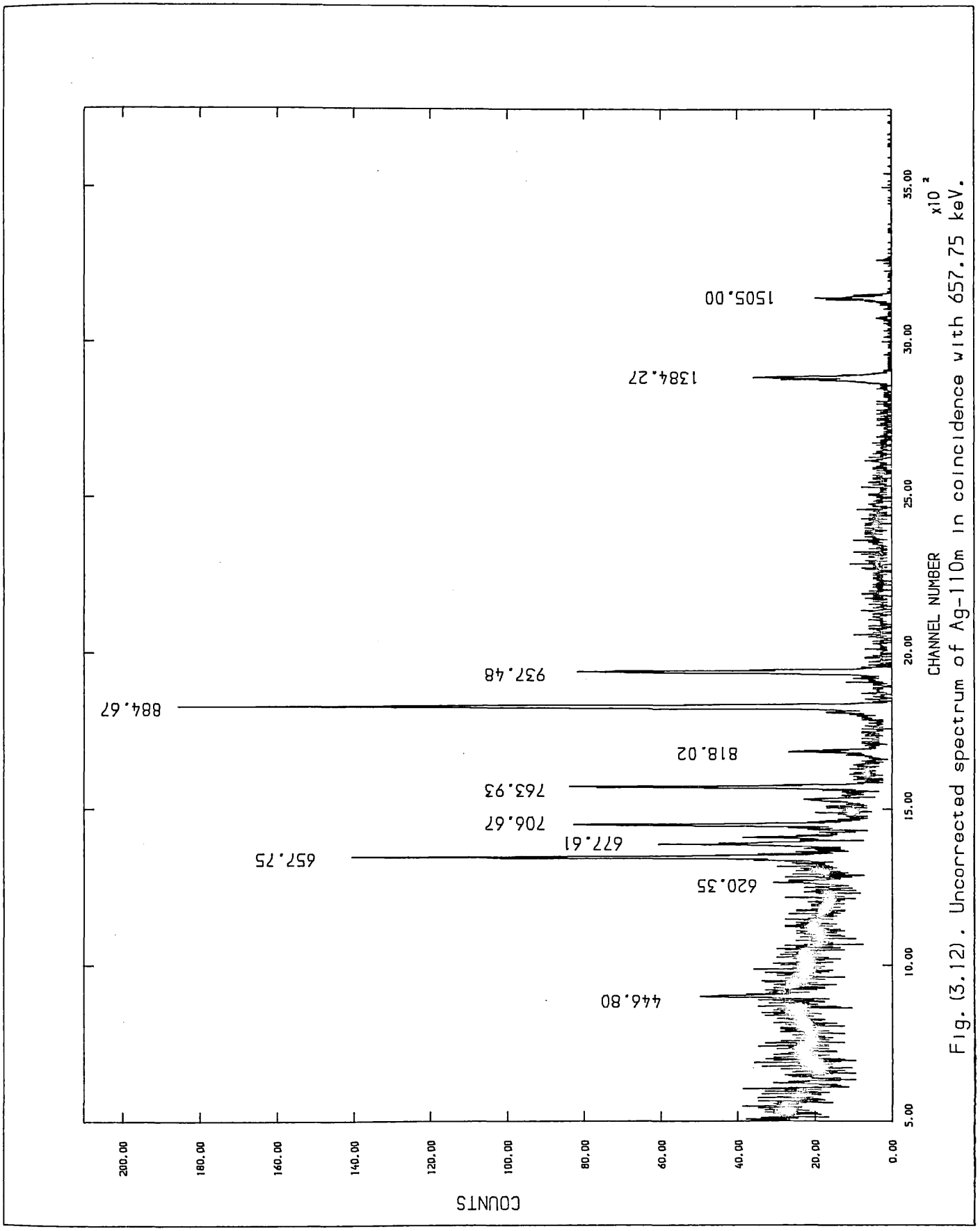

Fig. (3.12). Uncorrected spectrum of Ag-110m in coincidence with 657.75 keV.

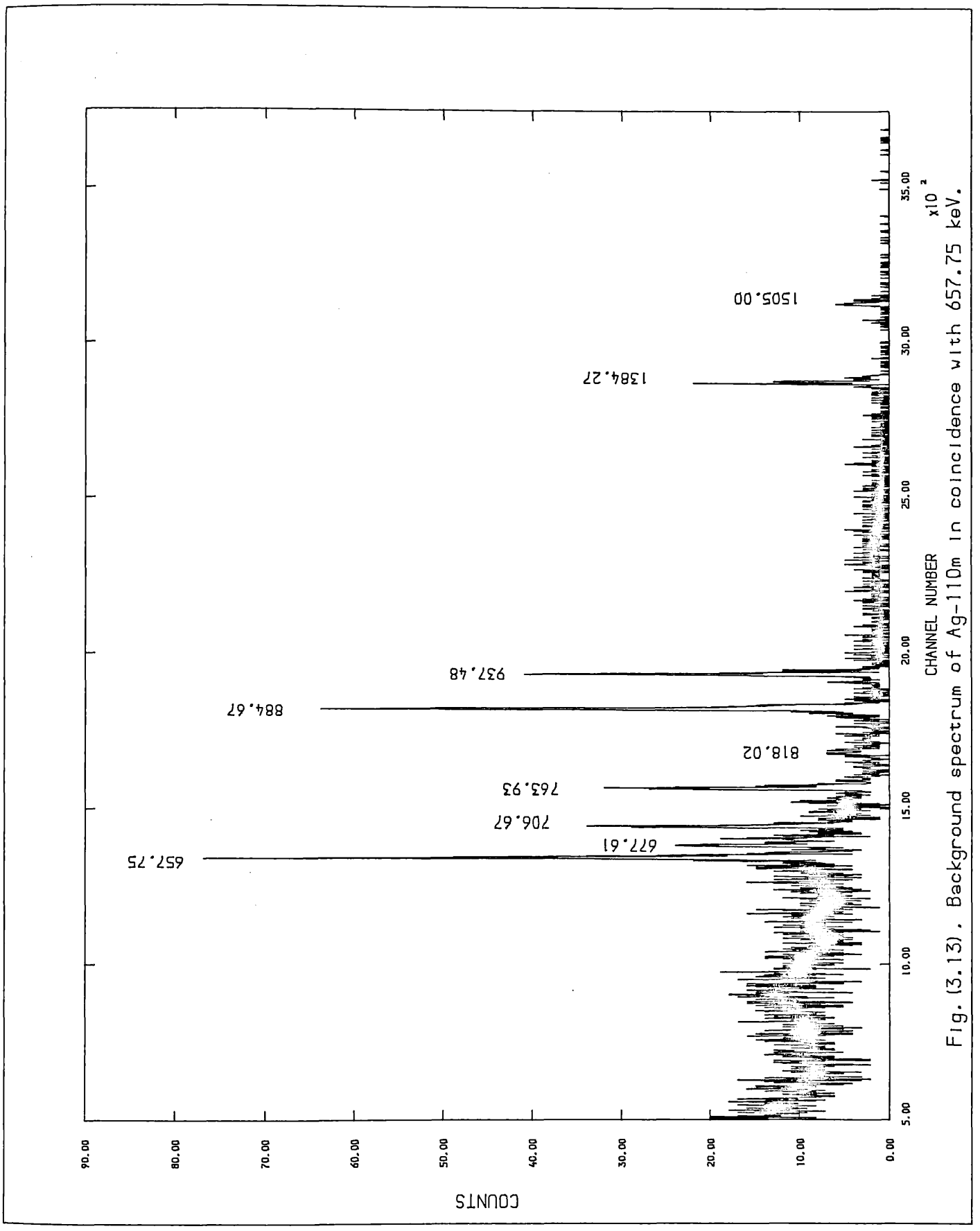

Fig.(3.13). Background spectrum of Ag-110m in coincidence with 657.75 keV.

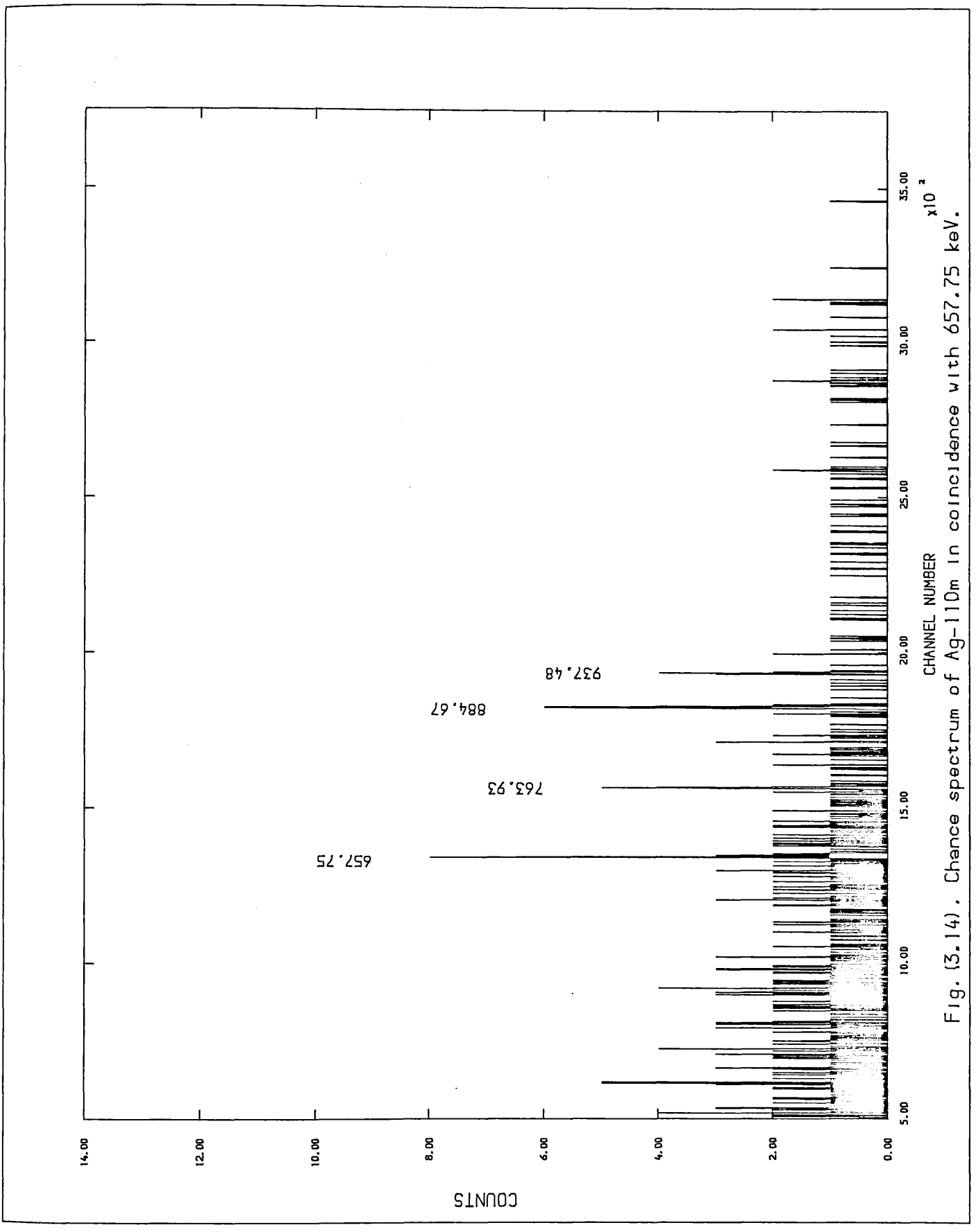

Fig. (3.14). Chance spectrum of Ag-110m in coincidence with 657.75 keV.

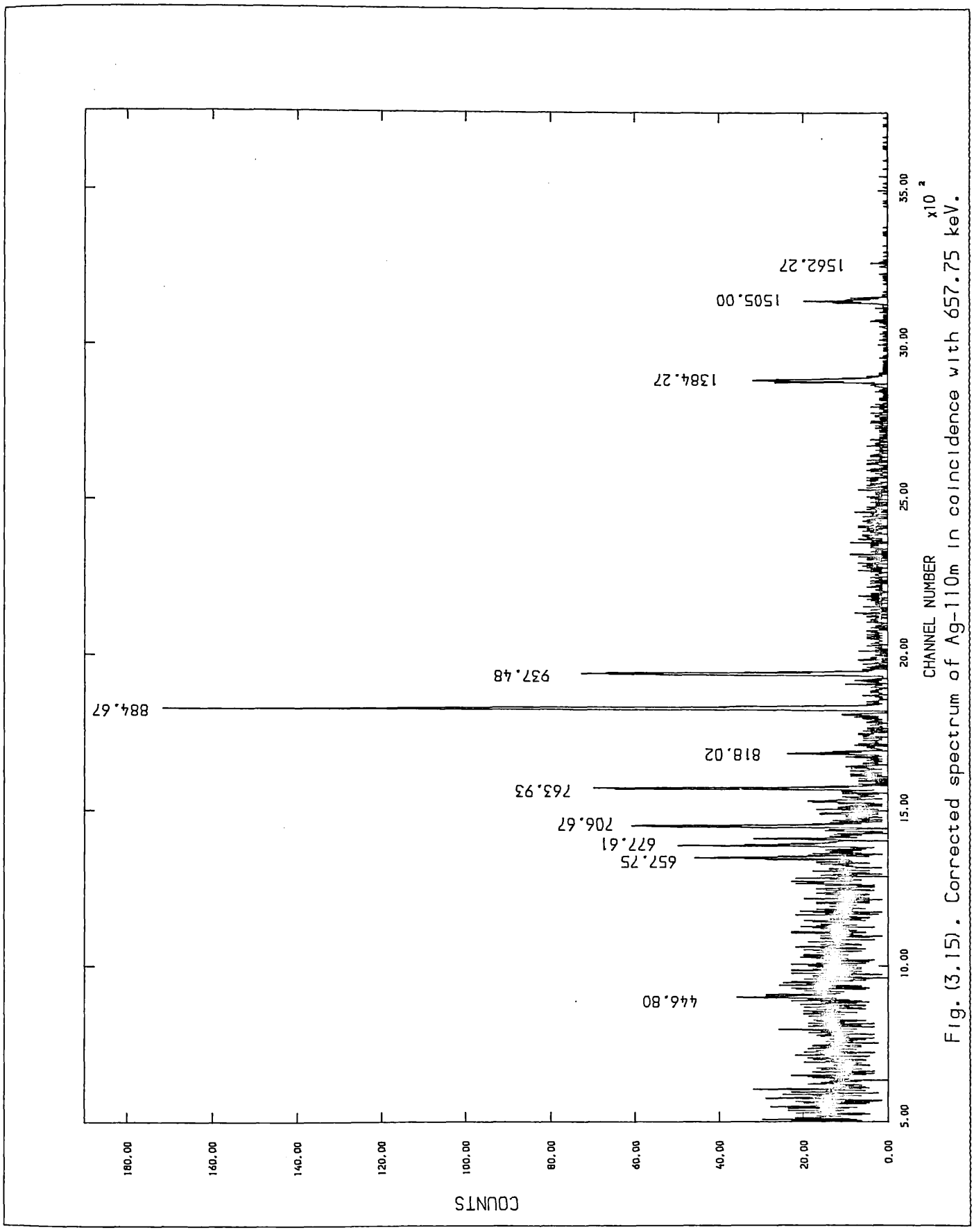

Fig. (3.15). Corrected spectrum of Ag-110m in coincidence with 657.75 keV.

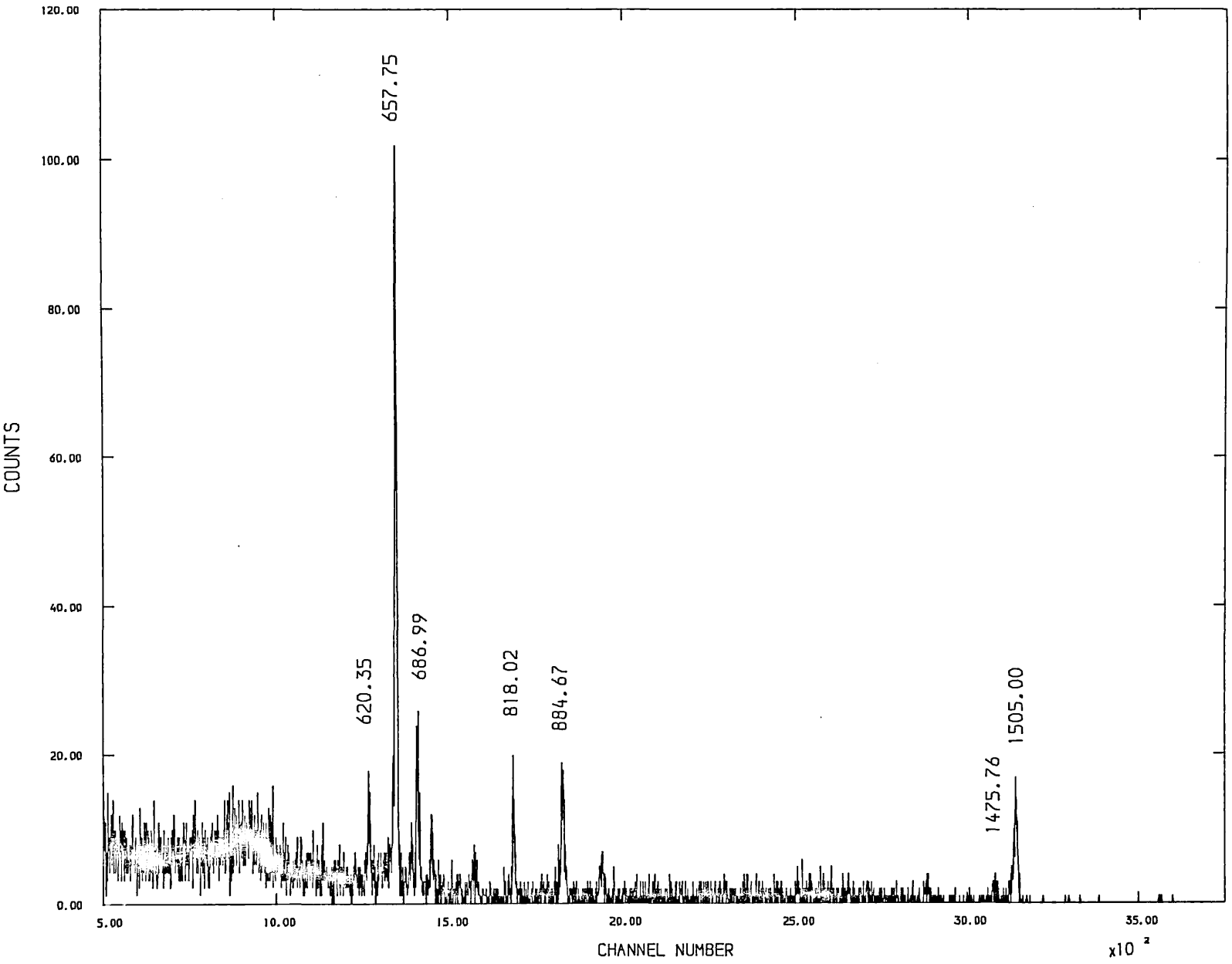

Fig. (3.16). Uncorrected spectrum of Ag-110m in coincidence with 763.93 keV.

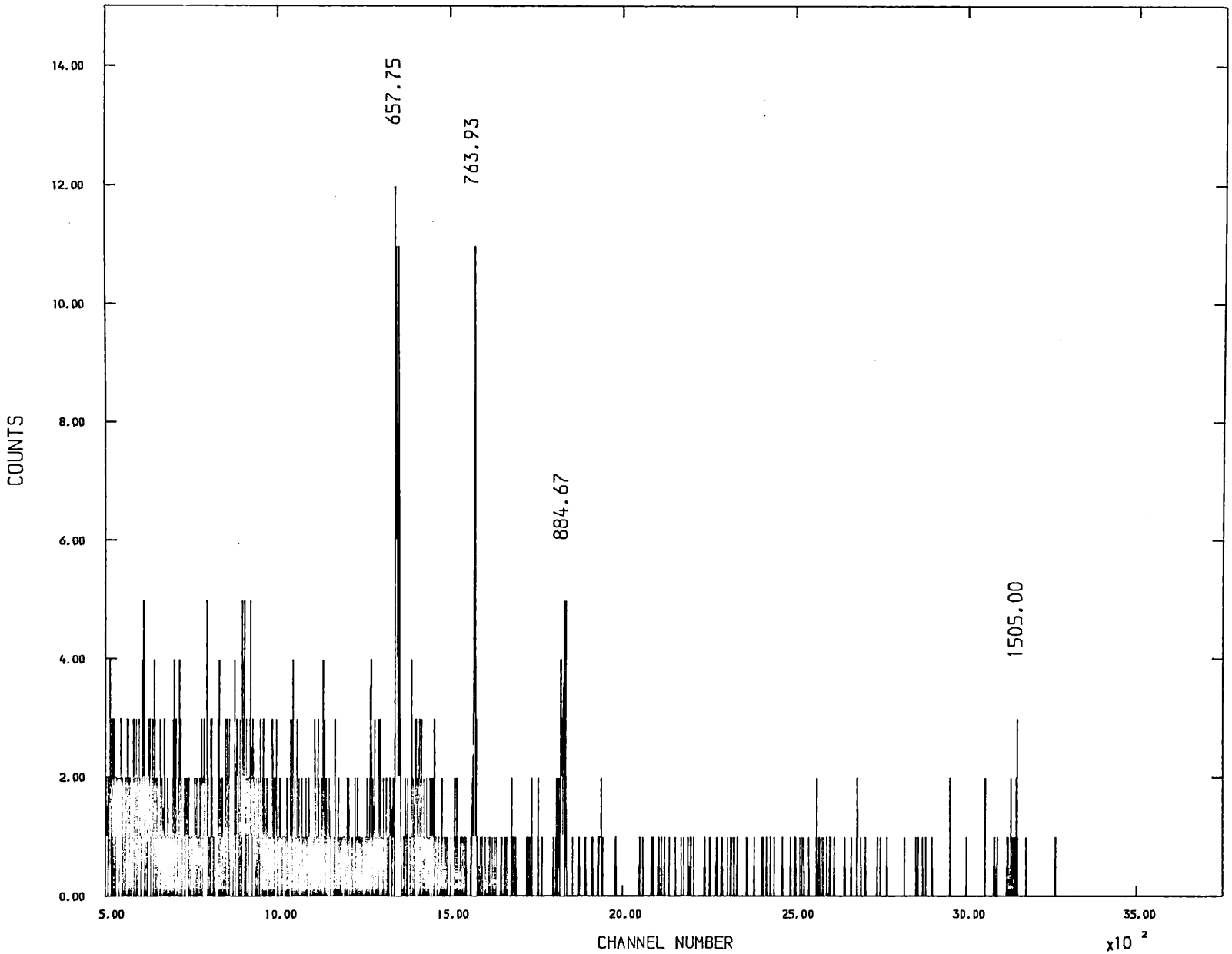

Fig. (3.17). Background spectrum of Ag-110m in coincidence with 763.93 keV.

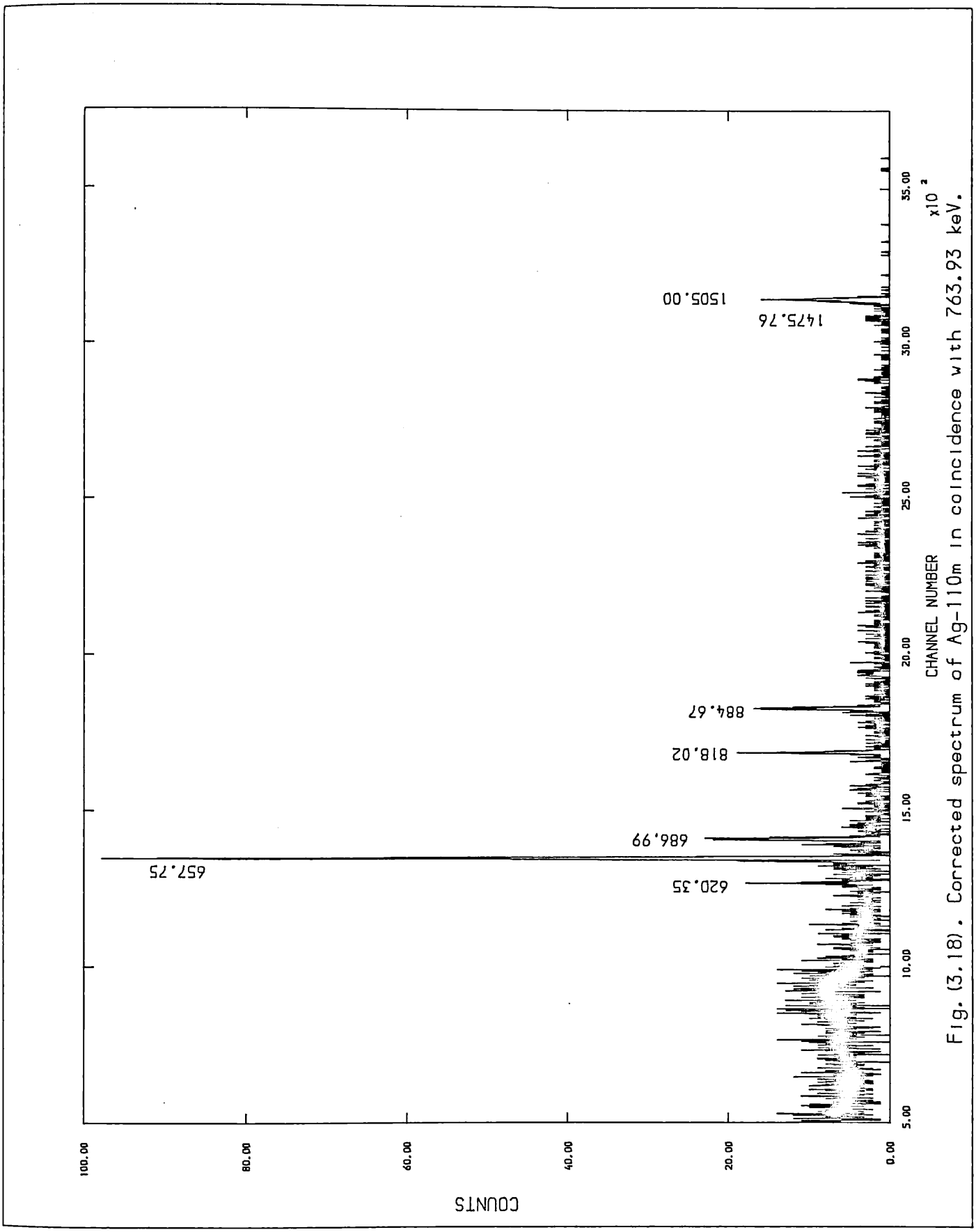

Fig. (3.18). Corrected spectrum of Ag-110m in coincidence with 763.93 keV.

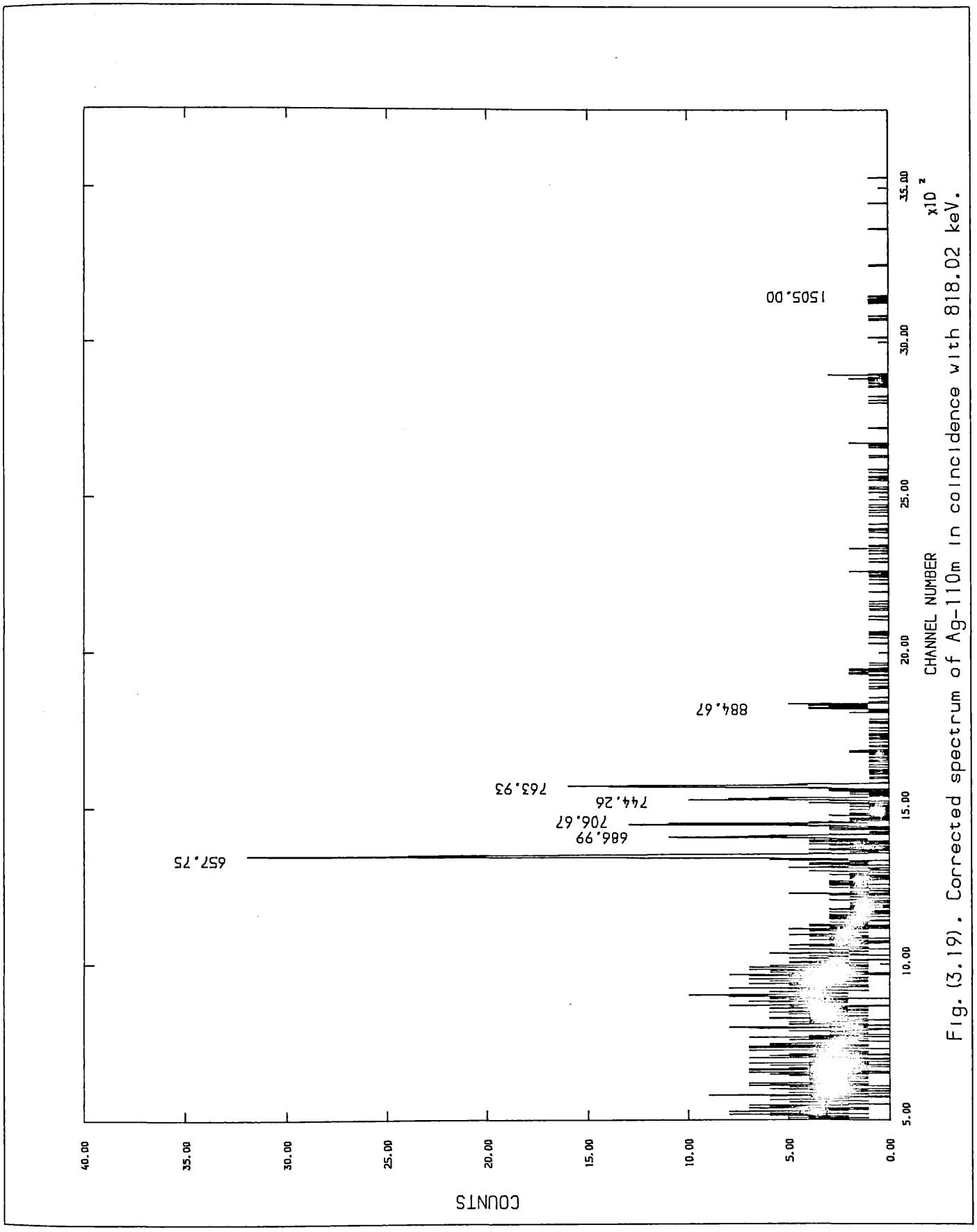

Fig. (3.19). Corrected spectrum of Ag-110m in coincidence with 818.02 keV.

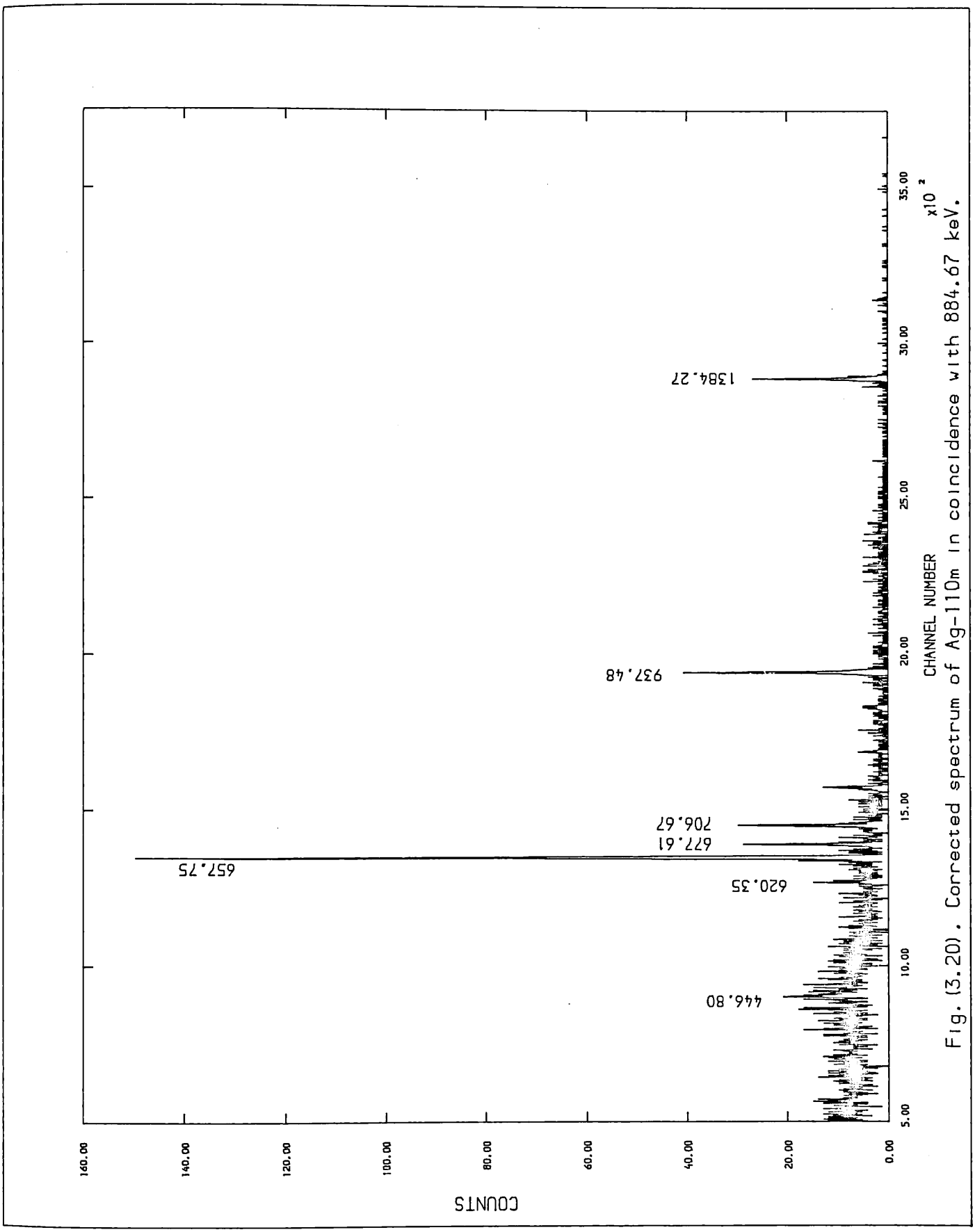

Fig. (3.20). Corrected spectrum of Ag-110m in coincidence with 884.67 keV.

Table(3.2). Results obtained from the decay of ^{110m}Ag.

Transition (keV)	Relative[a] Intensity	Coincidence gates(keV) 658	764	818	885
219.34	0.64(3)				
221.07	0.61(3)				
229.39	0.14(3)				
264.25	0.10(1)				
266.91	0.38(2)				
365.44	1.01(2)			W	
378.07	0.50(2)				
396.89	0.40(3)				
446.80	39.0(3)	VW			S
493.42	0.23(3)				
603.00	0.06(1)				
620.35	29.7(2)	W	VS		VS
626.25	2.28(7)				
657.75	1000.		S	VS	VS
677.61	111.6(7)	S			VS
686.99	69.2(5)	W	VS	VS	
706.67	175.8(9)	S		VW	
744.26	49.8(3)	W		VS	
763.93	236.8(14)	S		S	
818.02	78.0(5)	VS	S		
884.67	774.4(52)	VS	W	VW	
937.48	365.9(25)	S		P	VS
997.23	1.14(4)				S
1018.87	0.15(1)				
1085.43	0.75(4)			P	
1163.20	1.00(8)				W
1334.30	1.49(7)	VW			W
1384.27	263.6(24)	S			VS
1421.04	0.37(3)	P			
1475.76	42.4(5)		VW		
1505.00	139.8(17)	VS	VS	P	
1562.27	12.45(17)	VS			

[a] The relative intensities are normalised to $I_\gamma(657.75)=1000$.

with a respect to a reference peak as compared with the same intensity in the total spectrum. The reference peak is always referred to the most prominent peak in a gating spectrum, while the percentage ranges chosen correspond to 100-80, 80-60, 60-30 and less than 30%. P indicates a very weak peak, which probably exists, but owing to poor statistics cannot be conclusively identified. In Table(3.2) the main lines in the β^- decay of ^{110} Ag are given. The peaks that are truly in coincidence (S or VS) have intensities greater than theirs single intensities which explains very well the feature of the decay scheme [Fig.(3.10)] confirming the good performance of the DPDCS.

This same pattern for the data analysis of the coincidence results will be followed in the remaining part of this work.

CHAPTER IV

PROPERTIES OF ^{124}Te NUCLEUS FROM THE DECAY OF ^{124}Sb.

4.1 Introduction.

The doubly even Tellurium nuclei have been commonly considered to have vibrational-like properties since they belong to the transitional region between the "new" deformed region [Sheline et al.(1961)] of nuclides with N and Z between 50 and 82, and the spherical Z=50 closed shell nuclei. In particular ^{124}Te was expected to be of the type predicted by the hydrodynamical vibrational model [Bohr & Mottelson (1953), Scharff-Goldhaber et al.(1955)].

Early studies [Dorikens-Vanpract et al.(1965), Stelson (1967)] confirmed the general vibrational character of those few low-lying levels that had been reasonably well established. However, disagreements with experiment persisted: these were due to the well known fact that the vibrational model, in its usual form, yields vanishing probabilities for M1 transitions among any collective nuclear states. The non-existing M1 transition rate comes from an assumption of a uniform ratio of the proton and the neutron densities. Other striking changes are the displacement upwards of the first 0^+ state and the ratio 2_2-$2_1/2_1$-0_1 of E2 transition rate was reduced from the pure harmonic oscillator value of two. In order to meet these requirement and to make the magnetic nuclear properties consistent with the experimental observation, nuclear models definitely needed a more microscopic approach.

The introduction of a microscopic method, involving a pairing-plus-quadrupole force, was one attempt made by Lombard (1969) to overcome these difficulties, and it met with reasonable success for the first excited 2^+ and 3^- states of the tellurium nuclei.

Subsequently, a major contribution to the investigation of the isotopes of tellurium was made by the semi-microscopic approach of Lopac (1970). This model describes

the two protons outside closed proton shell at Z=50 as moving in the field of the core which performs harmonic oscillations around the spherical shape due to the collective effect of neutrons. The vibrational states of the core were taken up to three phonons whereas the proton configurations $1g_{7/2}$, $2d_{5/2}$, $2d_{3/2}$, $3s_{1/2}$ and $1h_{11/2}$ were assumed. The overall estimates of the parameters involved in this calculation produced the best agreement to the observed properties of ^{124}Te isotope to date.

Shortly after, Degrieck & Vander-Berghe (1974) applied the two proton-core coupling model to Te nuclei to explain the close energy spacing of the 6^+ and 4^+ levels found in A>126 nuclei which was not predicted by Lopac (1970). This model also describes the structure of the various members of the quasi-ground bands of the higher energy levels that were less well understood.

Deviations from the variable moment of inertia (VMI) predictions appeared to increase with increasing N for the neutron-rich Te nuclei [Scharff-Goldhaber et al.(1976)]. This implies a critical angular momentum at which the pairing energy for neutrons or protons suddenly decreases to a low value between J_c=4 and J_c=6. This phenomenon was attributed to strong overlap of proton pairs with a neutron pairs, i.e. α clustering.

Talmi (1979, 1981) pointed out that the interaction among only valence neutrons (or only valence protons) in semi-magic nuclei (only one closed shell) is not sufficient to cause nuclei to deform. On the other hand, as the number of proton pairs (or proton holes) increases away from a magic number, such as, i.e. $_{52}$Te (or $_{48}$Cd) deformation begins to take place. Also, as the neutron-holes increase (or neutrons), the proton neutron interaction increases in strength causing deformation behaviour near the middle of the 50 to 82 neutron closed shells. The striking as ymmetry with respect to the Z=50 shell has long been noticed [Mariscotti (1969)] by observing the R_4 ratio (E_4/E_2) and E2 energy behaviour in isotopes near the closed shell Z=50. These values for $_{46}$Pd and $_{54}$Xe

are very similar, but the asymmetry between the two-proton (Te) and two-proton hole nuclei (Cd) appear to be even more dramatic [Scharff-Goldhaber (1974)]. This asymmetry has been tentatively attributed to a good overlap between the extra-shell proton pair and an $h_{11/2}$ neutron pair missing from the same major shell (50 → 82). Several investigations have been carried out relating to these assymmetry properties, such as the work of Scholten (1980). Scholten stresses that in order to explain the properties of assymmetric nuclei about Z=50, one wants to distinguish between neutron and proton particles and introduces the interactions involving these particles.

Even so, a completely satisfactory description of the tellurium nuclei had not been acheived, and more recently the Interacting Boson Model (IBM) of Arima and Iachello was turned to. In an extension of the IBA-2 to account for even those region of the periodic table close to proton or neutron magic number, Sambataro (1982) studied the properties of Cd and Te nuclei: good agreement was provided for Cd nuclei by considering an existing two proton excitation across the shell gap at Z=50, an assumption made to explain the "unusual" 0^+ and 2^+ states observed at the energy of the two-phonon triplet for isotopes being in the middle of the shell. The neighbouring Te isotopes showed no evidence of similar proton excitations, but the results were not entirely successful, despite a fine description of the properties of some low-lying states.

The aim of the present work is to extend the previous IBM calculations to interpret the nuclear structure of ^{124}Te, highlighting the significance of the presence of several controversial low-lying 0^+ states, that have been experimentally observed in different experiments. By slightly moving away from a purely vibrational treatment, the first order perturbation to SU(5), suggested by Arima & Iachello (1976), is utilised and subsequently the programs PHINT and FBEM are used to study the possibility of greater SU(5) symmetry breaking leading towards the O(6) symmetry limit.

4.2 Previous investigations.

The energy levels in ^{124}Te can be populated by either

β^--decay of ^{124}Sb or β^+/EC-decay of ^{124}I, so previous investigators have used both these decay modes to build up the level scheme of ^{124}Te. The decay of antimony has been subject to numerous investigations in the past [Metzger (1953), Dzhelepov & Zhykovsky (1958)]. This is because of the relatively long half-life of ^{124}Sb(60 d), its large Q_β (2.9 MeV) and the β^--decay feeds high energy level make it favourable isotope to study. Typical of the earlier γ-γ or β-γ angular correlation experiments were those made by Weitkamp (1963), Korikens-Vanpract et al.(1965) and Stelson (1967), the first two of which used NaI(Tℓ) detectors, the last Ge(Li) detectors.

Further progress was made by Auer et al.(1969) who proposed fifteen energy levels as a result of their γ-γ coincidence studies with a curved crystal spectrometer and using Ge(Li) detectors. The γ-γ coincidence work of Meyer et al. (1969) led to the suggestion of twenty-two energy levels including confirmation of the fifteen previously suggested by Auer et al.(1969). All sixty-five γ-ray transitions incorporated in the decay scheme were observed by Ge(Li) detectors in a Compton suppression experiment. The same group also studied the ^{124}I decay [Ragaini et al.(1969)].

Johnson & Mann (1974) were able to use Ge(Li) and Si(Li) detectors to study β and γ spectra and the conversion electrons both singly and in coincidence. Compared with the results of Meyer et al.(1969), transitions at 185.7 and 1871.7 keV were not observed, nor could two levels at 1747. and 2411.8 keV be confirmed; instead new suggestions were made for five transitions at 159.4, 1248.3, 1732.1, 1957.7 and 1971.1 keV and for two other levels at 2335 and 2641.2 keV. A further eighteen transitions reported by Meyer et al.(1969) were only weakly supported. All spin-parity assignments of the ^{124}Te levels were determined from the deduced multipolarities of some transitions and from log ft values with varying degrees of confidence.

Extensive ^{124}Sb decay measurements were made by Sharma et al.(1979) who undertook a γ-γ correlation experiment of nine different cascades and confirmed the two transitions

reported by Johnson & Mann (1974) at 1248.6 and 1731.4 keV, along with eight others reported earlier by Meyer et al.(1969). However, fourteen transitions out of a total of seventy found by Sharma et al.(1979) could not be fitted into the decay scheme. Other experiments have also investigated the excited states of ^{124}Te by the methods of nuclear reactions such as that by Bushnel et al.(1969) using (n,γ) nuclear reaction and through (α,xn) made by Warner & Draper (1970).

The other aim of the present work is to try and resolve the differences remaining from previous studies regarding gamma transition intensities, energy level placement and spin/parity assignments in the decay scheme of ^{124}Te.

4.3 Experimental procedure and results.

4.3.1 Radioisotope:

The radioactive source of ^{124}Te was prepared from natural ^{123}Sb, of purity 99.9999 %, by thermal-neutron capture (n,γ) reaction at the University of London Reactor Centre (ULRC) following the method described in section (1.2). The source was left for three weeks after irradiation to allow undesirable activity from ^{122} Sb (4.2 m), ^{122}Sb (2d) and the isomer ^{124} Sb (21 m) to die away, and to provide a source strength of less than 10 μCi.

4.3.2 Singles:

Three separate determinations of the singles spectrum over the energy range 200 keV to 2694 keV were taken using the 12 % efficient Ge(Li) detector [detector no. 1 in Table (3.1)] placed at a standard source-to-detector distance of 25 cm.

Determination of the energy and efficiency calibrations was fully described in section (3.2). In addition, the presence of few sum, escape as well as background energies in the single spectra, as shown in Fig.(4.1), helped in the energy calibration that was determined by a least squares fitting procedure divided into two parts: transitions below 1.3 MeV

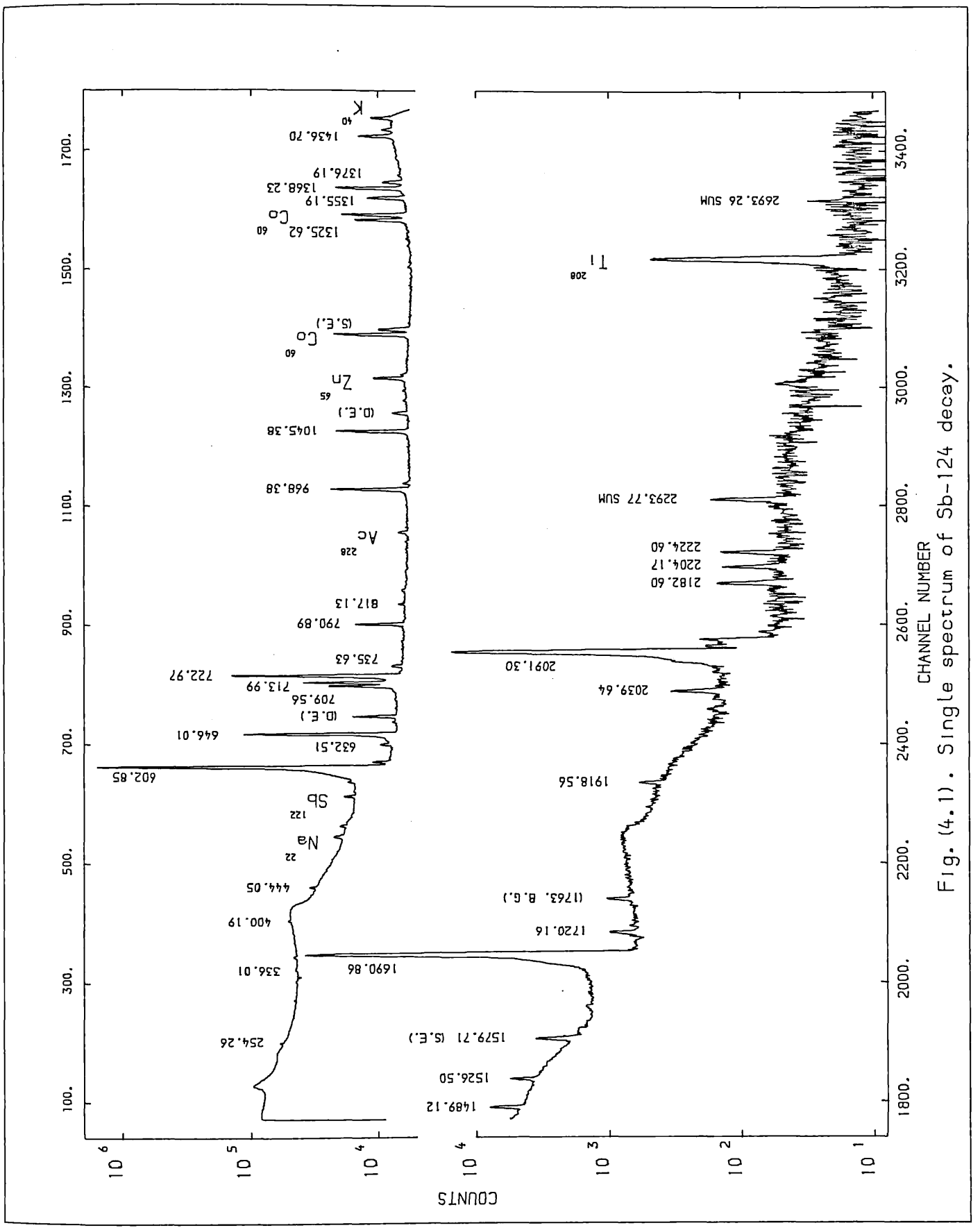

Fig. (4.1). Single spectrum of Sb-124 decay.

were linearly fitted, those above 1.3 MeV by a second order polynomial.

The energies and relative intensities of all transitions observed in the present work are listed in Table (4.1), together with those relative intensities and gamma-rays reported by Johnson & Mann (1974) and Sharma et al.(1979) for comparison. A total of ninety-two energies are reported, of which fourteen were observed for the first time in this work at energies 283.58, 358.79, 621.48, 1073.97, 1195.86, 1204.98, 1560.79, 1709.49, 1752.72, 1757.66, 1795.19, 2412.69, 2521.51 and 2642.2 keV. While the 498.10 keV energy was not fully confirmed in the singles obtained in this work, therefore is not treated as transition.

4.3.3 Coincidences.

The coincidence spectra were obtained with the two Ge(Li) detectors arranged in a 90^0 geometry. The 12 % efficient detector was used as the spectrum detector while the 10 % efficient detector [see Table (3.1) for specifications] provided the gate in a fast-slow coincidence system. It is referred to Chapter 3 for a resume of the operation of the Dual-parameter data collection system (DPDCS), and the method of correction for background and accidental coincidences. The total spectrum [Fig.(4.2)] was first obtained by spreading the gating window along the whole pulse height spectrum. Corrected spectra were obtained with seven energy gates as shown in Figs.(4.3-9) and a summary of the results of the γ-γ coincidence experiment is given in Table (4.2).

As the peak at 710 keV lies very close to the peak at 714 keV, the coincidence spectrum of the 710 keV line will not be completely corrected for the background mixture from the other two neighbouring peaks. Thus, wide gates covering the 710 + 714 + 723 peaks and the 710 + 714 keV peaks, as well as the 714 and 723 keV peaks were obtained, subsequently allowing the ^{124}Te spectrum in coincidence with the 710 keV peak to be deduced.

Table(4.1). Energies(keV) and relative intensities I_γ in the decay of ^{124}Sb. All relative intensities are normalised to $I_\gamma(602.85)=983000$.

E(keV) (Present)	E(keV) (Joh.)	E(keV) (Sha.)	I_γ (Joh.)	I_γ (Sha.)	I_γ (present)	Levels(keV) From	To
254.26(11)	254.40(30)	254.80	120(20)	205(20)	295(65)	2294	2040
283.58(27)					170(80)	2323	2040
336.07(12)	336.00(20)	336.10	560(35)	895(35)	765(70)	2294	1958
358.79(19)					325(90)	2694	2336
371.00(20)	371.20(20)	370.90	290(100)	310(25)	235(60)	2694	2323
387.26(26)	(380-390)		100		145(50)	2682	2294
400.19(07)	400.00(20)	400.24	1300(150)	2110(60)	1650(110)	2694	2294
444.05(09)	444.20(10)	444.24	1700(150)	2170(60)	2220(145)	2484	2040
468.91(14)	468.80(30)	468.93	300(100)	625(30)	775(50)	2694	2225
476.54(20)	(473-479)		100		75(35)	2702	2225
481.44(29)	481.40(20)	481.20	200(100)	250(20)	290(45)	2776	2294
498.10 P	498.60(30)		200(100)		40		
525.56(10)	525.40(20)	525.58	1300(100)	1590(40)	1750(110)	2484	1958
602.85(08)	602.80(06)	602.85	983000	983000	983000	603	000
621.48(27)					140(25)	[2580]	1958
632.51(10)	632.40(70)	632.57	1200(300)	1090(30)	1160(65)	1958	1326
646.01(08)	646.07(07)	645.94	74000(1600)	73900(1450)	76880(2135) †	1249	603
662.49(19)	662.70(50)	662.60	150(30)	145(15)	420(50)	2702	2040
709.56(09)	709.40(10)	709.42	13600(900)	14400(280)	14600(730)	1958	1249
713.99(09)	713.90(10)	713.93	23900(1000)	23750(460)	24160(880)	2040	1326
722.97(08)	722.90(07)	722.84	109700(2000)	111140(2200)	112620(1575)	1326	603
735.63(42)	735.40(20)	735.73	1400(300)	1430(35)	1400(45)	2694	1958
766.20(20)	765.40(50)	766.40	90(30)	85(20)	90(10)	2092	1326
774.83(24) *	(771-777)	775.00	<50	140(20)	110(40)	2733	1958
790.89(09)	790.78(08)	790.74	7500(150)	7220(160)	7530(80)	2040	1249
817.13(08)	816.90(10)	817.06	640(60)	820(30)	840(75)	2776	1958
856.98(21)	856.90(40)	856.80	220(60)	285(30)	265(60)	2183	1326
899.53(35)	900.00(20)	899.60	100(40)	275(35)	2580(55)	2225	1326
938.17(17) *	(935-942)	938.00	<50	60(10)	60(20)	[2263]	1326
968.38(09)	968.20(08)	968.22	20000(400)	19970(370)	20035(240)	2294	1326
976.55(40)	976.00(30)	976.40	1000(200)	950(40)	860(115)	2225	1249
997.15(10)	(995-1000)		<50		90(50)	2323	1326
1014.57(20) *	(1012-1019)	1015.00	<50	35(30)	30(30)	[2263]	1249

Continued

E(keV) (Present)	E(keV) (Joh.)	E(keV) (Sha.)	I_γ (Joh.)	I_γ (Sha.)	I_γ (present)	Levels(keV) From	To
1045.38(09)	1045.19(09)	1045.22	18900(400)	19370(400)	19790(230)	2294	1249
1054.22(40)	1054.40	1054.00	100(50)	45(30)	70(10)	1657	603
1073.97(32)					255(90)	2323	1249
1086.35(11)	1086.20(20)	1086.53	300(50)	450(40)	570(50)	2336	1249
1163.38(08)	(1160-1165)		<50		155(60)	2412	1249
1195.86(17)					165(60)	2522	1326
1199.24(26) *	1199.30(100)	1199.60	80(60)	60(50)	20(10)		
1204.98(10)					225(80)	2454	1249
1248.10(20) *	1248.30(30)	1248.62	50(10)	120(40)	110(60)†		
1253.96(25) *	(1250-1260)	1254.00	<50	40(40)	40(20)	[2580]	1326
1263.11(14) *	1263.40(40)	1263.41	440(100)	560(50)	530(100)	[2589]	1326
1272.38(33) *	(1267-1273)	1271.00	<50	60(40)	140(100)	{2522}	{1249}
						[2598]	1326
1301.71(21) *	(1298-1304)	1301.00	<50	440(40)	595(80)	[2627]	1326
1325.62(10)	1325.60(10)	1325.59	16400(400)	16800(350)	16610(280)	1326	000
1355.19(13)	1355.20(10)	1355.33	11200(350)	11500(240)	10890(220)	1958	603
1368.23(10)	1368.20(10)	1368.30	27100(600)	27700(570)	27110(680)	2694	1326
1376.19(10)	1376.00(20)	1376.20	5300(250)	5620(120)	5215(450)	2702	1326
1385.06(42)	1384.90(90)	1385.28	310(70)	525(25)	780(250)	2711	1326
1389.02(20)	(1385-1390)		<100		65(30)		
1428.56(21)					175(70)	[2754]	1326
1436.70(09)	1426.60(10)	1436.70	13600(400)	13440(270)	13170(265)	2040	603
1445.17(11) *	1445.00(20)	1445.24	2900(250)	4000(90)	3230(140)	2694	1249
1453.16 P	(1450-1457)	1454.00	<100	65(50)	200	2702	1249
1489.12(10)	1489.00(20)	1489.10	50(40)	7900(160)	7100(195)	2092	603
1526.50(09)	1526.30	1526.30	4400(200)	4785(100)	4260(80)	2776	1249
1557.24(10)	(1553-1560)		<50		80(45)†	[2806]	646
1560.79(20)					75(25)	2886	1326
1579.71(11)	1579.90(80)	1579.80	1500(500)	4800(100)	2335(70)	2183	603
1622.61(18)	1622.40(30)	1622.20	300(50)	465(30)	460(40)	2225	603
1690.86(10)	1691.05(09)	1690.89	504000(10000)	497800(9600)	500150(8660)	2294	603
1709.49(20)					45(10)		
1720.16(10)	1720.30(20)	1720.30	940(70)	1020(30)	990(50)	2323	603
1730.11(27) *		1731.40		65(20)	100(35)		
1733.00(26)	1732.10(20)		100(50)		60(20)	2336	603

Continued

E(keV) (Present)	E(keV) (Joh.)	E(keV) (Sha.)	I_γ (Joh.)	I_γ (Sha.)	I_γ (present)	Levels(keV) From	To
1752.72(20)					210(35)		
1757.66(30)					185(35)	[2360]	603
1795.19(15)					125(60)		
1851.40(30)*	(1845-1855)	1851.00	<25	90(20)	25(25)	2454	603
1918.58(11)	1918.60(20)	1918.80	270(40)	580(20)	540(30)	2522	603
2016.00(12)	2016.20(40)	2016.06	70(20)	115(10)	110(25)	2619	603
2039.64(11)	2039.30(20)	2039.68	660(40)	660(30)	665(25)	2642	603
2079.41(14)	2079.00(20)	2079.11	≤ 800	300(10)	365(85)	2682	603
2091.30(20)	2091.00(20)	2091.21	57600(1400)	56480(1170)	58190(950)†	2694	603
2099.75(21)	2098.70(30)	2099.06	500(200)	390(100)	360(50)	2702	603
2107.97(21)	2107.50(30)	2108.14	550(100)	465(20)	340(45)	2694	603
2151.08(25)	(2145-2155)		<5		13(10)	[2754]	603
2172.90(30)	2172.00(100)	2172.30	12(4)	20(5)	45(10)	2776	603
2182.60(15)*	2182.60(20)	2182.44	400(30)	430(10)	475(20)	2183	000
2204.17(13)*	2204.70(40)	2204.39	80(20)	70(5)	175(15)	[2806]	603
2224.70(30)		2224.00		9(5)	50(10)	2225	000
2283.38(29)	2283.30(50)	2283.75	70(20)	50(6)	95(20)	2886	603
2293.77(13)	2293.70(30)	2293.78	250(50)	580(15)	440(20)†	2294	000
2323.24(20)	2323.40(80)	2323.50	10(4)	20(5)	40(10)	2323	000
2412.69(14)					35(15)	2412	000
2454.50(30)	2454.60(100)	2454.54	9(4)	10(5)	10(5)	2454	000
2521.51(20)					35(7)	2522	000
2642.20(25)					95(15)	2642	000
2681.13(35)	2681.30(50)	2682.10	20(5)	20(5)	25(10)	2682	000
2693.26(28)	2693.10(60)	2693.90	24(5)	65(5)	55(10)†	2693	000

(Joh.) Refers to Johnson & Mann (1974).
(Sha.) Refers to Sharma et al.(1979).
* Transition was previously reported but not placed in the decay scheme.
[ ] Proposed level with no sufficient evidence.
{ } Transition is not firmly established in the decay scheme.
( ) Error corresponding to the last digital quoted value.
P Energy probably exist.
† Corrected relative intensity.

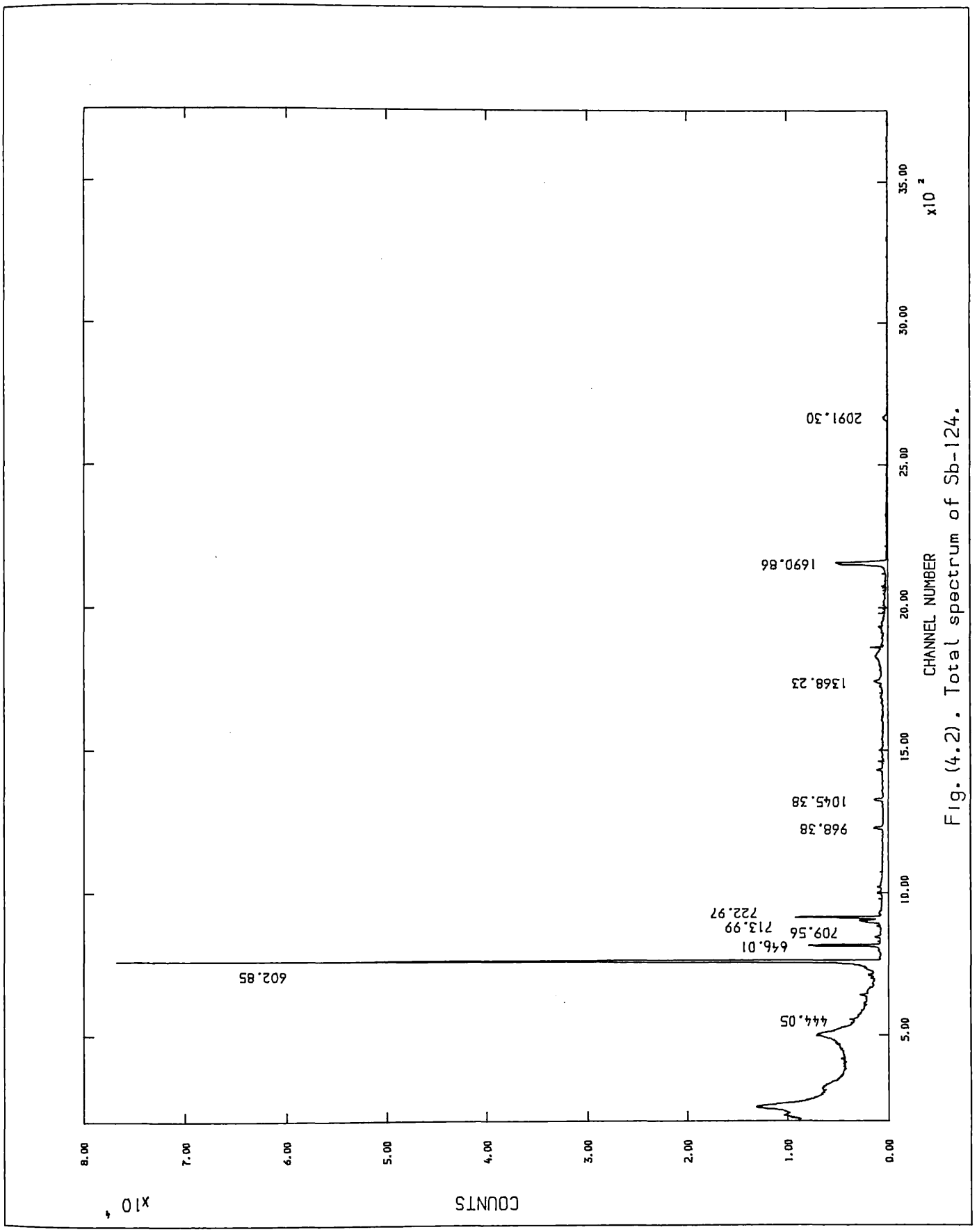

Fig.(4.2). Total spectrum of Sb-124.

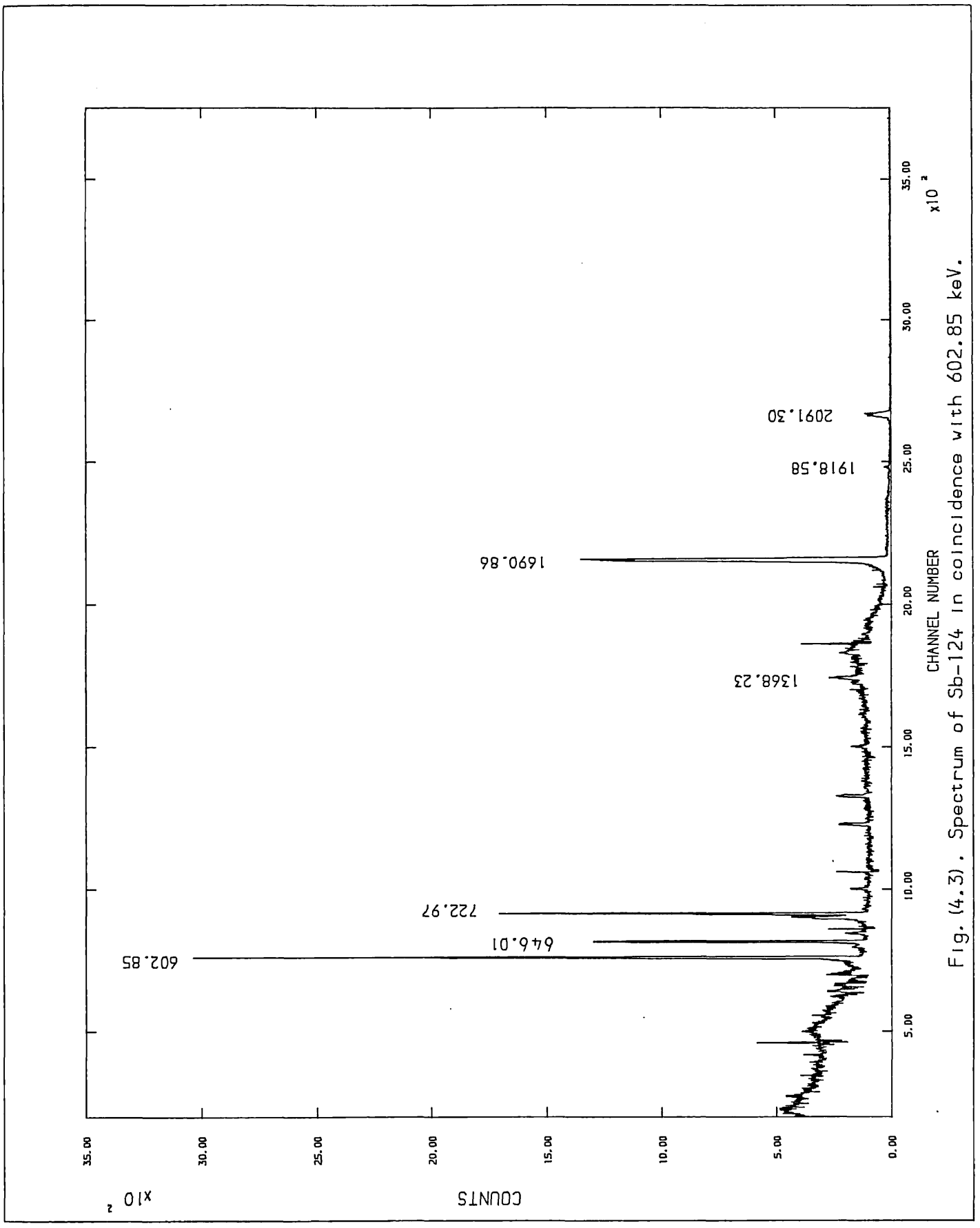

Fig. (4.3). Spectrum of Sb-124 in coincidence with 602.85 keV.

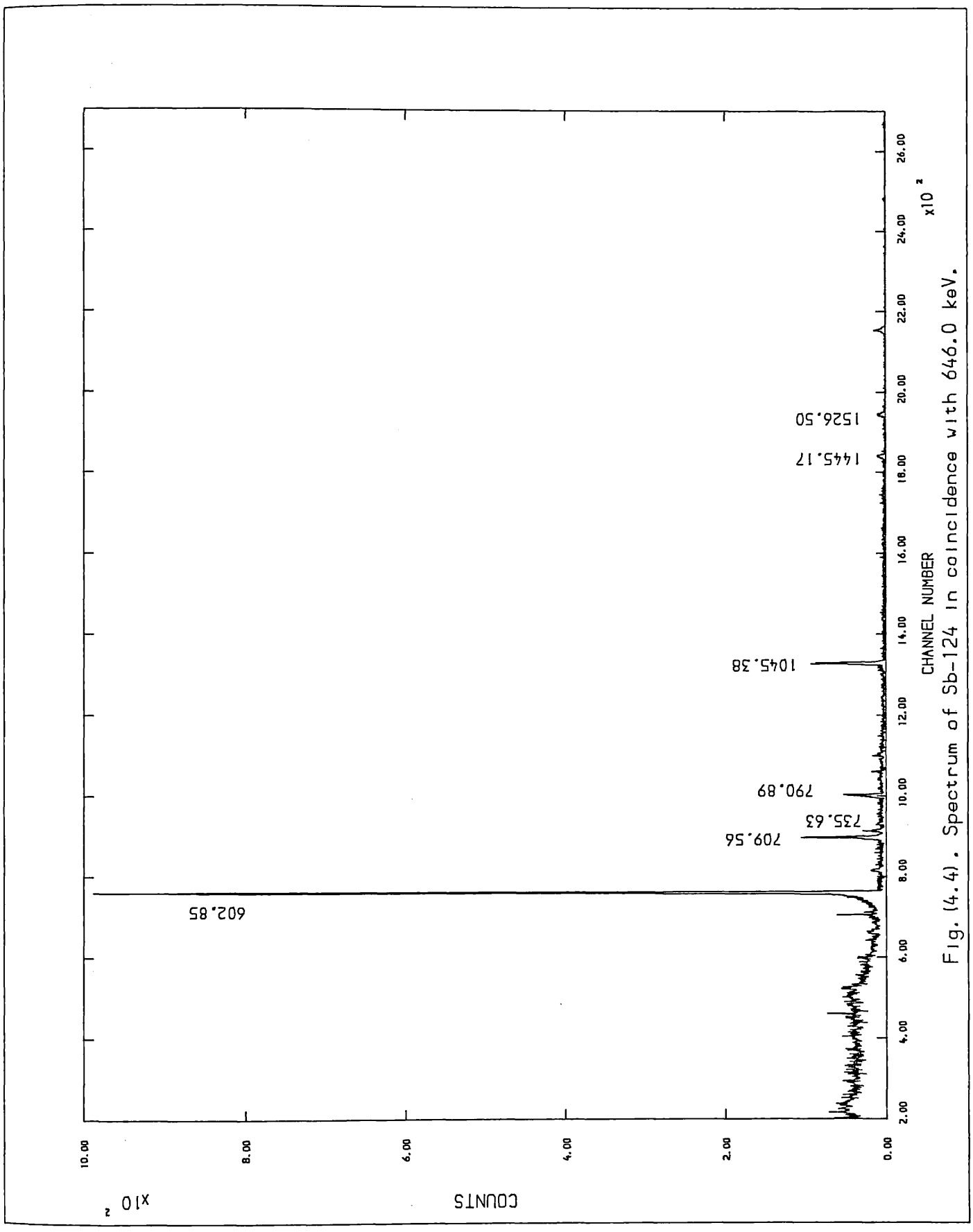

Fig. (4.4). Spectrum of Sb-124 in coincidence with 646.0 keV.

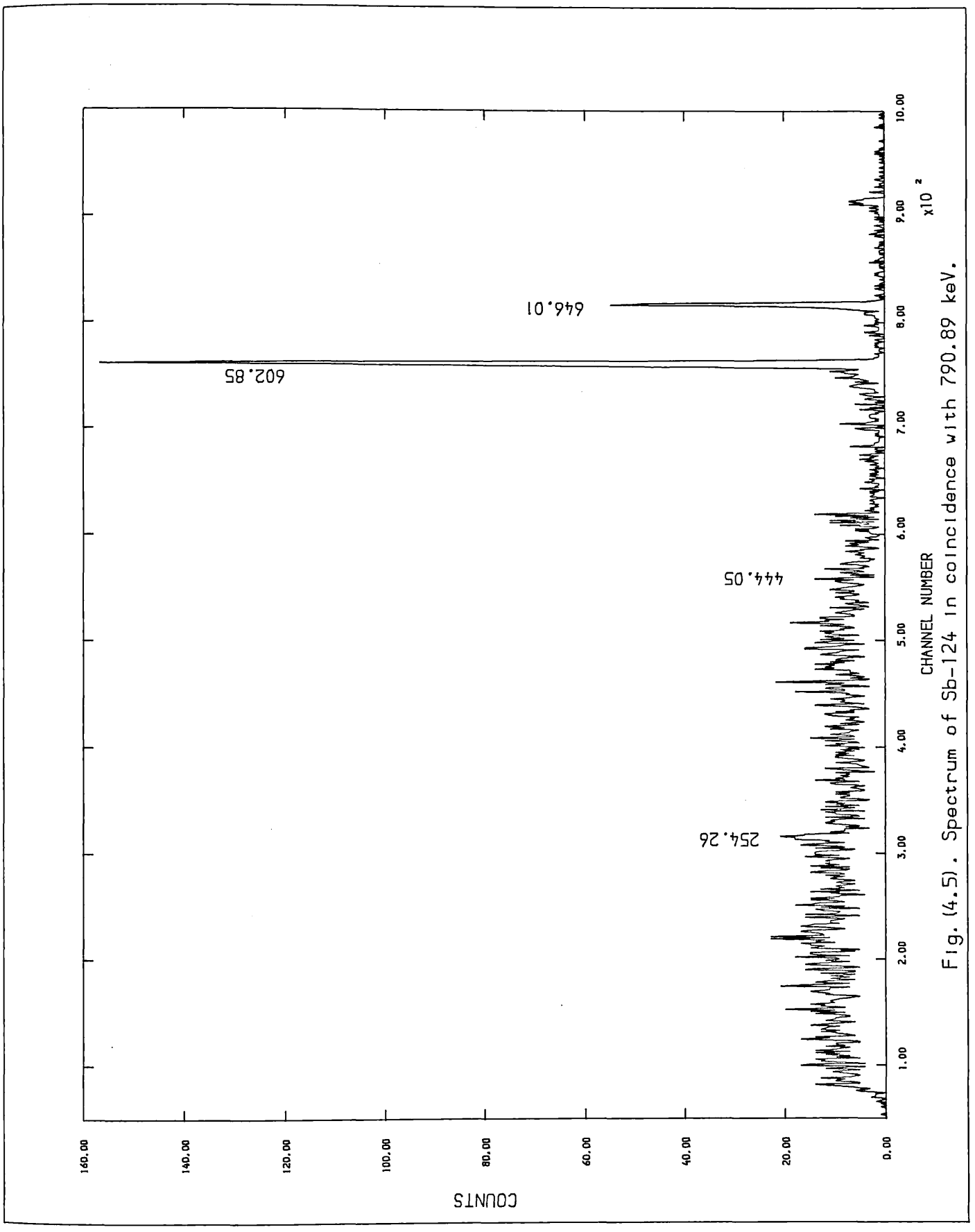

Fig. (4.5). Spectrum of Sb-124 in coincidence with 790.89 keV.

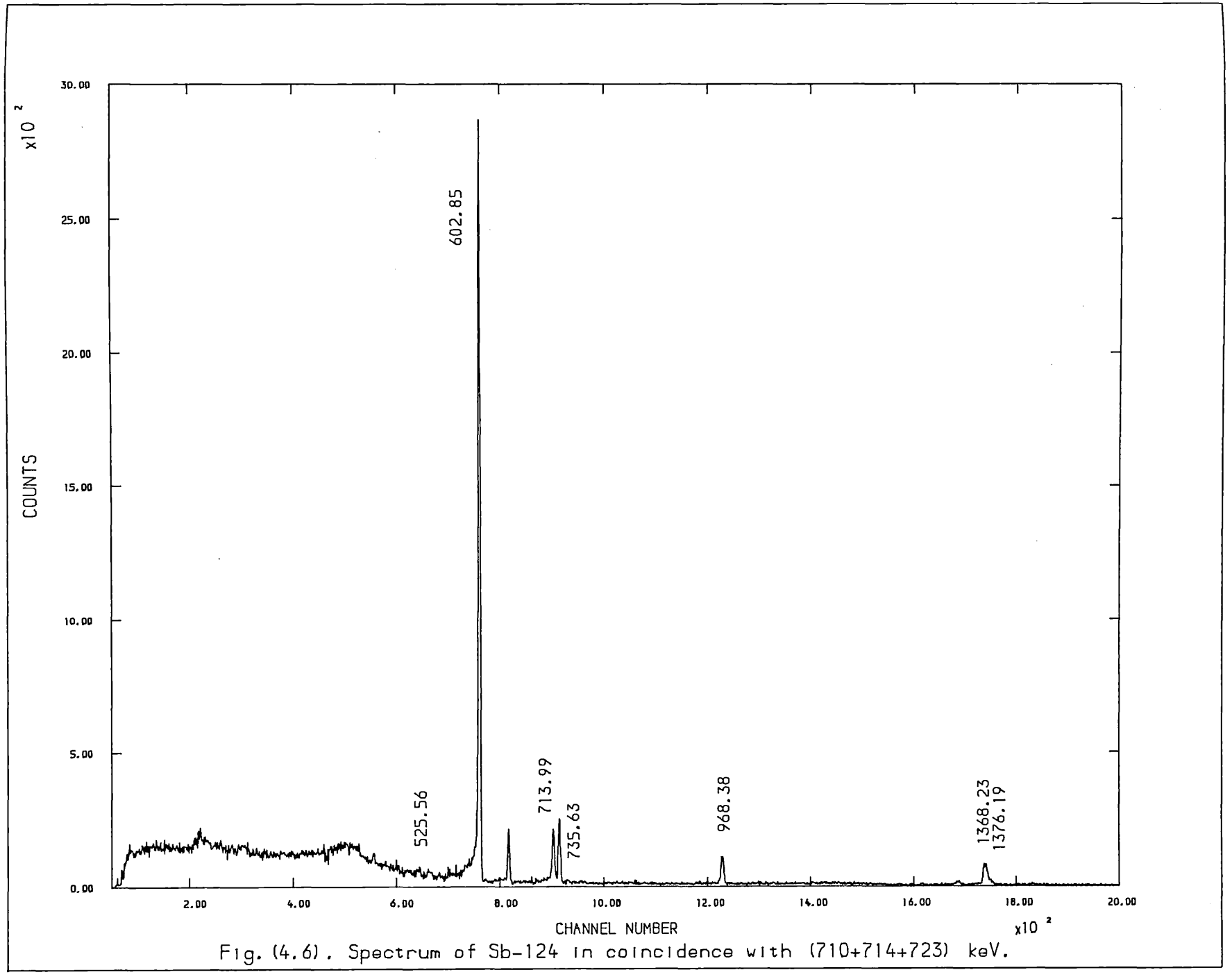

Fig. (4.6). Spectrum of Sb-124 in coincidence with (710+714+723) keV.

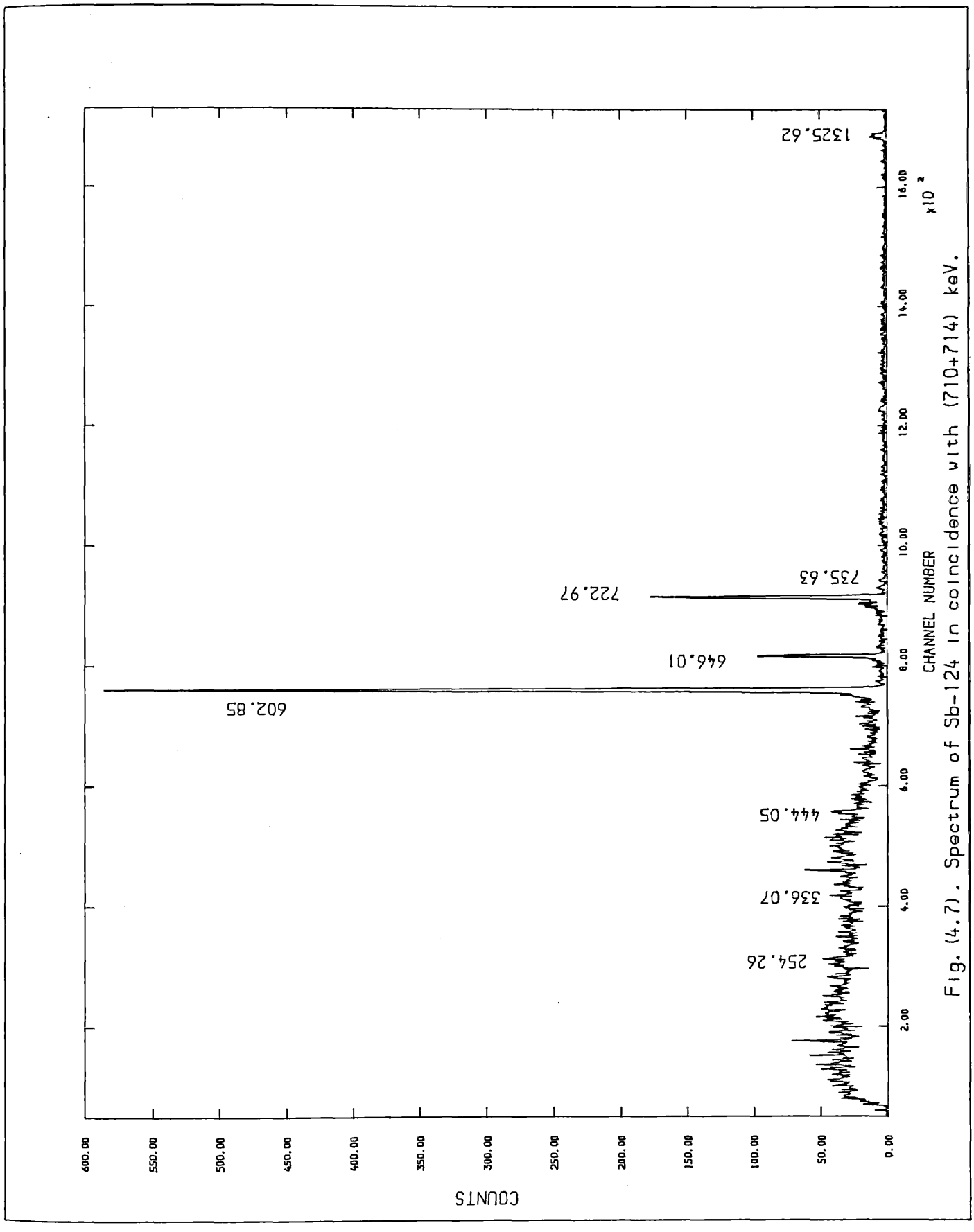

Fig. (4.7). Spectrum of Sb-124 in coincidence with (710+714) keV.

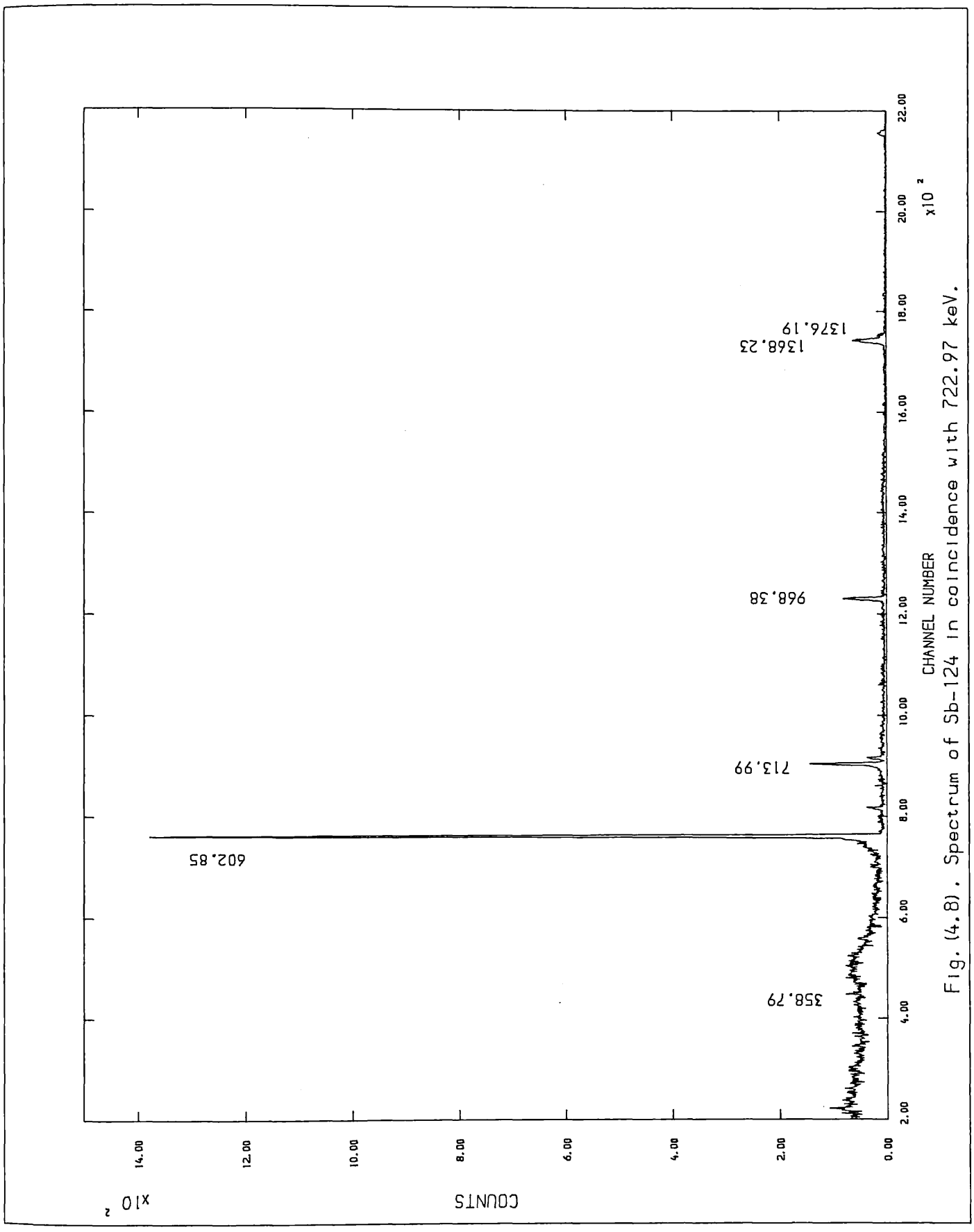

Fig. (4.8). Spectrum of Sb-124 in coincidence with 722.97 keV.

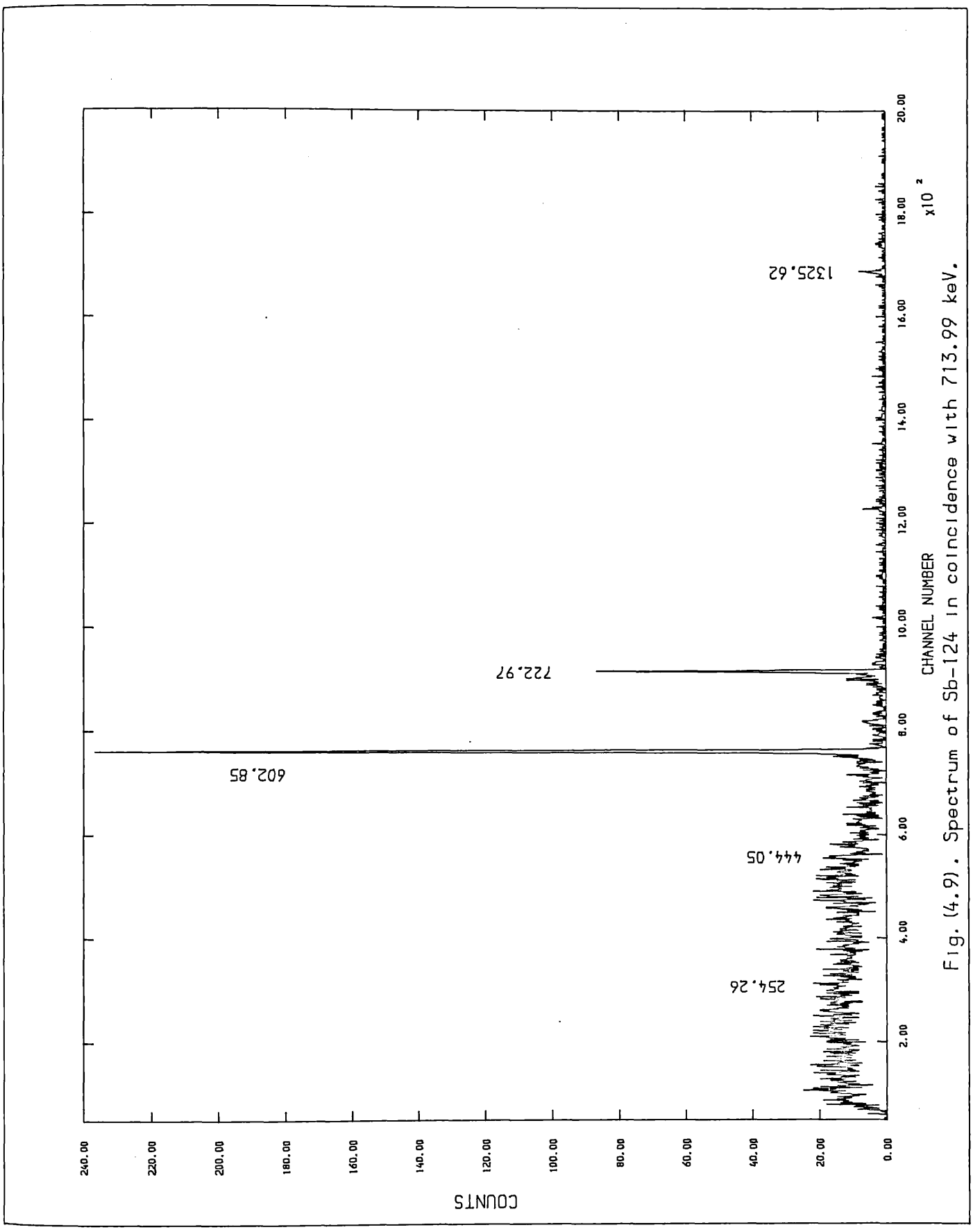

Fig. (4.9). Spectrum of Sb-124 in coincidence with 713.99 keV.

Table(4.2). Summary of the gamma-gamma coincidence measurements.

Transition (keV)	Gate (keV)							
	603	646	791	710 714 723	710 714	723	714	710
254.26			VS	VS	VS		VS	
283.58			P	S	VS		S	
336.07	S			W	S			VS
358.79	VS					VS		
371.00	S				P			
400.19	VW							
444.05	W	VW	VS	W	VS"	W	VS"	
525.56	S	W		S	VS			VS
602.85		VW	W	W	W	VW	W	
621.48					P			
632.51	S			VS		W		
646.01	VS		VS"	VW	W			S
662.49	W				P			
709.56	VW	VS						
713.99	W			S		VS		
722.97	VS			VW	W	VW	S	
735.63	S	S		VS	VS			VS
766.20	P							
774.83		W		P		W		S
790.89	W	VS						
817.13	VW			VW	W			S
968.38	W			VS"		VS"		
976.55	W	VS						
997.14						VS		
1014.57		VS						
1045.38	W	VS"						
1073.97		S						
1086.35	S	W						
1163.38		P						
1195.86				P		P		
1253.96						VW		
1263.11				VW		W		
1272.38		VW		VS		VS		
1301.71	S			S		P		
1325.62				VW	VS		S	
1355.19	VS			VW				
1368.23	S			VS		VS		
1376.19	S			VS		S		
1385.06				S		S		
1436.70	VS							
1445.17	W	VS						
1489.12	VS							
1526.50	VS	VS						
1560.79				P				
1579.71	VS							
1622.61	S							
1690.86	VS"							
1720.16	VS							
1757.66	P							
1851.40	P							
1918.58	VS							
2016.00	VS							
2039.64	S							
2079.41	VS							
2091.30	VS							
2099.75	P							
2107.97	VS							
2204.17	P							
2283.38	VS							

" The referrence line for a gate spectrum.

The observation of a γ-ray in coincidence with a γ-ray energy gate is indicated in Table (4.2) by the appropriate entries VS(Very Strong), S(Strong), W(Weak) or VW(Very Weak) as described in Chapter 3, while P indicates a very weak peak, which probably exists, but owing to poor statistics cannot be conclusively identified.

4.4 Decay Scheme.

Based on the coincidence results and energy sum relations the decay scheme of ^{124}Te was obtained as shown in Fig.(4.10); branching ratios, log ft values, spins, parities and level energy assignments are given on the left,and also listed in Table (4.3). The branching ratios were obtained from the gamma ray balance between transitions feeding and depopulating a level; using Q_{β}=2.905 MeV for ^{124}Sb [Lederer & Shirley (1978)] the log ft values were calculated, allowing spins and parities to be deduced consistent with β-decay selection rules.

The multipolarity of some transitions were determined by comparing experimental conversion coefficients α(K) with the theoretical values of α(K) for E1, E2 and M1 multipolarities as given by Rösel et al.(1978). The experimental α(K) were evaluated from the present gamma-ray intensities reported earlier and the K-shell conversion electron intensities I(K) given by Johnson & Mann (1974) and Grigoriev et al.(1968). Weighted mean values of results obtained by using both works are given in Table (4.4), and the multipolarities deduced are listed in the last column. A few differences were found on comparison with those reported by Johnson & Mann. For instance, the γ-ray of energy 254.26 keV was given an M1/E2 admixture in contradiction to parity conservation for a transition between levels with $I^{\pi} = 3^{-}$ and 3^{+}. As seen in Table (4.4), the multipolarity of this transition is assigned to be E1 in agreement with its placement in the ^{124}Te level scheme. Also, the present results differ from the mixed M1/E2 multipolarities of Johnson & Mann (1974) for the transitions at 400.19, 444.05 and 525.56 keV by suggesting pure electric quadrupole assignments. The transition with energy 766.2 keV was not given a multipolarity by Johnson & Mann (1974) while the

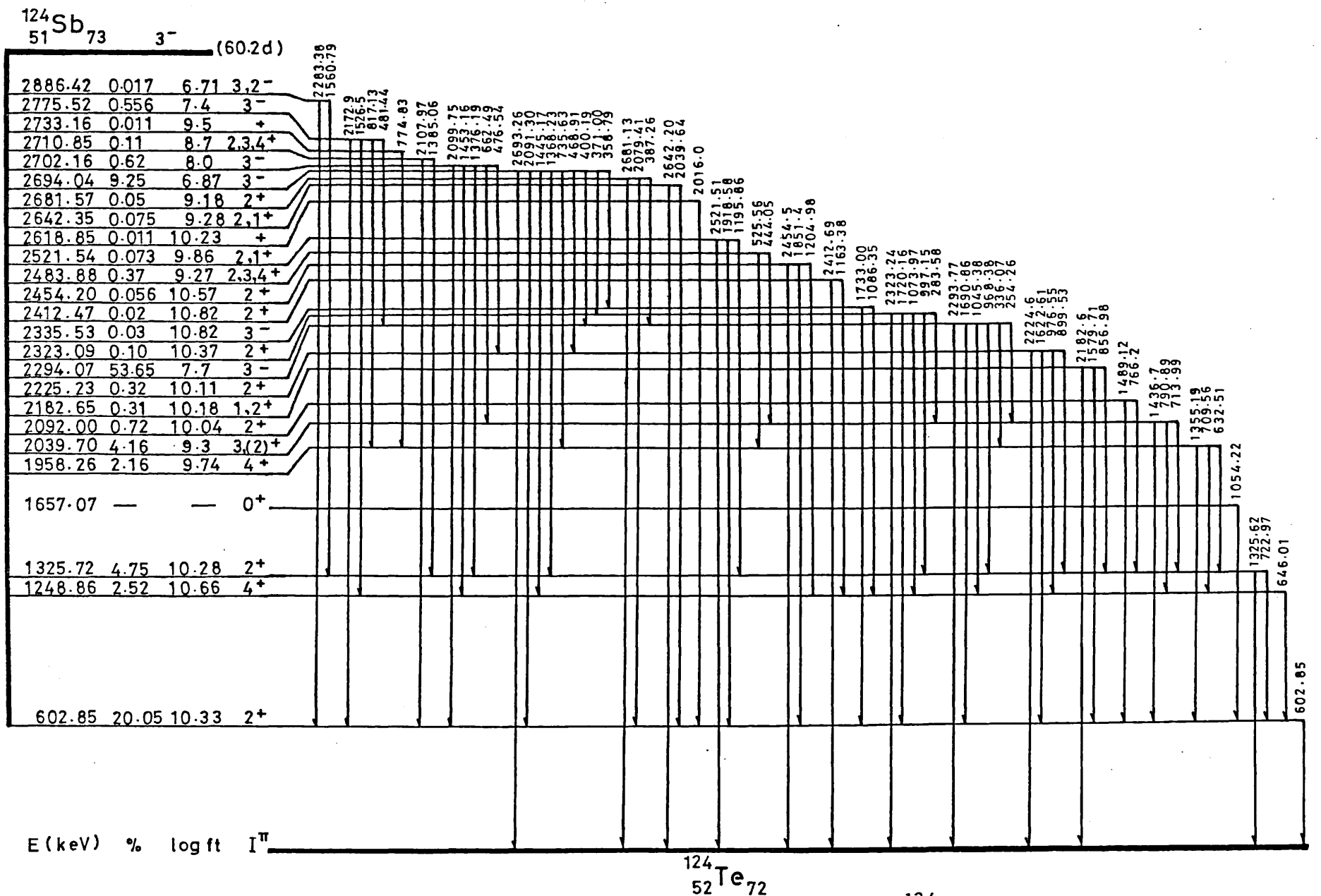

Fig.(4.10). The level scheme of ^{124}Te.

Table(4.3). Summary of the level properties in ^{124}Te.

E Level* (KeV)	E Beta (KeV)	Σ decay	Σ Feed	%B.R.	log ft	π	I
000.00						+	0
602.85(08)	2302.15	100.500	79.982	20.05	10.33	+	2
1248.86(08)	1656.14	7.854	5.2741	2.523	10.66	+	4
1325.72(14)	1579.28	13.185	8.3290	4.749	10.28	+	2
1657.07(24)						+	0
1958.26(20)	946.74	2.718	0.5097	2.160	9.74	+	4
2039.70(14)	865.30	4.575	0.3195	4.162	9.30	+	3,(2)
2092.00(10)	813.00	0.732	—	0.716	10.04	+	2
2182.65(13)	722.35	0.313	—	0.305	10.18	+	1,2
2225.23(36)	679.77	0.415	0.0865	0.321	10.11	+	2
2294.07(27)	610.93	55.088	0.2297	53.65	7.70	-	3
2323.09(22)	581.91	0.157	0.0594	0.096	10.37	+	2
2335.53(45)	569.47	0.065	0.0330	0.031	10.82	-	3
2412.47(32)	492.53	0.020	—	0.019	10.82	+	2
2454.20(33)	450.80	0.026	—	0.056	10.57	+	2
2483.88(12)	421.12	0.407	0.0260	0.372	9.27	+	2,3,4
2521.54(13)	383.46	0.075	—	0.073	9.86	+	2,1
2618.85(10)	286.15	0.011	—	0.011	10.23	+	
2642.35(20)	262.65	0.077	—	0.075	9.28	+	2,1
2681.57(60)	223.43	0.055	—	0.053	9.18	+	2
2694.04(33)	210.96	9.462	—	9.254	6.87	-	3
2702.16(29)	202.84	0.638	—	0.623	8.00	-	3
2710.85(10)	194.15	0.114	—	0.111	8.70	(+)	3,2,4
2733.16(12)	171.84	0.011	—	0.011	9.50	+	2,3,4,5
2775.52(16)	129.48	0.568	—	0.556	7.40	-	3
2886.42(27)	18.58	0.018	—	0.017	6.71	-	3,2

* Errors in the energy levels quoted are deduced from a single transition measurement, or the standard deviation of the spread of the energy sum relations.

Table(4.4). Deduced multipolarities from K-shell internal-conversion coefficients x(10^3) for ^{124}Te.

Energy (keV)	Experiment α(K)		Theoretical α(K) E1	E2	M1	Adopted multipolarity
254.26	13.88	(1.15)	12.8	54.0	45.5	E1
336.07	6.48	(4.36)	6.00	23.3	23.0	E1
400.19	11.27	(2.14)	3.87	13.5	14.7	E2
444.05	6.51	(3.24)	3.02	9.60	11.2	E2
468.91	< 7.47		2.69	8.25	9.80	E1
481.44	< 9.88		2.51	7.65	9.10	M1/E2
525.56	3.31	(1.90)	2.07	5.95	7.40	E2
602.85	4.2		1.54	4.20	5.30	E2
646.01	3.34	(16)	1.33	3.54	4.50	E2
709.56	3.42	(32)	1.07	2.86	3.60	M1/E2
713.99	2.73	(33)	1.05	2.77	3.52	E2/(M1)
722.97	2.30	(01)	1.03	2.68	3.40	E2
735.63	1.18	(59)	0.99	2.56	3.28	E1
766.20	21.26	(6.70)	0.91	2.35	3.00	E0+(E2,M1)
790.89	2.41	(16)	0.84	2.15	2.76	E2/M1
968.17	0.66	(06)	0.57	1.36	1.75	E1
1045.38	0.50	(06)	0.50	1.15	1.47	E1
1325.62	0.76	(07)	0.32	0.70	0.88	E2/M1
1355.19	0.75	(08)	0.32	0.67	0.84	E2/M1
1368.23	0.30	(04)	0.30	0.66	0.83	E1
1376.19	0.28	(24)	0.30	0.65	0.81	E1
1436.70	0.71	(29)	0.28	0.60	0.74	E2/M1
1489.12	0.76	(12)	0.26	0.56	0.68	M1/E2
1526.50	< 0.36		0.26	0.53	0.64	E1
1657.07	------		0.23	0.46	0.54	E0
1690.86	0.21	(04)	0.22	0.45	0.52	E1
2091.31	0.15	(04)	0.16	0.31	0.33	E1

possibility of a mixed E0 component with either E2 or E2/M1 multipolarities is suggested. The electric monopole character of the 766.2 keV transition is apparent from the large experimentally measured value of the K-shell conversion coefficient in Table (4.4).

Concerning the ninety-two γ-ray energies observed in this work, the present decay scheme generally agrees with those previously proposed with the restriction to the few following remarks.

– The energy at 498.1 keV was not firmly seen neither singly nor in coincidence, therefore no evidence in this work supportsa level at 1747 keV fed by the β-decay of ^{124}Sb, as was suggested by Meyer et al.(1969).

– Also, the following γ-ray energies of 1237.63 keV [Sharma et al.(1977)], 2254 keV [Meyer et al.(1969), Sharma et al.(1979)], 159.4, 1957.7 keV [Johnson & Mann (1974)], 553.8, 1950.4, 2274 keV [Meyer et al.(1969), Johnson & Mann (1974)] could not be confirmed. However the present results do confirm the transitions at 476.54, 997.15, 1163.38, 1557.24, 2151.08 keV [Meyer et al.(1969), Johnson & Mann (1974)] and at 387.26, 1389.02, 1733 keV [Johnson & Mann (1974)] none of which were confirmed by Sharma et al.(1979). The energies of 1428.56 keV [Meyer et al.(1969), 2224.7 keV Meyer et al.(1969), Sharma et al.(1979)] and 1730.11 keV [Sharma et al.(1979)] were also observed. Additionally, the present singles measurements detected fourteen new energies, eleven of which were placed in the decay scheme as a result of either of either coincidence evidence or energy sum considerations, whereas three of those fourteen at energies 1709.49, 1752.72 and 1795.19 keV were not placed.

– The 1958.76 keV level, with log ft value 9.74, was observed to de-excite through three transitions 632.51, 709.56, 1355.19 keV to the 2_2^+, 4_1^+ and 2_1^+ levels respectively. The second has an M1 component mixed with E2 [Table (4.4)] while the third has an E2/M1 indication; but no M1 admixture has been reported from angular correlation measurements, so

$I^{\pi} = 4^{+}$ is favoured for this level.

– The 2039.7 keV level populates the 2_2^+, 4_1^+ and 2_1^+ levels via the 713.99, 790.89 and 1436.7 keV transitions. Table (4.4) shows that all three transitions have a mixed M1/E2 multipolarity, which together with a log ft value of 9.3 favours a spin/parity assignment of 3^+, in agreement with the work of Johnson & Mann (1974) on ^{124}Sb decay, and that of Demidov et al.(1980) from a Te(n,n'γ) experiment. However, the angular correlation experiments of Sharma et al.(1979) indicate a 2^+ assignment.

– The 2412.47 keV level was proposed by Meyer et al. (1969) to be depopulated by the 1163.2 and 1086.3 keV transitions. Only the latter transition was observed by Johnson & Mann (1974), who could not confirm the level, whereas the present spectra gated with the 603 and 646 keV lines supported the proposal of Meyer et al.(1969). A new energy at 2412.69 keV, which would correspond to a transition to the ground state, is also reported in this work. The log ft value of 10.82 agrees with a spin/parity assignment of 2^+.

– The 2775.52 keV level was given a I^{π} of 4^- by Johnson & Mann (1974). The present results give a log ft value of 7.4 which agrees with the I^{π} of 3^- that is suggested by the presence of three depopulating transitions: 1526.5 keV with electric dipole (E1) characteristics to the 4^+ level, 481.44 keV with mixed M1/E2 multipolarity to the 3_1^- level and 2172.9 keV to the 602.85 keV (2_1^+) level.

– A new level at 2618.85 keV is proposed. It was established from the very strong coincidence of the 2016 keV transition with the 603 gate. The 2016 keV transition had been previously reported by Johnson & Mann (1974) and Sharma et al. (1979), but not placed in the decay scheme. It is also noted that a level with energy 2617 keV has been reported by Lederer & Shirley (1978) as the result of (n,γ) and (He, ^{124}Te) experiments.

– A new level at 2733.16 keV is proposed as a conseq-

uence of the coincidence measurements. The present singles have found a transition at 774.8 keV agreeing with singles measurements made by Johnson & Mann (1974) and Sharma et al. (1979), to the level at 1958.2 keV. The coincidence spectra gated with the 646, 723 and the 710 + 714 + 723 keV windows showed the 774.8 keV line detected with strengths of "W", "W" and "P" respectively; no coincidence was observed with the 714 keV gate, thus a strong coincidence with the 710 keV line is deduced. Although the 774.8 keV line was not seen in coincidence with the 710 + 714 keV gate (probably swamped by the large background from the 714 keV line) the foregoing observations are consistent with the existence of a level at 2733.16 keV.

— There are some evidences found for the presence of a further eight energy levels at 2263.66, 2360.51, 2579.7, 2589.04, 2598.1, 2754.11, 2806.56 and 2627.43 keV.

Three of these 2263.66, 2754.11 and 2806.56 keV had been suggested, but not confirmed by Meyer et al.(1969). Although the γ-energies observed at 938.17 and 1014.57 keV are consistent with a level at 2263.66 keV, their intensities were too weak to be seen in a coincidence spectrum. A similar argument applies to the γ-energies at 1428.56 and 2151.08 keV, which could depopulate a level at 2754.11 keV . The latter transition could be allowed, by Q_β restriction, to populate either the groundstate or the first excited state 602.85. The second choice was selected supported by the new energy 1428.56 keV that fits to also feed the 2_2^+ level. A level at 2806.56 keV could give rise to the transitions at 1557.24 and 2204.17 keV, but it was not supported by the coincidence evidence. In particular there was not a strong coincidence of the latter transition with the 603 keV gate [see Table (4.2)].

The 603 keV gating spectrum could not give a strong evidence for the new energy at 1757.66 [Table (4.2)] which could de-excite the proposed 2360.51 keV level.

Another level at 2579.7 keV is given on the evidence of the previously unplaced 1253.96 keV transition which very

weakly turned up in the 723 keV gate spectrum. On the other hand the new 621.48 keV energy was detected in the spectrum of the (710 + 714) gate with strength "P". This together with 1253.96 keV transition could be de-excited from 2529.7 keV level.

Previous investigations have confirmed the 1263.11 keV energy from ^{124}Sb decay, but were not able to put in the decay scheme of ^{124}Te. The present work detected this energy with strengths "W" and "VW" when the 723 and (710 + 714 + 723) keV windows were gated. Although these spectra do not provide a strong evidence, this transition might be ascribed to depopulate the 2589.04 keV level. Further support is given by the new 1340.38 keV energy, consistent to populate the 1248.86 keV level.

The 2598.1 keV level is mainly substantiated by the presence of a previously reported transition at 1272.38 keV, which had not been placed in the level scheme. This transition was strongly seen in the present coincidence with (710 + 714 + 723) keV gate, and subsequently could only populate the 1325.72 keV level since it cannot cascade with 710 keV nor with 714 keV line because of Q_β restrictions. As this transition did not show up in the spectrum of 723 keV gate, the coincidence events can possibly be due to a councidence with the background of the (710 + 714 + 723) keV window.

Another energy at 1301.71 keV, which had not been put in the decay scheme, was observed with strength "S" in both the spectra taken with gates 603 and (710 + 714 + 723) keV. As such the transition appears to be in coincidence with 723 keV line that in turn cascades to the 603 keV level. However, the 723 keV gating spectrum could only give a weak evidence, and so a level at 2627.43 is not firmly established.

The possibility of the existence of these eight levels could be inferred from the data given in Tables (4.1 and 2). However, the evidence was not regarded as strong enough to warrant their inclusion in the proposed decay scheme.

4.5 Discussion.

For ^{124}Te the energy level ratios R_4=2.1 and R_6=2.9 are far from the rotational expectations of 3.3 and 7.0, and are a consequence of the vibrational-like character of the nucleus (2.0 and 3.0 respectively). The interacting boson approximation (see Chapter 2) provides an elegant and powerful tool for the description of the collective properties of nuclei and the IBM will be applied to ^{124}Te.

The vibrational behaviour of collective states exhibited by the generators of the chain of sub-groups $U(6) \supset U(5) \supset O(5) \supset O(3) \supset O(2)$ is contained in the first two terms of Eq.(2.6.9). An analytical solution to the eigenvalue problem is achieved by diagonalysing H on the basis $|[N]n_d \; \nu \; n_\Delta \; L \; M>$ which labels the totally symmetric irreducible representations of SU(5). All the symbolic definitions of the quantum numbers and parameters given in this section are explicitly described in Chapter 2, unless specified.

In Fig.(4.11) each level is labelled by the quantum numbers (n_d, ν, n_Δ), and a close inspection of the decay scheme ^{124}Te [Fig.(4.10)] reveals few transitions which break the selection rules, Δn_d=0, ±1, of the SU(5) limit. One such case is the 3_1^+ (3,3,0) $\rightarrow$ 2_1^+ (1,1,0) transition at 1437 keV, but with only 3.6 % of the total B(E2) value of the 3_1^+ level. Also, 2.5 % of the B(E2) value from the 4_2^+ (3,3,0) level occurs to the 2_1^+ (1,1,0) level. Indications were that a slight breaking of SU(5) symmetry would suffice to explain the small splitting between members of the two phonon triplet (4_1^+, 2_2^+ and 0_2^+), especially if these were considered to fit experimentally determined levels at 1249, 1325 and 1156 keV.

One approach to considering a nearly vibrational nucleus in terms of a broken SU(5) symmetry has been suggested by Arima & Iachello (1976). As the last two terms in the Hamiltonian of Eq.(2.6.9) would be small (i.e. those other than the terms required in the SU(5) limit, they could be treated by the approximation of first order perturbation theory. A test of the first order perturbation applied to ^{110}Cd provided a

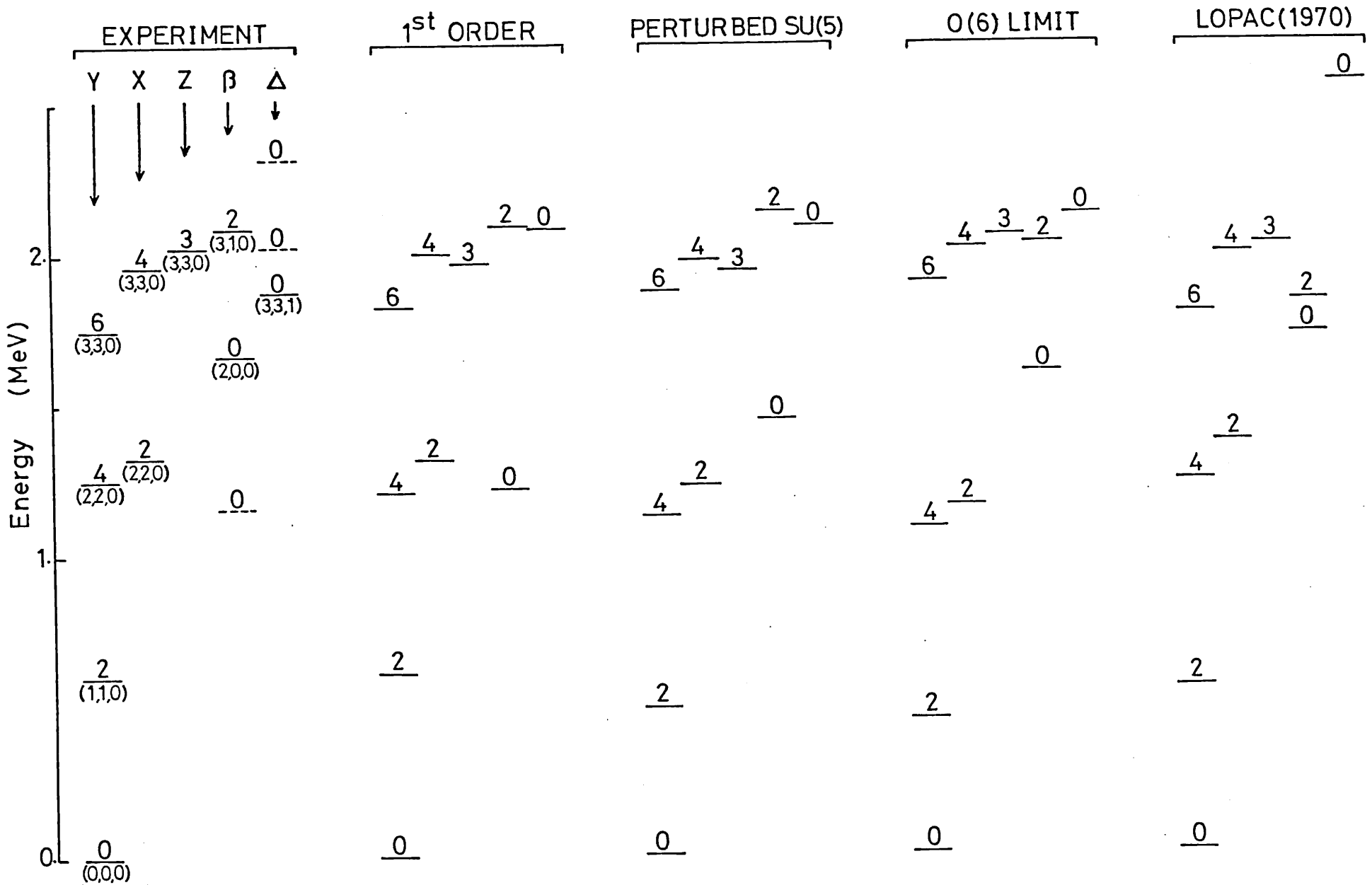

Fig.(4.11). The energy levels for the positive parity states of ^{124}Te are compared with IBA-1 predictions. The set on the right side is from the semi-microscopic description.

Table(4.5)
==========

The parameters used in the 1st order perterbation approximation to SU(5) ,and those obtained for the complete IBA-1 Hamiltonian.

1st order perturbation	: E 0.65	C(0) 0.0568	C(2) -0.0196	C(4) 0.0004	ξ 0.2	ξ' -0.3	q_2 0.2894	q_2' -0.0604
Complete Hamiltonian	: HBAR 0.37	C(0) -0.035	C(2) 0.09	C(4) 0.09	F 0.073	G -0.125	E2SD 0.1033	E2DD -0.0041
(UNITS)	: (MeV)	(MeV)	(MeV)	(MeV)			(eb)	(eb)

successful description of its collective behaviour [Arima & Iachello (1976)]. This treatment took N=6, as is required for ^{124}Te which has a similar assymmetry of protons with respect to the closed shell at Z=50. The application of the first order perturbation method to ^{124}Te produced the sequence of energy levels shown in column two of Fig.(4.11). The parameters used in this calculation are listed in Table (4.5), made to produce the best overall fit to the observed properties of ^{124}Te excited levels within the limited expansion of the parameters ($0.1 < \xi, -\xi' < 0.3$) and for the constraint $\xi' q_2' = 0.7/5^{\frac{1}{2}} \xi q_2$. It is seen from Fig.(4.11) that the overall agreement with the experimentally determined energy levels appears very good, especially if the fitted 0^+ states are those at 1156 and 2020 keV. Although the fitted 3^+ level at 1969 keV was shifted below the experimentally suggested 4_2^+ (3,3,0) level at 2040 keV, the B(E2) branching ratios for transitions depopulating this 3^+ level agree well with the calculated values as shown in Table (4.6).

The controversy surrounding the observance, with varying degrees of confidence by different authors, of several low-lying 0^+ states at 1156, 1290, 1657, 1883, 2020 and 2309 keV has been highlighted by the recent thermal-neutron capture work of Robinson et al.(1983), who confirmed only those at 1657 and 1883 keV, while suggesting the new level at 2309 keV.

TABLE(4.6)

Comparison between experimental [Johnson & Mann (1974) and present] B(E2) ratios and theoretical predictions of semi-microscopic approach [Lopac(1970)],1st order perturbation and perturbed SU(5) symmetry.

$\frac{B(E2;I_i-I_f)}{B(E2;I_i'-I_f'')}$	EXPERIMENT		THEORY		
	Johnson	Present	Lopac	1st order	SU(5)
$\frac{4_1 - 2_1}{2_1 - 0_1}$	--	1.43', 2."	1.46	1.64	1.38
$\frac{2_2 - 0_1}{2_2 - 2_1}$	0.0072	0.0067(2)	0.0034	0.026	0.035
$\frac{2_2 - 2_1}{2_1 - 0_1}$	--	5.80(16)	1.22	1.4	1.08
$\frac{4_2 - 2_1}{4_2 - 2_2}$	0.21	0.20(2)	2.6	0.04	0.012
$\frac{4_2 - 4_1}{4_2 - 2_1}$	30.0	34.0(20)	1.0	19.2	57.27
$\frac{4_2 - 2_2}{4_2 - 4_1}$	0.157	0.14(1)	0.38	1.3	1.41
$\frac{3_1 - 2_2}{3_1 - 4_1}$	5.3	5.35(34)	--	3.0	2.78
$\frac{3_1 - 2_2}{3_1 - 2_1}$	57.8	60.5(39)	800	22.8	22.22
$\frac{3_1 - 4_1}{3_1 - 2_1}$	10.9	11.3(6)	--	7.63	7.99

' Assuming a rotational model.
" A pure vibrational value.

The level at 1290 keV was reported by Christensen et al.(1970) on slender evidence from a ^{124}Te (d,d′) experiment and has not been confirmed since. The β^- decay of ^{124}Sb will preferentially populate the states with spin 2, 3, or 4 in ^{124}Te, while the EC/β^+ decay of ^{124}I can directly feed lower spin states. As a result of γ-γ coincidence studies of the latter decay, carried out to look for $0^+ \rightarrow 0^+$ transitions, Zhelev et al.(1972) reported 0^+ states at 1156, 1657 and 2020 keV. Of these, that at 1657 keV has been also established from ^{124}Sb decay experiments, such as the present work, in which it is accessible by gamma feeding. Although those levels at 1156 and 2020 keV have not been confirmed from other experiments, the ^{124}I decay has not been subsequently re-investigated. The present calculations clearly show [in Fig.(4.11), the unlabelled dashed lines of the experimental column are those 0^+ states that may be alternatives, in a given band, for other 0^+ levels with the same quantum numbers (n_d, ν, n_Δ)] that the existence, or otherwise, of such levels has an important bearing on the extent to which a purely vibrational description reveals the true character of the ^{124}Te nucleus.

In order to shift the first excited 0_2^+ state upwards, pushing the (2,0,0) level closer to the 0_3^+ (3,3,1) member of the three phonon quintet, a larger splitting between the levels of the two phonon triplet is required. This breaking of SU(5) symmetry can be accommodated by increasing the weight of the last two terms in the Hamiltonian of Eq.(2.6.9), thus moving away from a simple first order perturbation treatment. The program PHINT was used to investigate this possibility, and with the program FBEM the effect on B(E2) branching ratios was also determined; the levels shown in column three of Fig.(4.11) were obtained with the parameter listed in Table (4.5). These parameters, which were obtained using the methods described in the program package PHINT, indicate a departure from the SU(5) limit, but the branching ratios so obtained [Table (4.6)] show no overall improvement from those of the first order approximation as expected for the low-lying levels far from the top of the band n_d=N, a similar comment applies to the B(E2) values in Table (4.9). For the two phonon triplet, it was shown by Arima & Iachello (1976) that a higher value of

Table(4.7). Comparison between experiment and predicted B(E2) values (e^2 fm^4) in ^{124}Te and experimental and predicted (IBM) quadrupole moment of the first excited state 2_1^+.

Transition ($I_i - I_f$)	Experiment^	Lopac (1970)	1st order perturbation	Complete Hamiltonian	F
$2_1 - 0_1$	1140(18)	1420	1140	1145	31.
$4_1 - 2_1$	1630", 2280'	2080	1874	1581	51.
$2_2 - 0_1$	44(22)	6	41	44	1.1
$2_2 - 2_1$	6220(3230)	1740	1598	1242	169.

	EXPERIMENT*	CALCULATED
Q(2) (in eb)	- 0.16 (8) - 0.41 (8)	- 0.33

^ Lifetimes taken from Lederer et al. (1978).
" Assuming a rotational model.
' A vibrational model using the ($2_1 \rightarrow 0_1$) value.
* Quoted from Kleinfield et al.(1975).
F = $B(E2;I_i - I_f)/B(E2)_w$

ξ lowers the $0_2^+ - 2_1^+$ transition rate relative to the $4_1^+ - 2_1^+$ and $2_2^+ - 2_1^+$ (with respect to $2_1 - 0_1$). The experimental B(E2) ratio $(2_2 - 2_1/2_1 - 0_1)$=5.46 ± 2.84 was far from the first order perturbation prediction, which gave 1.4, though ξ was kept relatively low (0.2). However the complete Hamiltonian gives a value of 1.08 which indicates departure from the conventional vibrational value of 2.0. The predictions of the earlier semi-microscopic approach by Lopac (1970) are given for comparison in Fig.(4.11) and Tables (4.6 and 7).

The shift of the 0_2^+ level above its two phonon members has been interpreted by Jackson & Meyer (1977) as a softness of the nucleus with respect to γ-deformation since the partial filling of the $h_{11/2}$ shell is with pairs of neutrons occupying either prolate or oblate-driving orbitals. A similar effect was also noticed by Stachel et al.(1982) when studying the transitional SU(5)–O(6) trend of nuclei in the mass region near A=100. The latter work suggested that the onset of O(6) characteristics were signalled by observing the displacement

of 0^+ members of the two and three phonon multiplets (n_d=2, 3) of the SU(5) limit. Whereas the semi-microscopic approach of Lopac (1970) does not consider these behaviours as simple n phonon states as the phonon energy $\hbar\omega$ was partially treated as free parameter.

Recently the nucleus of ^{124}Te was considered in terms of the IBM O(6) limit by Robinson et al.(1983), and as a check their parameters were used to reproduce the levels in the O(6) limit [see Fig.(4.11)]. For comparison, when the two 0^+ states [given in notations as (2,0,0) and (3,3,1)] are considered to be at 1657 and 1883 keV respectively, it was found that the average energy spread quoted between the experimental and predicted levels is 115 keV for the full SU(5) Hamiltonian and 121 keV for the results of Robinson et al.(1983). Fig.(4.11) clearly shows the features of the level structure change as the transition from SU(5) to the O(6) limit is made. As a check, the brocken SU(5) parameters of the Hamiltonian produced in this work were tested with the parametrization given by Dieprink & Scholten (1980) in terms of ζ and η in order to inspect the deviation from SU(5) towards the O(6) limit.

$$\zeta = \frac{\eta}{1+\eta} \qquad \text{and} \qquad \eta = \frac{4a_0}{\varepsilon''}(N-1)$$

ε'' and a_0 referred to the parameters of the d-boson energy and the pairing force of the completely equivalent multipole expansion Hamiltonian [Eq.(2.6.1)]. These parameters mainly reflect the strength in character η of SU(5) ($\varepsilon''\neq 0$) and O(6) ($a_0\neq 0$). In this parametrization, the shape phase transition of ground state properties was reported to occur at ζ=0.5 which yields η=1, while the calculations of the present parameters give $\eta\simeq 3$ and ζ=0.75, indicating considerable shifting from SU(5) to O(6) limits. The movement of the 0_2^+ level away from the 4_1^+ and 2_2^+ levels is a clear consequence of the onset of an O(6) character. But also equally clear for the ground state band, as the O(6) limit is approached, is the closing up of the level spacing between the lower spin (0^+, 2^+, 4^+) members, while a much larger gap than experimentally observed is opened up between the spin 4 and spin 6 levels.

CHAPTER V

PROPERTIES OF ^{154}Gd NUCLEUS FROM THE DECAY OF ^{154}Eu.

5.1 Introduction.

The ^{154}Gd nucleus with 64 protons and 90 neutrons lies at the edge of the so-called region of strong deformation between the spherical and deformed nuclei. An abrupt transition from the vibrational to the rotational pattern is observed between 88 and 90 neutrons in Gd(Z=64) isotopes as well as in Sm(Z=62) isotopes [Scharff-Goldhaber et al.(1976)]. The reason appears to be that the $h_{11/2}$ shell breaks up as a function of deformation [Mottelson & Nilsson (1955)], which causes the similarity in character of the N=90 isotones as shown by the ^{152}Sm and ^{154}Gd nuclei. However ^{154}Gd is expected to exhibit some of the properties characteristic of spherical-transitional nuclei and the predictions of the collective model can be tested against the properties of this nucleus.

The simple Bohr-Mottelson approach is to assume that the nucleus is an axially symmetric rotor, the rotational and intrinsic motions of which do not disturb each other. This allows the E2 transition matrix element between members of two collective bands to be expressed as a product of a Clebsh-Gordan coefficient and a reduced matrix element which is independent of the spin of the levels involved. A ratio of reduced E2 transition probabilities between members of such bands is then merely a ratio of the appropriate Clebsh-Gordan coefficients squared [Alaga et al.(1955)]. However, it has been known that these simple predictions do not hold and that the adiabatic assumption for the axially-symmetric nucleus is the source of the problem. Non-adiabatic coupling of the intrinsic and rotational motion of the nucleus mixes the wave functions of the vibrational and rotational bands and leads to corrections in the predicted reduced E2 transition probability B(E2). The mixing β, γ and the ground state bands have been discussed for ^{154}Gd by Riedinger et al.(1967, 1969) in terms of a band mixing parameter Z_K which measures the rotational-vibrational interaction (the subscript K labels the vibrational band

considered). For the β- and γ- vibrational bands, the effect of band mixing is to redefine the reduced E2 transition probability B(E2) in terms of the unmixed transition probability, the mixing parameter and other spin-dependent terms. The inconsistency found in the Z_γ values as determined from different transitions [Riedinger et al.(1969)] for ^{154}Gd was significant and they showed that the additional inclusion of any M1 admixture in the 2_γ-2_1 transition, would result in clear disagreements between Z_γ values from the 2_γ state. There also appeared to be real differences in the Z_β values, which remained unexplained. A pure E2 component for 2_β-2_1 transition was adopted during their calculations [as reported by Hamilton et al.(1967)], which might had led to these variations. Furthermore, these discrepancies could not be fully removed by the inclusion of a correction for mixing of the β and γ bands, and it was thought that mixing of additional excitations into K=0 and K=2 bands would be required.

The simple I(I+1) rule for the energy level sequence of a deformed nucleus resulting from the adiabatic model is found experimentally to be incapable of describing its rotational spectrum. The non-adiabatic interaction affects the mean square radius of the rotating nucleus and can perturb the energies of the ground state rotational band. These effects have been experimentally tested in ^{154}Gd by means of the Z_K parameters by Riedinger et al.(1969), who also highlighted the similarities between ^{152}Sm and ^{154}Gd nuclei in terms of electric monopole matrix elements of radiations.

For the nucleus ^{154}Gd, Ng et al.(1968) compared the unified model of deformed nuclei, introduced by Bohr & Mottelson (1953), with the asymmetric rotator description of Davydov & Chaban (1960) and Davidson & Davidson (1965). Both models were found to give almost equal results for the B(E2) ratios when calculated for a few low-lying states. The energy levels of the g.s, β- and γ- bands were well produced up to levels spin of 4^+. On the other hand, the octupole states of a purely spherical nucleus are expected to be fragmented into components when the nucleus becomes deformed. Consequently, bands with K^π of 0^-, 1^-, 2^- and 3^- should be expected in the ^{154}Gd nucleus.

However, the suppressed levels in $K^{\pi}=0^{-}$ band and the inverted sequence of levels observed in $K^{\pi}=1^{-}$ band were suggested by Meyer (1968) to be a result of two types of Coriolis force acting on the $K^{\pi}=0^{-}$, 1^{-}, and 2^{-} bands: (1) a rotational-vibrational coupling (RVC) Coriolis type interaction acting on the $K^{\pi}=0^{-}$ and $K^{\pi}=1^{-}$ bands and (2) a pseudo-rotor-particle coupling (p.RPC) Coriolis-type force acting on the $K^{\pi}=1^{-}$ and $K^{\pi}=2^{-}$ bands. The latter suggestion is consistent with the previous calculations performed on the basis of a super-conducting model of strongly deformed nuclei as given by Soloviev et al.(1964 a and b). The states proposed by Soloviev were more pure two-quasi-particle than collective, so that higher K bands are less collective in nature.

In a later paper, Riedinger et al.(1970) pointed out that the inverted ordering of the states in the 1^{-} band in ^{154}Gd is in contrast to the normal level ordering in ^{152}Sm though the quadrupole-vibrational bands are quite similar. Neergard & Vogel (1970) also predicted the inverted sequence of the $K^{\pi}=1^{-}$ band in ^{154}Gd and a good agreement with the experimental results was obtained for the calculated band structure. The pairing plus modified octupole-octupole force was used as the residual interaction, and also included, the Coriolis interaction matrix elements between states with K and K+1 bands.

The energy spacing of successive high spin members of positive bands were studied by West et al.(1978): a comparison between the available data in ^{154}Gd and the theoretical predictions of Neergard & Vogel (1970) for the energy levels of negative parity states was also made. It is also worth mentioning that Giberti & Maglione (1981) have attempted to explain the properties of this nucleus by taking into account the coupling of

A) three $K^{\pi}=0^{+}$ and one $K^{\pi}=2^{+}$ bands,

B) two $K^{\pi}=0^{+}$, a $K^{\pi}=2^{+}$ and a $K^{\pi}=4^{+}$ bands.

This four band mixing analyses have nicely produced the properties of both the yrast and yrare states (energy levels and

B(E2) values up to high spin levels for both g.s. and beta bands) including the backbending phenomena observed in these bands.

Many attempts have been made to unify the description of rotational and vibrational nuclei. However, calculations of the energy spectra of transitional nuclei provide a strict test of models since the nuclei may not be adequately described by assuming some geometrical shape or symmetry limit. However the description provided in the IBA model has developed a unified algebraical description of the collective motion.

In fact, the first use of the IBM to describe Gd nuclei was given by Scholten (1980) in terms of IBA-2. This investigation provided a good level fit to the g.s. band but not for the β- or γ-bands. An extended version of the IBA model to account for states outside the s-, d-boson space was given by Van Isacker et al.(1982). It was made by the inclusion of s′-, d′-bosons to account for the so-called "intruder states", and g- (hexadecupole) bosons to incorporate the properties of $K^{\pi}=4^{+}$ band in Gd. This study concentrated on fitting the positive parity levels of the g.s., β-, γ-, second $K^{\pi}=0^{+}$ and $K^{\pi}=4^{+}$ bands. The B(E2) values obtained were in good agreement with the experimental data.

As it has been pointed out by Casten & Warner (1982), the structure of the IBA wave functions in the SU(3) limit (which in IBM applied to Gd refers the rotational limit) is such that the $K^{\pi}=2^{+}$ band contains a small admixture of $K^{\pi}=0^{+}$. This is related to the fact that the wave function of the SU(3) band can be expressed in terms of the Vergados basis whereas a scheme involving pure K bands is the Elliot basis. Therefore the deviations from Alaga rules, which in the geometrical model arise from band mixing, comes in the IBA space from two sources, one a kind of K mixing, and the other an explicit dependence on boson number. This is the background to the present work which examines the band structure in ^{154}Gd in the framework of the IBA-1. The observed bands in the present work are the g.s., β-, γ-, second $K^{\pi}=0^{+}$, second $K^{\pi}=2^{+}$ and $K^{\pi}=4^{+}$ bands for the positive parity levels. The common transitional

Hamiltonian that explains the region SU(3)-SU(5) was not adequate enough to cover the decay scheme of this nucleus. An additional perturbation of P.P or Q.Q terms are both considered. This has been calculated in the s- and d-boson space alone using the program codes PHINT & FBEM to get both levels and branching ratios. The discussion is also extended to examine the octupole states found in this work which are ascribed to $K^{\pi}=0^{-}$, 1^{-} and 2^{-} bands. Further test to the octupole states is made to measure the consequent effect of Coriolis force, acting on neighbouring bands with K and K+1, in predicting B(E1) values. The B(E1) values calculated show a good agreement with the experimental results.

Attention is also focussed to the expectation of the Z=64 closed shell on the behaviour of ^{154}Gd nucleus. As this nucleus has 64 protons and 90 neutrons, the use of the so-called "hybrid" parameters described by Gill et al.(1982) refer the proton boson number to the Z=82 closed shell. The consideration of the Z=64 closed shell would then result in an increase of the total boson number with respect to the normal way of counting the boson number from the valence nucleons to nearest closed shells.

5.2 Previous Investigations.

The nucleus of ^{154}Gd has always invited study as it exhibits interesting transitional characteristics and can be readily studied with high resolution γ detectors in order to build up such a complicated decay scheme. As the energy levels of ^{154}Gd can be fed by either the β^{-}decay of ^{154}Eu or from ^{154}Tb by electron capture and positron emission from at least three isomeric states: the methods of studying this nucleus varies and reaches high spin states through the latest development on nuclear excitation measurements.

The decay ^{154}Eu to ^{154}Gd reported by Ng et al.(1968) was able to add several γ-ray energies to the decay scheme of Harmatz et al.(1961) on the basis of energy fitting. A Ge(Li) detector and a magnetic spectrometer was used to study the γ-rays and the conversion electron spectra of ^{154}Eu decay. The

K and L internal conversion electron measurements were carried out by Brantley et al.(1968) on an iron-free double-focussing spectrometer.

More comprehensive work on ^{154}Eu decay was made by Meyer (1968) employing Ge(Li) Compton suppression spectrometer. Over one hundred and fifty γ-rays were detected and ascribed to thirty-two different levels. However only four γ-coincidence gates at 123, 248, 188 and 700 keV were taken to aid the construction of the level scheme. The energy levels were put into bands: five of these for positive parity states, are the g.s., β-, γ-, $K^{\pi}=0^{+}$ and $K^{\pi}=2^{+}$ bands, and three others with $K^{\pi}=0^{-}$, 1^{-} and 2^{-} bands for the negative parity states. Other levels were not ascribed to any of these bands and twenty-one energies were not placed in the decay scheme.

Riedinger et al.(1970) only detected 51 γ-rays in their studies on ^{154}Eu decay using Ge(Li) detectors, and did not confirm fourteen levels at 717.96, 1136.07, 1277.6, 1292.75, 1415.6, 1418.36, 1509.1, 1698.26, 1770.3, 1790.4, 1796.78, 1838.0, 1861.4 and 1894.69 keV as obtained by Meyer (1968).

The γ and electron conversion spectra of Nagpal & Gaucher (1972) observed in solid state detectors improved the available conversion electron data and reported 12 energies with low intensities already seen by Meyer (1968) but not confirmed by Riedinger et al.(1970).

The γ-γ directional correlations and coincidence studies of Gupta et al.(1977) provided additional information about the decay of ^{154}Eu made with a multiparameters γ-γ coincidence system, employing two Ge(Li) detectors. The twenty-one gating spectra confirmed some levels of Meyer (1968) at energies 718. , 1414.5, 1418.3,1698.3, 1790.4 and 1796.7 keV. These gates were at 123, 188, 248, 301, 305, 347, 557, 582, 625, 676, 692, 715, 757, 845, 892, 924, 996, 1005, 1118, 1128 and 1274 keV. The multipole mixing ratios of some transitions were also measured in their work. Additional information about the multipole mixing ratios were also given through β-γ-γ studies of Rathore & Singh (1979) and by Sharma et al.

(1982).

The latest work on ^{154}Eu decay studied the γ-ray energies and intensities was made by Sharma et al.(1979). A total of 82 transitions were observed and a few weak γ-transitions were reported. Thirty-two more energies of Meyer (1968) were given and the levels at 1136.07, 1277.6, 1292.75, 1509.1, 1698.26, 1770.3, 1790.4, 1838.0, 1861.4 and 1894 keV were not confirmed in their work.

Many studies have also been devoted to study ^{154}Tb decay to levels in ^{154}Gd from at least three isomeric states [Harmatz et al.(1961), Riedinger et al.(1971)]. The work of Sousa et al.(1974) provided a full study from three isomeric states of ^{154}Tb, measuring energies, intensities, conversion electron and multipolarities of γ-transitions using Ge(Li), Si(Li) and γ-γ coincidence measurements. Multipole admixtures of γ-ray transitions have also been investigated by Whitlock et al.(1971), Ober et al(1973), Gono & Sugihara (1974) and Sie et al.(1977). Inelastic deuteron scattering results of Block et al.(1967) were able to assign the spin-parity of a few high energy levels in the ^{154}Gd nucleus. While the levels populated from ^{154}Tb decay and those from (α, 2nγ) nuclear reaction studies by West et al.(1978) provided additional informations for higher spin levels of ^{154}Gd.

Single spectra and coincidence relationships with twenty-two gates have been obtained employing Ge(Li) & Ge detectors, Compton suppression spectrometer and the DPDCS. The half-life of the first excited state in ^{154}Gd was also measured using coupled Ge(Li) and plastic detectors in a delayed coincidence mode. One hundred and fifteen energies were identified and referred to thirty different levels that were established from γ-γ coincidence results. Many transitions reported earlier by Meyer (1968) from anti-Compton experiments in addition to six levels at 1277.33, 1509.1, 1770.3, 1838.22, 1860.86 and 1895.82 keV are confirmed and established in the decay scheme. The multipolarities of some of the transitions were deduced from K, L and M conversion coefficients using the latest works on conversion electron measurements.

The calculations were extended to determine the beta feeding branching ratios, log ft values, E_β, spins and parities of all observed thirty levels. These are also referred to nine bands (six positive bands and three negatives) and are discussed initially in terms of the adiabatic symmetric rotor model.

5.3 Experimental Procedure and Results.

5.3.1 Radioisotope.

Europium oxide (Eu_2O_3) powder (4mg) enriched in ^{153}Eu was irradiated in ULRC with neutron flux of 10^{12} $n.cm^{-2}.sec^{-1}$ for seven hours. The (n,γ) reaction gave ^{154}Eu having activity of ~10 μCi. Details of irradiation process have been described in Chapter I section 2.

^{154}Eu decays by β^- emission, with conflicting half-lives variously reported as 8y or 16y, to the stable even-even nucleus of ^{154}Gd. A negligible fraction (0.02%) decays through EC to ^{154}Sm. A recent experiment concerning the half-life of ^{154}Eu, still being carried out at ULRC, favours the value of 8-9y.

After irradiation, the isotope was kept for a month before use to allow background contamination to die away. A small percentage of ^{152}Eu (13y) had been observed to exist in the spectrum of ^{154}Eu, and special attention was taken to correct for some lines being superimposed from both spectra.

5.3.2 Single Spectra.

The γ-ray spectrum of ^{154}Eu contains more than one hundred energies between 50 and 1900 keV. Many of these γ-ray lines have also weak intensities.

Three spectra were collected from the 12% Ge(Li) detector [refer to Table(3.1) for specifications], together with a Compton suppression spectrometer, as only previously carried out by Meyer (1968), to be analysed with the computer program SAMPO for the purposes of peakfitting and energy

Table(5.1). Comparison between present relative intensities (I_γ) of gamma-ray transitions with previous works in ^{154}Eu decay (normalised to I_γ(1274.45)=100.).

Energy (keV)	I_γ Meyer	I_γ Riedinger	I_γ Sharma	I_γ Present	Levels(keV) From	To
58.32(22)	0.012(1)			0.0020(3)	1719	1661
79.92(22)	0.009(4)			0.009(1)	1128	1047
123.00(05)	121.	116.(6)	115.39(226)	113.62(134)	123	000
131.69(22)	0.033		0.037	0.037(4)	1128	996
134.81(10)	0.022		0.03	0.011(2)	815	681
138.00(24)	<0.003			0.008(4)		
142.98 P	<0.002			0.008 P		
145.93(21)	0.078	0.085(27)	0.021	0.028(3)	1397	1251
155.92(11)	0.03		0.025	0.022(3)	1397	1241
159.92 P	<0.003			0.0014 P		
180.72(36)	0.013(3)		0.015	0.005(2)	996	815
184.71 P	0.012(3)		0.017	0.012 P		
188.26(05)	0.68	0.61(12)	0.70(12)	0.623(8)	1719	1531
232.22(20)	0.072	0.079(43)	0.081(40)	0.078(4)	1048	815
237.03(22)	0.018(12)		0.026	0.0135(12)	1796	1560
247.93(05)	19.7	20.1(10)	19.34(37)	19.75(18)	371	123
260.81 P	0.006(3)			0.015 P		
263.45(15)				0.006(2)	1661	1559
267.77(08)	0.042		0.023	0.044(3)	1263	996
					1531	1264
269.89(13)	0.021(3)		0.01	0.020(2)	1397	1128
290.35(10)	0.01			0.032(10)	1531	1251
301.24(16)	0.004(3)		0.032	0.038(4)	1719	1418
305.02(13)	0.053		0.07	0.059(4)	1719	1415
309.07(49)	<0.005		0.01	0.039(5)		
312.12(13)	0.044		0.06	0.058(6)	1128	815
315.63(20)	0.014		0.03	0.028(4)	996	681
322.02(12)	0.2	0.16(4)	0.21(4)	0.170(5)	1719	1397
329.73(12)	0.027	0.036(26)	0.032	0.036(5)	1048	718
346.72(49)	0.09		0.067	0.104(20)	718	371
370.78(44)	0.016(4)		0.03	0.016(6)	1418	1048
382.10(13)	0.03		0.028	0.024(6)	1646	1263
397.23(13)	0.09	0.12(5)	0.12(4)	0.108(10)	1661	1264
401.27(09)	0.63	0.58(10)	0.57(8)	0.546(10)	1397	996
403.57(39)	0.081	0.054(32)	0.042(4)	0.045(7)	1531	1128
421.84(21)	<0.004			0.01(1)	1418	996
435.60(56)	<0.008			0.011(8)	1251	815
444.42(03)	1.5	1.69(15)	1.54(3)	1.6(2)	815	371
448.84(10)				0.017(5)	1264	815
467.98(06)	0.17	0.20(9)	0.16(8)	0.204(15)	1719	1251

Continued

Energy (keV)	I_γ Meyer	I_γ Riedinger	I_γ Sharma	I_γ Present	Levels(keV) From	To
478.29(10)	0.64	0.69(15)	0.63(10)	0.664(8)	1719	1241
483.79(10)	0.015		0.04	0.049(5)	1531	1048
506.28(20)	0.018(6)			0.014(2)	1770	1264
510.32(26)	0.11	0.17(8)	0.14(8)	0.058(8)	{1646	1136}
512.39(47)	<0.12			0.189(7)	1560	1048
518.05(12)	0.14	0.16(9)	0.18(8)	0.146(6)	1645	1128
524.40(06)				0.017(6)	{1160	1136}
532.80(09)	0.030(6)		0.032	0.035(8)	1661	1128
				0.071(16)	1796	1264
538.89(22)				0.0049(15)	1790	1251
546.00(22)	0.050(7)			0.048(9)	1264	718
557.59(10)	0.76	0.74(10)	0.72(10)	0.765(9)	681	123
569.36(22)	0.03		0.044	0.034(7)	1617	1048
574.35(08)				0.007(1)	1838	1263
582.12(09)	2.51	2.53(23)	2.45(5)	2.65(2)	1397	815
591.81(08)	14.5	14.8(8)	13.57(26)	14.57(8)	1719	1128
598.10(57)	0.018		0.026	0.031(15)	1646	1048
602.73(08)	0.018(12)		0.10	0.098(9)	1418	815
613.39(27)	<0.018	0.22(8)	0.25(8)	0.283(11)	1661	1048
625.33(08)	0.93	0.89(12)	0.84(5)	0.936(9)	996	371
649.56(09)	0.23	0.28(11)	0.25(8)	0.253(8)	1646	996
651.10(25)	0.03			0.020(2)	1699	1048
664.50(24)	0.09		0.072	0.089(12)	1661	996
669.2 (10)	0.035(9)		0.042	0.039(5)	1048	371
676.63(09)	0.43	0.43(11)	0.52(10)	0.471(13)	1048	371
692.41(09)	5.06	4.97(30)	4.92(10)	5.11(3)	815	123
701.91(12)	0.014			0.057(16)	1699	996
715.85(08)	0.52	0.32(13)	0.61(8)	0.554(23)	1531	815
723.30(08)	58.8	60.1(31)	55.33(106)	58.74(26)	1719	996
738.03(15)	<0.025			0.022(9)	1418	681
756.87(09)	13.0	12.9(6)	12.62(24)	13.36(6)	1128	371
800.31(23)	0.100(15)			0.057(8)	1796	996
815.54(09)	1.39	1.38(18)	1.47(10)	1.50(1)	815	000
845.43(09)	1.64	1.60(22)	1.58(10)	1.668(13)	1661	815
850.67(09)	0.69	0.60(13)	0.67(8)	0.689(13)	1531	681
873.19(09)	34.3	34.8(17)	34.47(70)	35.07(14)	996	123
880.70(24)	0.25	0.20(8)	0.28(8)	0.31(4)	1251	371
892.79(09)	1.37	1.31(10)	1.43(3)	1.427(14)	1264	371
904.09(09)	2.46	2.42(17)	2.49(5)	2.61(1)	1719	815
906.40(08)	0.036			0.031(31)	1277	371
919.48 P	0.037			0.016 P		
924.67(12)	0.18	0.19(10)	0.18(10)	0.192(8)	1048	123
943.90(34)				0.043(18)		
949.64(29)				0.051(12)		

Continued

Energy (keV)	I_γ Meyer	I_γ Riedinger	I_γ Sharma	I_γ Present	Levels (keV) From	To
981.59(49)	0.02	0.02		0.024(4)	1797	815
984.29 P	0.019(10)			0.031 P		
996.27(08)	30.8	29.4(15)	30.30(65)	30.21(12)	996	000
1004.77(08)	51.8	50.6(25)	51.40(103)	52.00(64)	1127	123
1012.79(21)	0.009(4)			0.010(1)	{1136	123}
1024.40(29)	0.020(9)			0.032(16)		
1029.18(21)				0.02(1)		
1032.93 P	0.036			0.0134 P		
1047.24(09)	0.15		0.23(10)	0.157(11)	1418	371
1049.79 P	0.052			0.028 P		
1056.01(12)				0.123(19)	{1179	123}
1059.43(19)				0.142(19)	1430	371
1072.16(19)	<0.01			0.0309(13)	1790	717
1118.44(19)	0.31	0.30(8)	0.37(10)	0.304(13)	1241	123
1128.68(09)	0.020(3)	0.79(9)	0.94(8)	0.864(11)	1251	123
1140.73(09)	0.65	0.69(10)	0.73(8)	0.661(9)	1264	123
1153.11(44)	0.04(1)			0.011(4)	{1524	371}
1160.48(09)	0.13	0.10(3)	0.13(10)	0.138(7)	1531	371
1180.69(10)				0.010(1)	1861	681
1188.27(09)	0.24	0.23(5)	0.29(8)	0.286(7)	1560	371
1216.70 P	<0.01			0.015 P		
1241.25(09)	0.39	0.30(7)	0.40(5)	0.355(12)	1241	000
1246.15(09)	2.08	2.40(22)	2.48(10)	2.42(2)	1617	371
1274.45(09)	100.	100.	100.	100.	1397	123
1290.47(22)	0.073	0.068(26)	0.086(20)	0.093(9)	1661	371
1292.19(42)	0.04			0.029(9)	1415	123
1295.50(32)	0.030(3)		0.026(3)	0.027(6)	1418	123
1317.07 P		0.074(29)	0.053(10)	0.009 P		
1408.50(20)	0.063(9)		0.082(10)	0.066(5)	1531	123
1414.90(19)	0.01		0.004	0.010(2)	1415	000
1418.05(20)	0.022	0.027(16)	0.039	0.044(4)	1418	000
1419.18(16)	0.005			0.0050(6)	1790	371
1489.91(60)	0.009(2)			0.0134(17)	1861	371
1494.10(11)	1.94	1.88(9)	1.91(8)	1.98(2)	1617	123
1509.20(12)	0.015(3)			0.039(5)	1509	000
1531.43(30)	0.018	0.009(5)	0.018(5)	0.018(4)	1531	000
1537.93(12)	0.15	0.15(2)	0.15(1)	0.157(7)	1661	123
1596.54(15)	4.98	5.15(26)	4.81(10)	5.02(4)	1719	123
1666.87(20)	0.0060(9)			0.0116(5)	1790	123
1673.84(15)	0.004(1)		0.006(1)	0.005(1)	1796	123
1737.47(40)				0.009(4)	1861	123
1838.21(25)	0.0024(6)			0.0072(8)	1837	000
1895.82(30)	0.0020(6)			0.0043(6)	1896	000

P Probable energy transition.
{ } Transition is not confirmed in this place.
( ) Error corresponding to the last digital quoted value.

calibration as described in Chapter III. The Compton suppression spectrum is shown in Fig.(5.1). Also the low energy region was further studied utilizing the Ge(I) detector (No.4) to confirm the small peaks observed in this region, and to complement the use of the Ge(Li) detector near the 100 keV region.

A total of one hundred and fifteen energies have been observed in the singles in addition to ten others not firmly confirmed in this work [denoted P for probable in Table(5.1)]. Many energies seen by Meyer (1968) have been identified as originated from background radiations. These are not listed in the table, whereas the present work confirms the twenty-five energies at 58.32, 79.92, 138.0, 290.35, 421.84, 435.6, 506.28, 512.39, 546.0, 651.1, 701.91, 738.03, 800.31, 906.4, 1012.79, 1024.4, 1072.16, 1153.11, 1292.19, 1419.68, 1489.91, 1509.2, 1666.87, 1838.21 and 1895.82 as reported by Meyer (1968), but not seen by Riedinger et al.(1970) nor Sharma et al.(1980). Twelve γ-ray energies are identified with small relative intensities and suggested for the first time. These energies are 263.45, 448.84, 524.4, 538.89, 574.35, 943.9, 949.64, 1029.18, 1056.01, 1059.43, 1180.69 and 1737.47 keV. Energies and intensities [Table(5.1)] are corrected for ^{152}Eu lines using the latest available data as by El-Daghmah (1982). The relative intensities are all normalized to 100 at 1274.45 keV and it is seen from Table(5.1) that the present results are consistent with and add to those given in the latest experiments.

5.3.3 Coincidence Spectra.

The coincidence spectra obtained were recorded on four large magnetic tapes to accumulate sufficient counts for a gating spectrum. A typical total spectrum of ^{154}Eu decay is shown in Fig.(5.2).

Constructing the decay scheme from coincidence relationships was achieved by gating twenty-two different peak at energies 123, 188, 248, 268, 301, 347, 444, 558, 582, 592, 677, 716, 723, 845, 873, 893, 1005, 1118, 1129, 1188, 1246 and 1292 keV: the gating spectra were generated from the 10% efficient

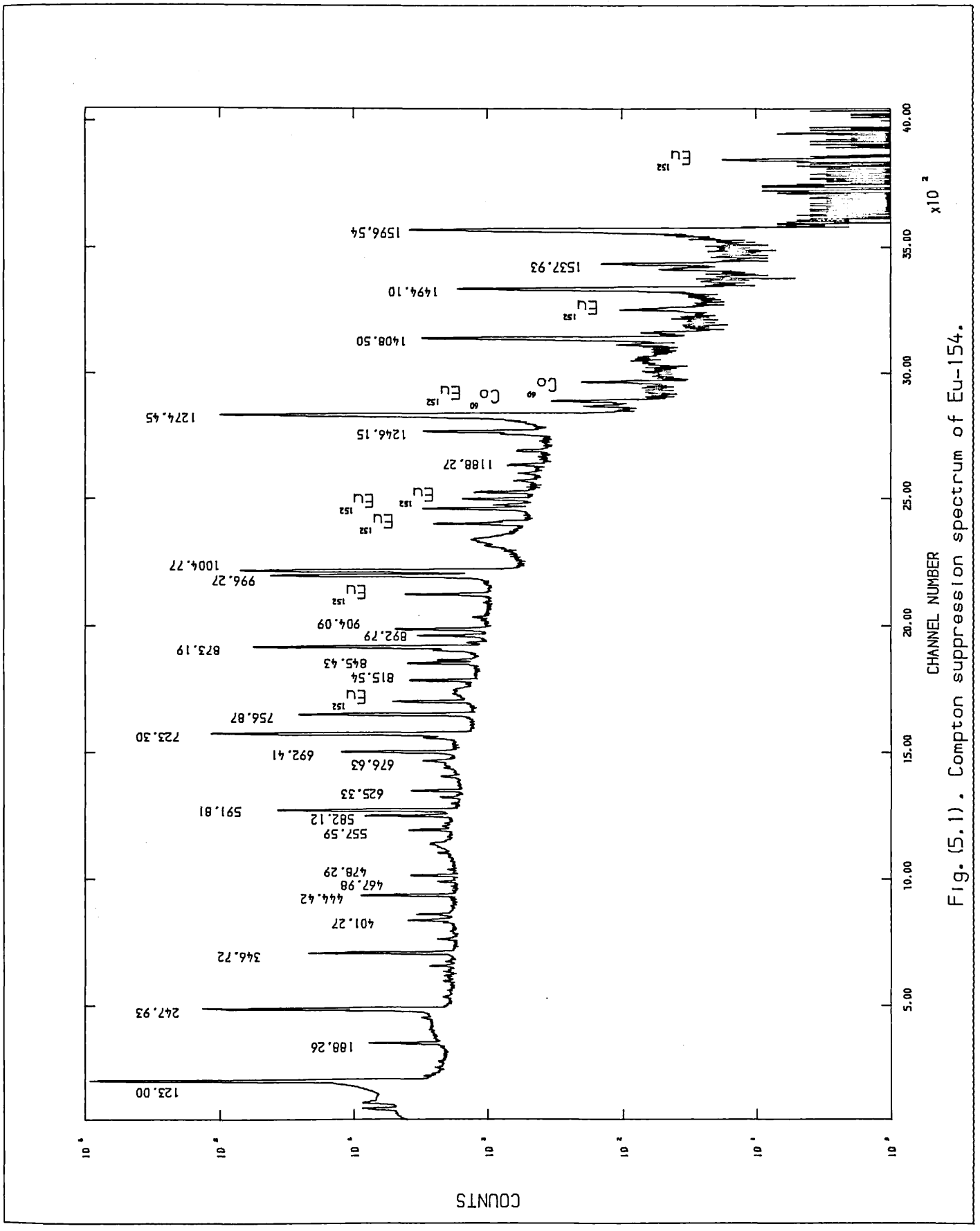

Fig. (5.1). Compton suppression spectrum of Eu-154.

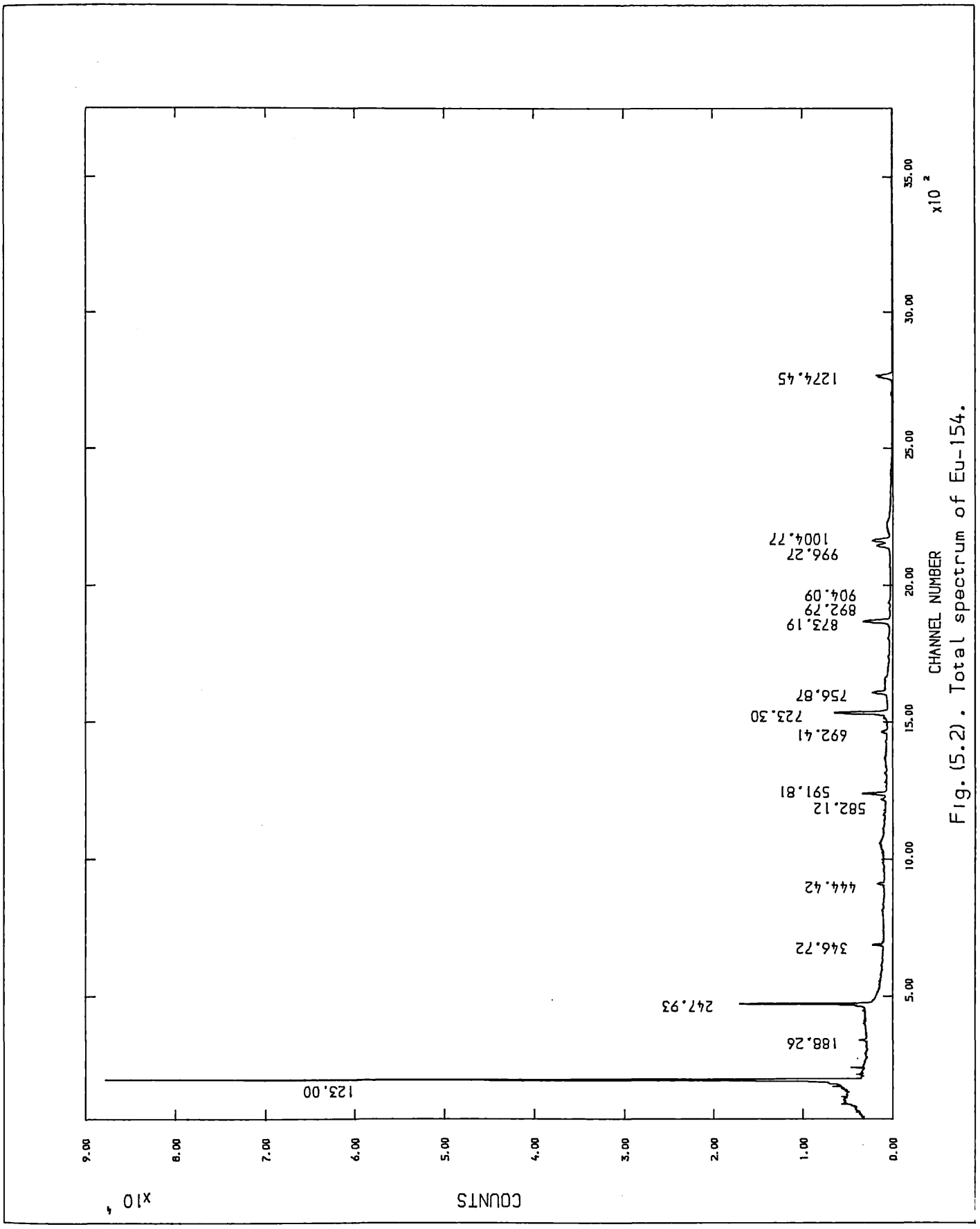

Fig. (5.2). Total spectrum of Eu-154.

Ge(Li) detector, hence any part of the spectrum originated from the 12% Ge(Li) detector, that is in coincidence relationship with the appropriate gate, is individually displayed for suitable corrections due to background and chance coincidences as previously described in Chapter III. These consequent spectra are shown in Figs.(5.3-24). Each gate was then analysed off-line by SAMPO on the CDC 7600 computer at ULCC in order to identify the strength of the observed lines in coincidence with gate. The results of these analyses are listed in Table(5.2) with the usual key entries VS, S, W, VW and P as defined in section (3.5.2). The first row of the table display the energy gates and the first column the transitions in coincidences. Other transitions that are not given in Table(5.2) could either decay to the ground state or too weak to be identified in coincidence. In the latter case, energies are placed in the decay scheme on energy fitting basis.

The energy levels have been determined from energy sum relations. Six of the energies found in the single spectra were not put in the decay scheme. These are the 138, 309.07, 943.9, 949.64, 1024.4 and 1029.18 keV; three of these are from the newly reported energies in this work (see section 5.3.2). Another two energies at 267.77 and 532.8 are established to be doublets which was confirmed from the coincidence results. The last two columns of Table(5.1) correspond to the levels that accommodate the transitions given in the first column.

5.3.4 Lifetime measurement.

The first excited state of ^{154}Gd at energy 123 keV has been found to have a half-life in the nanosecond region. The simultaneously correlated events for the lifetime measurement as described in section (3.4.1) was performed using the dual parameter energy-time spectrometer. The stability of the system was regularly checked as a long run was required to collect enough data.

The plastic detector was used to generate the start signal in the fast coincidence channel on the TPHC, while the

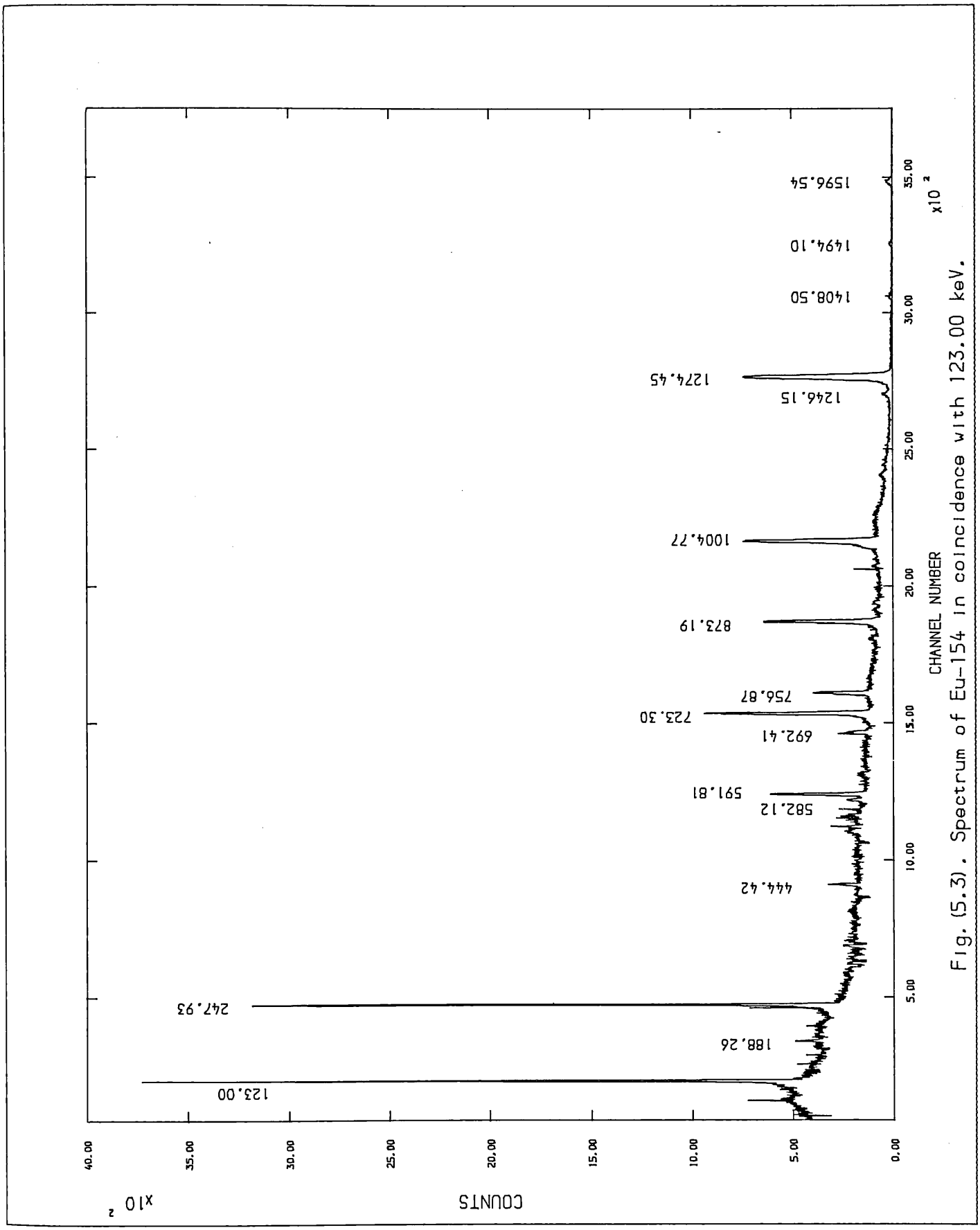

Fig. (5.3). Spectrum of Eu-154 in coincidence with 123.00 keV.

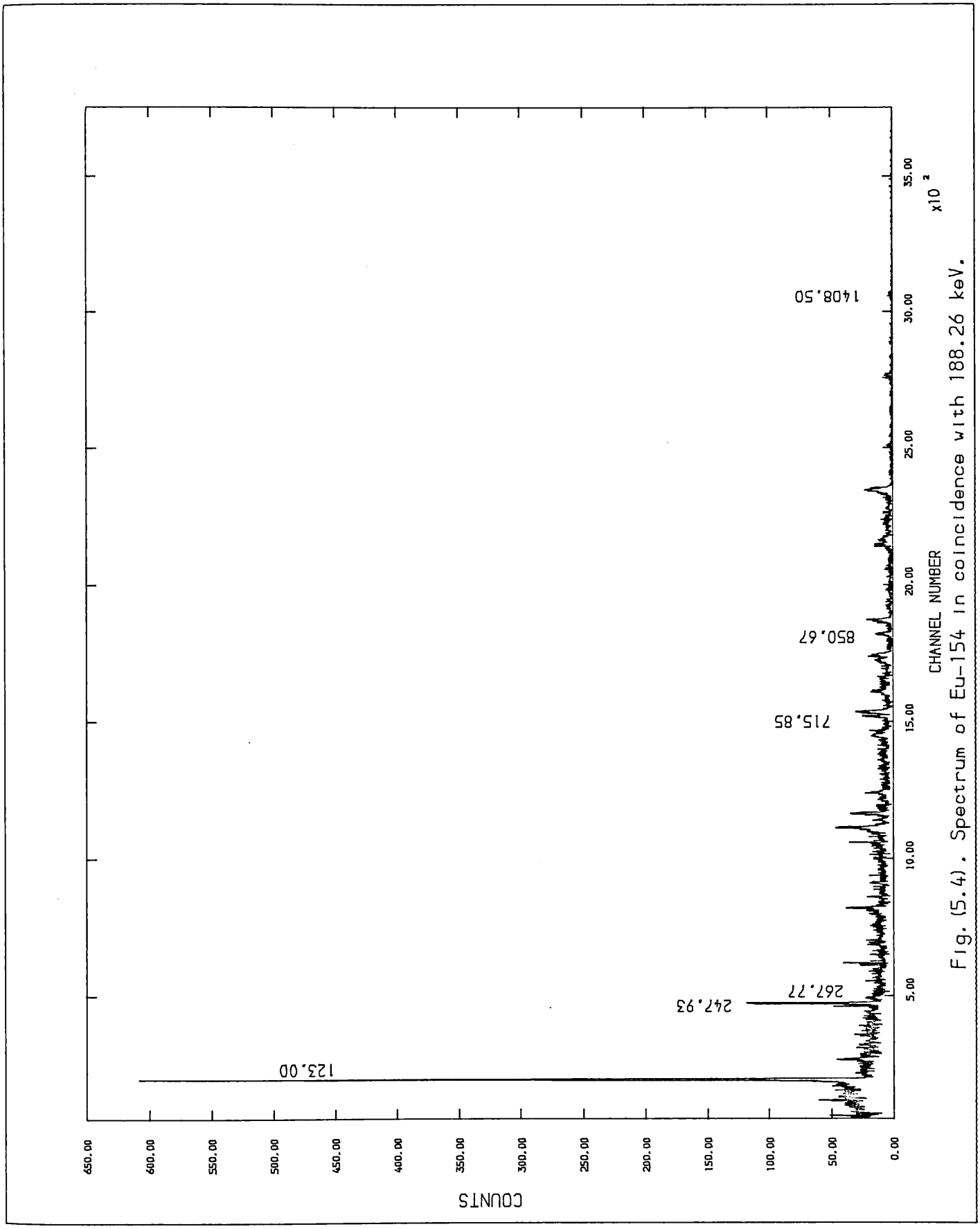

Fig. (5.4). Spectrum of Eu-154 in coincidence with 188.26 keV.

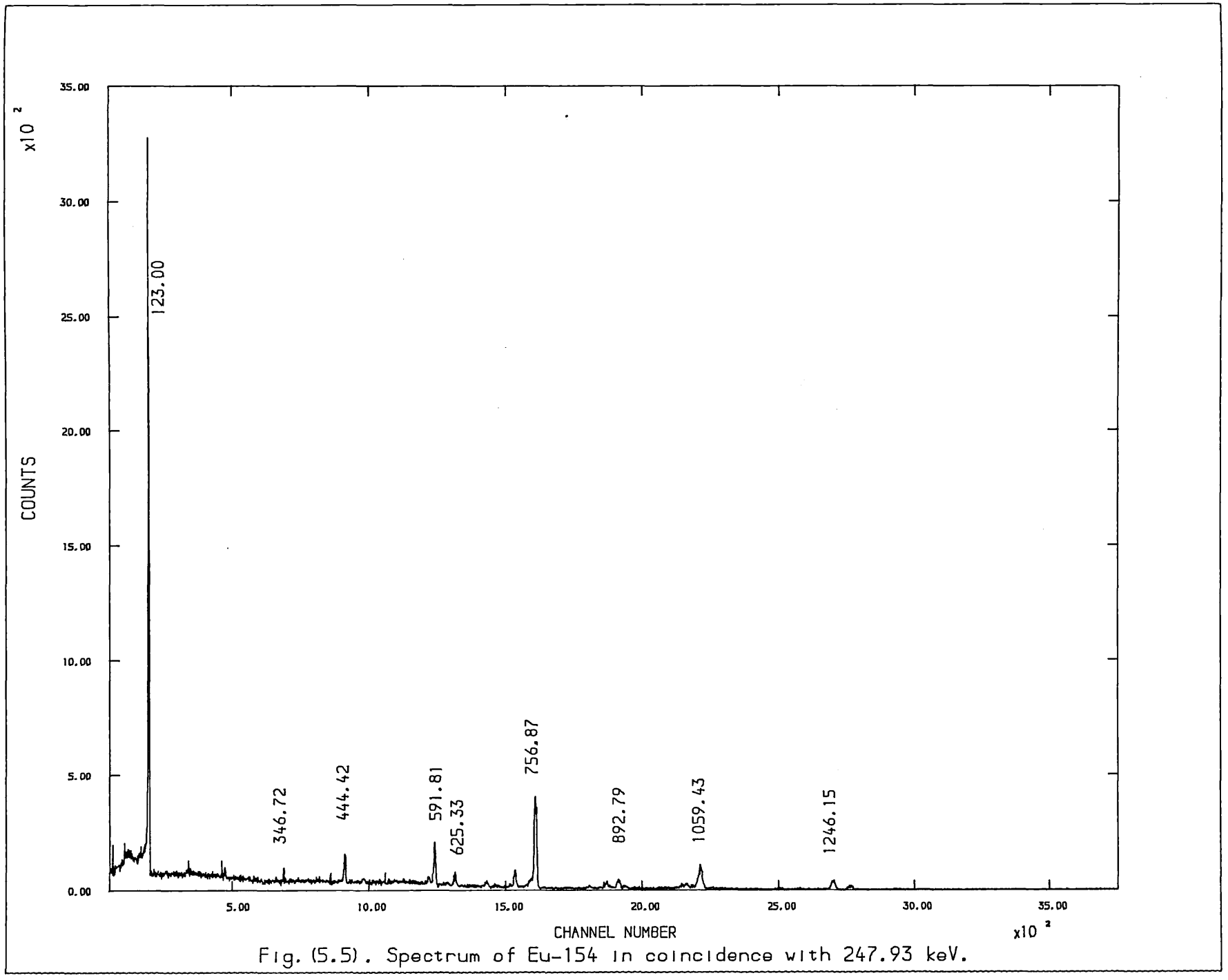

Fig. (5.5). Spectrum of Eu-154 in coincidence with 247.93 keV.

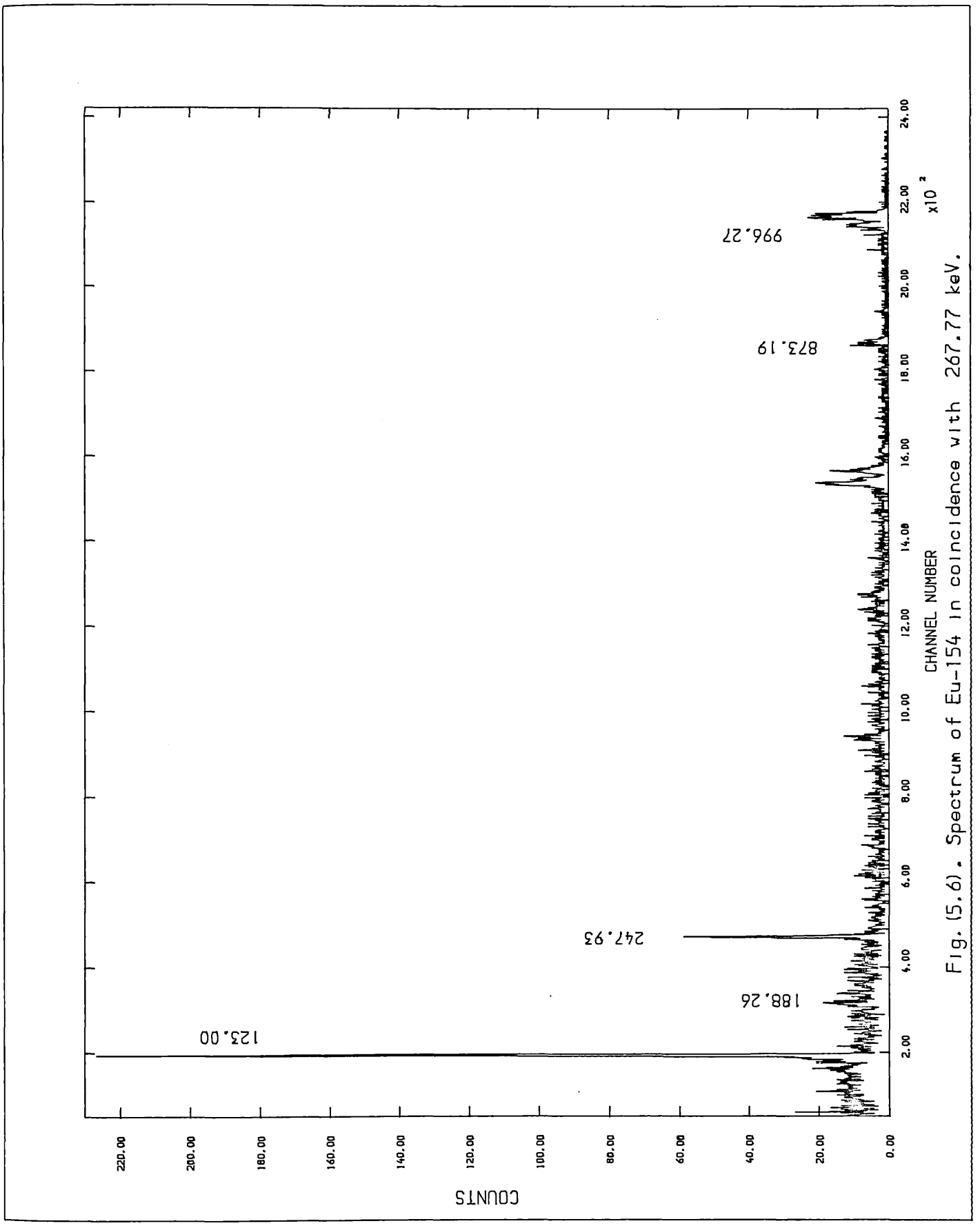

Fig. (5.6). Spectrum of Eu-154 in coincidence with 267.77 keV.

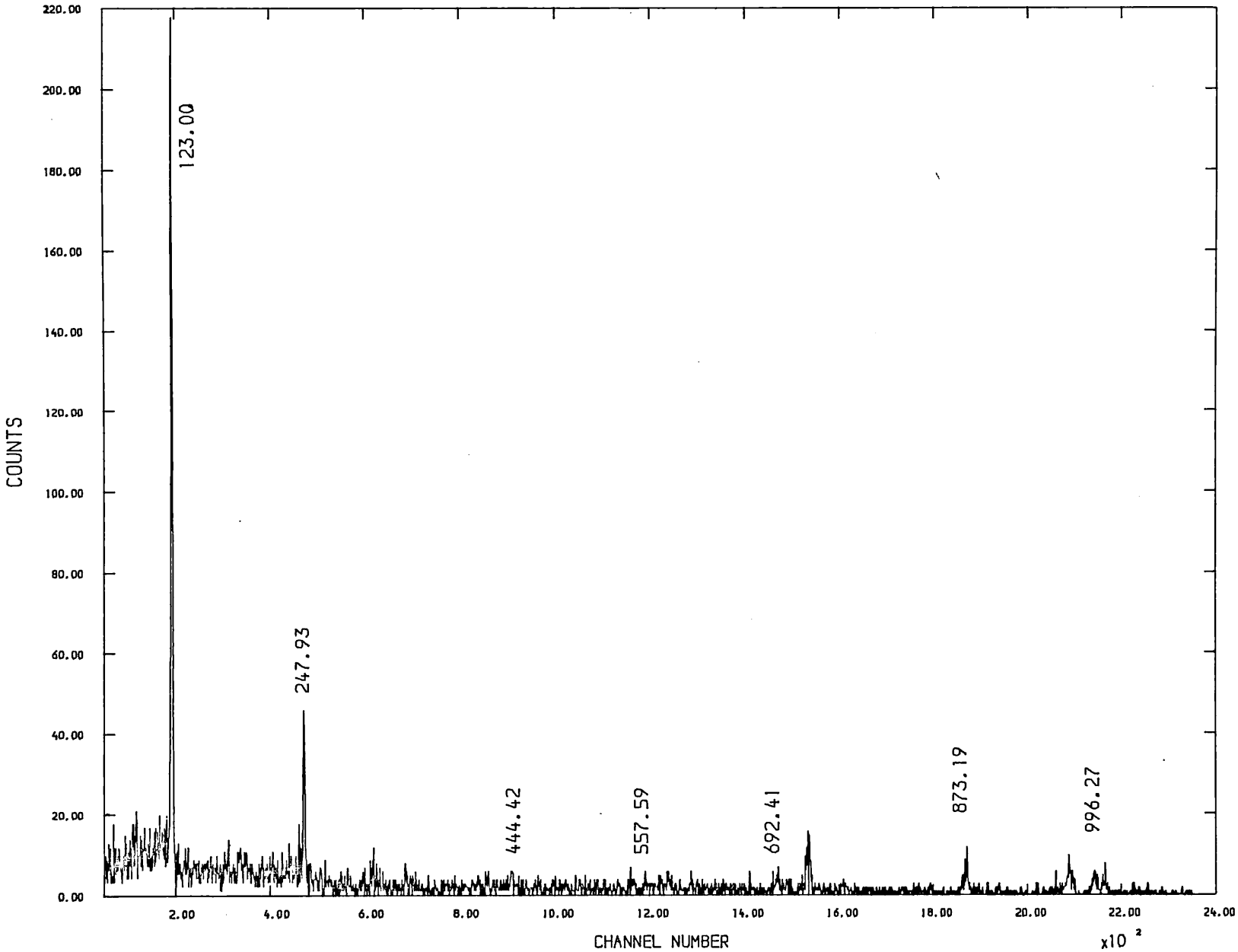

Fig. (5.7). Spectrum of Eu-154 in coincidence with 301.24 keV.

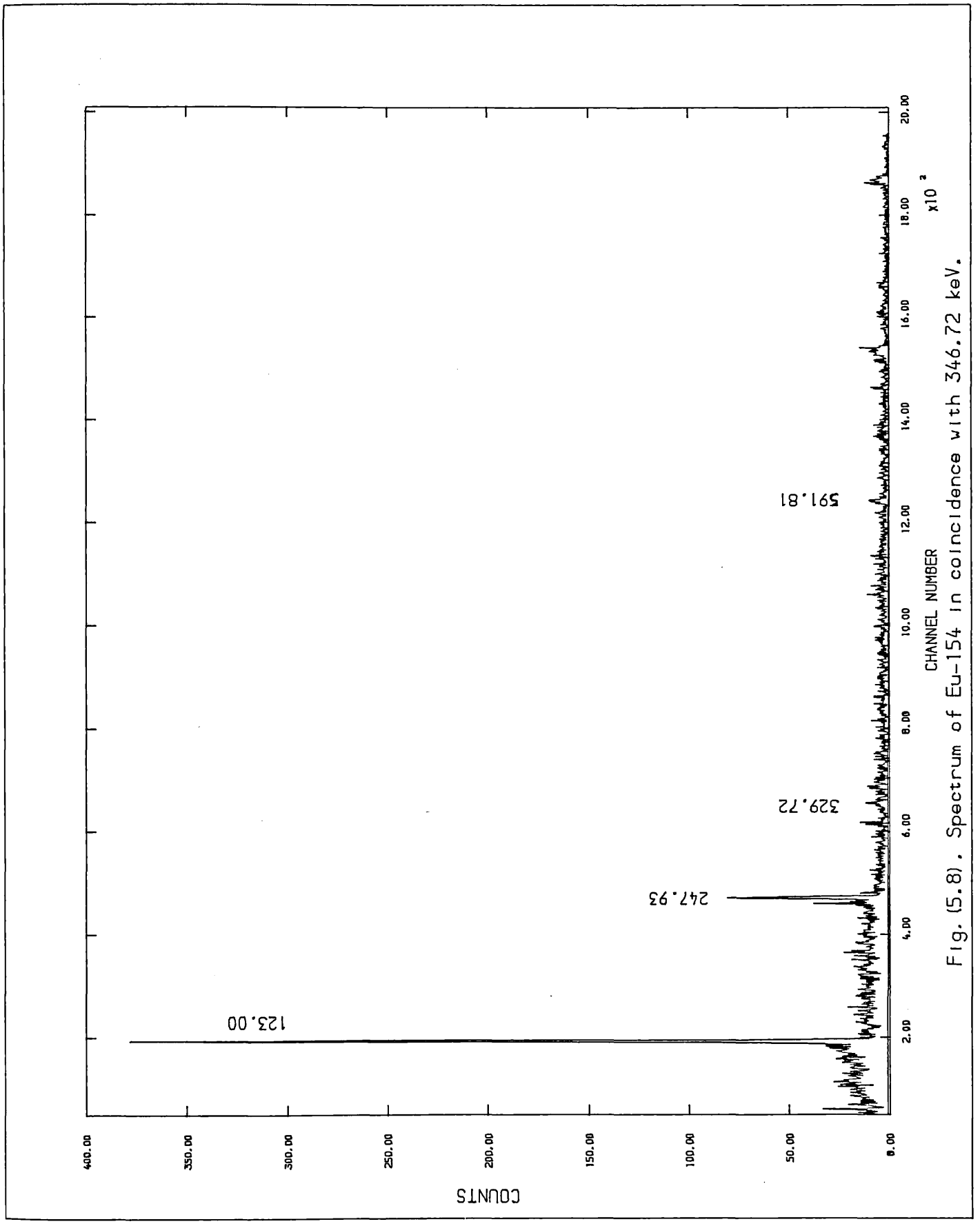

Fig. (5.8). Spectrum of Eu-154 in coincidence with 346.72 keV.

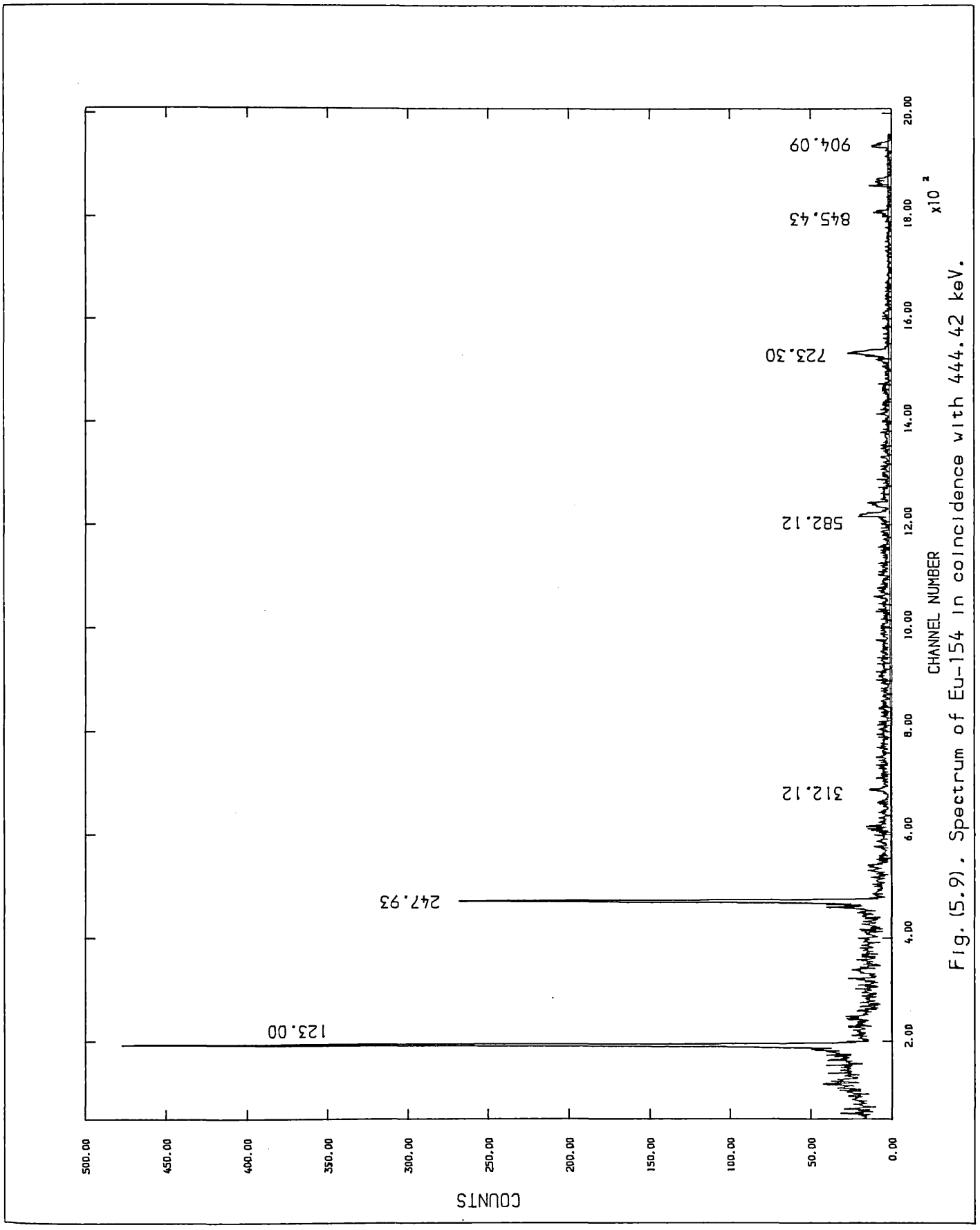

Fig. (5.9). Spectrum of Eu-154 in coincidence with 444.42 keV.

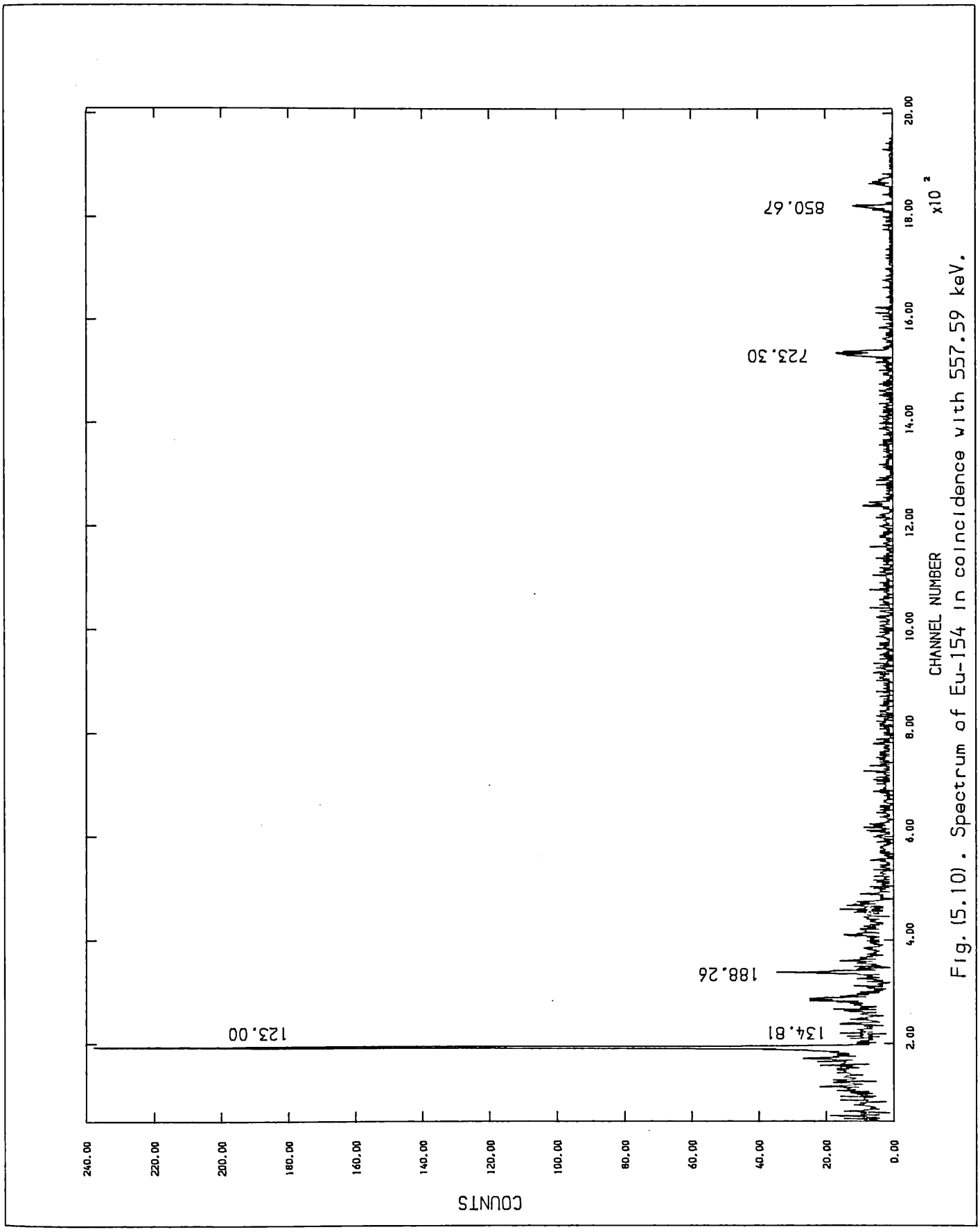

Fig. (5.10). Spectrum of Eu-154 in coincidence with 557.59 keV.

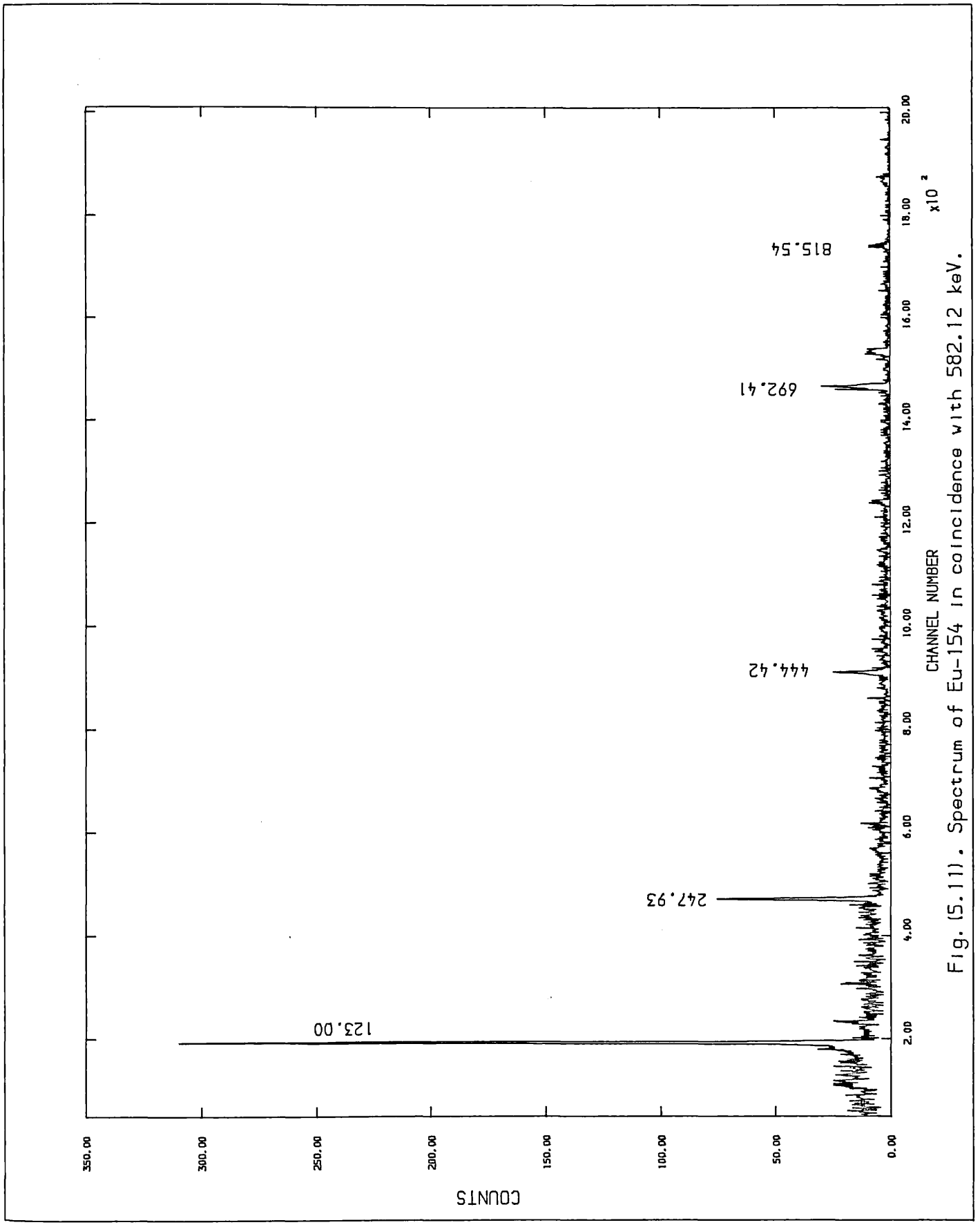

Fig. (5.11). Spectrum of Eu-154 in coincidence with 582.12 keV.

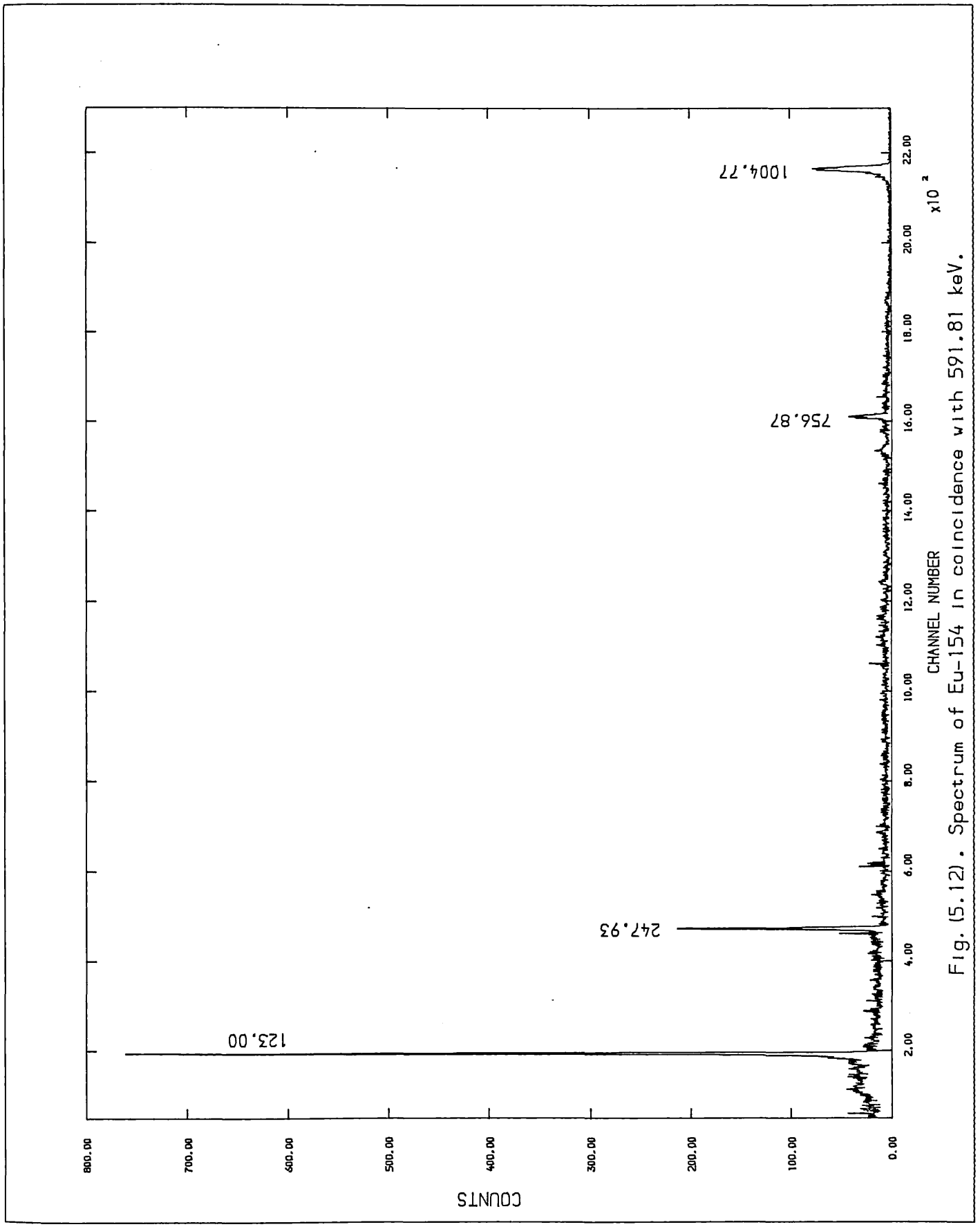

Fig. (5.12). Spectrum of Eu-154 in coincidence with 591.81 keV.

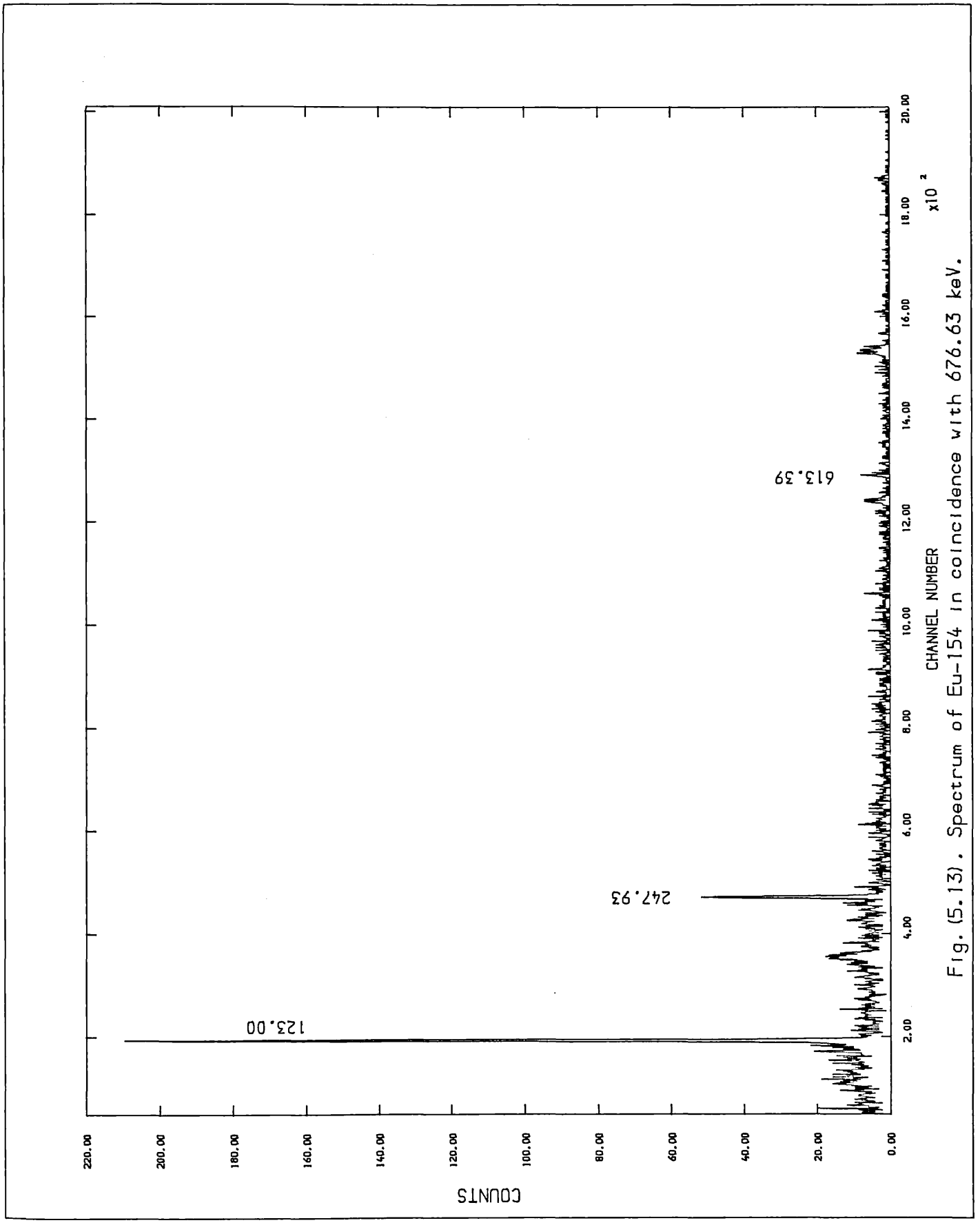

Fig. (5.13). Spectrum of Eu-154 in coincidence with 676.63 keV.

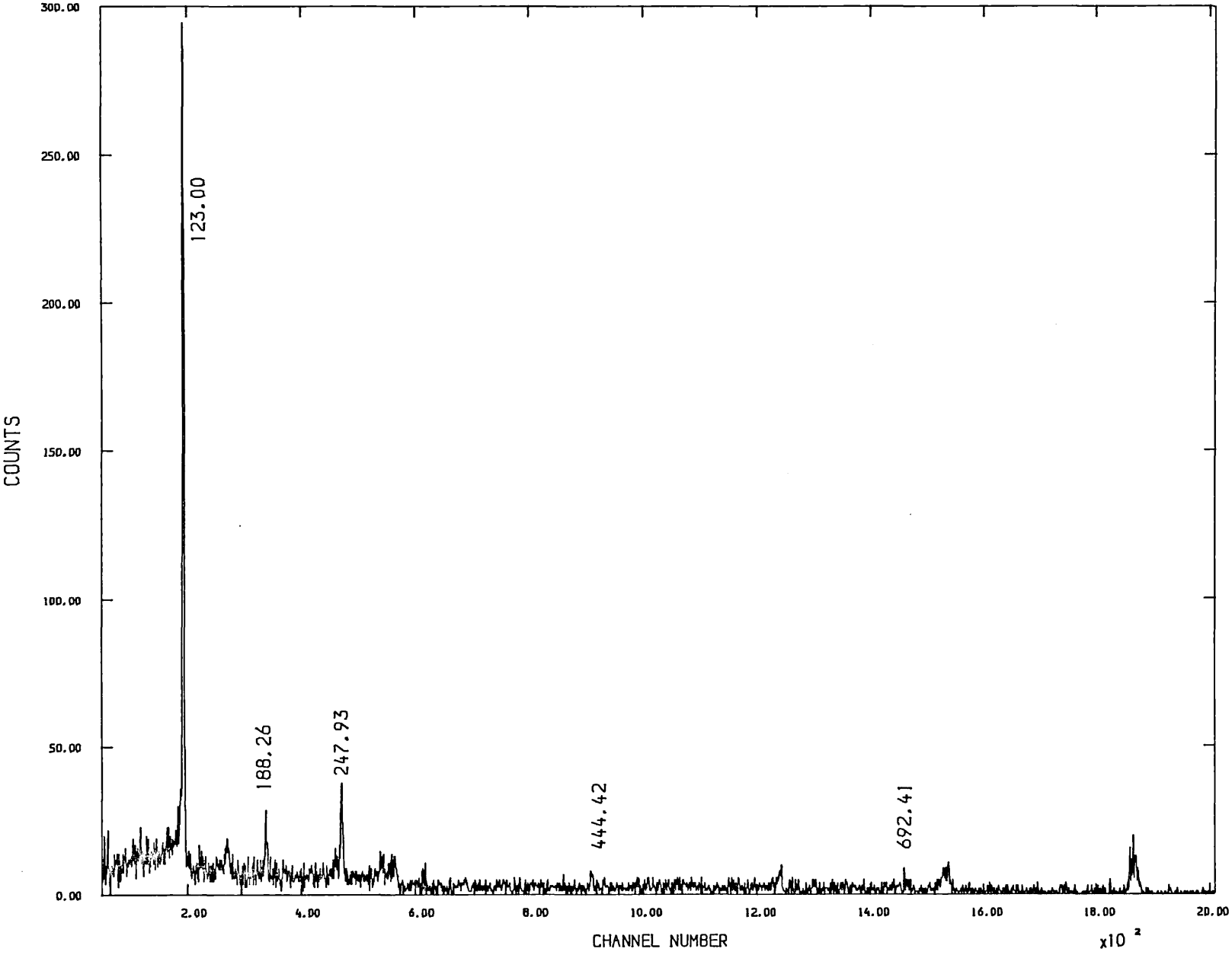

Fig. (5.14). Spectrum of Eu-154 in coincidence with 715.85 keV.

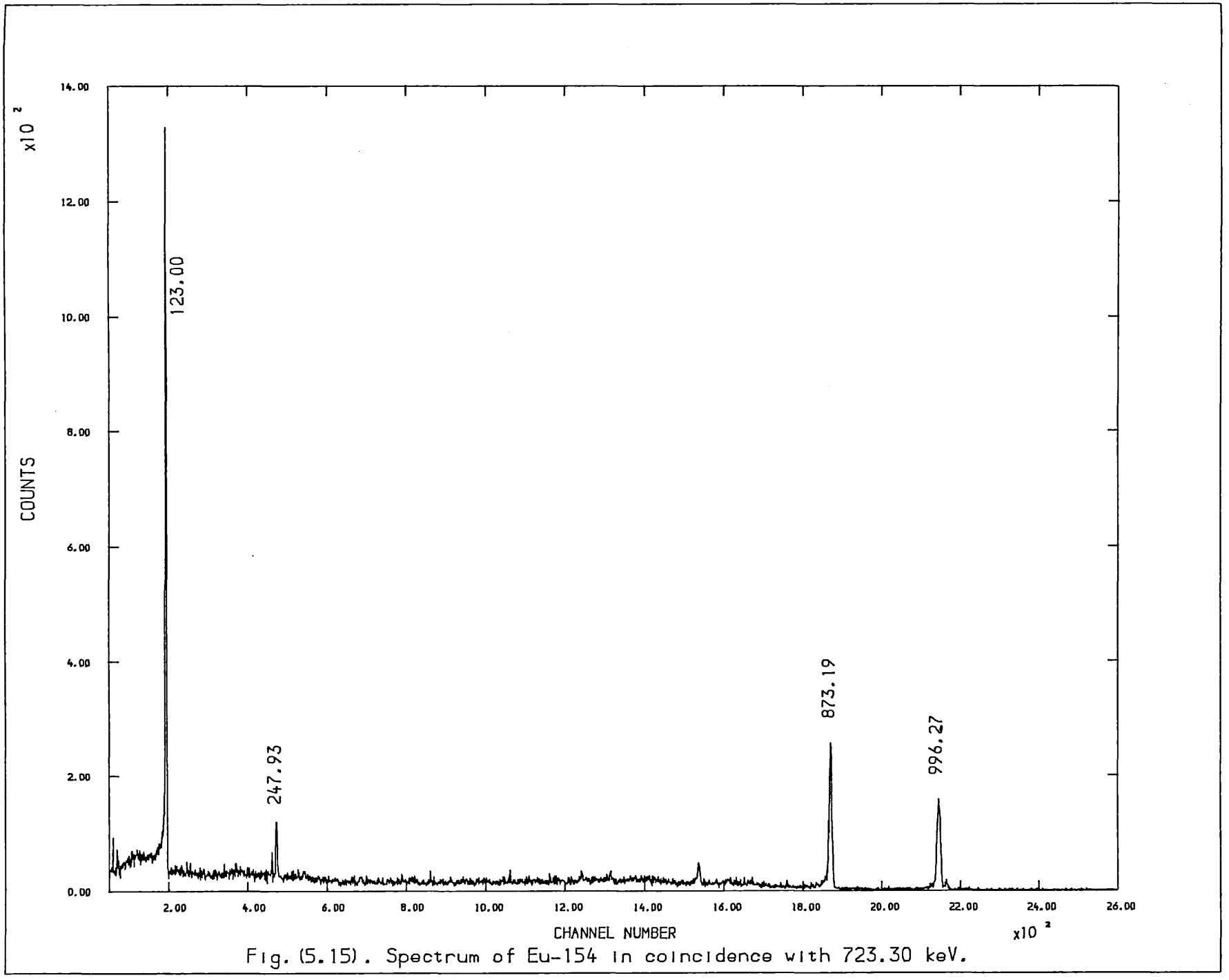

Fig. (5.15). Spectrum of Eu-154 in coincidence with 723.30 keV.

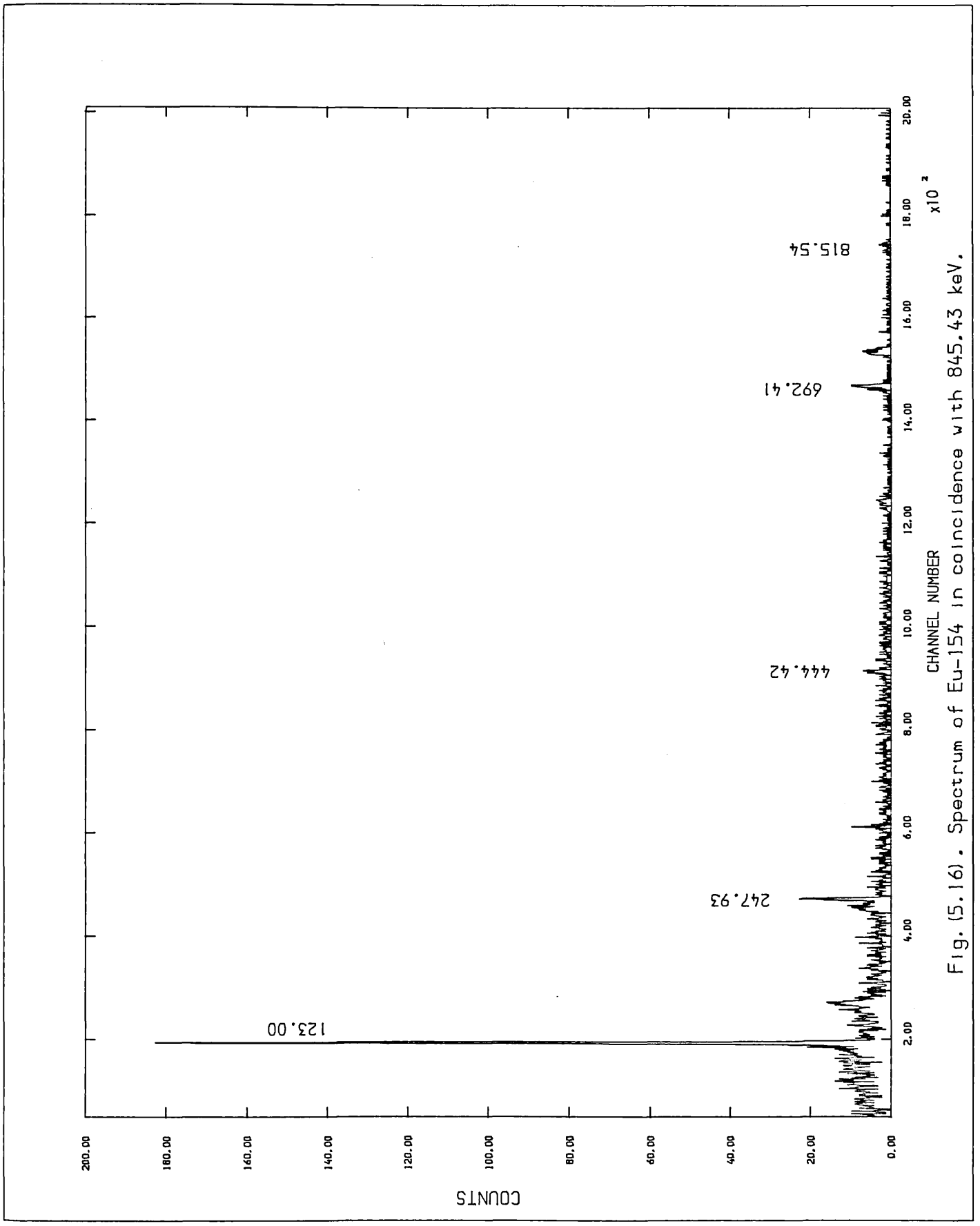

Fig. (5.16). Spectrum of Eu-154 in coincidence with 845.43 keV.

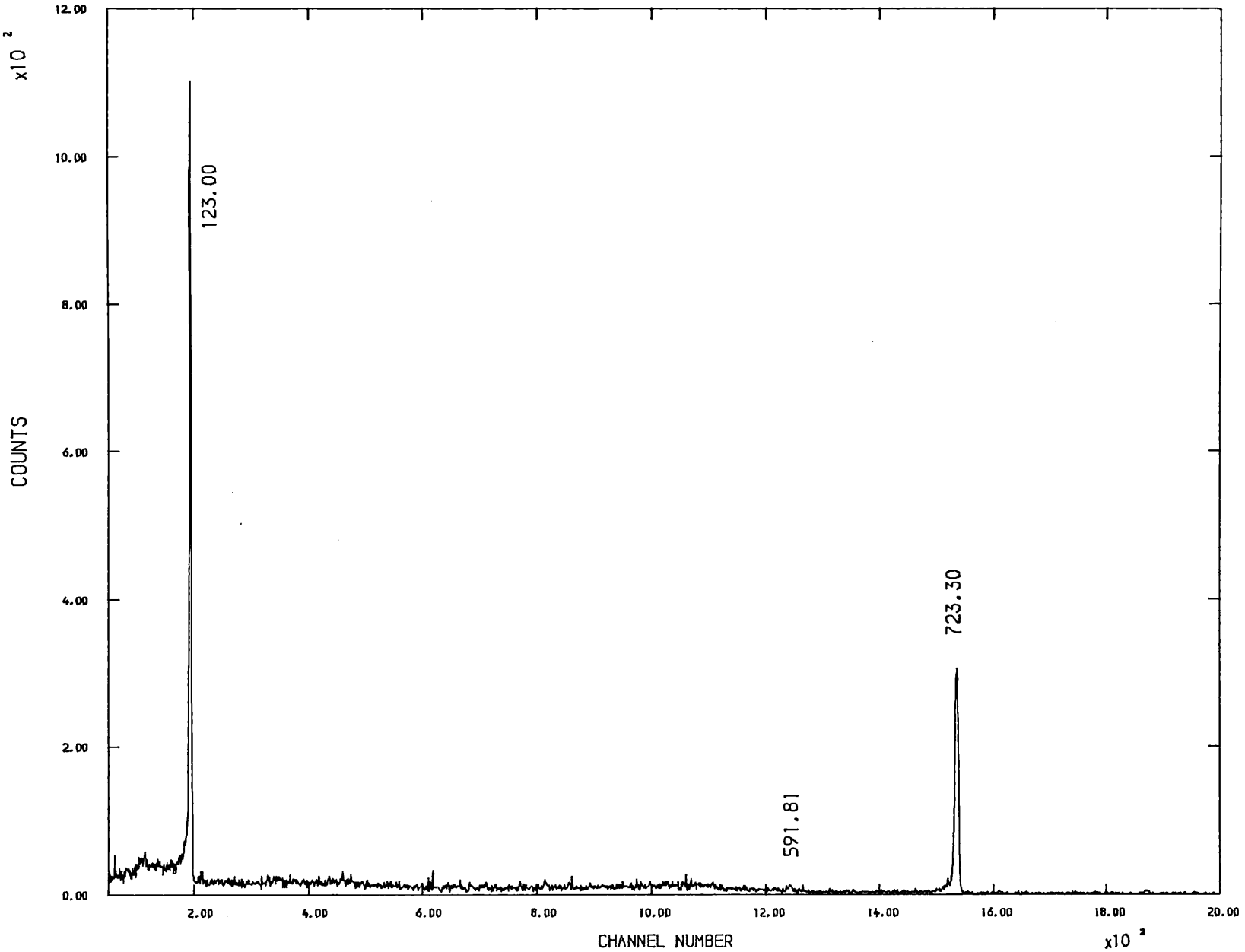

Fig. (5.17). Spectrum of Eu-154 in coincidence with 873.19 keV.

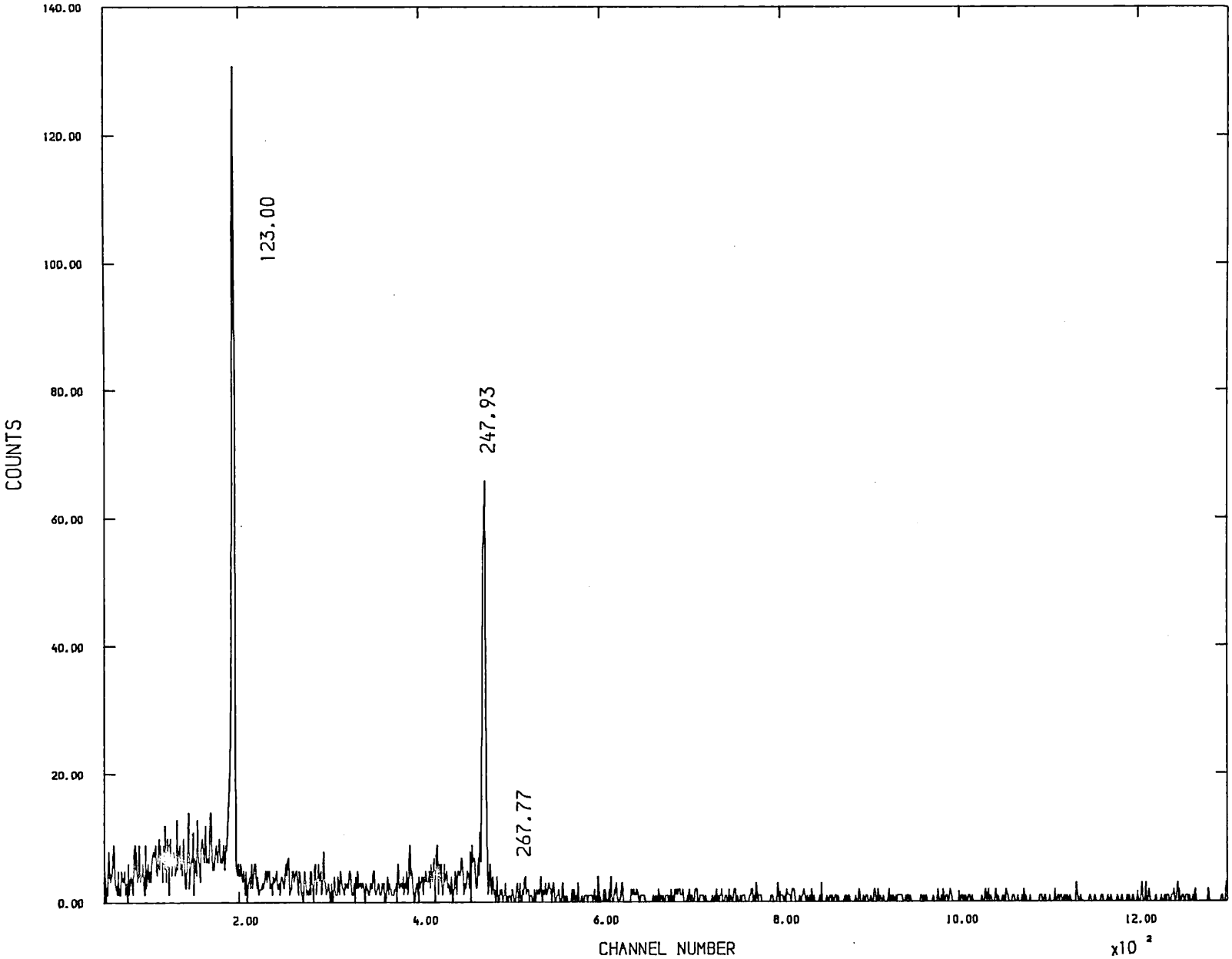

Fig. (5.18). Spectrum of Eu-154 in coincidence with 892.79 keV.

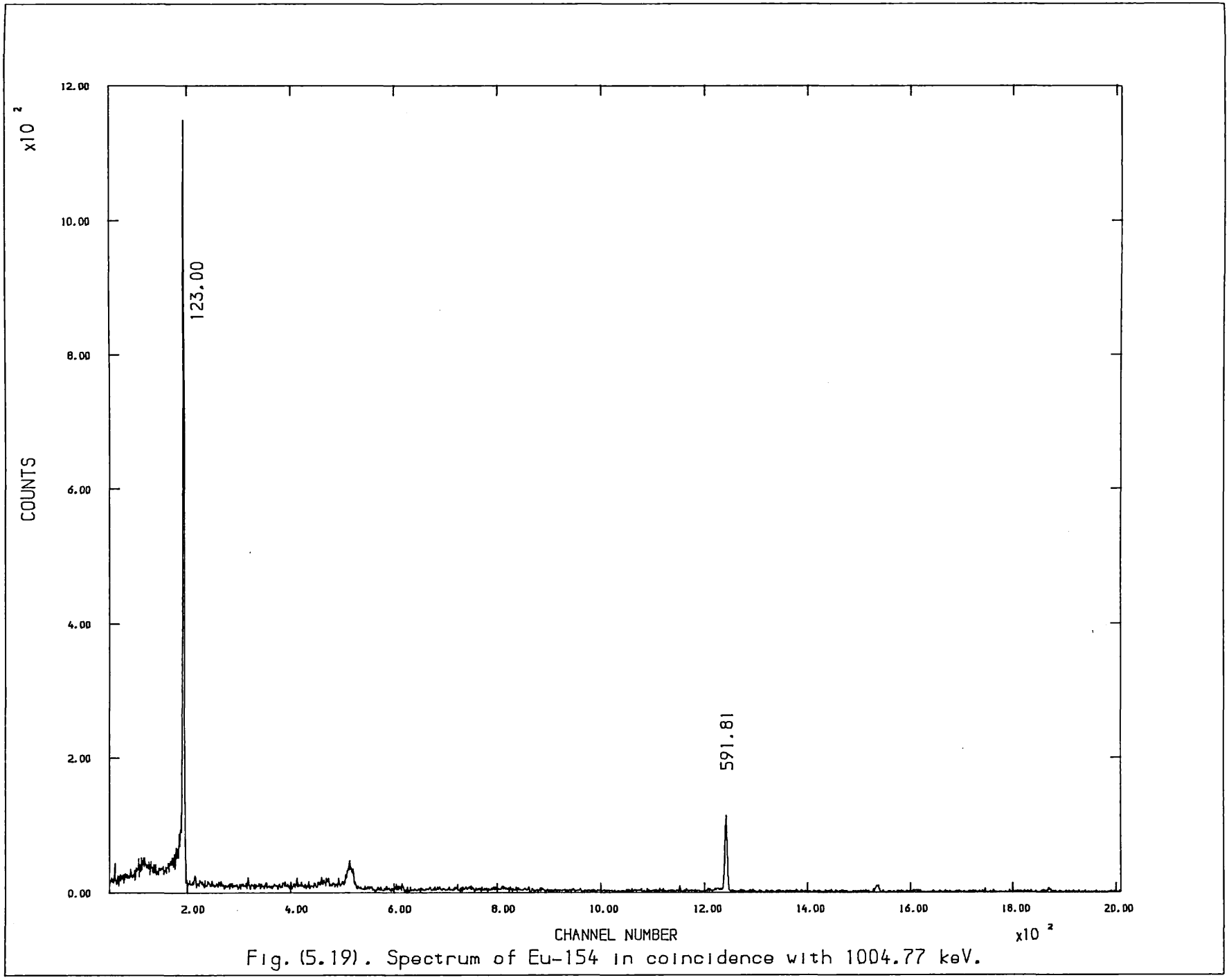

Fig. (5.19). Spectrum of Eu-154 in coincidence with 1004.77 keV.

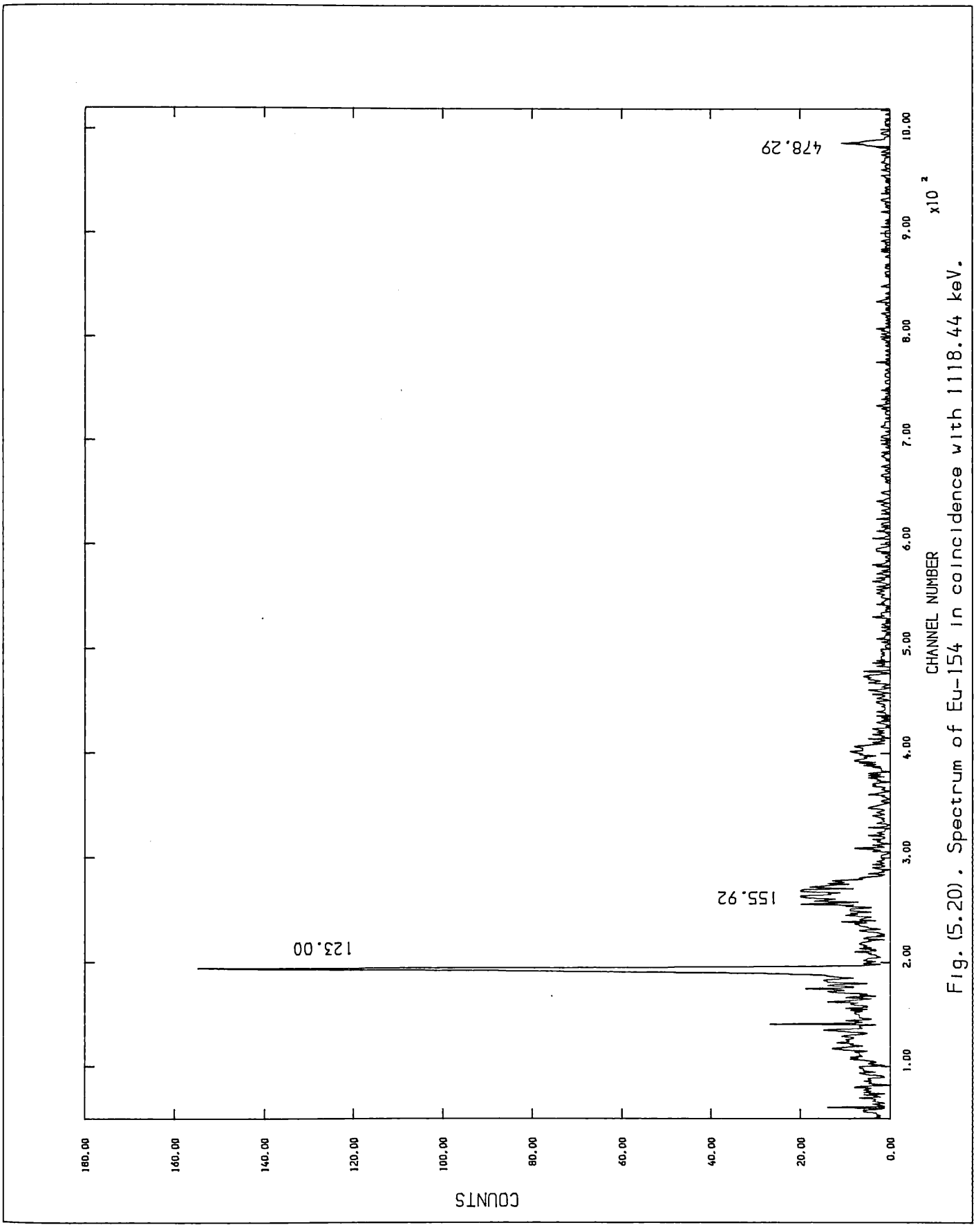

Fig. (5.20). Spectrum of Eu-154 in coincidence with 1118.44 keV.

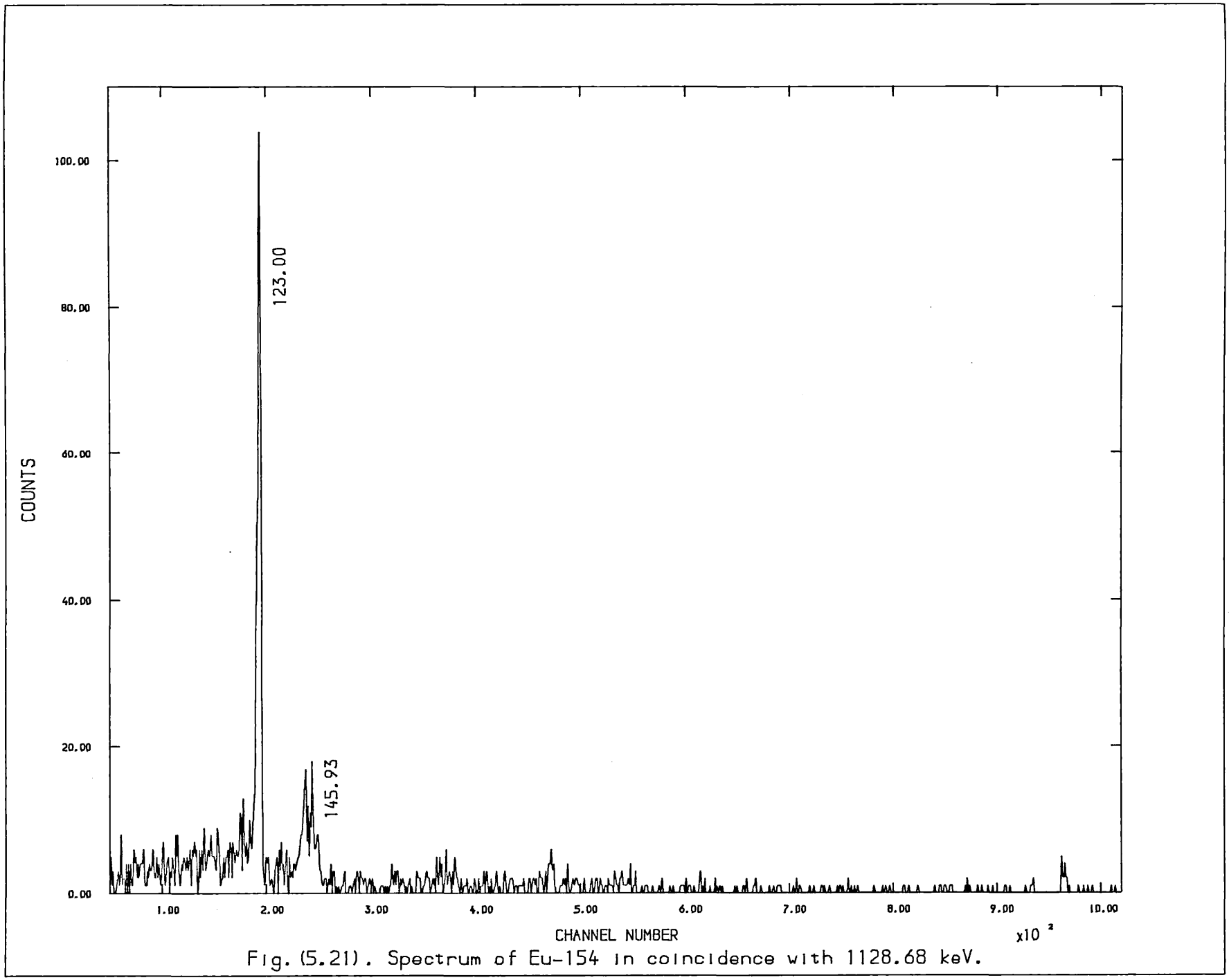

Fig. (5.21). Spectrum of Eu-154 in coincidence with 1128.68 keV.

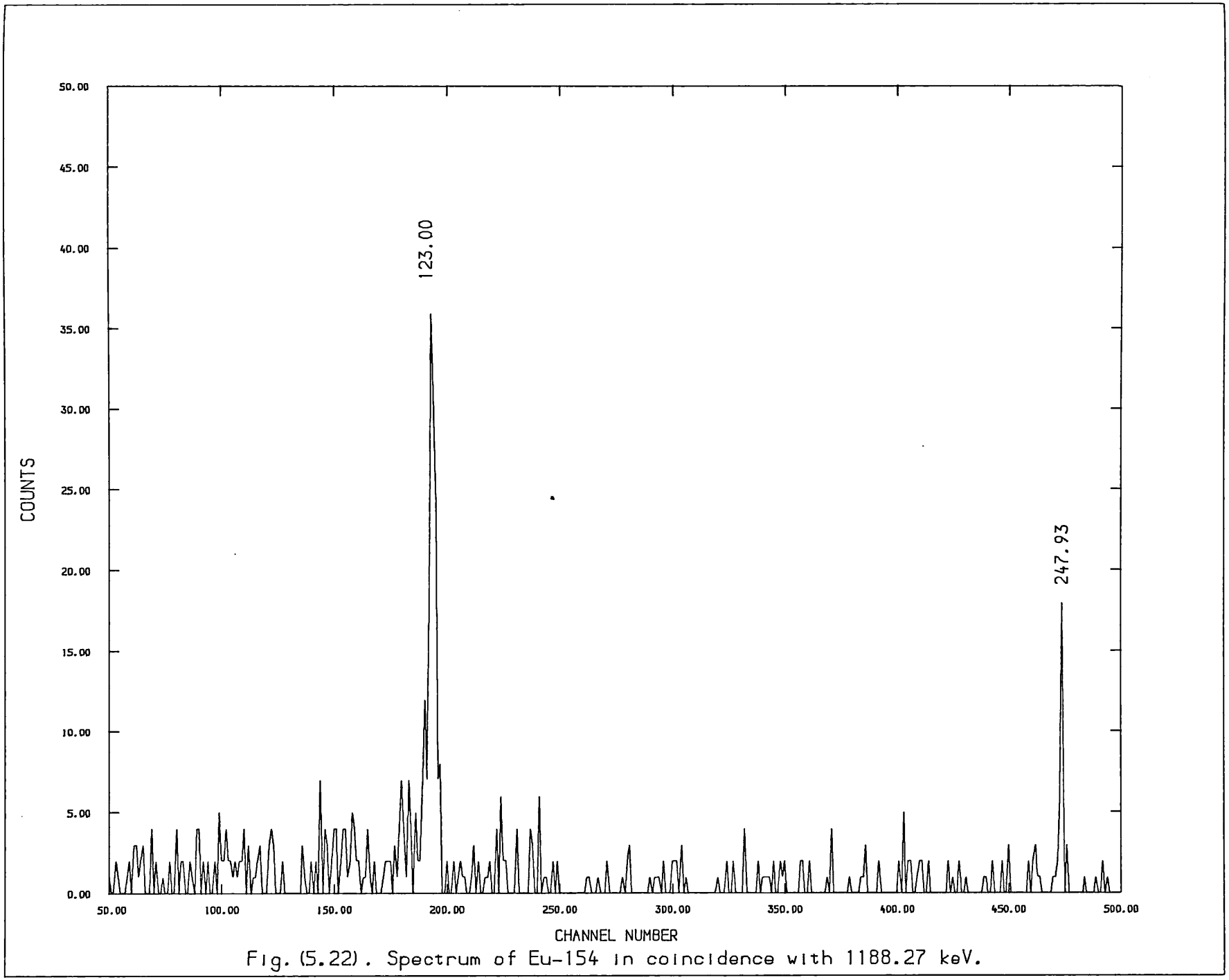

Fig. (5.22). Spectrum of Eu-154 in coincidence with 1188.27 keV.

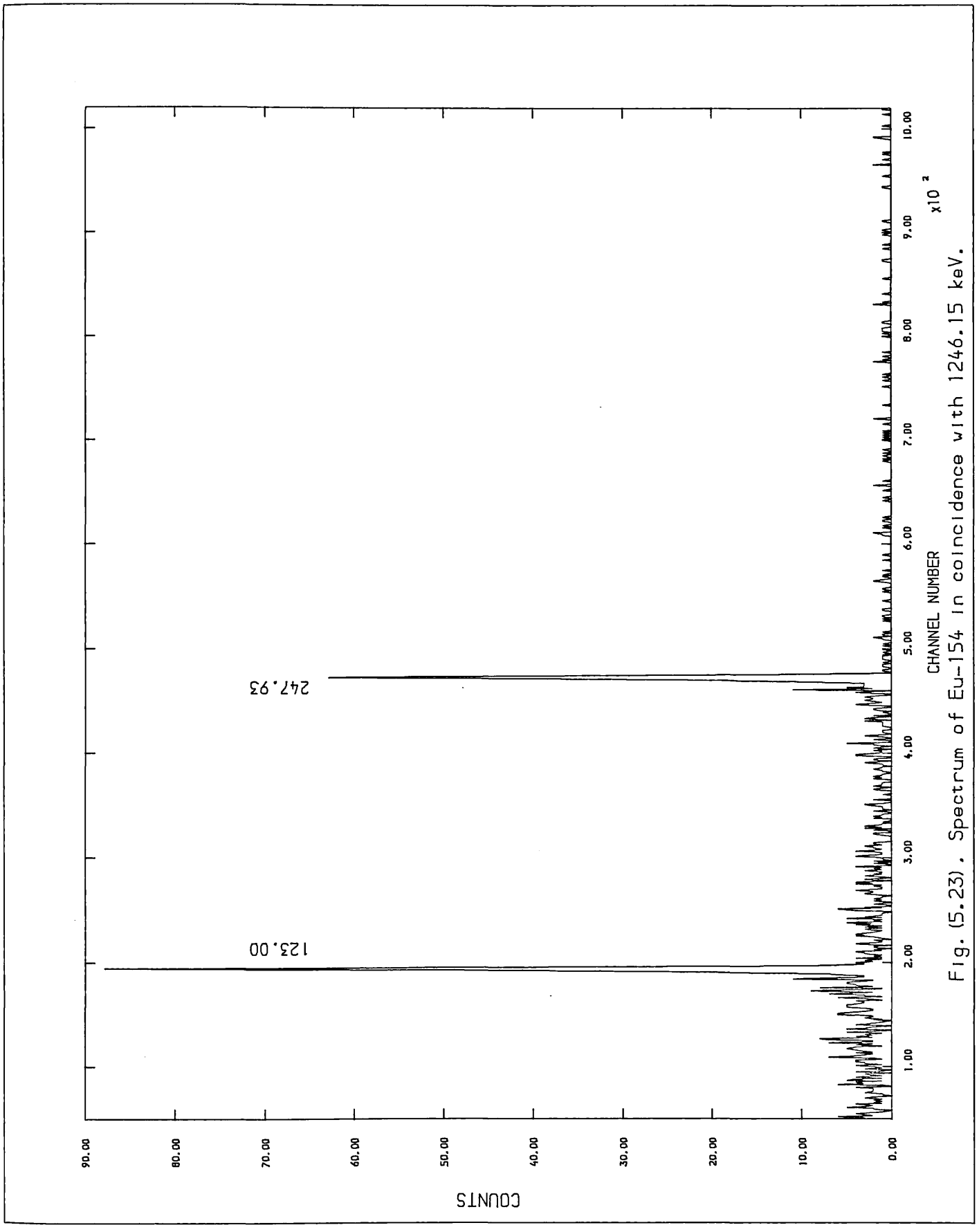

Fig. (5.23). Spectrum of Eu-154 in coincidence with 1246.15 keV.

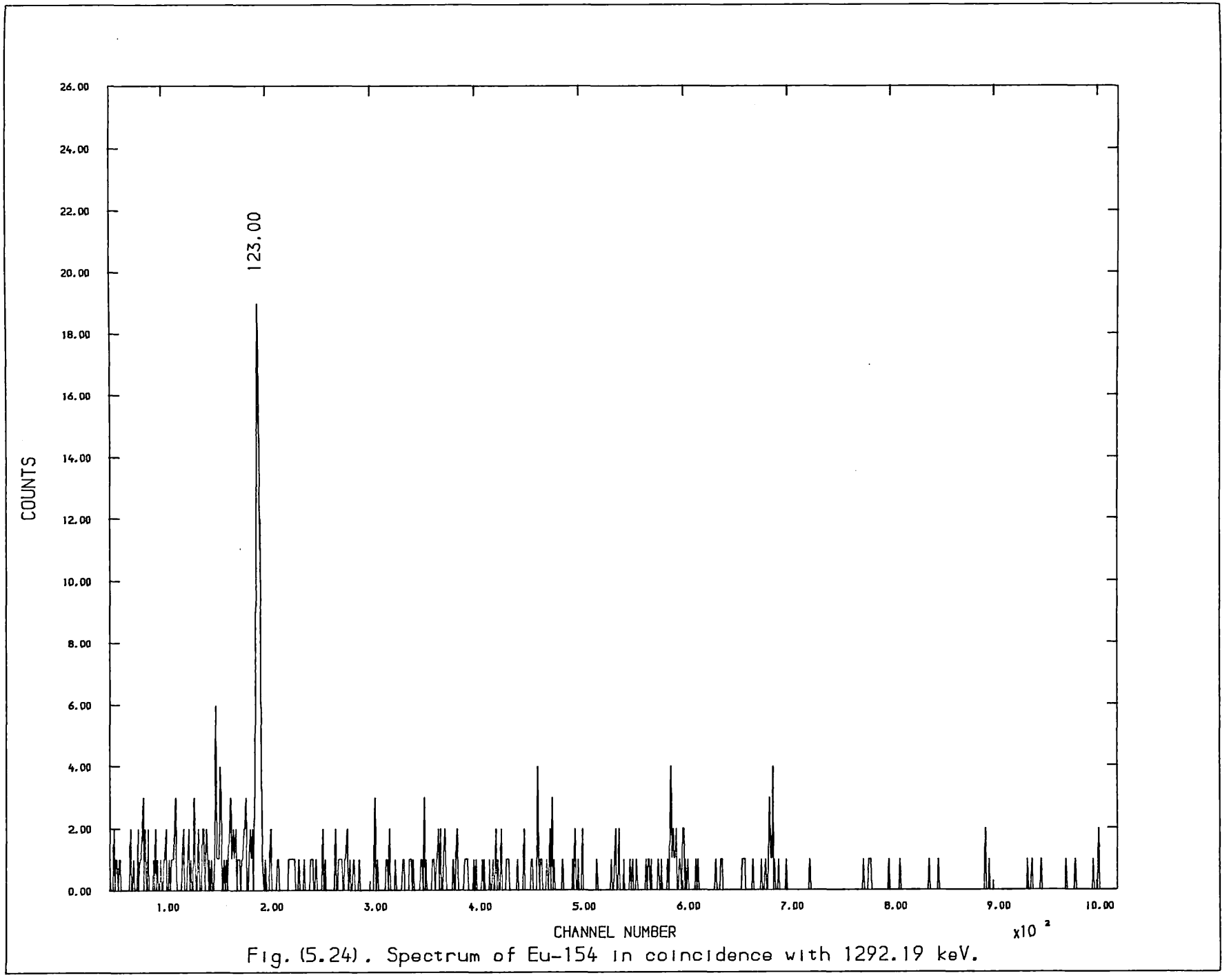

Fig. (5.24). Spectrum of Eu-154 in coincidence with 1292.19 keV.

Table(5.2). Summary of gamma-gamma coincidence results following the decay of ^{154}Eu to levels in ^{154}Gd. Transitions denoted (") correspond to the referrence line of a gate spectrum.

Transition (keV)	Gate (keV)																					
	123	188	248	268	301	347	444	558	582	592	677	716	723	845	873	893	1005	1118	1128	1188	1246	1292
123.00		P	VS	W	W	W	VW	S	VW	S	VW	VW	VW	VW	S	S	S	S	S	S	S	VS
131.69										W					VS							
134.81								S	S													
145.93																			VS			
155.92																		S				
188.26	S		VW	S				S				VS										
232.22							S															
247.93	VS"	P	P	W	W	W	S		VW	S	VW	VW	VW	VW		VS				VS	VS	
267.77		VS													VW	S						
290.35		S																P				
301.24	VW																					
312.12							VS															
315.63				S				VS"					W									
329.72						VS"																
346.72			S																			
370.78					W						W											
382.10	VS			VS											W	S	VW					
397.23				VS																		
401.27															VS							
403.57		VS"															VW					
444.42	S		VS						S	W		VS"		W								
478.29																		VS				
483.79		P																				
506.28				S												P						
510.32		W																				
512.39											S											
518.05			VW			S																
532.80				S											VW	VW	P					
546.00		W				VS																
557.59	VS	W			W					S		S	W									
582.12	S		VW				VS"															
591.81	VS		W			VW									VW		VS"					
598.10											W											
602.73					S		P															
613.39							S				VS"											
625.33	S		VS	VW																		
664.50															VW							

Continued

Transition (keV)	Gate (keV)																				
	123	188	248	268	301	347	444	558	582	592	677	716	723	845	873	893	1005	1118	1128	1188	1246	1292
676.63	VS		VS																			
692.41	S				W				VS"			W		W								
701.91															W							
715.85		VS	VW																			
723.30	S		P				P	W							VS"							
738.03								S														
756.87	VS	P	S							VS"												
800.31															W							
815.54			P						VS			VS		S								
845.43	S		VW				VS															
850.67		VS						VS														
873.19	VS	P		W	W								VS"									
880.70			VS																			
892.78	W		VS																			
904.09	S		VW				VS															
906.40	S		W																			
924.67	VS																					
981.56							P															
996.27				VS"	W								VS									
1004.77	VS									S												
1047.24					S																	
1056.02	VS																					
1059.43	VS		S																			
1118.44	S																					
1128.68	VS																					
1140.73	S																					
1153.11			P																			
1160.48		S	VS																			
1188.27			VS																			
1246.15	VS		VS																			
1274.45	VS																					
1290.74			S																			
1292.19	S																					
1295.50	P				P																	
1408.50	VS	S																				
1489.91			P																			
1494.10	VS																					
1537.93	VS																					
1596.54	VS																					
1666.87	P																					

10% Ge(Li) detector provided the stop pulse. The TSCA of the scintillation arm was set to collect the whole energy spectrum since the preceding events can be generated through direct β-decay (9%) to the first excited state as well as from γ-rays that are strongly de-exciting the 1127.69, 1397.34 and 1719.43 keV level to the first excited state as these are strongly fed by β-decay. The window at the TSCA of the Ge(Li) detector was set to select the 123 keV peak which is well defined in the spectrum.

The lifetime spectrum [Fig.(5.25)] was analysed using the slope method as described by Meiling & Stary (1968) to determine the half-life of the 123 keV level. A value of (1.20 ± 0.05) n.sec was obtained and is in agreement with those reported by Lederer & Shirley (1978) as well as with latest measurement given by Sharma et al.(1982) (1.19 ± 0.03 n.sec) using the 1275-123 delayed coincidence methods.

5.4 Decay Scheme.

The decay scheme of ^{154}Gd established from the coincidence results and energy sum relations is shown in Fig.(5.26). The log ft values, spin and parity assignments, together with the β energies and its feeding branching ratios for each level are given in Table(5.3). The log ft was evaluated using the Moszkowski monograms [section (1.3)]. The Q_β value of 1967.0 (20) keV used was taken from Nuclear Data Sheets (1979).

The branching ratios (B.R.) were calculated from the transition intensity balance (γ + conversion) for each level, while it was found that the energy levels at 680.59, 717.65, 1241.31 and 1415.04 keV are only fed by γ-transitions.

The experimental internal conversion coefficients were calculated for K-, L- and M-shells for those transitions for which the electron intensities (I_e) of these shells were available. Weighted mean values of the electron intensities were first calculated from Ng et al.(1968), Brantley et al. (1968), Andersson & Ewan (1969), Rud et al.(1971) and Nagpal & Gaucher (1972), and used together with the present γ-ray

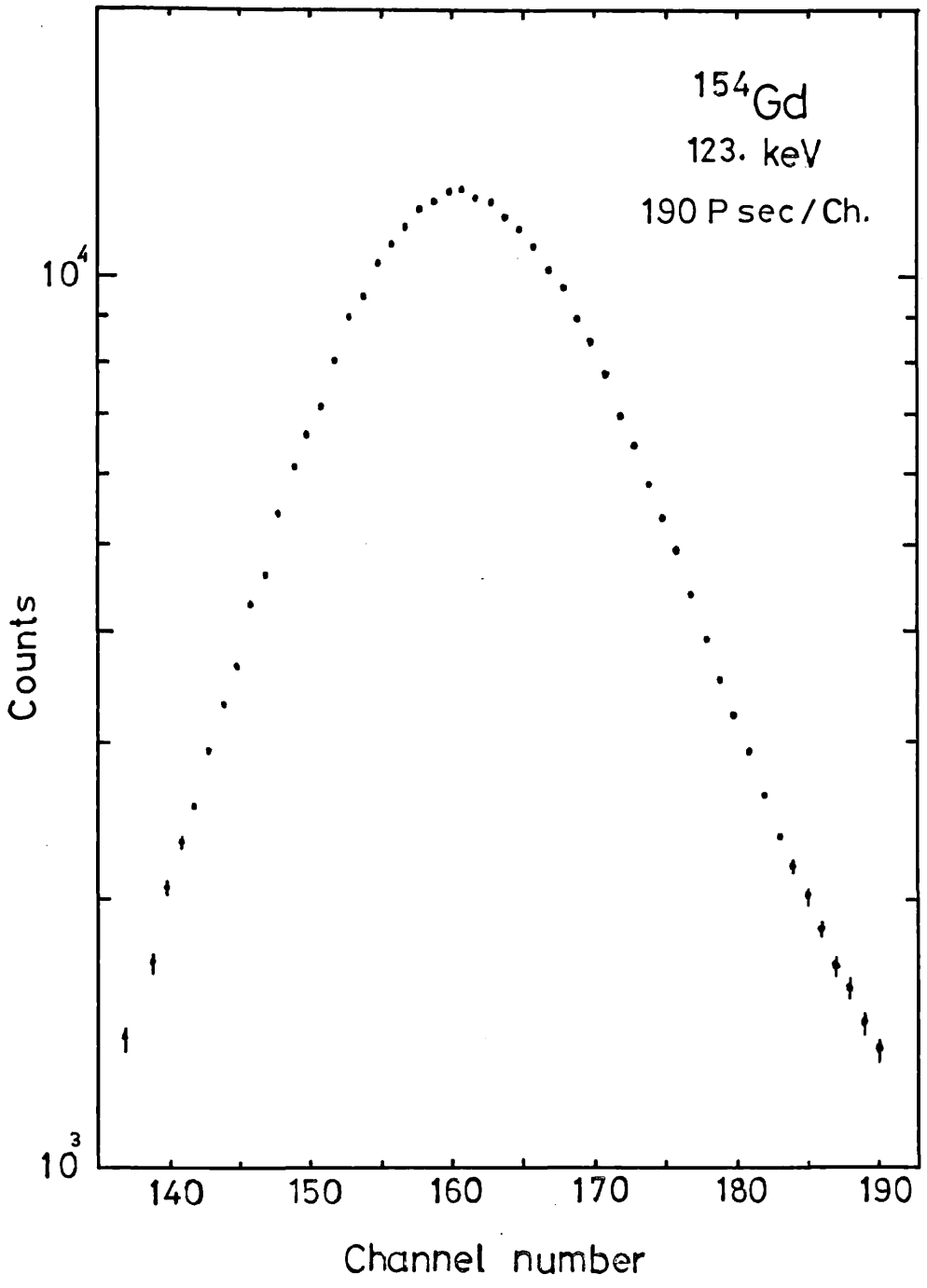

Fig.(5.25). The 123 keV level life-time spectrum.

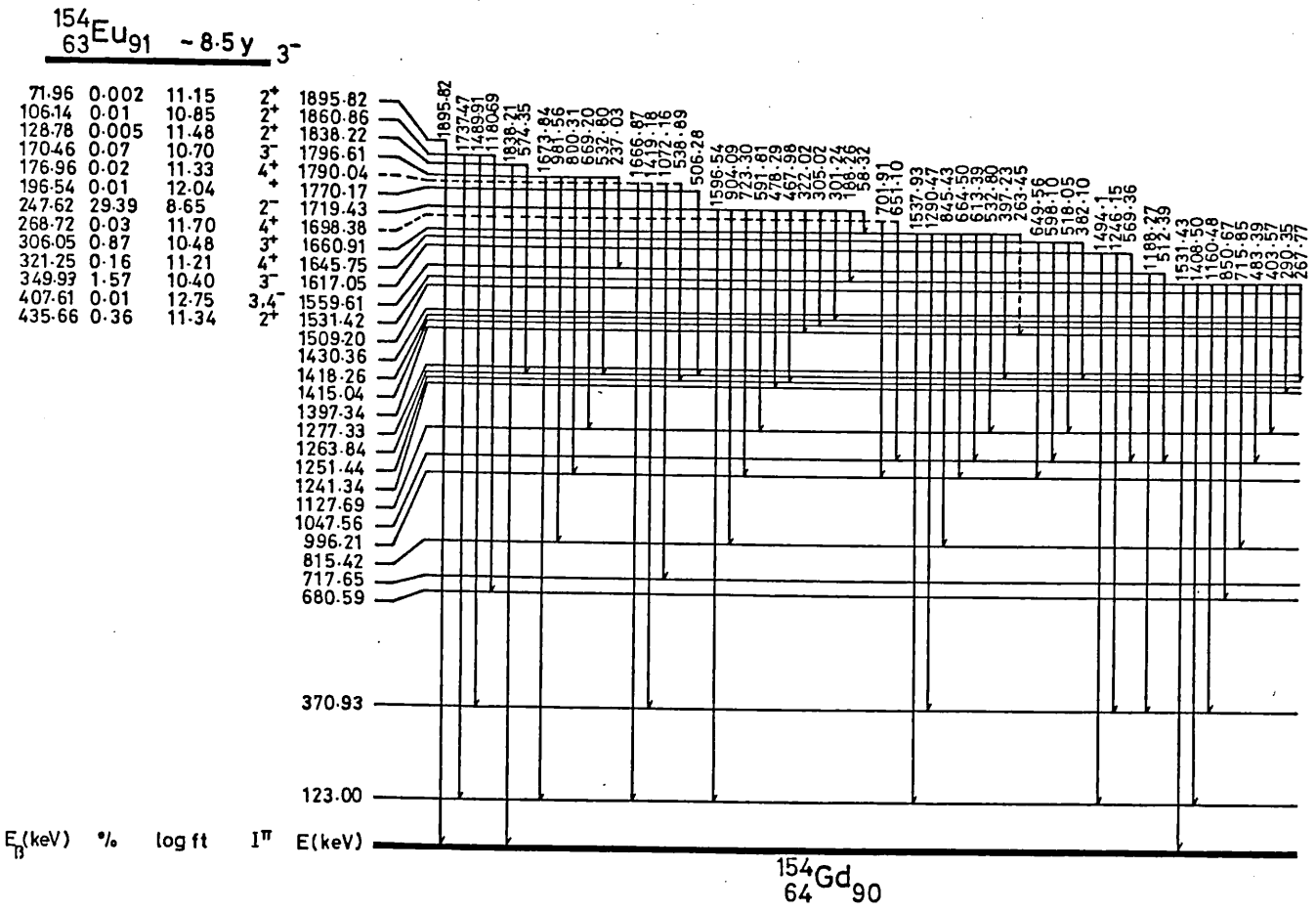

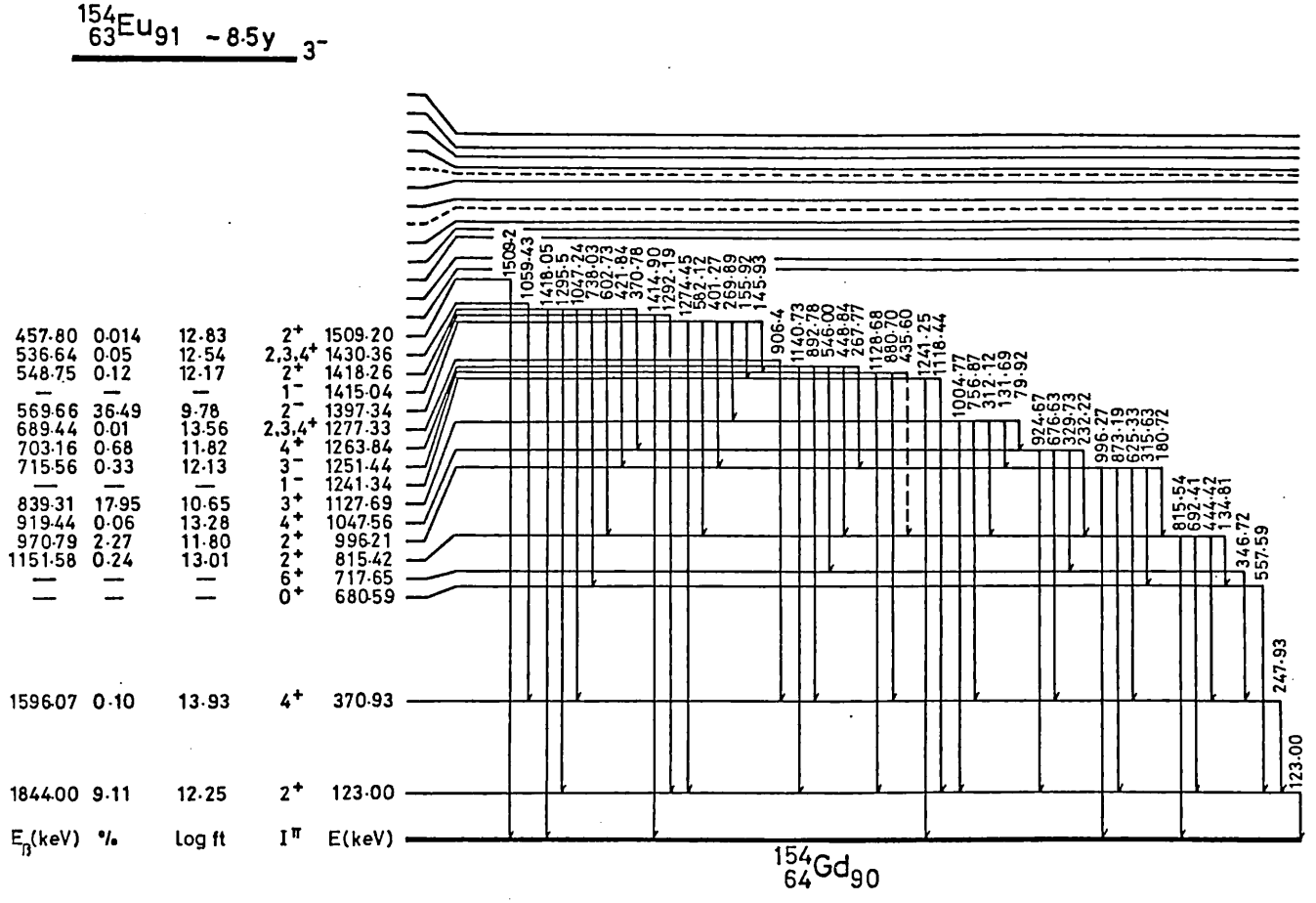

Fig.(5.26). The level scheme of ^{154}Gd.

Table(5.3). The beta branshing ratios, logft values, spins and parities assignments for levels in ^{154}Gd nucleus .

E(level)† (keV)	E (beta) (keV)	∑ Decay	∑ Feed	%B.R.	log ft	π	I
123.00(05)	1844.00	249.96	224.22	9.11	12.25	+	2
370.93(07)	1596.07	21.92	21.63	0.10	13.93	+	4
680.59(11)	--	0.773	0.760	--	---	+	0
717.65(49)	--	0.104	0.164	--	---	+	6
815.42(08)	1151.58	8.506	7.825	0.24	13.01	+	2
996.21(06)	970.79	66.47	60.05	2.27	11.80	+	2
1047.56(13)	919.44	0.799	0.630	0.06	13.28	+	4
1127.69(14)	839.31	65.67	14.94	17.95	10.65	+	3
1241.34(13)	--	0.659	0.732	--	---	-	1
1251.44(38)	715.56	1.181	0.241	0.33	12.13	-	3
1263.84(24)	703.16	2.181	0.268	0.68	11.82	+	4
1277.33(11)	689.44	0.071	---	0.01	13.56	+	2,3,4
1397.34(21)	569.66	103.35	0.176	36.49	9.78	-	2
1415.04(20)	--	0.039	0.059	--	---	-	1
1418.26(25)	548.75	0.374	0.038	0.12	12.17	+	2
1430.36(20)	536.64	0.142	---	0.05	12.54	+	2,3,4
1509.20(12)	457.80	0.039	---	0.014	12.83	+	2
1531.42(21)	435.66	1.728	0.623	0.36	11.34	+	2
1559.61(57)	407.61	0.044	0.014	0.01	12.75	-	4,3
1617.05(07)	349.93	4.437	0.002	1.57	10.40	-	3
1645.75(17)	321.25	0.454	---	0.16	11.21	+	4
1660.91(31)	306.05	2.465	0.002	0.87	10.48	+	3
1698.38(49)	268.72	0.092	---	0.03	11.70	+	4
1719.43(44)	247.62	83.083	---	29.39	8.65	-	2
1770.17(44)	196.54	0.014	---	0.006	12.04	+	
1790.04(13)	176.96	0.052	---	0.019	11.33	+	4
1796.61(35)	170.46	0.209	---	0.070	10.70	-	3
1838.22(02)	128.78	0.014	---	0.005	11.48	+	2
1860.86(40)	106.14	0.032	---	0.01	10.85	+	2
1895.82(30)	71.96	0.004	---	0.002	11.15	+	2

† Errors in the energy levels quoted are deduced from a single transition measurement,or the standard deviation of the spread of the energy sum relations.

relative intensities to find the experimental conversion coefficients. These results are shown in Table(5.4) normalized to the transition at 996.27 which has been previously well confirmed to pure E2. Theoretical conversion coefficients for K-, L- and M-shells corresponding to different multipolarities are taken from Rosel et al.(1978) and compared to the experimental values to deduce the types of transitions involved. The deduced multipolarities are listed in the last column of Table(5.4) and mostly confirm those reported earlier with the following exceptions: the 591.81 keV transition was reported by Ng et al.(1968) to be E2 in character while the present result agree with an E1 multipolarity, consistent with the transition between $2^- \rightarrow 3^+$ levels. The 873.19 and 892.79 keV transitions had been deduced as E2 in character from all previously reported conversion coefficient works, while here agreement is found with an E2/M1 admixture which is supported by the angular correlation expectations.

In Table(5.4) the electric monopole nature of the 680.56 keV line observed in ^{154}Eu decay as well as with EC experiment [Yamada et al.(1977)] is apparent as no γ-ray transition has been observed with this energy. The large values of conversion coefficients observed for 532.8, 676.63 and 692.41 keV transitions (in both K- and L-shells) suggest an admixture of an E0 component. The electric monopole components in transitions between K and K′ bands are evaluated from an E0 to E2 transition intensity ratio $\mu_{KK'}$,

$$\mu_{KK'} = I_e(E0;I_K-I_{K'})/I_\gamma(E2;I_K-I'_{K'}) \qquad (5.4.1)$$

$$= \alpha_K(E2)\cdot I_e(E0;0_K-0_{K'})/I_e(E2;0_K-2_{K'}) \qquad (5.4.2)$$

for $I_K=I_{K'}=0$ and $I'_{K'}=2$

$$= \delta^{-2}[\alpha_K(exp)-\alpha_K(M1)]+\alpha_K(exp)-\alpha_K(E2) \qquad (5.4.3)$$

for $I_K=I'_{K'}=I_{K'}\neq 0$

where δ is an E2/M1 mixing ratio. In present calculations, the values of δ, Krane (1975), were averaged to estimate $\mu_{KK'}$, and these are

Table(5.4). Deduced multipolarities from K- , L- or M-conversion coefficients .

Transition (KeV)	α(K) [1000] Experiment	Theory E1	Theory E2	Theory M1	Multipolarity (Present)
123.00	612. (7)	123.	660.	920.	E2
247.93	88. (5)	23.0	79.5	135.	E2
444.42	19.3 (34)	5.00	15.3	29.5	E2
478.29	11.9 (43)	4.50	12.8	24.7	E2
532.80	930. (350)	3.42	9.50	18.3	E0+(E2+M1)
557.59	7.7 (29)	3.13	8.60	16.3	E2
582.12	2.94 (76)	2.83	7.75	14.5	E1
591.81	3.0 (3)	2.75	7.47	14.1	E1
625.33	8.11 (23)	2.45	6.60	12.4	E2
676.63	47.4 (30)	2.11	5.50	10.4	E0+E2+M1
680.56	-----	2.08	5.40	10.2	E0
692.41	43.6 (3)	2.02	5.20	9.85	E0+E2+M1
715.85	8.9 (30)	1.90	4.87	9.25	M1/E2
723.30	2.06 (3)	1.87	4.72	8.90	E1
756.87	4.57 (12)	1.72	4.32	8.10	E2/(M1)
815.54	4.05 (68)	1.46	3.67	6.70	E2/(M1)
873.19	3.52 (6)	1.27	3.15	5.85	E2/M1
892.79	3.89 (38)	1.22	3.00	5.35	E2/M1
904.09	1.23 (68)	1.18	2.91	5.20	E1
996.27	2.36 (18)	0.99	2.36	4.10	E2
1004.77	2.34 (16)	0.97	2.30	3.98	E2
1274.45	0.707(12)	0.63	1.41	2.26	E1
1596.54	0.43 (13)	0.41	0.88	1.35	E1

Transition (KeV)	α(L) [1000] Experiment	Theory E1	Theory E2	Theory M1	Multipolarity (Present)
123.00	402. (80)	22.00	400.0	145.	E2
247.93	22.6 (13)	3.100	23.00	20.0	E2
532.80	107. (50)	0.480	1.730	2.66	E0+(E2+M1)
591.81	0.28 (11)	0.380	1.270	2.20	E1
692.41	5.2 (3)	0.268	0.830	1.35	E0+E2+M1
723.30	0.24 (3)	0.245	0.740	1.21	E1
756.87	0.65 (9)	0.222	0.665	1.08	E2/(M1)
873.19	0.56 (3)	0.165	0.460	0.76	E2/M1
996.27	0.315(74)	0.129	0.343	0.55	E2
1004.77	0.37 (6)	0.127	0.336	0.54	E2
1274.45	0.06 (2)	0.083	0.203	0.31	E1

Transition (KeV)	α(M) [1000] Experiment	Theory E1	Theory E2	Theory M1	Multipolarity (Present)
123.00	115. (5)		120.		E2
247.93	4.2 (4)		4.5		E2

$$\mu_{\beta g}(676.63 \text{ keV}) = (44.92 \pm 9.94) \times 10^{-3}$$

$$\mu_{\beta g}(692.41 \text{ keV}) = (38.72 \pm 5.50) \times 10^{-3}$$

for the transitions from β band. The estimation for the 532.8 keV transition is not well predicted due to a large error in α_K(exp) value. It is furthermore seen from the remainder of Table(5.4) that there is complete agreement with multipolarities deduced for different electron shells.

– The $K^\pi = 0^+$ ground state rotational band

Three members belonging to this band are observed in this work, the 2^+, 4^+ and 6^+ at energies of 123, 370.93 and 717.65 keV respectively. The percentage branching ratios of β decay feeding the first and second excited states (9.1 and 0.1%) are in disagreement with the values 14.3 and 0.56% reported by Meyer (1968) although their log ft are comparable to the present values. The present log ft values, 12.25 and 13.93, agree with the spin parity assignments of 2^+ and 4^+ which are also confirmed by the observed electric dipole characters of the 123 and 248 keV transitions as shown by K-, L- and M- conversion coefficients in Table(5.4). The 6^+ member at 717.65 keV is only fed by γ-rays depopulating several 4^+ higher energy spin states belonging to different bands.

The I(I+1) energy sequence of the simple rotational behaviour is not expected to fit this band (see the introduction). An admixture of $K^\pi = 0^+$ bands are responsible for this isomer shift in ^{154}Gd as was expected by Rud et al.(1971). The extension of the I(I+1) rules to a third power order has been shown by West et al.(1978) to nicely fit the levels up to 6^+, during their investigations on high excited spin states in ^{154}Gd by the reaction (α, 2nγ) and by the decay of the isomers ^{154}Tb.

– The $K^\pi = 0^+$ β-vibrational band.

The energies of the 0^+, 2^+ and 4^+ members of this

band observed in the present work are 680.59, 815.42 and 1047.56 keV respectively. The 680.59 keV level is fed by γ-rays predominantly from the 2^+ member of the second $K^\pi = 2^+$ band. This level decays by γ-ray transition with E2 component at 556 keV to the 123 keV level as established from coincidence results, and by an E0 component to the g.s. confirming the 0^+ assignment. The other two members of this band are directly fed from ^{154}Eu decay by β and γ transitions. A log ft values of 13.01 and 13.28 agree to the 2^+ and 4^+ spin-parity assignments to the 815.42 and 1047.56 keV levels respectively. On the other hand the presence of E0 components admixed with the γ-ray transitions depopulating these levels at energies 692 and 677 keV also support the spin-parity assignments.

The deviation of the energy levels from the I(I+1) sequence is noticed and is often suggested as being caused by a mixing of other bands with this band (see later). This is also reflected in a comparison of the experimental B(E2) ratios for transitions decaying from these levels to the g.s. band with the theoretical values predicted by the adiabatic symmetric-rotor model [Alaga et al.(1955)]. That is seen in Table (5.5.a) which shows these ratios for all allowed K_i values in these transitions.

– The $K^\pi = 2^+$ γ-vibrational band.

The levels of this band have caused great interest in the past [Riedinger et al.(1970), Meyer (1968 b)]. The 2^+, 3^+ and 4^+ members of this band at 996.21, 1127.69 and 1263.84 keV have been observed to be strongly fed from ^{154}Eu decay in this work. The spin and parity assignments are established from the log ft values and the types of transitions involved with these levels.

The energy spacings of successive spin members of this band exhibit a behaviours which could be due to bands coupling [the highest spin member of this band is 7^+ reported by West et al.(1978)]. The relative B(E2) values obtained in this work are compared in Table(5.5.b) to the adiabatic symmetric-rotor model with various K_f values. It must be noted

Table(5.5). Relative B(E2) values for transitions from (a) beta band, (b) gamma band are compared to the values predicted by the adiabatic symmetric rotor model.

- a -

I_i^+	I_f^+	Initial level (kev)	Final level (kev)	K_f^+	Experiment	K_i^+ 0	1	2
2	0	815.42	0.0	0	0.13(3)	0.7	2.78	0.7
	2		123.00	0	1.0	1.0	1.0	1.0
	4		370.93	0	2.88(12)	1.8	3.18	0.052
4	2	1047.56	123.00	0	0.086(7)	1.1	11.95	0.34
	4		270.93	0	1.0	1.0	1.0	1.0
	6		717.65	0	2.78(21)	1.75	12.15	0.09

- b -

I_i^+	I_f^+	Initial level (kev)	Final level (kev)	K_f^+	Experiment	K_i^+ 0	1	2
2	2	996.21	815.42	0	2.9(12)	1.43	0.36	1.43
	0		680.59	0	1.0	1.0	1.0	1.0
	0		00.0	0	0.24(10)	0.7	2.78	0.7
	2		123.00	0	1.0	1.0	1.0	1.0
	4		370.93	0	0.076(32)	1.8	3.18	0.052
3	2	1127.69	815.42	0	0.007(1)	0.0	0.4	2.5
	4		1047.56	0	1.0	1.0	1.0	1.0
	2		123.00	0	0.94(2)	0.0	0.4	2.5
	4		370.93	0	1.0	1.0	1.0	1.0
4	2	1263.84	123.00	0	0.035	1.1	11.95	0.35
	4		730.93	0	1.0	1.0	1.0	1.0
	6		717.65	0	0.10(4)	1.75	12.15	0.09

that the values of δ mixing ratios used in the present calculation of this chapter are taken as the average values of the following references; Krane (1979), Gupta et al.(1977), Hamilton & Kumar (1979), Whitlock & Hamilton (1971) and Rikovska et al.(1981), unless stated. Otherwise a transition was considered to be pure (E1 or E2) in character.

– The $K^{\pi} = 0^{-}$ octupole band.

This octupole-vibrational band has been first observed in the inelastic deuteron scattering work of Block et al. (1967). This was made with level spins of 1^{-}, 3^{-} and 5^{-} at energies 1241.3, 1251.7 and 1364.2 keV. In this work, the first two members are observed and confirmed by the singles and coincidence measurements.

The 1241.34 keV is populated only by γ-rays in disagreement with Meyer (1968). It decays through two transitions, 1241.25 keV to the g.s., and 1118.44 keV which feeds the first 2^{+} level. The E2 character of the 478.29 keV transition, which populates this level from the 2^{-} state member of the $K^{\pi} = 2^{-}$ band, confirms the 1^{-} spin-parity assignments.

The second level is observed at 1251.44 keV with a log ft value of 12.13. A new transition suggested in this work at energy 435.6 keV may depopulate this level to the 815.42 (2_2^{+}) keV level, and is consistent with the spin-parity assignment 3^{-}.

Using the assumption that all transitions depopulating these two levels are pure E1 transitions, the B(E1) ratios are calculated and compared in Table(5.6) with the values predicted by the adiabatic symmetric-rotor model. The ratio for the first 1^{-} level is closer to the predicted value for $K_i=0$. However, the experimental value of the B(E1) ratio of the first 3^{-} level is more difficult to explain at this stage, but as pointed out by Meyer (1968), the close energy spacing between these two levels indicates a large amount of Coriolis coupling.

Table(5.6). Comparison between the experimental B(Eλ) ratios and the prediction of the adiabatic symmetric rotor model.

Level (keV)	I_i^π	I_f^π	K_f^π	E (keV)	Experiment	K_i=0	K_i=1	K_i=2
1241.34	1^-	0^+	0^+	1241.25	0.85(5)	0.5	2.0	
		2^+	0^+	1118.44	1.0	1.0	1.0	
1251.44	3^-	4^+	0^+	880.70	1.0	1.0	1.0	
		2^+	0^+	1128.68	1.34(18)	0.75	1.33	
1397.34	2^-	3^+	2^+	269.89	0.12(2)		2.0	0.5
		2^+	2^+	401.27	1.0		1.0	1.0
		3^-	0^-	145.93	1.77(19)		4.0	0.25
		1^-	0^-	155.92	1.0		1.0	1.0
1617.05	3^-	4^+	0^+	1246.15	2.10(3)	1.33	0.75	
		2^+	0^+	1494.10	1.0	1.0	1.0	
1415.04	1^-	2^+	0^+	1292.19	1.0	1.0	1.0	
		0^+	0^+	1414.90	0.25(9)	0.5	2.0	
1719.43	2^-	2^+	2^+	723.30	1.0		1.0	1.0
		3^+	2^+	591.81	0.45(5)		2.0	0.5
1796.54	$(3)^-$	2^+	2^+	800.31	1.0		1.0	1.0
		3^+	2^+	669.2	1.17(23)		8.69	1.4

– Level at 1277.33 keV.

In this work, indications supporting the feeding of this level from the decay of ^{154}Eu appeared when the transition at 906.4 keV was seen in coincidence with the gates of 248 and 123 keV. These observations of the transition, and hence the level, give strong support to a level previously proposed by Meyer (1968) about this energy region, which had not been confirmed since. The present estimation of its spin-parity assignment, for a log ft value of 13.56, may take 2^+, 3^+ or 4^+, and without further information it is difficult to fully classify this level and it is possible that it might not be collective in nature.

– The $K^\pi = 1^-$ octupole band.

This band has been well studied in the past and was assigned $K^\pi = 1^-$ by Meyer (1968) and later confirmed by Riedinger et al.(1970). Four levels belong to this band are observed in this work and established by coincidence measurements at energies 1397.34 (2^-), 1415.04 (1^-), 1559.61 (4^-) and 1617.05 (3^-) keV.

The 1397.34 keV level is well established by the coincidence results. It is the most favoured level fed from ^{154}Eu decay, as 36.5% of the total beta branching ratio is consumed by this level, leading to small log ft value (9.78). In addition to two (E1) transitions, at energies 582.12 and 1274.45 keV, depopulating this level to the second and first 2^+ states, led to the level assignment of 2^-. An additional two transitions decaying to the 2^+ and 3^+ states members of the γ-vibrational band do not clearly favour the $K_i^\pi = 1^-$ assignment, as indicated in Table(5.6) if it assumed that they are pure E1 in character. The E2 transition rate ratios from transitions populating the 1^- and 3^- states of the $K^\pi = 0^-$ band showed better agreement to a $K^\pi = 1^-$ assignment [Table(5.6)]. A fact which strengthens the notion that these bands are not purely rotational in nature.

The 1415.04 keV level is seen not to be fed from β^--

decay as the total intensities of feeding transitions is almost equivalent to the output intensities within the error limits. This level is established when the transition at 1292.19 keV was observed in the coincidence spectrum of the 123 keV gate. All transitions which populate and depopulate this level give rise to the spin-parity 1^- assignment.

Both the levels 1559.61 and 1617.05 keV have a finite β-branching ratio, and the latter is strongly fed by β (1.57%). In this work, all information available about the former level could not uniquely define its spin assignment; Gupta et al. (1977) reported the electric dipole character of the 1188.27 keV transition which was also detected in the coincidence spectrum of 248 keV in this work, then the subsequent log ft value 12.75 equally supports the spin parity assignment 3^- and 4^-. The latter is more consistent with the spin sequence in this band and so will be adopted in this work as also reported by Meyer (1968).

As for the 1617.05 keV level, the present coincidences show the 1246 keV transition in both gates 123 and 248 keV, and the 1494 keV transition in the spectrum of 123 keV gate. Such observations are in agreement with the coincidence work of Gupta et al.(1977) who also suggested the E1 nature for the transitions at 1246 and 1494 keV. The subsequent negative parity character of the level is consistent with strong β feeding, and for a log ft = 10.4, the spin-parity 3^- is strongly favoured.

For B(E1) ratios, the predictions of the adiabatic symmetric-rotor model show considerable disagreements when compared to the experimental values for all levels belong to this band [Table(5.6)]. Also the inversion of the energy sequence in this band undoubtly indicates a large amount of Coriolis coupling acting between the $K^\pi = 0^-$ and $K^\pi = 1^-$ bands.

— The second $K^\pi = 0^+$ band.

Meyer (1968) reported a level at 1292.75 keV with spin-parity 0^+, and considered this level as the bandhead of

a second $K^{\pi} = 0^{+}$ band. However, his energy at 125.6 keV, which fed this level, and another two transitions at 612.0 and 1170. keV depopulating the level to the states 0_2^+ and 2_1^+, were not observed in the present singles work, not by Riedinger et al.(1970), Gupta et al.(1977) or Sharma et al.(1980). Strangely the 612.0 keV γ-ray transition was given to accommodate the $0^+ \rightarrow 0^+$ transition, but this could only be allowed through the transitionless E0 component.

Later Sousa et al.(1975) in their internal-conversion electron measurements performed on ^{154}Tb decay reported a strong 615.1 keV E0 transition corresponding to decay to the 680.7 keV (0_2^+) level. This led to a placement of a level at 1295.8 keV as the bandhead of a two-phonon character band.

From coincidence measurements, the 1418.26 keV level was established with seven transitions depopulating this level at energies 370.78, 421.84, 602.73, 738.03, 1047.24, 1295.5 and 1418.05 keV [see Table(5.1)]. With a log ft value of 12.15, the spin-parity 2^+ is confirmed for this level.

A third member of this band is tentatively suggested at 1698.38 keV with a possible two transition (651 and 702 keV) depopulating it to the 2_3^+ and 4_2^+ states. Meyer (1968) had reported a transition with energy 701.91 keV and did not put it in the level scheme, while in the present coincidence gate of 873 keV this transition is weakly observed, and so, could not produce firm evidence to establish this level (so this level indicated in Fig.(5.26) as dashed line). It is noted that a level near this energy had been observed in (d,d′) inelastic scattering by Block et al.(1967). If this level does exist from ^{154}Eu decay, the log ft value (11.52) would agree to 4^+ spin-parity assignment.

This band is strongly coupled to the β-vibrational band, as is indicated from the relative B(E2) ratios which favour decay to β-band. Such a fact, and also the occurrence of this band at twice the energy of the one phonon β-vibrational band indicates a two-phonon character for this band. Table(5.7) shows the relative B(E2) ratios for transitions depopulating

Table(5.7). Relative B(E2) values of other levels in ^{154}Gd .

Level (keV)	I_i	E (kev)	I_f	K_f	band	Experiment	K_i 0	1	2	3	4
1418.	2	370.78	4	0	β	1.85(71)	1.8	3.18	0.05		
		602.73	2	0	β	1.0	1.0	1.0	1.0		
		738.03	0	0	β	0.082(34)	0.7	2.78	0.7		
		1047.24	4	0	g.s.	16.9(39)	1.8	3.18	0.05		
		1295.5	2	0	g.s.	1.0	1.0	1.0	1.0		
		1418.05	0	0	g.s.	1.03(24)	0.7	2.78	0.7		
1531	2	267.7	4	2	γ	1.0	1.0	1.0	1.0		
		403.57	3	2	γ	0.13(3)	2.3	0.0	2.3		
		483.79	4	0	β	0.63(22)	1.8	3.18	0.05		
		717.85	2	0	β	1.0	1.0	1.0	1.0		
		850.67	0	0	β	0.53(18)	0.7	2.78	0.7		
		1160.48	4	0	g.s.	5.51(49)	1.8	3.18	0.05		
		1408.5	2	0	g.s.	1.0	1.0	1.0	1.0		
		1531.43	0	0	g.s.	0.18(4)	0.7	2.78	0.7		
1661	3	613.39	4	0	β	0.84(3)		2.5	0.4		
		845.43	2	0	β	1.0		1.0	1.0		
		1290.47	4	0	g.s.	1.43(15)		2.5	0.4		
		1537.93	2	0	g.s.	1.0		1.0	1.0		
1790	4	1072.16	6	0	g.s.	24.2(102)	1.59	1.02	0.26		
		1419.68	4	0	g.s.	0.96(12)	0.91	0.08	2.92		
		1666.87	2	0	g.s.	1.0	1.0	1.0	1.0		
1646	4	382.1	4	2	γ	1.35(36)	43.88	3.95	0.35	1.22	0.2
		518.05	3	2	γ	1.79(9)	14.0	6.82	2.22	0.14	0.56
		649.56	2	2	γ	1.0	1.0	1.0	1.0	1.0	1.0

the 2^+ member of this band to the β and g.s. bands. The decays to the β-band give a clear indication of a $K_i^\pi = 0^+$ assignment whereas the indications of those decays to the g.s. band are more ambiguous.

– Two levels at 1430.36 and 1509.2 keV.

The 1059.43 keV energy has been detected in this work both singly and in coincidences. It was regarded as a transition populating levels in ^{154}Gd nucleus since no background energy was identified about its energy region, and it also appeared in two coincidence spectra with 123 and 248 keV gates [Table(5.2)]. These observations of the transition resulted in proposing a new level at 1430.36 as it could only possible to populate the $371(4^+)$ keV level.

A level at $1509.1(1^-)$ keV had been previously reported only by Meyer (1968). He showed it was fed from the $1719.62(2^-)$ keV level via a γ-transition at energy 209.72 keV and that it decayed through γ-rays at 928.4, 1386 and 1509.1 keV to 0_2^+, 2_1^+ and 0_1^+ states, respectively. Of these transitions, only an energy at 1509.2 keV has been seen in this work. The Q_β restriction allow this energy to populate only the 4_1^+, 2_1^+ or the g.s. As no evidence for this energy was found in the 123 nor 248 keV coincidence gate spectra, the establishment of a level at 1509.2 keV is therefore in support of the work of Meyer (1968). On the other hand, this level was considered to be only β-fed since no γ-ray has been found to populate it yielding a log ft value of 12.83, which agree to either spin-parity assignments 2^+ or 1^-.

– The second $K^\pi = 2^+$ band.

Three members of this band have been observed in this work at energies $1531.42(2^+)$, $1660.91(3^+)$ and $1790.04(4^+)$ keV.

The first member at energy 1531.42 keV is heavily populated from ^{154}Eu decay. In present coincidence spectra, the 267.77 keV transition showed very strong, very weak and strong coincidences with gates 188, 873 and 893 keV respecti-

vely. As a result of the coincidence strengths, this indicates a doublet at this energy in agreement with the decay scheme of Meyer (1968); most of the γ-intensity (2/3 of I_γ estimated within 20% accuracy) is depopulating the 1531.42 to 1263.84 keV levels, while a weaker fraction (1/3 of total I_γ) occurs between the 1263.84 and 996.21 keV levels. The 290.35, 403.57, 483.79, 715.85, 850.67, 1160.48 and 1408.5 keV transitions were all seen in coincidence spectra to depopulate this level to the γ-, β- and g.s. bands, whereas the 1531.43 keV transition decays to the ground state. Those transitions at 267.77 and 483.79 keV were not established by Gupta et al. (1977) from their coincidences, while the present 188 keV spectrum shows a tentative indication at the latter energy. A 2^+ spin-parity is the most consistent assignment, as is also supported by the log ft value of 11.34.

The level at 1660.91 keV is the second member of this band and is established from coincidence results. It was found that the 397.23, 613.39, 664.5, 845.4, 1290.74 and 1537.93 keV transitions depopulate this level to the $4_3^+(\gamma)$, $4_2^+(\beta)$, $2_3^+(\gamma)$, $2_2^+(\beta)$, 4_1^+(g.s.) and 2_1^+(g.s.) states respectively. [refer to Table(5.2)]. Furthermore, the 532.8 keV line was seen in coincidence with the 268, 873, 893 and 1005 keV gates in respective strengths of S, VW, P and P. A case of doublet transition is also possible with an indication (1/3) of the total I_γ falling between the 1661 and 1127 keV levels, while the remaining intensity could only fit to the 1796-1263 keV cascade. When Gupta et al.(1977) gated with the 1005 and 757 keV lines they found very weak evidence for the 533 keV peak, but nevertheless they tentatively ascribed this transition to the 1661 keV level. The present 1005 keV gate also shows weak evidence for the 533 keV peak as most of the transition occurs between the 1796-1263 keV levels. Meyer (1968) reported an energy at 265 keV and the present singles detected an energy at 263.45 keV. This is too weak to be seen in coincidence, but could fit the 1660.9-1397.34 keV transition; on which evidence it was dashed in Fig.(5.26). An assignment of 3^+ was made by Meyer (1968), based upon the fact that no transition corresponding to decay to the 6^+ level of the ground state band is consistent with the predominant E0 character of the

533 keV transition [see Table(5.6)]. This also give an indication of the γ-band character of this level. It must also be noted that an E0 component at 535 keV reported by Anderson & Ewan enhances this postulation as this energy could go between the 1531-996 keV levels.

The 4^+ level at 1790 keV proposed by Meyer (1968) has not been fully confirmed. However, Gupta et al.(1977) reported an 1419.2 keV energy in their 248 keV gate and considered it to depopulate this level. The present singles agree with the work of Meyer (1968) about two close transitions at 1418.05 and 1419.18 keV. The former decays to the g.s. from the level 1418.26, whereas the latter is too weak to be seen in coincidence spectra. Other transitions have also very weak intensities, but could be ascribed to this level on energy fitting basis. These are 538.89, 1072.16 and 1666.87 keV. The 538.89 keV is newly reported in this work as was suggested from the present single measurements whereas the 123 keV gating spectrum gave a weak evidence for the 1666.87 keV transition. It is concluded that although this work supports the suggestion of Meyer (1968) about this level, more evidence is needed to confirm its presence. Nevertheless, a 4^+ assignment is strongly favoured and consistent with present assumptions as well as with the log ft value of 11.33.

Despite the inconsistency observed in Table(5.7) for the experimental relative B(E2) values in comparison with the theoretical values (adiabatic-symmetric-rotor model) for the $K^\pi = 2^+$ assignment, the spacing between the 2^+, 3^+ and 4^+ members of this band show close similarity to those of the $K^\pi = 2^+$ γ-vibrational band. Also the transitions from the 2^+ and 3^+ levels of this band decayed to the γ-band in preference to the β- or g.s. bands. It is also noticed that the 4^+ member does not show this preference. As Meyer (1968) pointed out, this band indicates a two-phonon (βγ) vibrational character; a suggestion further supported by the calculations of Gupta et al.(1977) for the occurrence of a βγ 2^+ level at about 1530 keV.

– The $K = 4^+$ band.

Two levels at 1645.9 and 1770.3 keV suggested by Harmatz et al.(1961) from ^{154}Tb decay were found by Meyer (1968) to be consistent with his energy sum relations. The present singles and coincidences suggest four transitions depopulating the 1645.75 keV level at energies 382.1, 518.05, 598.1 and 649.56 keV supporting the work of Gupta et al.(1977). However, the latter did not report any level at 1770 keV while in the present 268 keV gate spectrum, an energy at 506.28 keV is detected which could be depopulating the 1789.92 keV level. The 506.28 had been reported by Meyer (1968) to decay from 1770 keV level with three other transitions which are not observed in this work. Also the 893 keV gate gives only weak evidence to this level. However, the log ft values of 11.21 and 12.04 agree to the spin-parities 4 and 5^+ respectively assigned by Sousa et al.(1975) who also made the $K = 4^+$ assignment on a basis that almost pure E2 transition proceeding to the $K^\pi = 2^+$ γ-vibrational band. The presence of 598.1 keV depopulating the 4^+ member to the 4^+ state member of the β(K=0) band disturb the K = 4 assignment though the other transitions to γ-band are faster by ~10 times. This also noticed in Table (5.7) for the 1646 keV level which have been described [Riedinger et al.(1971) & Sousa et al.(1975)] as two quasi particle proton character of a state.

– The $K^\pi = 2^-$ octupole band.

The bandhead at 1719.43 keV is one of the levels most strongly populated from the decay of ^{154}Eu. The log ft value of 8.65 shows better agreement than the value of Meyer (1968) (9.05) for an allowed β transition (GT mode).

Gupta et al.(1977) supported the ten transitions, reported by Meyer (1968), depopulating this level at 188.26, 301.24, 305.02, 322.22, 467.98, 478.29, 591.81, 723.3, 904.09 and 1598.54 keV but did not observe those at 209.72, 73.4 and 58.7 keV. The present investigation also confirms these ten transitions in addition to an energy at 58.32 keV. The consequent decay of this level led to the 2^- assignment that is

also apparent from the dipole characters of the transitions 519.81, 723.3, 904.09 and 1598.54 keV which populate the 3_1^+, 2_3^+, 2_2^+ and 2_1^+ states respectively [see Table(5.4)]. Further confirmation from the E2 component of the 478.29 keV transition which populate the 1_1^- state of the $K^\pi = 0^-$ band.

The evidence for the presence of the 1796.61 keV level, the second member of this band, is related to an earlier discussion about the 532.8 keV transition from the 1660.91 keV level in the $K^\pi = 2^+$ band. Additionally, the 800.31 and 981.56 keV transitions are weakly detected in coincidence with the gates 873 and 444 respectively. The weakness of the latter transition in the coincidence spectrum could be referred to a missing part of its total intensity elsewhere in the decay scheme, i.e., the 1698-718 cascade, as pointed out by Sousa et al.(1975). Another energies at 669.2, 1673.84 and 237.03 keV are placed on the basis of energy sum relations. The latter transition was reported by Sharma et al.(1980)as well as the 669.2 keV. While three transitions have been reported by Sousa et al.(1975) at 669.2, 800.31 and 981.56 keV from ^{154}Tb decay but the 1724.6 keV was not seen in their singles as well as the present whereas Gupta et al.(1977) assign only the 982. keV transition to this level from coincidence work on ^{154}Eu decay.

The relatively low log ft value quoted in the present work (10.7) is in consistency with the negative parity character of this band. Also the spin 3 is clearly established from the present work. The assignment of the $K^\pi = 2^-$ for these two levels are apparent from the B(E1) ratios from transitions populating the γ-band as given in Table(5.6).

– Levels at 1838.22, 1860.86 and 1895.82 keV.

Two transitions at 574.35 and 1838.21 keV assign the 1838.22 keV level. The former is identified in the present singles and newly reported in this work, while the latter had been first reported by Meyer (1968) but not confirmed since. However, both transitions are too weak to be seen in coincidence. Therefore the level is established on energy sum

considerations and on the fact that the 1838.21 keV transition was unlikely to populate the first excited states 2_1^+ (123 keV) as the energy of the consequent level is just equivalent to Q_β value. Consequently the spin-parity 2^+ is the most likely assignment which is in agreement with the assignment of Meyer (1968).

Another two energies at 1180.69 and 1737.47 are proposed in this work after being detected in the single spectra. These two transitions and the 1489.91 keV transition were ascribed to the 1860.86 keV level, which had been first suggested by Meyer (1968). In fact, a slight indication in the coincidence gate of 248 was noticed for the 1489.91 keV transition, but this is not exclusive. A 2^+ spin-parity could only fit the present level. This is in disagreement to the assignment (4^-) made by Meyer (1968).

The last level at 1895.82 keV is established after identifying a transition with its energy value which could only depopulate to the g.s., because of Q_β restriction. Both the transition and the level were reported by Meyer (1968), and his spin-parity assignment (2^+) was reasonably suggested.

— Levels at 1135.79, 1179.01 and 1524.04 keV.

Meyer (1968) reported a level at 1136.07 keV populated by three transitions 591.74, 480.6 and 260.9 keV and accordingly de-excited via the 1013.1 and 1136.2 keV γ-rays. However, the present results only agree with the energy at 1012.79 keV, and because of its low intensity, it was not seen in any of the coincidence spectra. Instead, weak indication was detected for the 510.32 keV transition in the spectrum of the 188 keV, which together with 1012.79 keV transition, could lead to a level at 1135.79 keV. The latter coincidence is rather dubious as the background radiation at 511 keV (from ^{22}Na) might have affected the coincidence observation. Furthermore the new 524.4 keV energy is also consistent with fitting the transition between the levels 1661-1136 keV.

Weak indications for the 1056.01 and 1153.11 keV

transitions are also observed in the 123 and 248 keV gating spectra respectively, and accordingly, another two levels at 1179.01 and 1524.04 keV are also proposed in the course of this work.

The evidence for these three levels is not regarded as strong enough to warrant their inclusion in the present decay scheme.

5.5 Discussion.

5.5.1 Positive parity states.

The displacement of the level from the simple I(I+1) rule has been partly ascribed to band mixing. A second order modification giving

$$E(I) = (\hbar^2 / 2\mathcal{J})\ I(I+1) + BI^2(I+1)^2 \qquad (5.5.1)$$

where $\mathcal{J}$ is the moment of inertia and the coefficient B of the second order term has contributions from band mixing as discussed by Nathan & Nilsson (1965). The degree of mixing in the wave functions has a very strong effect on the E2 transition probabilities between the vibrational and ground state bands. Also, the inclusion of M1 components to reconcile the experimental B(E2) ratios to those of the Alaga rules did not produce an adequate effect as is shown by the disagreements of columns 2 & 3 in Table (5.8). The Z_γ values from various bands of ^{154}Gd were first estimated by Hamilton et al.(1964) from conversion electron data, and a similar estimation was given by Meyer (1968) from γ-ray results of ^{154}Eu decay. However, the calculations carried out by Riedinger et al.(1967, 1969) studied the Z_K mixing parameters for the β and γ transitions to the g.s. band and was extended to include a mixing between β and γ bands as well. Even though their calculations considered pure E2 transitions depopulating the β and γ bands to the g.s. band, the parameters produced often did not overlap within the quoted errors. As the multipolarity mixing ratios δ(E2/M1) are now experimentally available for the transitions concerned [Krane (1975), Gupta et al.(1977), Hamilton

Table(5.8). Experimental and theoretical ratios of reduced E2 transition probabilities from beta and gamma bands to the ground state band, and the deduced mixing parameters.

$\frac{I_i-I_f}{I_i-I_f'}$	Experiment	Theory"	Mixing parameters x10^{-2}			
			Z_β	$\xi_{\beta\gamma}$	Z_γ	$Z_{\beta\gamma}$
$\frac{2_2-4_1}{2_2-2_1}$	2.88(16)	1.8	1.89(11)	2.24(146)		
$\frac{2_2-0_1}{2_2-2_1}$	0.13(1)	0.7	9.48(51)	1.69(110)		
$\frac{2_2-4_1}{2_2-0_1}$	22.17(116)	2.6	6.09(32)	1.38(90)		
$\frac{4_2-2_1}{4_2-4_1}$	0.090(10)	1.1	5.1(5)	0.14(9)		
$\frac{4_2-6_1}{4_2-2_1}$	32.5(50)	1.59	4.13(64)	-0.36(24)		
$\frac{4_2-6_1}{4_2-4_1}$	2.78(45)	1.75	1.18(19)	0.95(63)		
$\frac{2_3-0_1}{2_3-4_1}$	3.14(16)	14.0			10.0(5)	2.6(13)
$\frac{2_3-2_1}{2_3-0_1}$	4.20(31)	1.43			19.2(15)	-7.5(38)
$\frac{2_3-2_1}{2_3-4_1}$	13.2(12)	20.0			3.5(3)	-2.1(11)
$\frac{3_1-4_1}{3_1-2_1}$	1.05(37)	0.4			8.2(29)	----
$\frac{4_3-4_1}{4_3-2_1}$	28.58(245)	2.94			12.04(103)	-1.56(79)
$\frac{4_3-4_1}{4_3-6_1}$	9.89(204)	11.32			0.64(13)	-2.19(118)
$\frac{4_3-2_1}{4_3-6_1}$	0.35(7)	3.87			7.85(153)	1.05(56)

" From the adiabatic symmetric-rotor model .

& Kumar (1979) and Rikovska et al.(1981)] it is worthwhile recalculating the mixing parameters for these bands in order to test their validity in the ^{154}Gd nucleus. From the above references, the weighted mean values were calculated and the B(E2) ratios for transitions $\beta \rightarrow g$ and $\gamma \rightarrow g$ were obtained as shown in Table (5.8). The parameters determined in the present calculations were evaluated the same way as described by Riedinger et al.(1969), these equations are reproduced in Table (5.9).

Table(5.9). Correction factors for the reduced E2 transition probability between members of the β- and γ-bands (K=0,2) and members of the ground state band.

		B(E2)	
I_i	I_f	Gamma band	Beta band
I-2	I	$[1+(2I+1)Z_\gamma+I(I-1)Z_{\beta\gamma}]^2$	$[1+2(2I-1)Z_\beta-(I-2)(I-3)\xi_{\beta\gamma}]^2$
I-1	I	$[1+(I+2)Z_\gamma]^2$	
I	I	$[1+2Z_\gamma-1/2I(I+1)Z_{\beta\gamma}]^2$	$[1+3(I-1)(I+2)\xi_{\beta\gamma}]^2$
I+1	I	$[1-(I-1)Z_\gamma]^2$	
I+2	I	$[1-(2I+1)Z_\gamma+(I+1)(I+2)Z_{\beta\gamma}]^2$	$[1-2(2I+3)Z_\beta-(I+3)(I+4)\xi_{\beta\gamma}]^2$

The Z_γ values calculated are listed in Table (5.8) column 6, and it is clearly seen that these set of parameters are not consistent as they do not overlap within the error limits; the (4-4/4-2) and (4-2/4-6) B(E2) ratios showing the greatest deviation with the rotational model predictions by about a factor of 10. These however, could be brought into agreement if the 4-2 transition has a considerable amount of M1 mixing, but this is not experimentally observed. In order

to test whether the mixing of the β and γ bands would cause the B(E2) ratios to have a consistent set of mixing parameters, the $Z_{\beta\gamma}$ parameters were recalculated using Z_{γ} value of the 3^+ level. This level contains no admixture from the β band since this band does not have a 3^+ member. The $Z_{\beta\gamma}$ values reported by Riedinger et al.(1969) could just overlap within their uncertainties. Whereas the present values, as shown in column 7 of Table (5.8), are in no way consistent, even with large (50%) reported errors. A similar argument is applied to the mixing parameters Z_{β} (for the $\beta \rightarrow g$ transitions) which also reveals that the inclusion of the β, γ band mixing could not predict the B(E2) ratios [Table(5.8)].

It is therefore concluded that the significant deviations of the experimental B(E2) ratios of the γ and β bands are not predictable only by the mixing of these bands with the ground state. Neither the inclusion of Z or ξ mixing parameters (for γ-β mixing) could explain the experimentally observed E2 transitions probabilities of the ^{154}Gd nucleus. Mixing of additional excitations into the K=0 and K=2 bands might be required.

A phenomenological three band mixing model was applied by Covello & Giberti (1979) to the nuclei $^{154-156}$Gd. Two $K^{\pi} = 0^+$ and one $K^{\pi} = 2^+$ bands was shown to be adequate to produce the B(E2) values and energy levels of the yrast band as well as the energy levels of the β and γ bands. However, a three band mixing model did not satisfactorily describe the back-bending effect observed in ^{154}Gd. Giberti & Maglione (1981) introduced two kinds of mixing for ^{154}Gd; 1) three $K^{\pi} = 0^+$ and one $K^{\pi} = 2^+$ bands, and 2) two $K^{\pi} = 0^+$, a $K^{\pi} = 2^+$ and a $K^{\pi} = 4^+$ band. These predictions have improved the B(E2) values for intraband and interband transitions, as well as the energy level spacing, for the β and g.s. bands.

As noted in Table (5.7) the ratio of the reduced transition probabilities for transitions between the $I_i=4$ member of the $K_i^{\pi} = 4^+$ band to the levels 3^+ and 4^+ of the γ-vibrational band have significant deviations from the rotational model predictions. This discrepancy could also be explained

by considering a mixing between the $K^{\pi} = 4^{+}$ and γ bands. The procedure is similar to that of the mixing of the β and γ bands with the ground state band.

Table(5.10). Esperimental and theoretical ratios of reduced E2 transition probabilities from K=4 band and the gamma vibrational band, and the mixing parameters Z.

$\frac{I_i - I_f}{I_i - I_f'}$	Experiment	Theory*	Z (×100)
$\frac{4_5 - 4_3}{4_5 - 2_3}$	1.35(36)	0.197	3.82(103)
$\frac{4_5 - 3_1}{4_5 - 2_3}$	1.79(9)	0.56	4.24(22)
$\frac{4_5 - 4_3}{4_5 - 3_1}$	0.75(20)	0.353	3.05(88)

* From the adiabatic symmetric-rotor model.

The unmixed B(E2) value for a transition between the two bands is modified by a factor $[1 + ZF]^2$, where Z is the mixing parameter and F is the spin-dependent factor which is given [Sousa et al. (1975)] by,

$$F(I_i,I_f) = f(I_i)\frac{< I_i 220 | I_f 2 >}{< I_i 42\text{-}2 | I_f 2 >} - f(I_f)\frac{< I_i 420 | I_f 4 >}{< I_i 42\text{-}2 | I_f 2 >} \qquad (5.5.2)$$

with $$f(I) = [(I-2)(I-3)(I+3)(I+4)]^{\frac{1}{2}} \qquad (5.5.3)$$

The factors $< I_i K_i L\ K_f - K_i | I_f K_f >$ represent the Clebsch-Gordon coefficients for a transition with L multipolarity depopulating the initial level of spin I_i of the band K_i to a final spin I_f of the K_f band. The Z parameters found in this calculations are listed in the last column of Table (5.10). In Table (5.10), large deviations are noted between ratios of reduced transition probabilities experimentally found and the rotational model predictions. These deviations, which are reported for the $I^\pi = 4^+$ level of the $K^\pi = 4^+$ band (transitions from I=4 level only being available in this work) could be understood and referred to a simple two bands mixing ($K^\pi = 4^+$ and $K^\pi = 2^+$ γ-vibrational band), since the mixing parameters (Z) are consistent within the errors. The average value of Z=3.7 obtained from Table (5.10) is identical to that reported by Sousa et al.(1975), who also included the parameters produced from higher spin levels (5^+ and 6^+).

Inspection of Fig.(5.27) reveals the transitional structure of ^{154}Gd with respect to its neighbouring nuclei. ^{150}Gd is not shown as its high band structures are not clearly defined. But its vibrational behaviour is apparent by the one phonon 2^+ state at 638 keV, and the two phonon triplets, with I=0, 2 and 4, at energies 1207, 1430 and 1288 keV respectively. The vibrational behaviour is also reflected by the ^{152}Gd spectrum as seen in Fig.(5.27) for N=88. On the other hand, ^{156}Gd was a good example of the SU(3) limit [Arima & Iachello (1978)], while the rotational structure of ^{158}Gd (N=94) is observed from the energy sequence of its levels. The second $K^\pi = 2^+$ band is not shown in Fig.(5.27) as it is not observed in $^{156-158}$Gd while it was earlier shown to exist in ^{154}Gd, and its presence in ^{152}Gd could well start at a bandhead of 1605 keV (2^+) and follow with the 1771 keV (3^+) level [Lederer et al.(1978)].

As also noticed in Fig.(5.27) the rotational character, which is described in the IBA model by the SU(3) limit, gradually decreases away from N=94 towards lighter nuclides. From the β, γ and the second $K^\pi = 0^+$ band it is clear that the SU(3) sequence is heavily disturbed at N=90 to "follow" with the N=88 nucleus, which is dominantly characterized by SU(5)

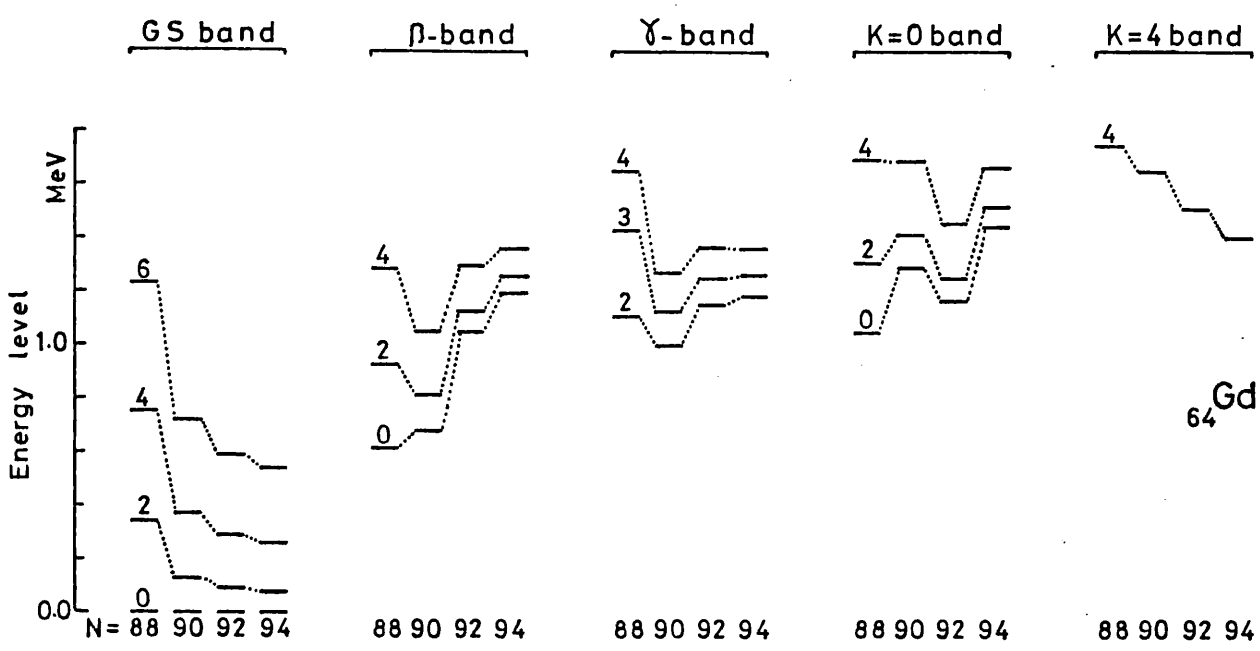

Fig.(5.27) The collective characters of the positive parity states in $_{64}$Gd nuclei between the neutron numbers N=88 to 94.

behaviour. On the contrary, the $K^{\pi} = 4^{+}$ and g.s. bands do not exhibit this abrupt change of behaviour. Hence ^{154}Gd (N=90) could be expected to possess vibrational as well as rotational characteristics. Assessment for the predominant collective features (rotational-vibrational) of the spectrum of ^{154}Gd, which can be revealed by its nuclear properties, will be discussed next.

The application of the IBA model [see chapter II for the theory] to the region of transitional nuclei is of crucial interest, since it offers perhaps the best opportunity to link the IBA Hamiltonian to the more familiar concepts of the collective descriptions, in a region where the latter is broadly applicable. The boson number found for ^{154}Gd with 64 protons and 90 neutrons is 11, since it is referred to the Z=50 and N=82 closed shells [N(total boson number)=$N_{\pi}+N_{\nu}$=7+4=11].

The energy levels produced in the present experimental work are shown together with theoretical levels predicted from the IBM in Fig.(5.28). A few higher spin levels, that were

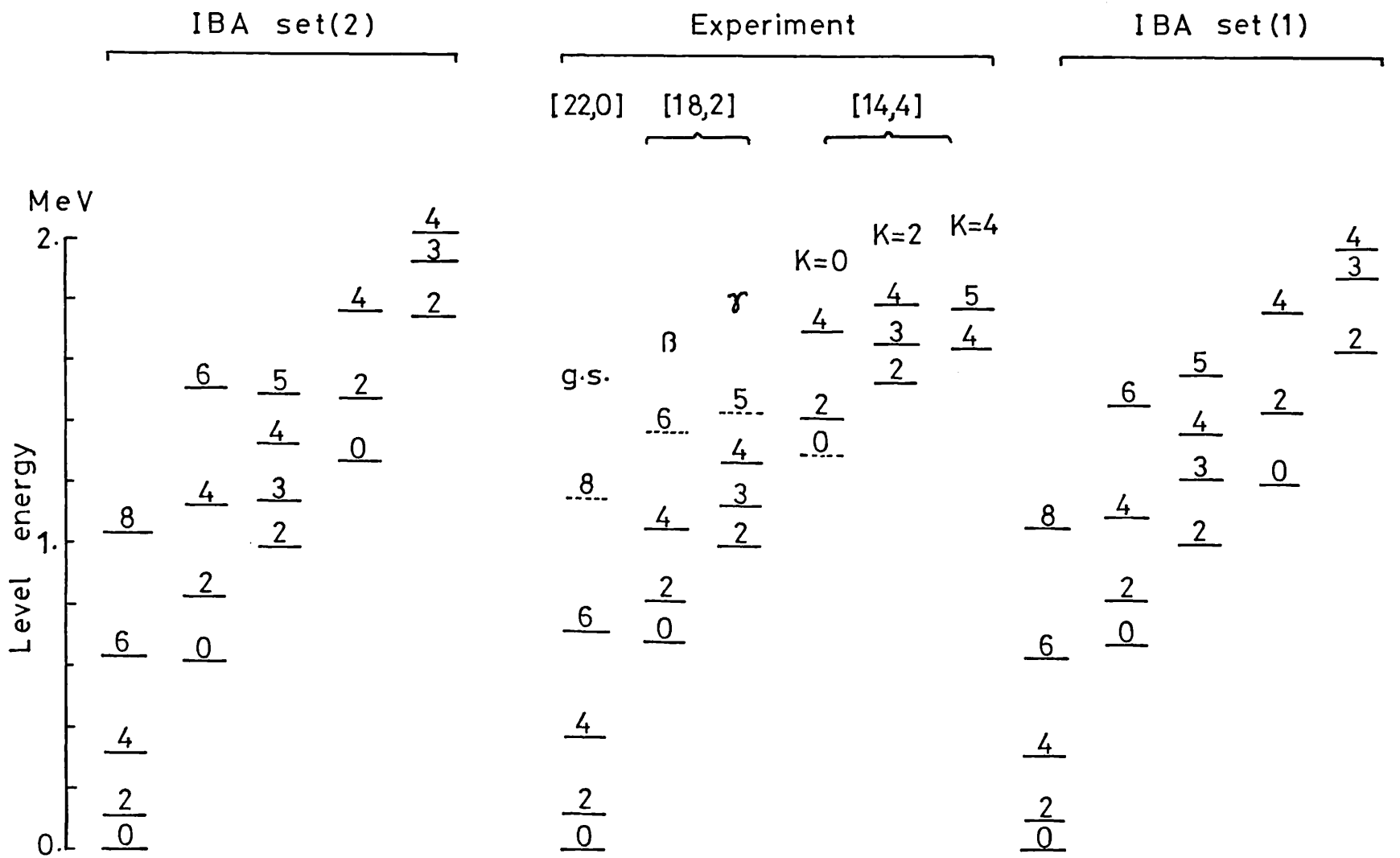

Fig.(5.28). The collective $^{+}_{\lambda}$parity states of ^{154}Gd observed experimentally are compared with IBA-1 predictions of sets (1) and (2).

not populated by ^{154}Eu decay, are also shown as dotted lines for comparison with the theoretical predictions. These theoretical predictions were obtained using the IBA computer code PHINT. The interaction parameters in the IBA Hamiltonian, adjusted to fit 20 state energies of this nucleus, are given in Table (5.11) in two sets, (1) and (2).

Table(5.11). The parameters obtained from IBA model for (a) positive parity bands, (b) negative parity bands (all the parameters are in MeV units except the last two columns in eb).

- a -

Present	EPS	PAIR	ELL	QQ	OCT	E2SD	E2DD
Set(1)	0.338	0.00	0.006	-0.0285	0.0038	0.1749	-0.506
Set(2)	0.465	0.0038	0.003	-0.028	0.00	0.1749	-0.1166
Set(3)	0.368	0.0031	0.01	-0.022	0.0018	0.1749	-0.506

- b -

Present	HBAR3	FELL	FQQ	E1SD	E1DD
Set(1)	0.9872	0.005	-0.13	0.33	-0.1
Set(2)	1.3111	0.005	-0.015		
Set(3)	1.271	0.005	-0.0109	0.495	-0.15

As a good description of the $^{156-158}$Gd properties, made by McGowan & Milner (1981), used the IBA model in the transitional SU(3)-O(6) limits, the inclusion of O(6) parameters in this work is also made with the parameters OCT in set (1) and PAIR in set (2). They play a crucial role in refining the energy level sequences to produce the best fit

to the twenty state energies as well as for the contribution in the B(E2) values. The pairing term displaces the $K^{\pi} = 0^{+}$ bands, while the octupole term mainly affects the high spin states and leaves the lower spin states almost unchanged. As these two parameters are equal in magnitude, the I(I+1) term (ELL parameter) and the boson energy term (EPS) had to be re-adjusted to produce the best fit. Hence, one finds the β and the $K^{\pi} = 0^{+}$ bands produced in set(2) are not as good as in set(1) and vice versa for the γ-vibrational band. This fact gave equal average spreads of both sets(1) and (2) with respect to the experimentally observed level as given in Table (5.28) [about 75 keV for both sets(1) and (2)]. In this work, the $K^{\pi} = 4^{+}$ band has not been predicted because the s-, d-boson space of the IBA model does not have enough degrees of freedom. The inclusion of a g-boson, however, is necessary to produce this kind of effect, as was pointed out by Van Isacker et al.(1982) who predicted this band for Gd nuclei using the hexadecupole operator in the IBA Hamiltonian. On the other hand in their work no explanation was given to justify the lack of the $K^{\pi} = 2^{+}$ band, which is nicely predicted in this work.

Recently, Lipas (1983) made an interesting comparison between the IBA-1 model and the "projection model" (PM) [Lipas et al.(1976)] using the sequence $^{150-156}$Gd. The agreement given by the IBA model to the experiments was stated to be better than that of the simple boson (PM) model which does not include a s-boson. As a check, his IBA parameters given for the ^{154}Gd nucleus were used to reproduce the energy levels by the present PHINT program. Furthermore, his parameters (E2SD and E2DD) for E2 transition probabilities were used to recalculate the B(E2) values. These could be compared with the present parameters, which have been selected to give the best overall agreement to all available transitions found in ^{154}Gd in this work. It was done by the computer code FBEM, and all the results obtained are listed in Table (5.12, 13). The results of Van Isacker et al.(1982) are also included in Table (5.12) for comparison.

The interband and intraband B(E2) values of transitions

Table(5.12). Comparison between experimental and IBM predictions of absolute B(E2) values ($10^{-2}e^2b^2$) and B(E2) ratios for inter- and intra-band transitions of the ground state ,beta and gamma bands .

I_i^+	I_f^+	Transition (keV)	Experiment Present	Experiment Van I."	IBM Set(1)	IBM Set(2)	IBM Set(3)	IBM Van I."	IBM Lipas*
2_1	0_1	123.00	76.75(334)	77.3(15)	76.75	76.75	76.75	76.3	76.75
4_1	2_1	247.59	118.4(39)	117.8(39)	109.33	111.14	109.93	109.8	107.75
6_1	4_1	346.72	138.7(106)	138.8(65)	118.6	122.14	120.56	119.0	114.83
0_2	2_1	557.59	24.7(37)	25.8(35)	7.11	10.45	7.78	13.6	2.47
2_2	0_1	815.54	0.44(3)	0.4(1)	0.35	0.28	0.43	1.68	0.36
	2_1	692.41	3.39(36)	3.3(8)	1.59	5.29	1.87	2.54	0.58
	4_1	625.33	9.75(102)	9.0(23)	3.9	2.9	4.41	8.73	1.49
4_2	2_1	924.67	0.33(5)	0.30(8)	0.26	0.22	0.30	1.64	0.40
	4_1	676.63	3.86(47)	2.7(7)	1.57	6.32	1.96	1.54	0.48
	6_1	329.73	10.73(186)	7.1(20)	3.11	0.978	3.52	8.94	1.52
2_3	0_1	996.27	0.24(2)	0.46(12)	0.49	0.66	0.69	0.52	0.6
	2_1	873.19	1.0	1.0	1.0	1.0	1.0	1.0	1.0
	4_1	625.33	0.076(7)	0.139(18)	0.23	0.34	0.34	0.038	0.073
3_1	2_1	1004.77	0.94(33)	1.031(68)	0.78	1.22	1.03	1.76	1.74
	4_1	756.87	1.0	1.0	1.0	1.0	1.0	1.0	1.0
	4_2	79.92	14.1(23)	----	17.85	12.08	61.42	---	0.53
	2_2	312.12	1.0	1.0	1.0	1.0	1.0	1.0	1.0
4_3	2_1	1140.73	0.035(3)	0.142(25)	0.1	0.237	0.28	0.185	0.24
	4_1	892.78	1.0	1.0	1.0	1.0	1.0	1.0	1.0
	6_1	546.00	0.10(2)	0.43(7)	0.47	0.62	0.92	0.081	0.16
2_2	0_2	134.81	26.1(55)	49.(16)	50.8	48.8	52.37	51.0	55.7
4_2	2_2	232.22	113.7(128)	122.(35)	76.5	74.15	78.77	78.	77.61
2_2	0_1	134.81	0.017(3)	0.008(2)	0.007	0.006	0.008	0.033	0.006
	0_2	815.54	1.0	1.0	1.0	1.0	1.0	1.0	1.0
4_2	2_1	924.67	0.0025(2)	0.0025(3)	0.0034	0.0029	0.0038	0.021	0.005
	2_2	232.22	1.0	1.0	1.0	1.0	1.0	1.0	1.0
2_3	2_2	180.72	2.9(5)	2.5	95.4	35.6	1777	13.	1.5
	0_2	315.63	1.0	1.0	1.0	1.0	1.0	1.0	1.0
2_3	0_1	996.27	3.44(52)	2.5	4.6	3.3	97.5	5.3	4.38
	0_2	315.63	1.0	1.0	1.0	1.0	1.0	1.0	1.0
2_3	2_2	180.72	0.20(8)	1.00(2)	10.	7.1	12.7	1.3	0.21
	2_1	873.19	1.0	1.0	1.0	1.0	1.0	1.0	1.0

" Van Isacker et al.(1982).
* Lipas(1983).

Table(5.13). Comparison between experimental and IBM B(E2) ratios for high bands in ^{154}Gd .

Level (keV)	Transition I_i^+	(keV)	I_f^+ K_f^+	Present	Theory Set(1)	Set(2)	Set(3)	Lipas"
1418	2_4	370.78	4_2 0	1.85(71)	1.71	0.43	1.57	2.75
		602.73	2_2 0	1.0	1.0	1.0	1.0	1.0
		738.03	0_2 0	0.82(34)	0.051	0.18	0.002	0.62
		1047.24	4_1 0	16.85(393)	0.0	0.05	0.21	
		1295.50	2_1 0	1.0	1.0	1.0	1.0	
		1418.05	0_1 0	1.03(24)	0.17	0.37	0.0	
1698	4_4	701.91	2_3 2	1.96(58)	0.12	0.35	0.09	0.0
		651.1	4_2 0	1.0	1.0	1.0	1.0	1.0
1531	2_5	267.7	4_3 2	7.61(129)	44.57	11.68	6.3	0.066
		403.57	3_1 2	1.0	1.0	1.0	1.0	1.0
		483.79	4_2 0	0.63(22)	2.34	4.69	307.0	0.075
		715.85	2_2 0	1.0	1.0	1.0	1.0	1.0
		850.67	0_2 0	0.53(18)	1.07	0.82	1.0	0.59
		1160.48	4_1 0	5.51(49)	0.51	0.18	5.4	
		1408.50	2_1 0	1.0	1.0	1.0	1.0	
		1531.43	0_1 0	0.18(4)	0.71	0.4	3.0	
1661	3_2	397.23	4_3 2	15.9(26)	0.2	0.01	0.38	1.46
		532.80	3_1 2	1.2(5)	0.0	0.0	0.0	0.0
		664.50	2_3 2	1.0	1.0	1.0	1.0	1.0
		613.39	4_2 0	0.84(3)	0.55	0.65	6.28	0.58
		845.43	2_2 0	1.0	1.0	1.0	1.0	1.0
		1290.47	4_1 0	1.43(15)	0.96	0.76	0.92	0.59
		1537.93	2_1 0	1.0	1.0	1.0	1.0	1.0
1790	4_5	1072.16	6_1 0	24.2(102)		0.0		
		1419.68	4_1 0	0.96(12)		4.0		
		1666.87	2_1 0	1.0		1.0		
1646	4_6	382.10	4_3 2	1.35(36)	0.75	0.18	0.044	0.3
		518.05	3_1 2	1.79(9)	4.54	15.3	7.68	0.6
		649.56	2_3 2	1.0	1.0	1.0	1.0	1.0

" Lipas(1983).

obtained from both sets (1) and (2) for the g.s., β- and γ-bands are more or less equal [Table (5.12)]. Agreement between the experimental and theoretical values has been achieved to within an average factor of 2. With exceptions are the theoretical ratios (2-2 / 2-0) and (2-2 / 2-2) which are larger than the experimentally observed values by a factor of ~10.

The B(E2) data for higher bands, though scarce, give an insight into the validity of the predictions concerning transitions that are forbidden by the selection rules of the IBA limits. In Table (5.13), for example, despite the fact that most of the B(E2) ratios for transitions from higher bands are not well predicted by the present IBA parameters, these parameters still provide better predictions than the parameters given by Lipas (1983). The difference could be understood by referring to Fig.(5.29). For ^{154}Gd (N=90): the EPS parameter that mainly characterizes the SU(5) vibrational limit, is rather smaller in magnitude than the present value of set (2), which is shown along the dotted line; also, it is noticed that the present ELL parameter of the SU(3) limit is smaller by almost a factor of 10 than the value of Lipas (1983). In other words, the present parameters predict the nucleus of ^{154}Gd to contain predominantly vibrational type characteristics in its structure properties, while Lipas (1983) infers it to a continuation of the rotational behaviour exhibited by $^{154-160}$Gd. It is noted that the selection rules put the reduced matrix elements for transition with $\Delta\lambda > 4$ [see section (2.6.2) for definitions] at zero in the SU(3) representations [Warner & Casten (1982)] which therefore explain the vanishing values of the transition probabilities for some transitions predicted by Lipas (1983) in Table (5.13). The parameters of set (2) were used in the comparison of Fig.(5.29) since this set has a finite value of the pairing parameter, as in Lipas (1983): whereas in set (1), the OCT term replaced the pairing parameter, which was set to zero. However, the striking property of set (1) is that its R value, which represents the ratio of the two operator terms of Eq.(2.6.7), is found to be -2.89 which is very close to the SU(3) prediction [R takes the value 0 in the O(6) or SU(5) limits and $-\sqrt{35}/2$ in the SU(3) limit as explained by Warner & Casten (1982)]. Yet, set

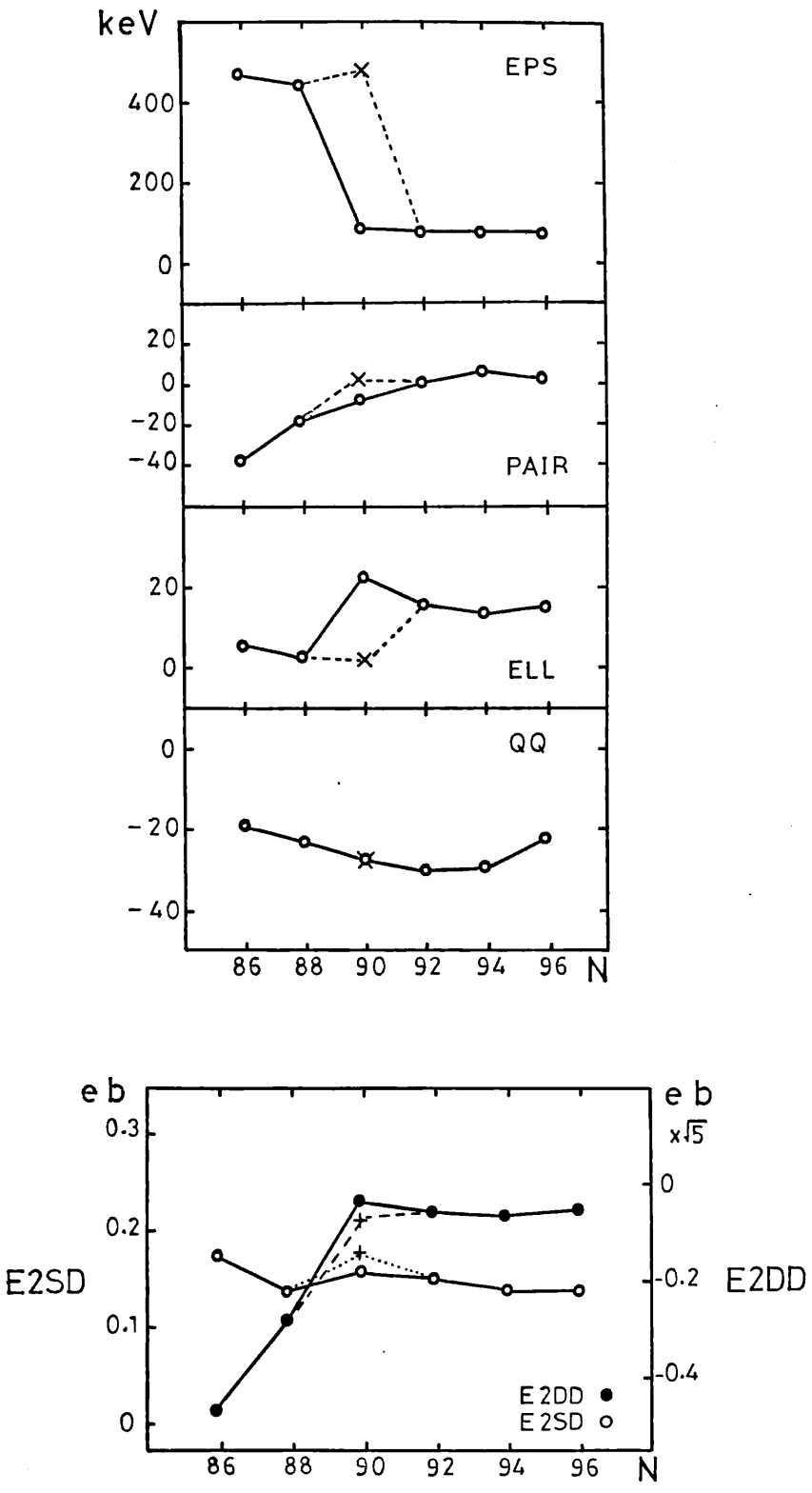

Fig.(5.29). IBA energy parameters for $^{150-160}$Gd. The circles are the results of Lipas (1983) and the crosses indicate the present values for ^{154}Gd.

(1) B(E2) values of transitions with $\Delta\lambda > 4$ are still nonzero. This could be due to large perturbing effect of the operators in the OCT term which greatly breaks the rigorous representation of SU(3) limit.

The discovery of a major subshell closure at Z=64 and the existence of substantial shape phase transition in the N=88-90 transition region from spherical to quadrupole prolate deformation have been discussed by Casten et al.(1981) for all nuclei known to exist in that region. The recognition that the Z=64 shell closure effectively reduces the number of valence particles appeared to be well justified. Gd nuclei, however, are expected to be "singly magic" as Z=64 is an exact subshell. Indeed, as Talmi (1964) and (1962) has repeatedly emphasized "nuclei which are magic or near magic in one type of nucleon exhibit a remarkable resistance to deformation and a constancy in $E(2_1^+)$ that is a characteristic feature of an unbroken generalized seniority scheme". Also, as the deformation is strongly reliant on the neutron-proton interaction, this led Gill et al.(1982) to introduce what is so-called the "hybrid" parameters which shows that the Z=64 shell has to be used for $N < 88$ and the Z=82 shell for $N \geq 90$. The latter statement is rather astonishing as it refers the proton number to the furthest closed shell (Z=82) rather than to the nearest (Z=50). Nevertheless, this possibility has been tested in this work using the program codes PHINT and FBEM to calculate the energy levels and B(E2) values. As ^{154}Gd has 90 neutrons, the total boson number $N=N_\pi+N_\nu=13$ is used in this case, and two more bosons are added to account for the Z=64 subshell. The parameters used to indicate this case, catagorised set (3) in Table (5.11), have produced energy levels which are generally better than those obtained by set (1) and set (2), and are shown together with those levels produced by Lipas (1983) in Fig.(5.30) [The average spread between the experimental and predicted energy levels produced by the parameters of set (3) is 40 keV and those given by Lipas about 35 keV]. In set (3), both PAIR and OCT parameters, which are characteristic of the O(6) limit, have been used to obtain the ultimate level sequence. The parameter ELL, which does nothing to B(E2) values, is larger than in both sets (1) and (2). The E2

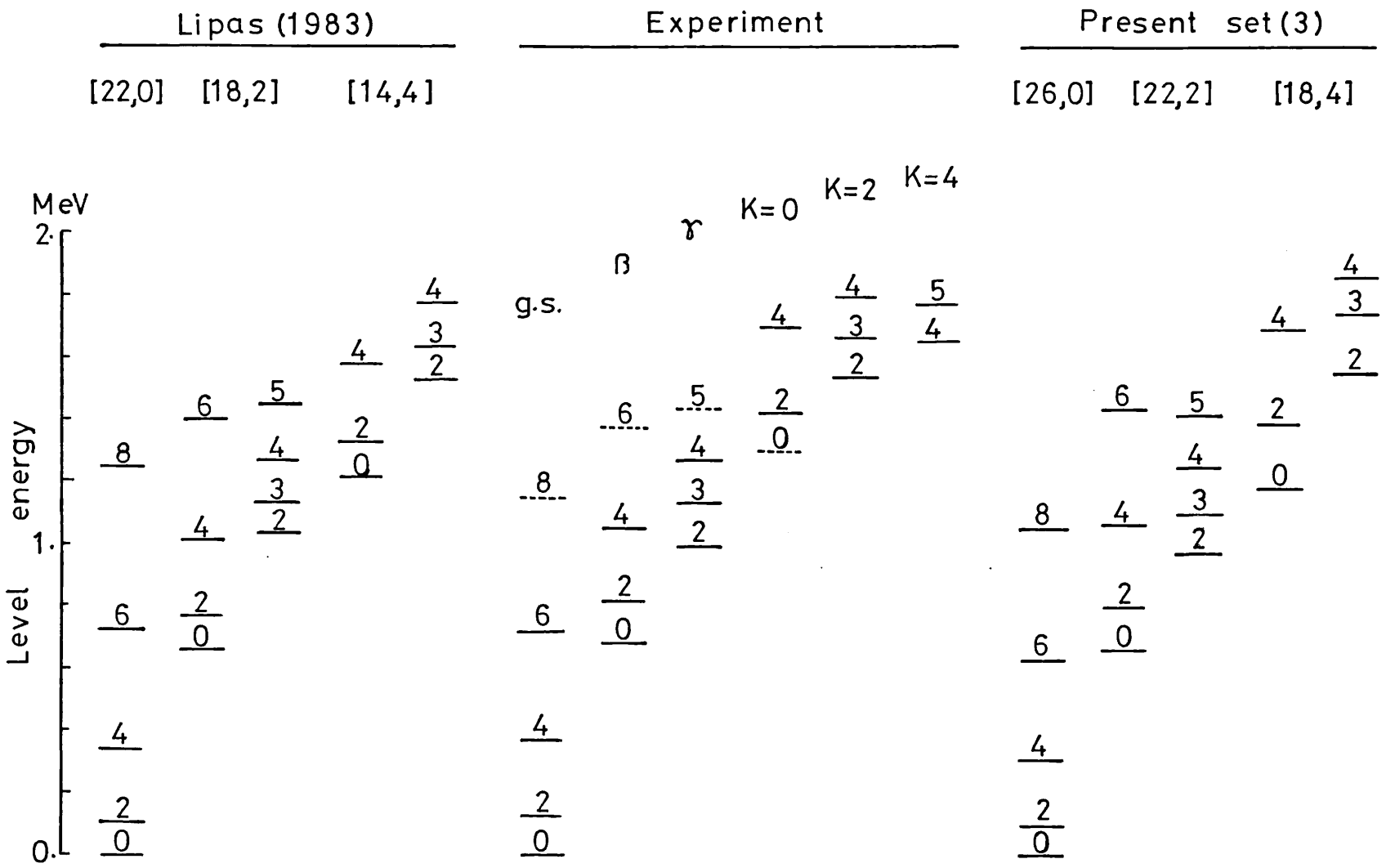

Fig.(5.30). The positive parity states of ^{154}Gd are compared with IBA-1 predictions in the case of subshell closure at Z=64 (set(3)) and with Lipas estimates.

reduced transition probabilities [Table (5.12, 13)] are in good agreement to the experiment and in general do not differ significantly from those produced by sets (1) and (2).

5.5.2 Negative parity states.

The general disagreement between the observed and theoretical B(E1) branching ratios from the $K^{\pi} = 0^-$ and 1^- bands, as shown in Table (5.6), indicates the existence of a strong Coriolis coupling between these bands. This is supported by the inverted ordering of the states in the 1^- band and the suppressed levels in $K^{\pi} = 0^-$ band.

Neergard & Vogel (1970) attempted to describe the negative parity bands by using the random-phase approximation (RPA) for low lying octupole states by incorporating an octupole-octupole force and Coriolis coupling between the lowest $K^{\pi} = 0^-$ to 3^- bands. Their theoretical levels are shown in Fig.(5.31). However, the IBA predictions to the negative parity states, although not including Coriolis type interactions, provide good results by including the three extra parameters HBAR3, FQQ and FELL. This was done by fixing the parameters of the positive parity states [Table (5.11-a)] and varying these three parameters to obtain the final levels to be compared with experiment. The parameters for the three sets (1), (2) and (3) are given in Table (5.11-b) and the results are shown in Fig.(5.32). The 5^- state is shown dashed in the experimental column as this level is not populated by ^{154}Eu.

A treatment of the Coriolis interaction has been worked out by Günther et al.(1968) to describe the properties of ^{160}Dy. This produced a successful interpretation of its negative states and the B(E1) branching ratios. A similar procedure is used in this work to estimate the B(E1) values by considering Coriolis interactions acting on the bands 0^-, 1^- and 2^- of ^{154}Gd. The method as described by Günther et al. (1968) is briefly outlined in this section.

The Coriolis interaction is the interaction that gives rise to a coupling between bands with $\Delta K=1$. It is

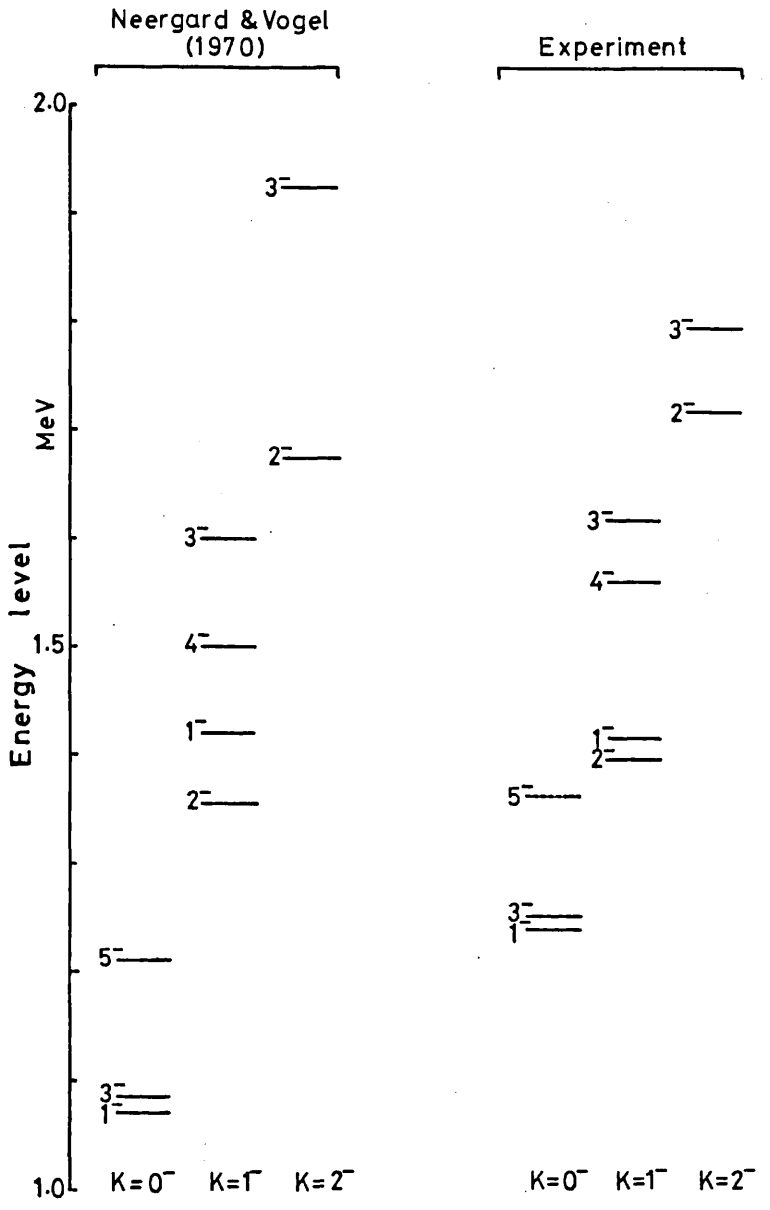

Fig.(5.31). The negative parity states of ^{154}Gd. Dashed line indicates a level which is not populated from ^{154}Eu decay.

assumed that the intrinsic degrees of freedom of these bands is described in terms of one or a few particles moving in an average potential produced by the rest of nucleons and also that this potential is independent of the rotational motion. The first order effect of Coriolis coupling gives rise to a mixing of bands:

$$\psi_I = \Sigma_{K=0}^{I} \alpha_K |IK\rangle \qquad (5.5.4)$$

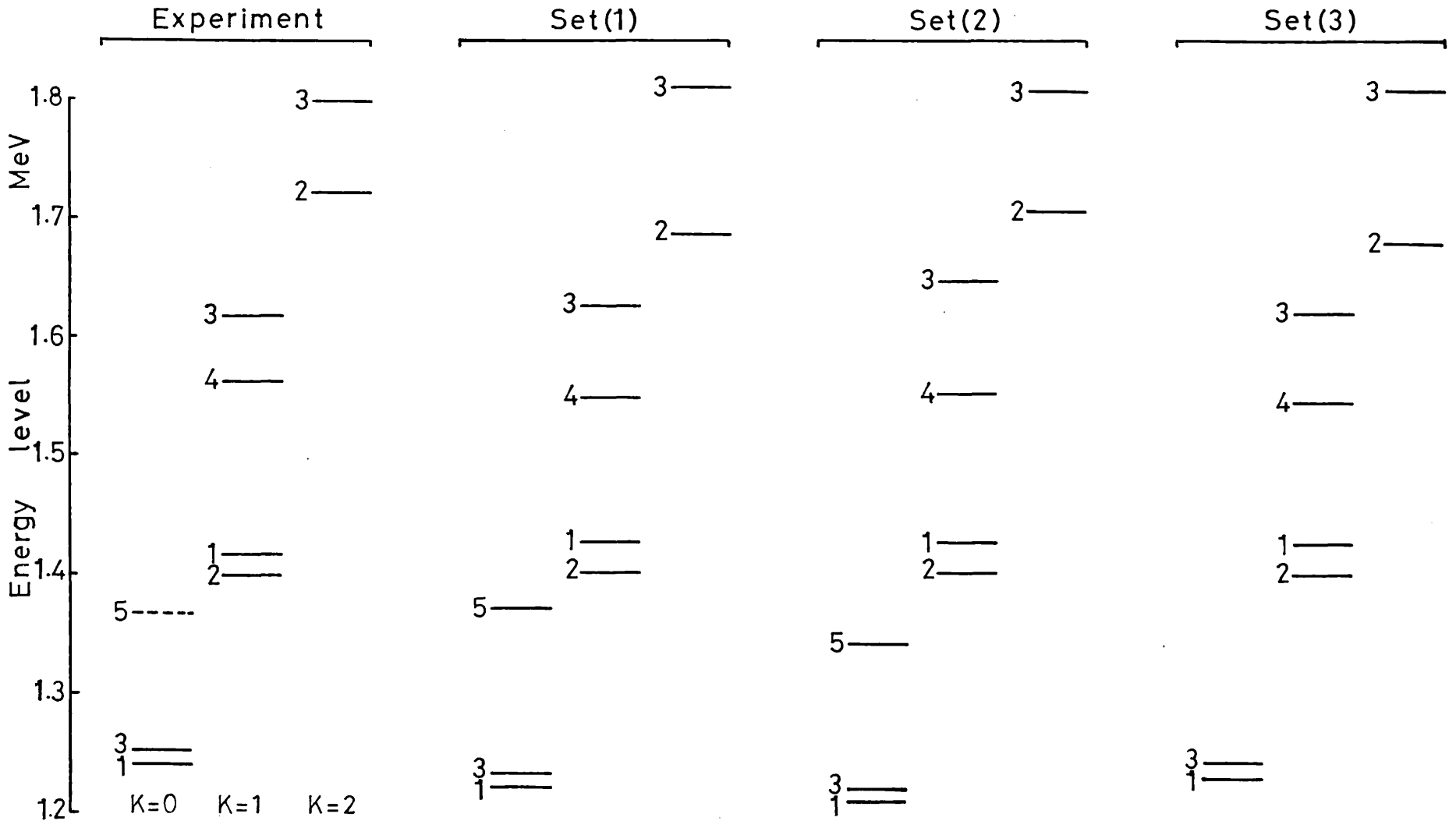

Fig.(5.32). IBA-1 predictions to the negative parity states of ^{154}Gd .

where ψ_I is the wave function of the coupled (or renormalized) state and the first order amplitude of admixture

$$C(I) = < K+1|\varepsilon_{+1}|K > (1-K)^{\frac{1}{2}}(I+K+1)^{\frac{1}{2}} \times \begin{cases} \sqrt{2}\,, & K=0 \\ 1\,, & K\neq 0 \end{cases} \qquad (5.5.5)$$

where $C(I)$ is the ratio of the sizes of amplitude admixture (α_K) of states K and K+1 with normalization function $\Sigma\alpha_K^2 = 1$, and

$$< K_2|\varepsilon_{+1}|K_1 > \equiv \frac{< K_2|h_{+1}|K_1 >}{E(K_2) - E(K_1)} \qquad (K_2 = K_1+1) \qquad (5.5.6)$$

where $$h_{+1} = \frac{\hbar^2}{2\mathfrak{J}_0} J_+ \qquad (5.5.7)$$

and $\mathfrak{J}_0$ is the intrinsic moment of inertia of the residual nucleus and $J_+ = J_1 + iJ_2$ is the component of the total angular momentum of the particles considered. From the energy level spacings E(MeV), one calculates the coefficients α_K of the wave function ψ_I and the results listed here are obtained for $\frac{\hbar^2}{2\mathfrak{J}_0} = 20.5$ keV [Brink (1960)] and $< K=1|J_+|K=0 > = 3.38$, $< K=2|J_+|K=1 > = 3.3$ [Neergard & Vogel (1970)]

$$\begin{aligned}
\psi_2(1398) &= +0.92\,|1,1> -0.39\,|1,2> \\
\psi_2(1719) &= +0.39\,|2,1> +0.92\,|2,2> \\
\psi_3(1617) &= 0.51\,|3,0> +0.55\,|3,1> -0.66\,|3,2> \\
\psi_3(1796) &= +0.77\,|3,1> +0.64\,|3,2> \\
\psi_3(1252) &= 0.73\,|3,0> -0.68\,|3,1> \qquad (5.5.8) \\
\psi_1(1415) &= 0.62\,|1,0> +0.78\,|1,1> \\
\psi_1(1241) &= 0.78\,|1,0> -0.62\,|1,1> \\
\psi_4(1560) &= +0.76\,|4,1> -0.65\,|4,2> \\
\psi_4(1898) &= +0.65\,|4,1> +0.76\,|4,2>
\end{aligned}$$

The last wave function ψ_4 corresponds to the 1898 keV level, which is theoretically considered to exist as a member of the $K^\pi = 2^-$ band. A consideration based on the rotational characteristics of the band, as exhibited by the energies of its 2^- & 3^- members, as well as their modes of decay [see Table (5.6)]. This level has been used instead of the level at 1861 keV (assigned by Meyer (1968) to be the 4^- member of the $K^\pi = 2^-$ band) since the present work disagreed with the 4^- assignment, as described at the last stage of section (5.4).

The reduced matrix element of a transition with multipole λ is given

$$< I_f K_f || M(\lambda) || I_i K_i > =$$

$$(2I_i+1)^{\frac{1}{2}} \{ < I_i K_i \lambda (K_f - K_i) | I_f K_f > < K_f | M'(\lambda, K_f - K_i) | K_i > + \qquad (5.5.9)$$

$$(-1)^{I_i + K_i} < I_i (-K_i) \lambda (K_i + K_f) | I_f K_f > < K_f | M'(\lambda, K_i + K_f) | -K_i > \}$$

where $M'(\lambda, K_f - K_i)$ is the matrix element of the intrinsic coordinate system, and the quantum numbers between the bra-kets define the Clebsch-Gordon coefficients. The reduce transition probability is related to the matrix element in a simple manner.

$$B(\lambda;\ I_i K_i \longrightarrow I_f K_f) = (2I_i+1)^{-1} < I_f K_f || M(\lambda) || I_i K_i >^2 \qquad (5.5.10)$$

The last term of Eq.(5.5.9) vanishes if one of the bands has K=0 or for $\lambda < K_i + K_f$. This is implied for E1 components of transitions depopulating the K_i^-(i=0, 2) to members of the rotational-vibrational bands in ^{154}Gd. Therefore the B(E1) reduced transition probability is given by the expression

$$B(E1;I_i \rightarrow I_f) =$$

$$\alpha_a \langle I_i a 1 (K_f-1) | I_f K_f \rangle \langle K_f | M'(1,K_f-a) | a \rangle \left[1 + \frac{\alpha_b \langle I_i b 1 (K_f-1) | I_f K_f \rangle}{\alpha_a \langle I_i a 1 (K_f-2) | I_f K_f \rangle} R\right] \qquad (5.5.11)$$

$$\text{for} \qquad R = \frac{\langle K_f | M'(1,K_f-b) | b \rangle}{\langle K_f | M'(1,K_f-a) | a \rangle} \qquad (5.5.12)$$

where a and b are the K quantum number of the mixed states (a, b=0, 1, or 2). Hence, in order to calculate the B(E1) ratio one needs to evaluate R from experimental data. In the present work, the R values for transitions depopulating the spin states I from two bands K and K+1, were not seen to be consistent, as should be the case for only this type of Coriolis coupling. This has been expected and arises from the assumption that the K quantum numbers of the ground-state band and the vibrational bands are considered pure. Thus, the final R values used in the present calculations, chosen to give the nearest results to the experimental data, are the following:

$$\frac{\langle 0^+ | M' | 1^- \rangle}{\langle 0^+ | M' | 0^- \rangle} = 0.184(43)$$

$$\frac{\langle 2^+ | M' | 2^- \rangle}{\langle 2^+ | M' | 1^- \rangle} = 8.19\ (193)$$

$$\frac{\langle 2^+ | M' | 1^- \rangle}{\langle 0^+ | M' | 1^- \rangle} = 0.164(13)$$

The relative B(E1) values obtained from this calculation are listed in Table (5.14) show the general agreement between the theoretical and experimental values. In Table (5.14), most theoretical B(E1) ratios deviated by a factor of 2 or less from the experimental value, three of these by

Table(5.14). The experimental B(El) ratios of negative parity states are compared to different theoretical approches.

Level (keV)	I_i^-	K_i^-	I_f^+	K_f^+	Transition (keV)	EXP.	Coriolis	Theory Set(1)	Set(3)
1241	1	0	0	0	1241.25	0.85(5)	0.77	4.38	4.27
			2	0	1118.44	1.0	1.0	1.0	1.0
1251	3	0	2	0	435.60	1.0	1.0	1.0	1.0
			4	0	880.70	3.5(27)	1.1	1.62	1.91
			2	0	1128.68	4.76(359)	1.0	38.43	43.5
1398	2	1	2	0	1274.45	5.72(31)	1.62	64.93	90.55
			2	0	582.12	1.59(9)	1.62	0.95	1.2
			3	2	269.89	0.12(2)	0.12	0.187	0.12
			3	2	401.27	1.0	1.0	1.0	1.0
1415	1	1	2	0	1292.19	1.0	1.0	1.0	1.0
			0	0	1414.90	0.25(9)	0.24	0.08	0.08
1560	4	1	4	2	512.39	8.23(163)	0.77	0.02	0.02
			4	0	1188.27	1.0	1.0	1.0	1.0
1617	3	1	2	2	621.00	0.34(5)	0.34	0.45	0.24
			4	0	1246.15	2.10(3)	2.38	66.0	57.95
			2	0	1494.10	1.0	1.0	1.0	1.0
			4	0	569.36	0.31(6)	2.38	0.78	0.6
1719	2	2	2	0	1596.54	0.008(3)	0.08	2.98	4.98
			3	2	591.81	0.45(6)	0.62	0.63	0.56
			2	2	723.30	1.0	1.0	1.0	1.0
			2	0	904.09	0.023(13)	0.08	0.019	0.023
1796	3	2	4	2	532.80	1.0	1.0	1.0	1.0
			3	2	669.20	0.28(5)	0.49	0.68	0.044
			2	2	800.31	0.24(4)	0.57	3.8	0.53
			2	0	1673.84	0.0021(3)	0.21	3.05	2.96

factor of 10, and that corresponding to the 1673.84 keV transition depopulating the $3^-(K^\pi = 2^-)$ state by a factor of 100. The predicted B(E1) ratio of transitions $(4^- \rightarrow 4_3^+ \; / \; 4^- \rightarrow 4_1^+)$ is found to be 0.77 for the wave function ψ_4 (1560) of Eq.(5.5.8). If however, the 1861 keV level was considered to be the 4^- member of the $K^\pi = 2^-$ band, this ratio would become 0.9 showing no significant difference.

The B(E2) values from the IBA model are obtained from the program FBEM by including the electric dipole parameters E1SD and E1DD. These parameters were allowed to vary freely as the limits on their absolute values are not yet well understood in context of the IBM. The final ratios of E1 transition rates obtained with the parameters of Table (5.11-b) are listed in Table (5.14) for comparison with the predictions of the Coriolis interaction. The latter estimates show remarkable agreement to the experimental values, better than those of IBM.

CHAPTER VI

SUMMARY AND CONCLUSION

A common method of approaching a problem in nuclear physics is to introduce models that simulate, more or less accurately, nuclear behaviour, and when necessary to introduce empirical parameters that help in the description. As a consequence of different nuclear approaches, one may find various models useful, depending on the property under consideration and on the mass number of the nucleus studied. For example: despite the considerable success of collective models, there has nevertheless been applied, for each different type of nucleus (vibrational, transitional, quadrupole symmetric, triaxial, etc.) a different phenomenological model; or, if a microscopic approach is used, its success has generally not been uniform across a broad series of nuclei, i.e. the boson expansion models often converge much more poorly for deformed than for spherical nuclei. In the spirit of overcoming this limitation, the IBA model has greatly simplified the nuclear structure problem by truncating the shell model space so as to lead to a simple boson Hamiltonian, that is applicable equally throughout broad regions of the periodic table. There are two respects, moreover, in which the IBA can be preferable. First, it indicates a finite number of particles outside closed shells, whereas the geometrical models implicitly assume an infinite dimensional space. Secondly, the IBA automatically includes full sequences of intrinsic excitations, including some of their mutual interactions, whereas in geometrical models the higher lying intrinsic collective excitations often have to be introduced explicitly, and their interactions parametrized (i.e. band mixing). In IBA-1 model space, the group decomposition of this space has three non-trivial subgroups, SU(5), SU(3) and O(6). The first two correspond to the familiar vibrational and symmetric rotor limits, while the O(6) limit corresponds to the γ-unstable picture. One of the most powerful and appealing aspects of the IBA is the treatment of the transitional regions between these extreme limiting coupling schemes. The information offered by the structure properties of the two medium mass isotopes ^{124}Te and ^{154}Gd, have allowed a valuable

test of the applicability of the IBA in such transitional regions; the former performs an apparently vibrational motion with γ-unstable characteristics, while the latter is deformed and predominantly transitional (rotational-vibrational) in character. The test has been carried out using the computer program "PHINT" which calculates the energies and eigenvectors for positive and negative parity states by an exact diagonalization of the full IBA Hamiltonian. Also, the electromagnetic transition rates are calculated by mean of the program code "FBEM". The IBA model is currently still being developed, and though it is not independent of other models, it is a significant attempt at a global theory that still does not exist for all nuclei.

The experimental treatment has employed the dual-parameter energy-time spectrometer, which incorporates two large volume Ge(Li) detectors and plastic scintillation counter in order to record coincidence events. The gamma-gamma coincidence measurements following the decay of ^{124}Sb have enabled the energy level scheme of ^{124}Te to be established based on the observation of eighty-four transitions.

The present singles were able to confirm some previously reported transitions, but not confirmed by others, while also proposing fourteen new energies, most of which placed in the decay scheme. The analyses of the coincidence spectra, that were obtained by gating seven lines in the spectrum of ^{124}Te, resulted in establishing two new levels at 2412.69 and 2733.06 keV. The former had been reported in the studies on ^{124}I decay by Ragaini et al.(1969). Another eight levels 2264, 2361, 2580, 2589, 2598, 2754, 2807 and 2627 keV appeared to be newly indicated, but due to the weakness of their de-exciting transitions, these levels were not firmly established, although the three levels at 2264, 2754 and 2807 keV had been proposed in the past Meyer et al.(1969) .

Experimentally determined properties of the ^{124}Te nucleus have been examined in the framework of the IBA-1 model with the number of proton pairs N_π=1 and the number of neutron-hole pairs N_ν=5, so that there are six interacting bosons,

$N=N_\pi+N_\nu$. Small deviations from the SU(5), or vibrational, limit were investigated by means of a first order perturbation calculation. This approximation provided energy levels and B(E2) transition rates in reasonable agreement with experiment. Not all 0^+ states could be predicted, although energy level ratios and B(E2) ratios were well reproduced. The best fits were obtained for a lowest reported 0^+ state at 1156 keV. However, this level has not been recently confirmed and its existence must be regarded as dubious. Higher 0^+ excited states can be obtained by moving away from the SU(5) limit and using the full IBM Hamiltonian, as provided for in the computer code PHINT. However, the corresponding B(E2) values generated by FBEM were not in better agreement with experiment. Clearly, the existence of excited 0^+ states, especially without a level at 1156 keV, points to the nucleus having O(6) characteristics. But it is noted that a nucleus characterised by the O(6) limit of the IBM should possess some fewer gamma-transition probabilities than are experimentally observed in ^{124}Te. For example, the $0_2^+ - 2_1^+$ transition becomes forbidden, and both the observed $2_3^+ - 2_2^+$ and $2_3^+ - 2_1^+$ transitions break the selection rules for E2 transitions in the O(6) limit. It is also noted that the quadrupole moment (Q_2) of the first excited state is zero in the O(6) representation and has a non-vanishing value in the SU(5) limit. Experimentally, the latest Q_2 values [-0.16(8), -0.41(8) eb] of ^{124}Te were reported by Kleinfield et al.(1975), which are consistent with the value of -0.33 eb obtained with the calculation using the complete Hamiltonian. Furthermore, it has been pointed out by Heyde et al.(1982) and Wood (1983) that it is just in those regions where the SU(5) limit is approximately realised that the excitation of a proton (or neutron) pair across a shell or subshell gap would give rise to a low-lying excited 0^+ state, outside the normal s, d boson model space.

In view of the present work the nucleus of ^{124}Te tends to lie closer to the SU(5) limit than the O(6) limit of the IBM, but is most probably transitional as there are indications of a two phase nature, characteristic of a vibrational and γ-unstable "soft" nucleus [Wilets & Jean (1956)].

The decay scheme of ^{154}Gd has been established following the decay of ^{154}Eu from energy sum relations and γ-γ coincidence measurements employing twenty-two gates. Twelve new transitions have been identified, and twenty-five other transitions only previously reported by Meyer (1968) have been confirmed, in the present single spectra from Ge, Ge(Li) detectors and a Compton suppression spectrometer. Transitions are usually obtained with energies having less than 0.1 % accuracy.

Conversion electron coefficients have been measured by combining present γ-ray intensities with the twenty-three conversion electron intensities reported from conversion electron experiments, thereby allowing the multipolarities of transitions contributing to the conversion electron process be deduced. This is achieved by comparing the experimental conversion coefficients with the theoretical values predicted for different multipole orders. Branching ratios of β^--decay, and therefore log ft values, have been determined from the intensity balance between transitions feeding and depopulating a level; using the log ft values and multipolarities obtained the spin-parity assignment of thirty excited states of ^{154}Gd were determined consistent with β-decay and γ-emission selection rules. Of these, the six levels at 1277.33, 1509.1, 1770.3, 1838.22, 1860.86 and 1895.82 keV, which were previously only reported by Meyer (1968), are now regarded as confirmed. Less evidence is available for the 1790.4 and 1698.38 keV levels, and so they are considered not firmly established. A new level is proposed at 1430.36 keV which has been confirmed both from singles and from coincidences. It is also proposed that the level 1860.86 keV Meyer (1968) might not be the third member of the $K^\pi = 2^-$ band (4^-), the present results agree with the 2^+ spin-parity assignment. The lifetime of the first excited state (2^+) of ^{154}Gd has been remeasured by the delayed coincidence method. The present half-life of 1.20 ± 0.05 n. sec. is in agreement with previously reported values, and is used to calculate the absolute B(E2; $2^+_1 \rightarrow 0^+_1$) for the 123 keV transition. It has been recently confirmed by experiments that transitions between the lowest positive parity bands (g.s., β- and γ-bands) possess considerable amounts of M1 characters mixed with E2 components. The presence of magnetic dipole

moments, along with deviations of the energy level spacing in these bands from the simple I(I+1) rule, supports the view that ^{154}Gd is not of a pure rotational character. In order to account for these deviations, calculations of band mixings have been carried out incorporating M1+E2 modes. As a result of these calculations, it appears that ascribing the deviations of ^{154}Gd to a simple mixing of two bands is not adequate to justify the structure of this nucleus. Nor did the inclusion of a second order mixing perturbation ($\beta\gamma$ mixing) produced the proper effect. In general, calculations concerning mixing of bands seem to successfully describe phenomena linked to higher energy excitations than the collective states, i.e. phenomena such as band-crossings or backbendings [Gioberti & Maglione (1981)].

In the case of negative parity states, however, the treatment involves a Coriolis type of interaction. Also Coriolis interactions between $\Delta K=1$ bands assume that the intrinsic potential of the nucleus is independent from the rotational motion. If further assumes that wave functions belong to levels having the same spin in two adjacent bands ($\Delta K=1$) could overlap. As such, the levels are mixed and that affect the rate of their transition probability. The B(E1) values obtained from this calculation were evaluated by applying the same methods of Günther et al.(1968) in their treatment on ^{160}Dy. As agreement between calculated B(E1) ratios and those experimentally observed is achieved, the Coriolis description could provide an evidence for the rotational-like characteristics of the octupole states of this nucleus.

The validity of the IBA Hamiltonian, including the three symmetries SU(5), SU(3) and O(6), has been tested for ^{154}Gd within the framework of s- and d-boson space. The inclusion of O(6) parameters in the Hamiltonian is small, enabling fine adjustment to the overall fit. Five positive parity bands were predicted, the g.s. band, β-, γ-, $K^{\pi} = 0^{+}$ and $K^{\pi} = 2^{+}$ bands, and three negative parity bands with $K^{\pi} = 0^{-}$, 1^{-} and 2^{-}, all of which have been experimentally confirmed in this work. Another band experimentally found with $K^{\pi} = 4^{+}$, was not predicted by the present Hamiltonain and could require

additional degrees of freedom, such as the hexadecupole g-boson, that is outside the limits of the s- and d-boson space [Van Isacker et al.(1982)]. Both rotational and vibrational properties are exhibited by the nucleus of ^{154}Gd because of its transition phase characteristics. The recent work of Lipas (1983) suggested the major characteristics were rotational in nature while the present work gives the vibrational mode a greater significance. In both, agreement with the experimental energy levels and E2 transition probabilities for the g.s., β- and γ-bands was achieved. But for higher bands the present results were able to produce non-vanishing transition probabilities, particularly for the $\Delta\lambda > 4$ transitions, consistent with the departure from the rigorous SU(3) representation, as experimentally observed.

The effect of Z=64 subshell closure involving the use of the so-called "hybrid" parameters [Gill et al.(1982)] has also been considered. The description, which requires shell closure to be referred to 82 for isotopes with Z=64 ($N \geqslant 90$) rather than Z=50, subsequently led to an increase of the total boson member by 2. In the context of the IBA model better estimations have been produced for level properties of ^{154}Gd. The agreement of energy levels with experiment has particularly improved over the usual IBA predictions; the mean spread of energy differences between experiment and theory has reduced by a factor of two. The B(E2) values did not show considerable differences [a chi squares test used to inspect the goodness of the predicted absolute B(E2) values of Table (5.12) suggests the best estimate is produced by set (3); chi squares for sets (1) and (2) were larger by 20 % and 50 % respectively. By comparison, chi square estimates from the results of Lipas (1983) were larger by over a factor of two, and those of Van Isacker et al.(1982) by a factor of 18]. Within the subshell description, both the parameters (OCT, PAIR) of the O(6) representation had to be used in order to produce the fit. An estimation for the quadrupole moment Q_2 of the first excited state (empirically calculated to be -1.78 eb for the deformation parameter β=0.31) was found in the framework of IBA calculation to be -1.79 eb for set (3), -1.78, -1.74 for sets (1) and (2) and also -1.76 from the parameters

of Lipas (1983). One consequence of subshell closure at Z=64 is the formation of a second low-lying 0^+ (s-boson) or 2^+ (d-boson) state [Van Isacker et al.(1982)]. Such possible intruder 2^+ states could be the newly observed levels at 1430.36 keV and at 1509.2 keV, which were not ascribed to any of the available positive bands. This provides further evidence concerning the effectiveness of Z=64 subshell closure in nuclei [Ibrahim & Stewart (1983)].

It is concluded from the present observations that the transitional nature of the ^{154}Gd nucleus is mainly exhibited withinavibrational-to-rotational region. Although the rotational sequences are apparent in its energy level spacings, there is strong evidence from B(E2) values to indicate the vibrational nature of the nucleus. Furthermore, the inclusion of a small amount of the O(6) representation is required to explain its overall properties. In view of a possible subshell closure at Z=64, the hybrid parameters were investigated and these were found not to enhance the deformation [SU(3)] mode despite the increase of total boson number. Better estimates were obtained with the hybrid approach reflecting the usefulness of this description and highlighting the effectiveness of a subshell closure in the concept of nuclear physics.

REFERENCES

- Ahmad A., P.W.Gray, T.D.MacMahon and M.Macwani, 1981, 6th international conference on modern trends in activation analysis. Toronto, Canada.

- Ahmad A., 1982, Ph.D thesis, Imperial College, University of London.

- Alaga G., K.Alder, A.Bohr and B.R.Mottelson, 1955, Kgl. Dansk. Videnskab. Selskab, Mat. Fys. Medd. 29, 9.

- Alder K., A.Bohr, T.Huus, B.Mottelson and A.Winter, 1956, Rev. Mod. Phys. 28, 432.

- Anderson G.I. and G.T.Ewan, 1969, Nucl. Phys. A 123, 609.

- Arima A. and F.Iachello, 1976, Ann. Phys. (N.Y) 99, 253.

- Arima A. and F.Iachello, 1978, Ann. Phys. (N.Y) 111, 201.

- Arima A. and F.Iachello, 1979, Ann. Phys. (N.Y) 123, 468.

- Arima A. and F.Iachello, 1981, Ann. Rev. Nucl. Part. Sci. 31, 75.

- Auer I.P., J.J.Reidy and M.L.Wiedenberck, 1969, Nucl. Phys. A 124, 199.

- Baranger M. and K.Kumar, 1965, Nucl. Phys. A 62, 113.

- Baranger M. and K.Kumar, 1968a, Nucl. Phys. A 110, 490.

- Baranger M. and K.Kumar, 1968b, Nucl. Phys, A 122, 241.

- Belyaev S.T. and V.G.Zelevinsky, 1962, Nucl. Phys. 39, 582.

- Bertolini G. and A.Coche, 1968, Semiconductor detectors (North Holand Pub. Comp. Amsterdam).

- Blatt J.M. and V.F.Weisskopf, 1952, Theoretical Nuclear Physics, (John Wiley & Son, New York).

- Bloch R., B.Elbeck and P.O.Ty m, 1967, Nucl. Phys. A91, 576.

- Bohr A., 1952, Kgl. Dansk Videnskab Selskab, Mat. Fys. Medd. 26, 14.

- Bohr A. and B.Mottelson, 1953, Kgl. Dansk Videnskab Selskab, Mat. Fys. Medd. 27, 16.

- Bohr A., 1957, Amr. J. Phys. 25, 547.

- Bohr A. and B.F.Bayman, 1958a, Nucl. Phys. 9, 596.

- Bohr A., B.Mottelson and D.Pines, 1958b, Phys. Rev. 110, 936.

- Brantley W.H., J.H.Hamilton, T.Katoh and E.F.Zganijar, 1968, Nucl. Phys. A 118, 677.

- Brink D.M., 1960, Process in Nucl. Phys. 8, 99.

- Brink D.M., A.F.R.de Toledo Piza and A.K.Kerman, 1965, Phys. Lett. 19, 413; G.Gneuss and W.Greiner, Nucl. Phys. A 171 (1971) 449 and references therein.

- Bushnel D.L., R.P.Chaturvedi and R.K.Smither, 1969, Phys. Rev. 179, 1113.

- Casten R.F. and J.A.Cizewski, 1978, Nucl. Phys. A 309, 477.

- Casten R.F., 1980, Nucl. Phys. A 347, 173.

- Casten R.F. 1981, see Iachello 1981.

- Casten R.F., D.D.Warner, D.S.Brenner and R.L.Gill, 1981, Phys. Rev. Lett. 47, 1433.

- Casten R.F. and D.D.Warner, 1982, Neutron Capture Gamma-ray Spectroscopy and Related Topics (Inst. Phys. Conf.

Ser. 62) P. 28.

- Christensen P.R., G.Lovhoiden and J.Rasmussen, 1970, Nucl. Phys. A 49, 302.

- Covello A. and G.Giberti, 1979, J. Phys. G. 5, 989.

- Davidson J.P. and M.G.Davidson, 1965, Phys. Rev. 138 B, 316.

- Davydov A.S. and A.A.Chaban, 1960, Nucl. Phys. 20, 499.

- De-Shalit A. and H.Feshbach, 1974, Theoretical Nuclear Physics, Vol.1, Nuclear Structure (J.Wiley & Sons, Inc. New York).

- Degrieck E. and G.Vander-Berghe, 1974, Nucl. Phys. A 231, 141.

- Demidov A.M., L.I.Gover, I.B.Shukalov, M.R.Akhmed, S.Al-Nadzhar, N.A.Al-Anil, N.Rammo and N.Al-Assafi, 1980, Izv. Aka. Nank USSR Ser. Fiz. 44, 135.

- Diamond R.M., F.S.Stephens and W.J.Swiatecki, 1964, Phys. Rev. Lett. 11, 315.

- Dieperink A.E.L. and O.Scholten, 1980, Nucl. Phys. A 346, 125.

- Dorikens-Vanpract L., J.Demuynck and M.Dorikens, 1965, Nucl. Phys. 73, 539.

- Dzhelepov B.S. and N.N.Zhykovsky, 1958, Nucl. Phys. 6, 655.

- Enge H., 1966, Introduction to Nuclear Physics, Addison-Wesley, Reading, Mass.

- El-Daghmah M.S.S., 1982, Ph.D thesis, University of London, Bedford College, London.

- El-Daghmah M.S.S. and N.M.Stewart, 1983, Z. Physik A 309, 219.

- Fano U., 1947, Phys. Rev. 72, 26.

- Feenberg E., 1949, Phys. Rev. 75, 320.

- Fermi E., 1933, Ric. Sci. 2 part 12.

- Fermi E., 1934, Zf. Physick, 88, 161.

- Giberti G. and E.Maglione, 1981, Letters Al Nuovo Cimento, vol.32, N 16, 433.

- Gill R.L., R.F.Casten, D.D.Warner, D.S.Brenner and W.B.Walters, 1982, Phys. Lett. 118b, 251.

- Gono Y. and T.T.Sugihara, 1974, Phys. Rev. C 10, 2460.

- Goulding F.S., 1966, Nucl. Inst. Meth. 43. 1.

- Gove N.B. and M.J.Martin, 1971, Nucl. Data Tables 10, 206.

- Grigoriev E.P., A.V.Zolotavin, V.O.Sergeev and M.I.Soubv, 1968, Bull. Acad. Sci. USSR Phys. Ser. (USA) 32, 711.

- Groseclose B.C. and G.D.Loper, 1965, Phys. Rev. A 137, 939.

- Günther C., H.Ryde and K.Krien, 1968, Nucl. Phys. A 122, 401.

- Gupta J.B., S.S.Gupta, J.H.Hamilton and A.V.Ramayya, 1977, Z. Phys. A 282, 179.

- Hamilton J.H., T.Katoh, W.H.Brantely and E.F.Zganjar, 1964, Phys. Lett. 13, 43.

- Hamilton J.H., A.V.Ramaya, L.C.Whitlock and A.Menlenberg, 1967, Phys. Rev. Lett. 19, 1484.

- Hamilton W.D. and K.Kumar, 1979, J. Phys. G. vol.5, No.1, 1567.

- Harmatz B., T.H.Handley and J.W.Milhelich, 1961, Phys. Rev. 123, 1758.

- Harris S.H., 1965, Phys. Rev. B 138, 509.

- Haxel O., J.H.D.Jensen and H.E.Suess, 1949, Phys. Rev. 75, 1766.

- Helmer R.G., J.E.Clive and R.C.Greenwood, 1975, The Electromagnetic Interaction in Nuclear Spectroscopy, ed. W.D.Hamilton. Chapter 17.

- Heyde K., P.Van Isacker, G.Wenes, M.Waroquier, J.San and J. Maldegham, 1982, Neutron Capture Gamma-ray Spectroscopy and Related Topics (Inst. Phys. Conf. Ser. 62) P. 63.

- Iachello F., 1979, Interacting Bosons in Nuclear Physics (Plenum Press, New York).

- Iachello F., 1981, Interacting Bose-Fermi Systems in Nuclei (Plenum Press, New York).

- Ibrahim N. and N.M.Stewart, 1983, J. Phys. G: Nucl. Phys. 9, L 195.

- Jackson S.V. and R.A.Meyer, 1977, Phys. Rev. C15, 1806.

- Janssen D., R.V.Jolos and F.Dönan, 1974, A224, 93.

- Jensen J.H.D., 1964, Zur Geschichte der Theories des Atomkens, in Les Prix Nobel en 1963.

- Johnson J.R. and K.C. Mann, 1974, Can. J. Phys. 52, 406

- Kishimoto T. and T.Tamura, 1972, Nucl. Phys. A 192, 246.

- Kishimoto T. and T.Tamura, 1976, Nucl. Phys. A 270, 317.

- Kleinfield A.M., C.Mäggi and D.Werdecker, 1975, Nucl. Phys. A 248, 342.

- Krane K.S., 1975, Atomic Data and Nuclear Data Tables, 16,

No.4, 391.

- Kumar K. and M.Baranger, 1967a, Nucl. Phys. A 92, 608.

- Kumar K. and M.Baranger, 1967b, Nucl. Phys. A 92, 673.

- Kumar K. and M.Baranger, 1968a, Nucl. Phys. A 110, 529 and 490., or A 122, 241.

- Kumar K. and M.Baranger, 1968b, Nucl. Phys. A 122, 273.

- Lederer C.M. and V.Shirley, 1978, Table of Isotopes, 7th ed. New York, J.Wiley & Sons.

- Lipas P.O., 1983, Prog. Part. and Nucl. Phys. 9, 511.
- Lombard R.J., 1969, Nucl. Phys. A 114,449.
- Lopac V., 1970, Nucl. Phys. A 115,513.
- Mallman C., 1959, Phys. Rev. Lett. 2, 507.

- Mariscotti M.A.J., G.Scharff-Goldhaber and B.Buck, 1969, Phys. Rev. 178, 1864.

- Mayer M.G., 1949, Phys. Rev. 75, 1969.

- Mayer M.G., 1950, Phys. Rev. 78, 22.

- Mayer M.G. and J.H.D.Jensen, 1955, Elementary Theory of Nuclear Shell Structure (Wiley, New York).

- Meiling W. and F.Stray, 1968, Nanosecond Pulse Techniques (Gordon & Breach Science Pub. INC.).

- Metzger F.R., 1953, Phys. Rev. 90, 328.

- Meyer R.A., 1968, Phys. Rev. 170, 1089.

- Meyer R.A., 1968b, Phys. Rev. 174, 1478.

- Meyer R.A., W.B.Walters and R.C. Ragaini, 1969, Nucl. Phys. A 127, 295.

- Morinaga H., 1966, Nucl. Phys. 75, 385.

- Moszkowski S.A., 1951, Phys. Rev. 82, 35.

- Mottelson B.R. and S.G.Nilsson, 1955, Phys. Rev. 99, 1615.

- Myers W.D. and W.J.Swiatecki, 1966, Nucl. Phys. 81, 1.

- McGowan F.K. and W.T.Milner, 1981, Phys. Rev. C 23, 1926.

- Nagpal T.S. and R.E.Gaucher, 1972, Can. J. Phys. 50, 2688.

- Nathan O. and S.G.Nilsson, 1965, in Alpha-, Beta-, and Gamma-ray Spectroscopy, ed. K.Siegbhn (North Holand Pub. Comp. Amsterdam) P. 601.

- Neergard K. and P.Vogel, 1970, Nucl. Phys. A 145, 33.

- Ng L.K., K.C.Mann and T.G.Walton, 1968, Nucl. Phys. A 116, 433.

- Nicholson P.W., 1974, Nuclear Electronics (J.Wiley & Sons).

- Nilsson S.G., 1955, Math. Fys. Nedd. 29, 16.

- Nuclear Data Sheets, 1977, 22, No.1.

- Nuclear Data Sheets, 1979, 26, No.2.

- Ober D.R., W.Weeber and R.L.Place, 1973, Phys. Rev. C 7, 738.

- Ragaini R.C., W.B.Walters and R.A.Meyer, 1969, Phys. Rev. 187, 1721.

- Rathore I.V.S. and B.P.Singh, 1979, Indian J. of pure and Appl. Phys. 17, 518.

- Riedinger L.L., N.R.Johnson and J.H.Hamilton, 1967, Phys. Rev. Lett. 19, 1243.

- Riedinger L.L., N.R.Johnson and J.H.Hamilton, 1969, Phys. Rev. 179, 1214.

- Riedinger L.L., N.R.Johnson and J.H.Hamilton, 1970, Phys. Rev. C 2, 2358.

- Riedinger L.L., D.C.Sousa, F.G.Funk and J.W.Milhelich, 1971, Phys. Rev. C 4, 1352.

- Rikovska J., A.Machova and D.W.Hamilton, 1981, Czech. J. Phys. B 31, 511.

- Robinson S.J., W.D.Hamilton and D.M.Snelling, 1983, J. Phys. G. Nucl. Phys. 9, L 71.

- Rose M.E., 1937, Phys. Rev. 51, 484.

- Rose M.E., G.H.Goertzel, B.I.Spinral, J.Harr and P.Strong, 1955, see M.E.Rose in Beta and Gamma-ray Spectroscopy, ed. K. Siegbahn (North Holand Pub. Comp, Amsterdam)P.P. 905., or, M.E.Rose, 1958, Internal Conversion Coefficient, (North Holand Pub. Comp., Amsterdam).

- Rosel F., H.M.Fries, K.Alder and H.C.Pauli, 1978, Atomic Data and Nuclear Data Tables, 21, 205.

- Routti J.T., 1969, Lawrence Berkeley Laboratory Report UCRL 19452.

- Routti J.T. and S.G.Prussin, 1969, Nucl. Inst. Meth. 72, 125.

- Rud N., H.L.Nielsen and K.Wilsky, 1971, Nucl. Phys. A 167,401.

- Sambataro M., 1982, Nucl. Phys. A 380, 365.

- Scharff-Goldhaber G. and J.Weneser, 1955, Phys. Rev. 98, 212.

- Scharff-Goldhaber G., D.E.Alburger and M.McKeown, 1958, Phys. Rev. 111, 913.

- Scharff-Goldhaber G., 1974, J. Phys. A: Math. Nucl. Gen 7: L 212.

- Scharff-Goldhaber G., C.B.Dover and A.L.Goodman, 1976, Ann. Rev. Nucl. Sci. 26, 239.

- Scharenberg R. and G.Goldring, 1958, Phys. Rev. 110, 701.

- Scholten O., 1975, Computer program PHINT. Univ. Groningen, The Netherlands.

- Scholten O., F.Iachello and A.Arima, 1978, Ann. Phys. (N.Y) 115, 325.

- Scholten O., 1980, The Interacting Boson Model and Some Applications. Ph.D thesis, Univ. Groningen, The Netherlands.

- Segrè E., 1977, Nuclei and Particles, Second ed., W.A.Benjamin, INC. Reading Mass.

- Shaban A.M., 1980, Ph.D thesis, Univ. London, Bedford College, London.

- Sharma A.K., Ravinger Kaur, H.R.Verma, K.K.Suri and P.N.Trehan, 1979, J. Phys. Japan, vol.46, No.4, 1057.

- Sharma A.K., R.Kaur, H.R.Verma and P.N.Terhan, 1980, J. Phys. Soc, Japan, 48, NO.5, 1407.

- Sharma A.K., R.Kaur, H.R.Verma, S.S.Sooch and P.N.Trehan, 1982, Proc. Indian Natn. Sci. Acad. 48 A, No.2, 182.

- Sheline R.K., T.Sikkeland and R.N.Chanada, 1961, Phys. Rev. Lett. 7, 446.

- Sie S.H., D.Ward, J.S.Seiger, R.L.Graham and H.R.Andrews, 1977, Nucl. Phys. A 291, 443.

- Siegbahn K., 1965, Alpha-, Beta- and Gamma-ray Spectroscopy,

vol.1, (North Holand Pub. Comp., Amsterdam).

- Soloviev V.G., P.Fogel and A.A.Korneichuk, 1964a, Dokl. Akad. Nauk SSSR 154, 72, or English translation; Soviet. Phys. Doklady 9, 45.

- Soloviev V.G., P.Fogel and A.A.Korneichuk, 1964b, Bull. Acad. Sci. USSR Phys. Ser. 28, 1495.

- Sorensen B., 1967, Nucl. Phys. A 97, 1.

- Sorensen B., 1968, Nucl. Phys. A 119, 65.

- Sorensen B., 1970, Nucl. Phys. A 142, 392 and 411.

- Sousa D.C., L.L.Riedinger, E.G.Funk and J.W.Milhelich, 1975, Nucl. Phys. A 238, 365.

- Stachel J., P.Van Isacker and K.Heyde, 1982, Phys. Rev. C 25, 650.

- Stelson P.H., 1967, Phys. Rev. 157, 1098.

- Stewart N.M. and A.M.Shaban, 1980, Z. Physik A 296, 165.

- Sulaiman M.Y.B., 1977, Ph.D thesis, Univ. London, Bedford College, London.

- Sulaiman M.Y.B. and R.N.Thomas, 1979, Nucl. Inst. Meth. 166, 305.

- Talmi I., 1962, Rev. Mod. Phys. 34, 704.

- Talmi I., 1964, in Selected Topics in Nuclear Spectroscopy, ed. Verhaan (J.Wiley, New York) P. 106.

- Talmi I., 1981, in "Proc. Int. Conference on Dynamical Properties of Heavy-Ion Reactions" S.Afr. J. Phys. 1, 183; In Frontier Research in Nuclear Physics, ed. by D.H.Feny et al. (Plenum Press, New York) or

Iachello (1979) P. 79.

- Tamura T., K.Weeks and T.Kishimoto, 1979, Phys. Rev. C 20, 307.

- Thein M., 1977, Ph.D thesis, Imperial College, Univ. of London, London,

- Verral R.I., J.C.Hardy and R.E.Bell, 1966, Nucl. Just. Meth. 42, 258 and references therein.

- Van Isacker P., K.Heyde, M.Waroquier and G.Wenes, 1982, Nucl. Phys. A 380, 383.

- Warner D.D., R.R.Casten and W.F.Davidson, 1980, Phys. Rev. Lett. 45, 1761.

- Warner D.D. and R.F.Casten, 1982, Phys. Rev. C 25, 2019

- Weitkamp C., 1963, Nucl. Phys. 43, 57.

- West R.L., E.G.Funk and J.W.Mihelich, 1978, Phys. Rev. C 18, 679.

- Whitlock L.C., J.H.Hamilton and A.V.Ramaya, 1971, Phys. Rev. C 3, 313.

- Wilets L. and M.Jean, 1956, Phys. Rev. 1 02, 788.

- Wilson R.K., P.O.Johnson and R.Stump, 1963, Phys. Rev. 129, 2091.

- Wood J.L., 1983, Nucl. Phys. A 396, 245.

- Wu W.M., C.S. and S.A.Moszkowski, 1966, Beta Decay, Wiley-Interscience, New York.

- Yamada H., H.Kawakami, M.Koike and K.Komura, 1977, J. Phys. Soc. Japan, 42, 1448.

- Zhelev Z.T., N.G.Zaitsera and S.S.Sabinov, 1972, Bull. Acad. Sci. USSR Phys. Ser. 35, 40.

- Zelnowski D.R. and T.Kishimoto, 1974, Cyclotron Inst., Texas A & M Univ., Progress Report, unpublished.

Acknowledgements

I would like to express my gratitude to Dr. N.M. Stewart for his supervision, support and encouragement during the course of this work.

Thanks are due to the Director and staff at the University of London Reactor Centre, in particular Dr. T.D. MacMahon, for their hospitality and help in obtaining the radioactive source materials and making available some of the equipment described in this work.

The assistance given by the staff and technicians in both the physics department and the computer centre at Bedford College have been invaluable, and I would especially like to thank Professor Dobbs for his support of this work.

I wish to thank Dr. W.Gelletly and Dr. Jo Mo for very helpful discussions on the use of the programs PHINT and FBEM, their help in providing these programs are sincerely appreciated.

I wish to acknowledge Dr. M.S.S. El-Daghmah and Mr. N.Ibrahim for valuable discussions, and particularly my parents and Mrs. M.Arita without whom this work would not have been possible.

I am indebted to the Syrian Government for a post-graduate scholarship granted by the University of Aleppo.